Structure-based design, synthesis and biophysical studies of artificial ribonucleases

A thesis submitted to the University of Manchester for the degree of Doctor of Philosophy in the Faculty of Medical and Human Sciences

2009

Jasbir Kumar Rattu

School of Pharmacy and Pharmaceutical Sciences

List of Contents

List of Figures

List of Tables

Abstract

Research into the design of artificial ribonucleases, a class of RNA phosphodiester bond recognising and cleaving molecules, has been inspired by their potential use in both therapy and as tools in molecular biology. These artificial mimics offer the prospect of sequence-specific cleavage of target RNA sequences which is a prominent advantage over natural ribonucleases.

The challenging approach to artificial ribonuclease design normally includes conjugation of structural elements which function separately as a binding and a cleaving moiety. The cleaving moiety design has normally been based on the imitation of the catalytic active centre of natural RNases with hydrolytically active functional groups. Other elements which are responsible for binding may consist of (antisense) oligonucleotides for specific recognition *via* Watson-Crick hydrogen bonding and small molecules with non-specific affinity for RNA (also known as anchor groups), for example *N*-(2-hydroxyethyl)-phenazinium, used in this study. The function of the *N*-(2-hydroxyethyl)-phenazinium anchor group is to increase the affinity of the designed artificial ribonucleases to the RNA target and improve stability of the corresponding *RNA:DNA* hybrid. This may (potentially) enhance the probability of the cleaving group(s) being located near the RNA cleavage site and thus improve their hydrolytic performance.

The objective of this study was to devise a novel and flexible approach to the synthesis of novel artificial ribonucleases which can vary in location of an *N*-(2-hydroxyethyl)-phenazinium anchor group and specific recognition oligonucleotide moiety relative to the *bis*-imidazole cleaving moiety. The cleaving constructs for the studied artificial ribonucleases were synthesised by standard peptide synthesis, followed by conjugation to the oligonucleotide recognition element. A number of the structural variants of such artificial ribonucleases have been successfully synthesised and characterised by various analytical techniques (NMR, mass spectrometry, UV-visible spectroscopy, HPLC and fluorescence spectroscopy).

Synthesised artificial ribonucleases were subjected to binding studies using UV-visible spectroscopy and thermal denaturation experiments by monitoring changes to the absorption of the *N*-hydroxyethylphenazinium's distinct chromophore. UV-visible spectroscopy experiments were able to demonstrate the considerable contribution from electrostatic interactions between *N*-(2-hydroxyethyl)phenazinium anchor and the RNA target (in addition to stacking interactions from the hydrophobic heteroaromatic phenazinium ring).

The hydrolytic ability of the synthesised artificial ribonucleases was assessed by our collaborators from the research groups of Professor M. Zenkova's, Novosibirsk, Russia. The synthesised AR were also able to cleave $tRNA^{Phe}$ in a sequence-specific manner at sites typical of RNases. However, the presence of the *N*-hydroxyethylphenazinium in the artificial ribonucleases did not show an enhanced rate of hydrolysis compared to similar cleaving constructs without this anchor group.

Declaration

No portion of the work referred to in the thesis has been submitted in support of an application for another degree or qualification of this or any other university or other institute of learning.

Copyright statement

i. The author of this thesis (including any appendices and/or schedules to this thesis) owns any copyright in it (the "Copyright") and he has given The University of Manchester the right to use such Copyright for any administrative, promotional, educational and/or teaching purposes.

ii. Copies of this thesis, either in full or in extracts, may be made **only** in accordance with the John Rylands University Library of Manchester. Details of these regulations may be obtained from the Librarian. This page must form part of any such copies made.

iii. The ownership of any patents, designs, trade marks, and any other intellectual property rights except for the Copyright (the "Intellectual Property Rights") and any reproductions of copyright works, for example graphs and tables ("Reproductions"), which may be described in this thesis, may not be owned by the author and may be owned by third parties. Such Intellectual Property Rights must not be made available for use without the proper written permission of the owner(s) of the relevant Intellectual Property Rights and/or Reproductions.

iv. Further information on the conditions under which disclosure, publication and exploitation of this thesis, the Copyright and any Intellectual property Rights and/or Reproductions described in it may take place is available from the Head of School of Pharmacy and Pharmaceutical Sciences.

Acknowledgements

I would like to thank my supervisor Dr Elena Bichenkova for all her help and support throughout this degree on all aspects of my work.

I would also like to thank Dr Dmitry Stetsenko for his expert advice and support with my chemistry work.

Thanks to Dr. N. Tamkovich and Professor Marina Zenkova from the Institute of Chemical Biology and Fundamental Medicine, Novosibirsk, Russia for their collaborative biochemical work.

Thanks also to my assessor Professor Ken Douglas for useful advice and motivation on assessments.

More thanks to all the friendly characters in the labs (past and present) for their scientific and technical help, the laughs, the philosophical talks, and for creating a pleasant environment to work in.

Finally, last but not least, I would like to thank my friends and family for all their encouragement and especially my nephew Suraj (Sunshine) and niece Priya (beloved) for enriching my life.

Abbreviations

A_{260}, A_{520}	Absorbance at 260 nm, 520 nm, etc
Ala	Alanine
Å	Angstrom
AML	Acute myeloid leukaemia
ApoB	Apolipoprotein B
Aq	Aqueous
AR	Artificial ribonuclease(s)
AS-ON	Antisense oligonucleotide(s)
AS-ON-AR	Antisense oligonucleotide based artificial ribonuclease
Boc	*tert*-Butoxycarbonyl
Boc_2O	Di-tert-butyl-dicarbonate or Boc anhydride
Boc-β-ala-OH	Boc-β-alanine
Boc-β-ala-OPFP	Boc-β-alanine pentafluorophenol ester
Boc-His-(Boc)-OSu	Boc-Histidine-(1-Boc)-*N*-hydroxysuccinimide
Boc-lys-(Fmoc)-OH	*N*-α-t-Boc-*N*-ε-Fmoc-L-lysine
Boc-lys-(Fmoc)-OSu	*N*-α-t-Boc-*N*-ε-Fmoc-L-lysine- *N*-hydroxysuccinimide
Boc-Lys-(Tfa)-OH	*N*-α-t-Boc-*N*-ε-trifluoroacetyl-L-lysine
Boc-Lys-(Tfa)-OSu	*N*-α-t-Boc-*N*-ε-trifluoroacetyl-L-lysine-*N*-hydroxysuccinimide
Bp	base pairs
CABG	Coronary artery bypass graft
C	Cytidine
Ca	*Circa*
Cbz	Carbonyloxybenzyl
$CHCl_3$	Chloroform
CMV	Cytomegalovirus
CNS	Central nervous system
Conc	Concentrated
COSY	Correlated spectroscopy
CPP	Cell Penetrating Peptide(s)
CTAB	*N*-Cetyl-*N,N,N*-trimethylammonium bromide
D_2O	Deuterium oxide
DCC	*N,N'*-dicyclohexylcarbodiimide
DCM	Dichloromethane
DEPT	Distortionless enhancement by polarization transfer
DIEA or DIPEA	Diisopropylethylamine

DMAP	4-Dimethylaminopyridine
DMF	Dimethylformamide
DMSO	Dimethylsulfoxide
DNA	Deoxyribonucleic acid
dsDNA	Double-stranded deoxyribonucleic acid
dsRNA	Double-stranded ribonucleic acid
EDTA	Ethylenediaminetetraacetic acid
Eqn	Equation
Et_3N	Triethylamine
Et_3SiH	Triethylsilane
EtOAc	Ethyl acetate
Fmoc	Fluoren-9-ylmethoxycarbonyl
Fmoc-lys-(Mtt)-OH	*N*-α-Fmoc- *N*-ε-4- methyltrityl-L-lysine
GI	Gastrointestinal
HAART	Highly active antiretroviral therapy
HBV	Hepatitis B virus
HCl	Hydrochloric acid
HCV	Hepatitis C virus
HIF-1	Hypoxia-Inducible Factor
His	Histidine
HIV	Human Immunodeficiency Virus
HMCV	Human cytomegalovirus
HPLC	High performance liquid chromatography
HPNP	2-Hydroxypropyl-*p*-nitrophenyl phosphate
HPV	Human papillomavirus
Hz	Hertz
IE2	Immediate early region 2
IR	Infra red
K	Kelvin
Li	Lithium
LDL	Low density lipoprotein
LNA	Locked nucleic acid
Lys	lysine
MALDI-TOF/TOF	Matrix Assisted Laser Desorption Ionisation- Time of Flight/ Time of flight
MeCN	Acetonitrile
MeOH	Methanol
MeOD	Deuterated methanol

min	Minute
MM	Malignant mesothelioma
Mmt	Monomethoxytrityl
MO	Morpholino oligonucleotides
m.p.	Melting point
MS	Mass spectrometry
MST	Mean survival time
Mtt	4-Methyltrityl
MW	Molecular weight
NA	Nucleic acids
N-BuOH	1-Butanol
NH_3	Ammonia
NH_4OH (aq)	Ammonia water
NHS	*N*-hydroxysuccinimide
nm	Nanometer
NMM	*N*-methyl morpholine
NMR	Nuclear magnetic resonance
NSCLC	Non-small cell lung cancer
nt	Nucleotides
2'OMe RNA	2' O-methyl ribonucleic acid
ON	Oligonucleotide
OPfp	Pentafluorophenyl ester
OSu	*N*-hydroxysuccinimide
OD	Optical density
ON-AR	Oligonucleotide-based artificial ribonuclease
OU	Optical units
PCN	Peptidyloligonucleotide
Pd/C	Palladium on activated charcoal
PfpOH	Pentafluorophenol
Phn	Phenazinium
PNA	Peptide nucleic acid
ppm	Parts per million
PS	Phosphorothioate
Pur	Purine
Pyr	Pyrimidine
$(PyS)_2$	2,2'-dipyridyl disulfide
RI	Ribonuclease inhibitor
RISC	RNA-inducing silencing complex

RP-HPLC	Reverse-phase high performance liquid chromatography
RNA	Ribonucleic acid
RNAi	Ribonucleic acid interference
RNase	Ribonuclease
RT	Room temperature
s	Second
SARS	Severe acute respiratory syndrome
siRNA	Small interfering ribonucleic acid
SNase	Staphylococcal nuclease
ssRNA	Single-stranded ribonucleic acid
SPPS	Solid phase peptide synthesis
T	Thymidine
TEA	Triethylamine
TES	Triethylsilane
TFA	Trifluoroacetic acid
Tfa	Trifluoroacetyl
THF	Tetrahydrofuran
TLC	Thin layer chromatography
T_m	Melting temperature
TMS	Tetramethylsilane
U	Uracil
UMM	Unresectable malignant mesothelioma
UTR	Untranslated region
UV	Ultraviolet
VEGF	Vascular endothelial growth factor
Z	Benzyloxycarbonyl
Z-lys-(Boc)-OH	*N*-α-Benzyloxycarbonyl-*N*-ε-t-Boc-L-lysine
λ_{EX}	Excitation wavelength
λ_{EM}	Emission wavelength

1. Introduction

1.1. Global pharmaceutical challenges

Many factors drive the continual need to find novel chemotherapeutics with new pharmacological mechanisms and targets. These include the ongoing threat and occurrence of resistance to current anti-infective therapy and the unmet medical need in many other areas, such as cancer.

Infectious diseases alone are still the leading cause of death in the world. According to the 'World Health Report 1996- Fighting disease, fostering development' by the World Health Organisation (WHO), infectious diseases are killing over 17 million people every year, costing millions of lives and threatening global socioeconomic development [28]. Another major challenge facing us today is the developing resistance of infectious diseases to antibiotics [29], with some infections virtually untreatable due to multiresistant bacteria [30, 31]. As an example, diseases such as tuberculosis and malaria once believed to be under control are re-emerging with multi-drug resistant strains [32, 33]. Aside from the looming threat of drug resistance, there are still many infections with no or inadequate treatment or cure. One example is HIV for which there has been no satisfactory curative treatment in over 25 years. There is also the rarer threat of 'new' infectious agents such as the severe acute respiratory syndrome (SARS) virus.

Consequently, one of the major challenges in medicine today is the development of new antimicrobials such as antibiotics and antiviral agents to combat these problems. Research to develop new medicines with innovative ways to fight disease in these areas is gravely needed and a multitude and diversity of approaches will increase the probability of success. One promising target class is the multifunctional RNA molecule whose biological importance and potential as a drug target has become increasingly recognised over the last decade [34-37]. This target class offers a route to fulfil the need for the development of novel therapeutics, particularly with approaches affecting specific messenger RNAs (e.g. against abnormal gene expression) and viral genomic RNAs (e.g. to fight viral infectious diseases).

Treatments for common serious diseases such as cancer also require therapy which is more cancer specific with fewer, more tolerable or no side effects.

Currently, management of unresectable or metastatic tumours often relies on the cytotoxic effect of radiotherapy and/or chemotherapies. This area would benefit from the gene-specific approach to chemotherapy where the production of harmful, oncogenic protein(s) could be treated using antisense interference of an oncogene-relevant mRNA. This in effect would very specifically block the translation of the cancer-causing oncogenic information. This promising approach therefore may result in highly selective anticancer drugs for the abnormal gene expression of disease states, identified by post-genomic studies, in place of the currently indicated combination therapies comprising toxic drug cocktails [38-40].

The approach taken in this study involves a type of molecule designed to target specific RNA sequences called antisense-oligonucleotide based artificial ribonucleases. This method utilises efficient, specific and irreversible RNA damage in its mechanism of action and therefore has promise in the field of RNA targeting both in therapeutics and as a tool in molecular biology.

1.2. RNA as a potential pharmaceutical target

RNA plays a vital role in all living organisms and does much more than physically convey genetic information stored in DNA to functionally acting proteins.

In the scheme of translation of messenger RNA (mRNA) to specific proteins, targeting at the RNA translation stage can be seen as an 'earlier step', even before the protein is produced, compared to the traditional targeting of drugs to proteins.

Figure 1.1. Schematic diagram showing mRNA is prevented from being translated into its encoded protein.

In the last few years, several novel and biologically important small RNAs have been discovered in a variety of organisms from bacteria to mammalian cells. A large number of non coding RNAs (ncRNA), including small RNAs, sometimes referred to as micro RNA (miRNA) and small interfering RNA (siRNA) have also recently been identified. Today we know that such ncRNA molecules have several

fundamental functions essential for cell growth, survival, and development. This large collection of novel small and non coding RNAs (ncRNAs) have been demonstrated to be involved in gene silencing via RNA and to play essential roles in controlling all steps of gene expression, including transcription, chromatin modification, epigenetic memory, and alternative splicing. Also, since many miRNAs have been implicated in disease they too provide a promising new (miRNA antagonising) target [41].

The plethora of properties and functions associated with RNA molecules, i.e., non-coding RNA (ncRNA), has led to the realisation that RNA molecules are frequently associated with the development and progression of diseases: particularly genetic disorders, tumour progression and autoimmune diseases [42]. Numerous RNA molecules are also essential for the growth of microbial pathogens (*e.g.*, bacteria, virus, parasites, etc.) and thereby are essential for the progression of infectious diseases [43]. Other key roles of RNA include structural, functional, regulatory, and informational roles. The functions that RNA carries out or participates in also include RNA processing and protein translation, acting as structural scaffolds, transporters, gene regulators, and biocatalysts. These many roles have been reviewed by John S Mattick [44]. Further, the many roles of RNA highlight its importance and the abundance of opportunities for its potential targeting.

Based on its key role in many biochemical pathways, RNA has been recognised as a possible drug target for many years [45]. Most prominently, it has been a prime target because it has been identified to play a major role in many macromolecular processes, e.g. as a mediator (mRNA) in the passage of genetic information from DNA to protein (protein synthesis), in mRNA splicing, in transcriptional regulation and also in retroviral replication [36].

RNA is the genetic material of certain viruses; hence the viral genome lends itself to selective targeting (as well as mRNA) in potential antiviral chemotherapy, theoretically clearing the virus completely. However, for DNA viruses or retroviruses which integrate their proviral DNA into the host genome, only mRNA (or newly synthesised genome RNA for retroviruses) can be targeted [46].

Lastly, RNA's validity as a potential drug target (a validated drug target for over 50 years), has been proven by the fact that several important classes of

antibiotics such as aminoglycosides, macrolides and tetracyclines interact with RNA and interfere with its function to effect their antimicrobial action [47, 48].

1.3. RNA targeting

1.3.1. General overview

There are three major approaches to targeting mRNA for gene silencing: antisense oligonucleotides (AS-ON), ribozymes and RNA interference (RNAi) with small interfering RNA (siRNA) which are explained in more detail later in sections 1.3.2- 1.3.4.

Figure 1.2. Mechanisms of antisense strategies for inhibiting gene expression (taken from [1]). Ribozyme mechanism (left), oligonucleotide mechanism (centre) and RNAi mechanism (right).

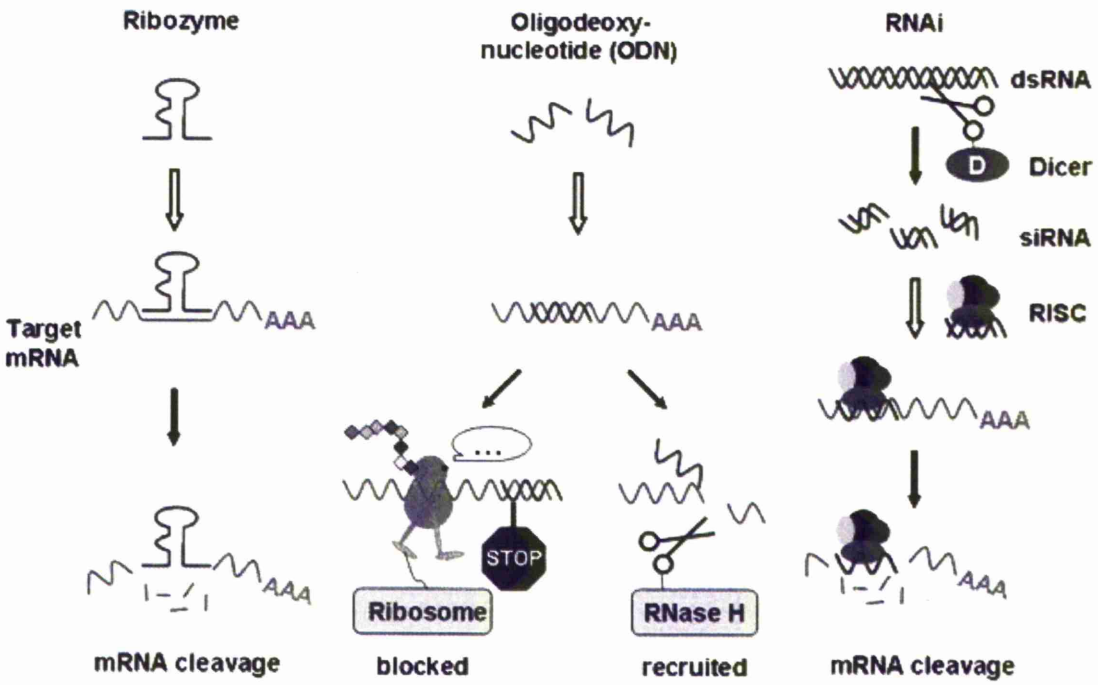

The diagram above summarises the three major approaches to RNA targeting. The ribozyme binds specifically to the substrate RNA via the Watson–Crick base pairing, and subsequently attacks the RNA with a non-hydrolytic cleavage which degrades the target. AS-ON hybridises with the target mRNA of a

complementary sequence and blocks mRNA translation through translation arrest by blocking ribosomal machinery or RNase H-dependent cleavage. In RNA interference (RNAi), siRNA assembles with Argonaute proteins, Dicer and other cellular factors into the RNA-induced silencing complex (RISC), which unwinds the siRNA. Then the antisense strand guides RISC to cleave the target mRNA in a sequence-specific manner.

The use of these approaches had lead to the development of many investigational drugs although the application of RNA-based drugs in therapy still remains in its infancy. Currently there are only two RNA-based drugs on the market: fomivirsen (Vitravene®, see section 1.4.1) and pegaptanib (Macugen®, see section 1.3.4). Although neither can be considered to be commercially successful [49] there are many hopeful RNA targeting medicines in clinical trials [50]. These include: natural RNases (e.g. Onconase®, see section 1.7), several RNase activators and many siRNA and antisense oligonucleotides which are in clinical trials for cancer treatment (e.g. mesothelioma, renal cell carcinoma), inhibition of chronic virus infections (e.g. HIV, Hepatitis C), diabetes, restenosis, coronary artery bypass graft (CABG), asthma, multiple sclerosis, ocular diseases and amyotrophic lateral sclerosis [51].

1.3.2. Antisense oligonucleotides

One of the most popular approaches has been the design of antisense oligonucleotides.

An antisense oligonucleotide is a single-stranded nucleic acid sequence or its analogue, which is complementary to the target region of the sense RNA or DNA strand. Antisense oligonucleotide technology involves the recognition of a single-stranded target mRNA by Watson-Crick base pairing (hybridisation) with a complementary nucleic acid. Antisense technology, however, is more than simply a method of binding sense RNA. It is the general principle of several gene silencing technologies.

Figure 1.3. Schematic illustration of mRNA translational arrest using antisense oligonucleotide approaches. Antisense oligonucleotide either blocks transcribed mRNA from translation sterically or by inducing RNA degradation by RNase H, taken from [2].

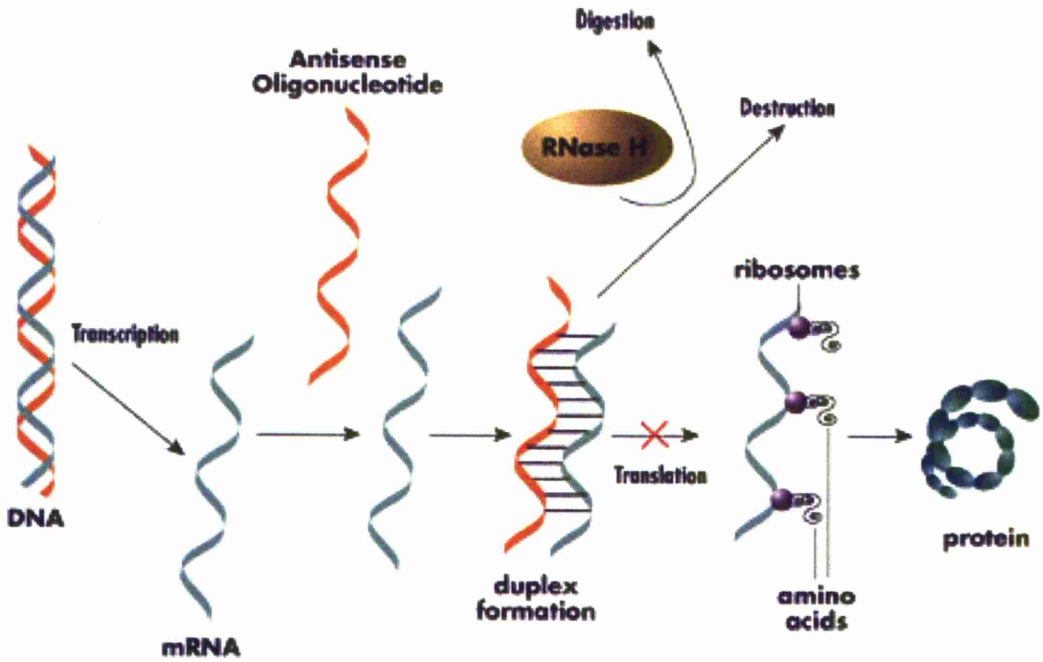

There are two major classes of AS-ON (depending on the mode of action). The first approach is based on disruption of translation by (only) steric blocking of the functionally significant mRNA regions. Once inside the cellular cytoplasm, single stranded oligonucleotides block gene expression by interfering with RNA translation: by simple hybridisation and steric blockage they prevent translation of the intended message by hindering ribosomal assembly and translation.

The other approach is based upon degrading the RNA in a DNA/RNA heteroduplex *via* a RNase H dependent pathway using RNase-H mediated cleavage [2] of RNA sequences. RNase-H is a natural endogenous ribonuclease which is often necessary for a successful antisense effect. When antisense oligonucleotides bind to RNA to form a duplex, RNase H destroys the bound RNA by its hydrolytic activity, freeing the oligonucleotide to rehybridise with another copy of mRNA. However, this blocking does not prevent more mRNA being produced.

Target RNA has to be selected rationally as knocking down one gene may lead to an overexpression of a compensatory gene. Alternatively, a target RNA may not be the only important target in the disease or it may only be involved at one stage e.g. in the early stages of the disease but become unimportant as the disease progresses. If the target protein is overexpressed only in the disease state, antisense approach is expected to be highly specific with low or zero cytotoxicity. However, if target is similarly expressed in both normal and malignant cells both types may be induced to undergo apoptosis [52], thus leading to non-specific cytotoxicity.

1.3.3. Ribozymes

Ribozymes (also known as RNA enzymes or catalytic RNA) are ribonucleic acids with enzymatic properties that catalyse the hydrolysis of phosphodiester bonds in RNA molecules. In ribozymes the RNA functions as the catalytic component. They bind to their specific RNA target by Watson-Crick base pairing and can cleave it without the aid of cellular proteins, relying on their nucleobases for catalytic chemistry [53]. Aside from their use as tools in functional studies several ribozymes have reached testing in clinical trials for viral infections and inhibiting cancer growth [42, 54].

1.3.4. RNAi with siRNA

A related technology which has benefited from progress in antisense development is the area of RNA interference (RNAi). This is mediated by small interfering RNA (siRNA) molecules, which are double stranded RNA (dsRNA) molecules, usually 21- 25 base pairs in length. They mediate RNA interference, an antiviral response initially identified in *C elegans* and subsequently found active in specific gene silencing in many other organisms including mammalian cells. The sense and antisense strands of a siRNA first unwind and the antisense strand binds to the target mRNA and recruits RNA-inducing silencing complex (RISC). The sense strand is released from RISC and catalyses the mRNA cleavage (see Figure 1.2.). The gene silencing efficiency of siRNA has reportedly been greater than antisense in general, typically reaching 80-90%, but it too has its advantages and disadvantages. Although siRNAs and related approaches achieve sufficient gene silencing with mRNA target specificity and benefit from a catalytic amplification, the biological cascade triggered by siRNAs is complex and may be associated with off-target effects, raising concerns of their potential safe

use in humans. This has been a prolific area of growth in the last decade and the state of the art has recently been reviewed by Grimm D., Masiero M. and Sioud M [55-57].

1.3.5. Advantages and disadvantages of using RNA as a target

1.3.5.1. Disadvantages

There are a number of disadvantages in using RNA as a pharmaceutical target which are summarised below.

Unless antisense oligonucleotides are designed to inhibit transcription, they would rarely be 100% inhibitory because the antisense inhibition of RNA does not shut down transcription of endogenous copies of mRNA. The antisense RNA interference competes with RNA being produced by the cell, and the resulting effect is gene knockdown, not knockout [52, 58].

The delivery into cells aspect of antisense oligonucleotide design is not straightforward and can be a problem. Antisense oligonucleotides must enter the cell through an uptake mechanism and escape from endosomes and lysosomes within cells in sufficient amounts to avoid complete intracellular degradation [59].

If target mRNA is shielded or coiled it makes it difficult for antisense to access and hybridise target regions. Also, usually RNA are folded and often studded with regulated proteins, which makes accessibility problematic. Predicting folding and secondary RNA structures in a living cell is still very difficult.

Stability of *Antisense:RNA* hybrids is affected by the proportion of G-C base pairing which has three hydrogen bonds as opposed to two hydrogen bonds between A-T and may therefore be uncontrollably sequence dependent. Sufficient base pairs are required to make a specific match and thus identify a *unique* RNA sequence. However, too much base-pairing may cause non-specific RNA binding resulting in more than a single target being affected, thus leading to off-target effects [60, 61].

The RNA target may not be the only important target in the disease and knocking down one gene may lead to a compensatory gene overexpression.

Antisense oligonucleotides designed to destroy cancer cells by down-regulation of disease-relevant RNA might be unsuccessful due to a competition between RNA inhibition using antisense oligonucleotides versus endogenous production of copies of relevant mRNA in a cell [62].

The importance of the gene relevant to the disease state has to be fully understood. One gene may be important at the early stage of the disease, but as it progresses it may have a diminished role, while another gene may become more important. Targeting transcription factors or signalling pathway proteins which are important in regulating cells may not be sufficiently specific [58, 62].

If the target protein is only overexpressed in the disease state then antisense interference could be highly selective. However, the specificity of RNA targeting might be compromised if relevant RNA is expressed in both normal and malignant cells, which may cause both types of cell to undergo apoptosis leading to indesirable cytotoxicity [63].

1.3.5.2. Advantages

Potential targeting of RNA is vast because of its abundance and ubiquity. On a scientific level, antisense gene knockdown has been the quickest way to study therapeutic targets in drug discovery [60].

Another advantage of using RNA as a target is that it lacks repair mechanisms to overcome any damage made to its structure unlike DNA which has repair mechanisms to preserve genetic data. Also, RNA has a relaxed structure with less intensive puckering and greater tertiary structural diversity than DNA [16]. Finally, RNA is located within the cellular cytoplasm as opposed to DNA, which is located in the nucleus. Therefore, RNA can be easily accessed in comparison to targeting DNA within the nucleus. Furthermore, the nature of the RNA molecule (which has prolonged single stranded nucleotide regions) presents a degree of structural diversity upon folding in the space. Therefore, RNAs could also be targeted according to a particular tertiary structure rather than simply by base sequence [16].

The antisense artificial ribonuclease (AS-AR) approach has the potential of making the whole genome amenable to targeting, hypothetically rendering all

proteins drugable, which is particularly desirable in areas intractable to classical pharmaceutical approaches.

1.4. Application of antisense oligonucleotides as new pharmacological chemotherapeutics

1.4.1. General overview

Grineva et al, in 1967, suggested the use of RNA sequences as endogenous inhibitors of prokaryotic gene expression. However, the potential therapeutic use of antisense technology was first proposed in 1978 with the demonstration that oligonucleotides could be used as antisense agents to inhibit viral replication in cell cultures [45].

The therapeutic goal envisioned is a gene-specific approach to chemotherapy, where any disease that involves the production of a harmful protein (or one essential to its existence or pathogenicity) can be treated by antisense interference with a disease-relevant mRNA [59, 64]. This antisense method of controlling gene expression or protein production is based on the natural method of gene regulation.

A big advantage of antisense oligonucleotides (AS-ONs) when considering their use in humans is that theoretically they are 'physiologically-friendly' agents because they neither cause a mutation to DNA nor prevent a protein involved in normal physiology from performing its role [60]. Antisense oligonucleotides are effective in reducing overexpression of proteins that cause disease states. To date, several human trials have shown how well antisense technology can be tolerated, with more than 2000 people having received investigative antisense products.

Multi-specific targeting of RNA using selected overlapping regions of mRNA transcripts encoding disease relevant proteins would allow more efficient translational arrest and thus would give more chance of success. This approach, which is expected to offer a synergistic effect, has already been successfully demonstrated in human prostate PC3 cells [65].

Choice of RNA sequences for specific targeting by antisense oligonucleotide is an important issue. Theoretically AS-ON can be directed against any region of the target RNA. However, long RNA molecules form complex secondary and tertiary structures, unaccessible for targeting. Moreover, RNA may form *RNA:protein* complexes, thus precluding ONs from hybridizing with the target regions. Therefore it is important to identify the regions of target RNA which can be accessible to AS-ON. The problem associated with inaccessible structure can be mitigated by molecular modeling and *in silico* searching of accessible structural sites, including prediction of accessibility of the target mRNA sequence using secondary structure and folding algorithms (*e.g.* mfold, RNAstructure). Various methods have been developed for this and are summarised by Sohail and Southern [66, 67].

1.4.2. Antisense oligonucleotides as potential antivirals

Viruses with RNA genomes contain both mRNA and genomic RNA and therefore are particularly well suited to attack by AS-ON to theoretically achieve complete viral clearance. However, in the genome for retroviruses the proviral DNA is stably integrated into the host genome and so only mRNA (or newly synthesised genomic RNA) can be targeted by AS-ONs. In the latter case only inhibition of virus spreading can be expected, rather than complete clearance, requiring continous treatment [46]. However, the genome of RNA viruses is sensitive to antisense targeting and reverse transcriptase is particularly sensitive to the blockage of the virus RNA template [68]. This has lead to oligonucleotide based antiviral strategies.

Prevalence of chronic viral infections such as Human immunodeficiency virus (HIV), Hepatitis B virus (HBV) and Hepatitis C virus (HCV) have increased and new viruses e.g. SARS coronavirus have emerged. Approximately 40 small molecular compounds are approved for treating viral infections; over half of which are for HIV infections [69]. Incidently, groups of inhibitors of DNA and RNA synthesis, namely nucleoside analogues represent the most prominent class of drugs used to inhibit viral propogation. However, these are not fully specific for viral polymerases and cause serious side effects and toxicity on long-term treatment meaning specific antiviral therapy is needed [70-72].

Antisense strategies employ oligonucleotides (ON) complementary to a given viral RNA and taking into account frequent viral mutations, offer the opportunity

for the development of an antiviral compound as soon as the sequence of a virus is known [46]. Such strategies have been applied to inhibit pathological viruses.

Of the approximately 20 AS-ONs which have reached clinical trials, a high proportion is for the potential treatment of viral infections. Companies responsible for their development include: Isis (CMV), Coley (HBV, HCV), Novopharm (HIV-1) and Hybridon (HIV-1 and HPV).

As an example, infection with hepatitis C virus (HCV) is a major health problem worldwide with unsatisfactory current treatment [73]. Chronic infection causes liver cirrhosis, liver failure, hepatocellular carcinoma, often leading to needing a liver transplant. In this therapeutic area AS-ONs have been applied to inhibit HCV replication, mostly targeting one of the most highly conserved regions of the genome: the 5′ untranslated region (UTR) [46, 73].

Vitravene® (Fomivirsen) is an example of a licensed and commercially marketed drug. It is a phosphorothioate oligonucleotide that inhibits human cytomegalovirus (CMV) replication through an antisense mechanism. CMV is a virus which belongs to the herpes group. HIV patients, especially those failing highly active anti-retroviral therapy (HAART), may suffer with CMV retinitis (the most common viral opportunistic infection), which can lead to significant loss of vision and blindness. Fomivirsen is an effective treatment for CMV retinitis in patients with AIDS that has a different mechanism of action to the other antivirals used such as ganciclovir, foscarnet, and cidofovir. The nucleotide sequence of Fomivirsen is complementary to a sequence in the mRNA transcripts of the major immediate early region 2 (IE2) of HCMV. This region of mRNA encodes several proteins responsible for regulation of viral gene expression that are essential for production of infectious CMV. Binding of fomivirsen to the target mRNA, results in inhibition of IE2 protein synthesis, subsequently inhibiting virus replication [74-76].

HIV is one of the most severe causes of infectious disease and has over 40 million infected individuals worldwide. Current drugs are too expensive for patients in poorer countries. They also exert severe side-effects on long term treatment and eventually become ineffective from the emergence of resistant mutants. Numerous efforts to prevent HIV with ON have been reviewed by Jing and Xu [77].

Many AS-ONs have been designed to bind at various sites along the genome of HIV. Anti-HIV ONs are not necessarily required to induce virus RNA degradation by RNase H as they can be used to inhibit essential proceses of viral lifecycle by steric blocking. For example, Arzumanov *et al* developed AS-ONs against the HIV-1 *trans*-activating response region (TAR), a 59- residue stem-loop that interacts with the *trans*-activator protein Tat. Steric blockade with a chimeric 2'-O-methyl RNA/Locked Nucleic Acid (LNA) ON prevented full-length HIV transcription [78-80]. In another study, the HIV-1 dimerisation initiation site was chosen as an AS-ON target [81]. An LNA/DNA mix-mer directed against this region prevented dimerisation of the genome and inhibited replication of a clinical HIV-1 isolate in a human T cell line.

A large number of the clinical trials involving AS-ONs are for viral diseases including trials for hepatitis C virus (HCV), hepatitis B virus (HBV), human immunodeficiency virus (HIV-1) and human papilloma virus (HPV).

1.4.3. Antisense oligonucleotides for anti-cancer chemotherapy

Cancer is a major target of ongoing clinical trials with antisense therapies, followed by HIV and other immune related diseases. Conventional cancer therapies involving surgical resection, ionising radiation and chemotherapy designed to perturb DNA synthesis or the mitotic event are either invasive or highly toxic. The antisense approach has been used to silence the crucial proteins over-expressed at the gene expression level, and has seen over 10 AS-ON in human phase II clinical trials. This antisense approach is expected to cause fewer and less severe side effects due to its specificity to genes aberrantly expressed in diseased cells. Also, the antisense oligonucleotide approach is especially attractive when targeting products not amenable to small molecule or monoclonal antibodies. Antisense cancer targets include genes involved in cell growth, apoptosis, angiogenesis and metastasis [52]. Several of these genes implicated in cancer have been studied as potential targets for antisense therapy. Such targeted genes and their proteins such as BCL-2 and BCL-xL, Protein Kinase C, RAF-1, clusterin, HSP27, STAT3, Insulin Growth Factor Binding Proteins, H-RAS, Ribonucleotide Reductase, Survivin, XIAP, cMYB, etc, have been reviewed by Gleave [38], Dean [82], Orr [83, 84] and Hadaschik [85, 86]. A few examples of these genes are given below.

1.4.3.1. The BCL-2 family

The BCL-2 gene belongs to a class of oncogenes which inhibit apoptosis to enhance cell survival and therefore is a key regulator of programmed cell death. Hence, overexpression of this antiapoptotic protein can contribute to cancer progression and chemoresistance. G3139, also referred to as oblimersen sodium or Genasense®, is a first generation 18-mer phosphorothioate AS-ON that is complementary to the first six codons of the initiating sequence of the human *BCL-2* mRNA. G3139 has moved into a clinical trial level, both as a single agent and in combnation therapy studies, based on promising activity in preclinical models of many cancers [38, 87]. Many of the studies have shown Genasense to have a good safety profile and it continues to be involved in many ongoing cancer clinical trials.

1.4.3.2. Protein kinase C-α (PKC-α)

Protein kinase C belongs to a class of serine/threonine kinases and has been implicated in tumour progression and oncogenesis. ISIS 3521, also refered to as LY900003 or Affinitak® or Aprinocarsen) is a phosphorothiate AS-ON directed against the mRNA of Protein kinase C-α. However, results of its efficacy in non-small cell lung cancer (NSCLC) trials have been disappointing and may be attributable to the need for longer-lived antisense oligonucleotides (e.g. second generation ON) or higher doses for treatment [88].

1.4.3.3. Heat Shock Protein 27 (HSP27)

Heat shock proteins are ubiquitous proteins classed as cytoprotective molecular chaperones. High levels of HSP27 are commonly detected in many cancers including prostate, breast, ovarian and gastric tumours. It is crucial in maintaining the balance between cell death and cell survival and is consequently an important therapeutic target. A second generation 2'– O- MOE gapmer (see Fig. 1.21) antisense drug OGX-427 significantly decreases the production of HSP27 in preclinical experiments, induces apoptosis in several human cancer cell lines, and has single agent anti-tumor activity. OGX-427 is currently being evaluated in a Phase 1 study in patients with breast, prostate, ovarian, non-small cell lung, or bladder cancer who have failed potentially curative treatments or for which a curative treatment does not exist [89].

1.4.3.4. Hypoxia-inducible factor-1 (HIF-1)

Hypoxia-inducible factor-1 (HIF-1) is an important gene which can contribute in promoting angiogenesis (blood vessel formation) under hypoxic stress (low oxygenation level) in the case of ischaemia in cardiovascular disease and tumours. Manipulating the activity of this gene therefore has therapeutic anti-cancer potential since it could prevent spread of cancerous cells by inhibiting the supply of blood to tumours. HIF-1 inhibition has been shown in various cell types and animal studies but has yet to be replicated in humans. However, there is some early stage promise as plasmid delivery of antisense HIF-1α has lead to diminished microvessel density in lymphoma T-cell line (EL-4) tumours in mice [39]. Further, Chang *et al* [90] have demonstrated decreased progression and metastasis of pancreatic cancer when antisense HIF-1α was transfected into pancreatic carcinoma (BxPc-3) cells [91]. The successful application of antisense oligonucleotide analogues to the mRNA sequences encoding *HIF-1α* protein have been also demonstrated by Sun *et al* and Greenberger *et al* [39, 92].

Many phase I clinical trials have shown that systemic treatment with AS-ONs can be safely performed in cancer patients. However, while examples of AS-ONs such as Genesense® and Affinitak® have reached phase III clinical trials, the oncology area of medicine has still not received clear proof of AS-ON efficacy, but looks to medicinal chemistry improvements with new antisense modifications to resolve a number of crucial issues including low *in vivo* stability, numerous side effects and high cytotoxicity, high commercial cost and delivery issues [45].

1.4.4. Antisense oligonucleotides for other conditions

An ISIS investigative drug called ISIS301012 is a second generation antisense agent with 2'-O-methoxyethyl modified riboses (see Fig. 1.21) which suppresses expression of apolipoprotein B (ApoB); a carrier of plaque thickening low density lipoprotein (LDL) into arteries. It is being clinically trialled in phase II studies for reducing high cholesterol and has been reported to lower cholesterol by 62%. This result is promising and better than Atorvastatin and Simvastatin (the market leaders in cholesterol-lowering HMG-CoA reductase inhibitors) at treating familial hypercholesterolaemia for which it has subsequently been granted orphan drug status by the FDA in June 2006 [93].

1.5. Artificial ribonucleases: general concept

Artificial ribonucleases (AR), also known as chemical nucleases, are functional mimics of the active centre of natural ribonucleases (RNA depolymerase) [94]. Their creation is one of the most challenging approaches to RNA targeting. Natural RNases play an important role in the regulation of RNA molecules and being able to imitate their ability to cleave RNA efficiently offers a highly desirable route to targeting RNA.

A successful artificially engineered 'ribonuclease' would, similarly to natural RNases, be able to (i) recognise RNA molecules, (ii) cleave RNA with high efficacy and (iii) in a catalytic manner (iV) preferably under physiological conditions [94]. These four features are desirable for their potential use in research and therapy.

Although a molecule with the essential cleaving groups to mimic the RNase active centre could be defined as an artificial ribonuclease, these compounds are generally more complex. Hence, ARs range from small molecules to much larger molecules incorporating antisense oligonucleotide as a recognition element [95].

The simplest AR may consist of only a simple cleaving domain and a binding site, but in reality their complexity requires them to be classified to differentiate the different types that exist. They can be categorized in terms of either their cleaving sites (*e.g.* organic, inorganic or mixed organic and inorganic catalytic centre) or binding site (*e.g.* non-specific binding groups of small molecule constructs or sequence-specific binding domains of oligonucleotide-based ARs).

ARs typically comprise three functional domains. These three domains include a cleaving moiety (cleaver), a binding domain (binder) and a linker. The cleaving domain should cleave RNA effectively and irreversibly. The binding domain allows accurate delivery of the cleaver to the correct target sequence of RNA. Finally, the linker acts to join and optimise the spatial arrangement of the cleaving and binding sites.

Restriction enzymes, although recognising specific 4-6 base pair DNA sequences, result in multiple cleaving sites. Similarly, none of the naturally occurring ribonucleases, although nucleobase-specific, show high sequence-selectivity; hence they would not be able to distinguish between a desired, specific, single therapeutic target and their natural target.

In contrast to this, oligonucleotide-based ARs (typically between 17 and 23-mer in length) have the potential to be directed to any desired specific site (single site, if required) in a transcriptosome/genome by varying the length and content of the nucleic acid sequence. For example, statistically, a 17-mer genetic sequence only occurs once in the human genome. The targeted RNA can therefore be perceived as a highly specific receptor [46].

A potential goal for artificially engineered 'ribonucleases' is the effective and specific cleavage of specific mRNA or viral genomic RNA. It is hoped this may lead to the development of new therapeutics in the form of potential antivirals, antibiotics or anti-cancer drugs. ARs may also be used as biological tools such as probes to investigate nucleic acid structure.

1.6. Antisense oligonucleotide based artificial ribonucleases

One promising approach in searching for a new pharmacological chemotherapeutic is in the design and development of molecules which bind and irreversibly cleave selected RNA sequences, i.e. oligonucleotide based artificial ribonucleases (ON-AR). This approach would lead to translation arrest of a vital or important target protein, hence desirably interfering with an important function of the organism or cell.

The approach presented in this study is based on an antisense oligonucleotide-based artificial ribonuclease (ON-AR). The major structural elements of an oligonucleotide-based AR include an oligonucleotide moiety as the binding site and a cleaving site. Antisense oligonucleotides complementary to target regions in the RNA can deliver the cleaving domain to the desired RNA site *via* formation of specific Watson-Crick hydrogen-bonding. A linker is usually used to assist in the desired spatial arrangement of both sites [96]. This technology can be considered to be a particular type of antisense oligonucleotide approach which combines irreversible RNA phosphodiester bond cleavage with sequence-selective antisense Watson-Crick binding to target RNA. Many of the advances in antisense technology can be applied to the oligonucleotide component of ON-AR, whereas the advances in RNA cleavage strategies can be refered to the catalytic components of ON-AR.

Although in this approach the antisense component is used for sequence-specific recognition of RNA sequences, additional binding elements (e.g. anchor group), which could potentially enhance affinity to the RNA target sites, may prove to be a double-edged sword to enhance overall translational arrest. A further benefit of this approach is incorporating of an artificially engineered cleaver in ON-AR to provide potential independence from the RNase mechanism (*e.g.* RNase H) for the full antisense effect. Since RNase-H is a natural endogenous ribonuclease which is often necessary for a successful antisense effect, this dependence on RNase H mechanism theoretically supports the incorporation of a cleaving moiety in ARs to also mimic RNase H's important involvement.

1.7. Current and potential pharmaceutical applications of *engineered* and natural ribonucleases

Natural and artificially engineered 'ribonucleases' could be useful as molecular biology tools, namely as RNA-cleaving compounds for investigating RNA structure and RNA-protein interactions [97, 98].

Also, ribonucleases (both natural and engineered) have been seen as an attractive alternative approach to conventional small-molecule drugs. The *unspecific* immunotoxin ribonuclease of diphtheria or AB5 toxins has been selectively delivered to tumour cells using antibody or tumour-ligand targeting approaches [99, 100]. Although this approach was very encouraging, the cytotoxic specificity of the above ribonucleases relies wholly on the targeting ligand to prevent wide-scale systemic toxicity. Further, the toxin ribonucleases damage RNA uncontrollably and their high imunogenicity leads to a rapid clearance from the bloodstream.

Another example is Onconase®, a homologue of RNase A, which has shown anti-cancer and antiviral activity [101]. Onconase® has shown antiviral activity by inhibiting HIV-1 replication in human cells by degrading viral RNA [100, 101].

Onconase® (or Ranpirnase or P-30 protein), a RNase enzyme, derived from the eggs and early embryos of the leopard frog *Rana pipens* has been shown to be toxic to tumours both *in vitro* (showing activity against a wide range of human tumour cell lines) and also *in vivo.* It represents a 'first in class' in a potential therapeutic class for the ribonuclease family and is currently in phase III human

clinical trials in combination with doxorubicin as a cancer chemotherapeutic for patients with unresectable malignant mesothelioma (UMM) [102]. Cytotoxic ribonuclease Onconase® catalyses *unspecific* cleavage of cellular RNA, leading to cell death. Its cytotoxicity is due to its ribonucleolytic activity and is more toxic to cancer cells than non-cancer cells in cell culture systems, animal models and human clinical trials [101]. The observed higher cytotoxicity towards tumours as compared to normal cells could be attributed predominantly on the rapid proliferation of cancer cells making them more reliant on the integrity of their RNA. Within certain tumour cells, it has been found to break down tRNA, preventing protein synthesis and leading to apoptosis [3, 103]. The structure of Onconase® interacting with tRNA [3, 104] is shown in Figure 1.4 below.

Onconase® is a homolog of RNase A [103], however, in contrast to RNase A, it has been shown to preferentially cleave at the phosphodiester bond on the 5' side of guanine [103]. When its mechanism of action was studied closely it was found to be cytotoxic due to its catalytic activity rather than as a result of its conformational stability [105].

Results from phase III clinical trials have shown some survival benefits in patients with malignant mesothelioma (MM), non-small cell lung cancer (NSCLC), advanced breast cancer and renal cell carcinoma, although further investigations are ongoing into its full therapeutic effect [106].

Figure 1.4. A 3D ribbon image of the Onconase®-nucleic acid complex with the 3′ and the 5′ termini of the nucleic acid and the N and C termini of the protein highlighted [3].

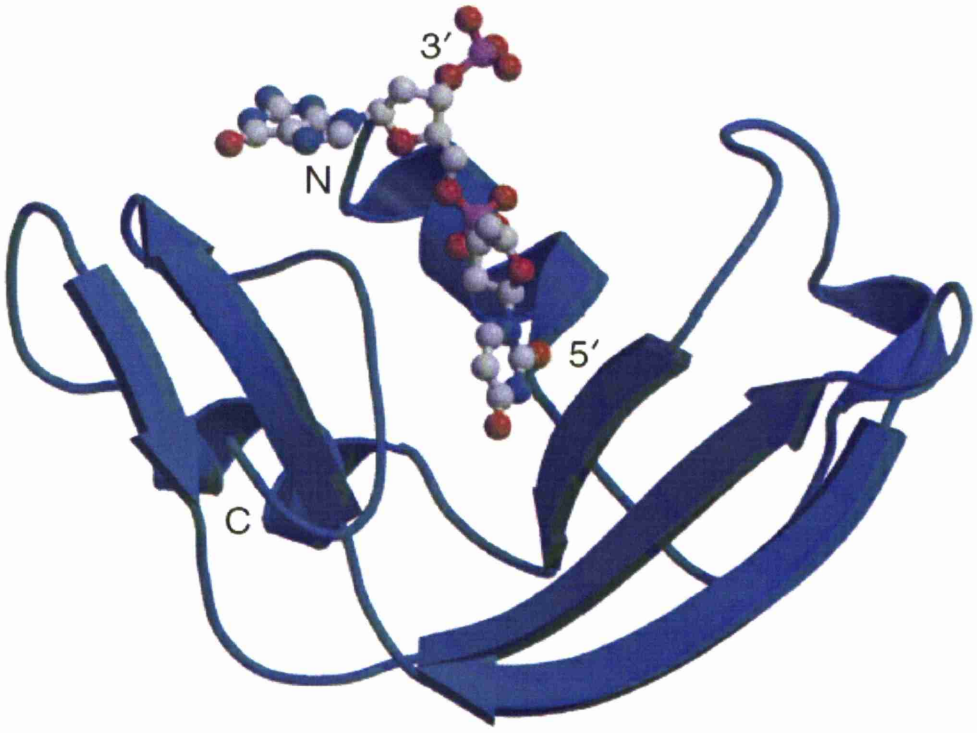

Results of the drug's phase IIIb human clinical trial in UMM showed 'significant improvement' for patients treated with Onconase® alone and based on these encouraging results, a randomized phase III multicenter trial of Onconase® versus doxorubicin was conducted in patients with unresectable MM.

Investigators concluded that Onconase® is at least as active as doxorubicin for the treatment of UMM and may be more active in certain patient subsets [102]. Unfortunately, the results did not meet statistical significance for the primary endpoint of survival in UMM. However, a statistically significant improvement in survival was seen in the treatment of UMM patients who failed one prior chemotherapy regimen, a pre-defined primary data set for this sub-group of patients in the trial, which represents a currently unmet medical need [107].

Several Onconase® clinical trials are still ongoing including a phase III study comparing doxorubicin alone versus the combination doxorubicin/Onconase® in patients with UMM [102] and a phase I/II trial in non-small cell lung cancer (NSCLC).

Overall, these clinical trial results have been encouraging, especially in demonstrating the principle of how RNase can be utilised as an anti-cancer agent.

1.8. Natural RNases as models to design AR

Existing artificial ribonucleases can be classified into two general groups using their type of cleaving domain for differentiation as either organic or inorganic complexes.

Organic constructs are designed to mimic the structural properties of the active centre of natural ribonucleases (RNase A and/ or RNase T1 [108]), incorporating the essential hydrolytically active organic groups (e.g. imidazoles, aliphatic amino groups, carboxy-groups, *etc.*) which constitute their catalytic centre. Three dimentional structures of many natural ribonucleases are available from X-ray analysis and/or NMR structural investigations [73-74].

Figure 1.5. Schematic diagram of the RNase A sites/subsites involved in RNA binding and cleavage (extracted from [4]).

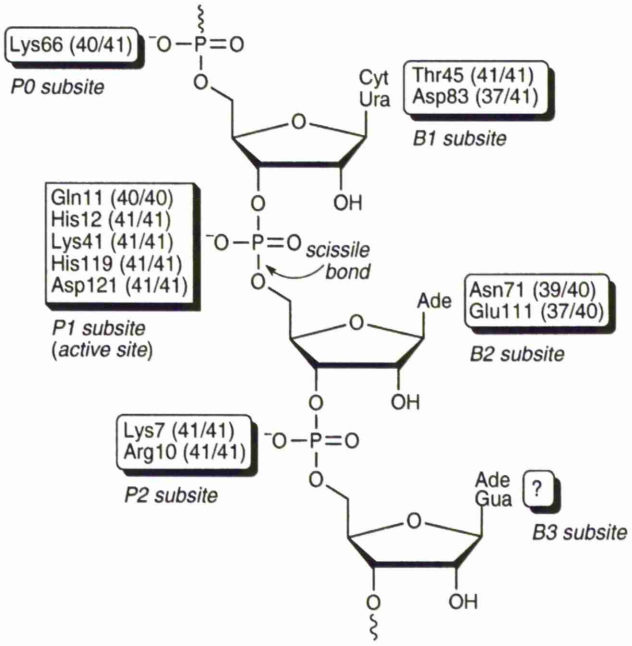

Figure 1.5 shows a schematic representation of all RNase A sites/subsites involved in binding and cleavage of single-stranded RNA substrate [4]. His 12, His 119 and Lys 41 are the most important amino acids in the active site (P1). Non-catalytic subsites are involved either in interactions with the nucleotide bases (B1, B2, B3) or with the other phosphodiester groups of the bound substrate (P0, P2) [109].

Figure 1.6. Crystal structure of ribonuclease A in complex with thymidylic acid tetramer ($d(pT)_4$) [5]. Important residues for RNA binding (Lys 66, Asn 91, Thr 45) and cleavage (His 12, His 119, Lys 41) are shown.

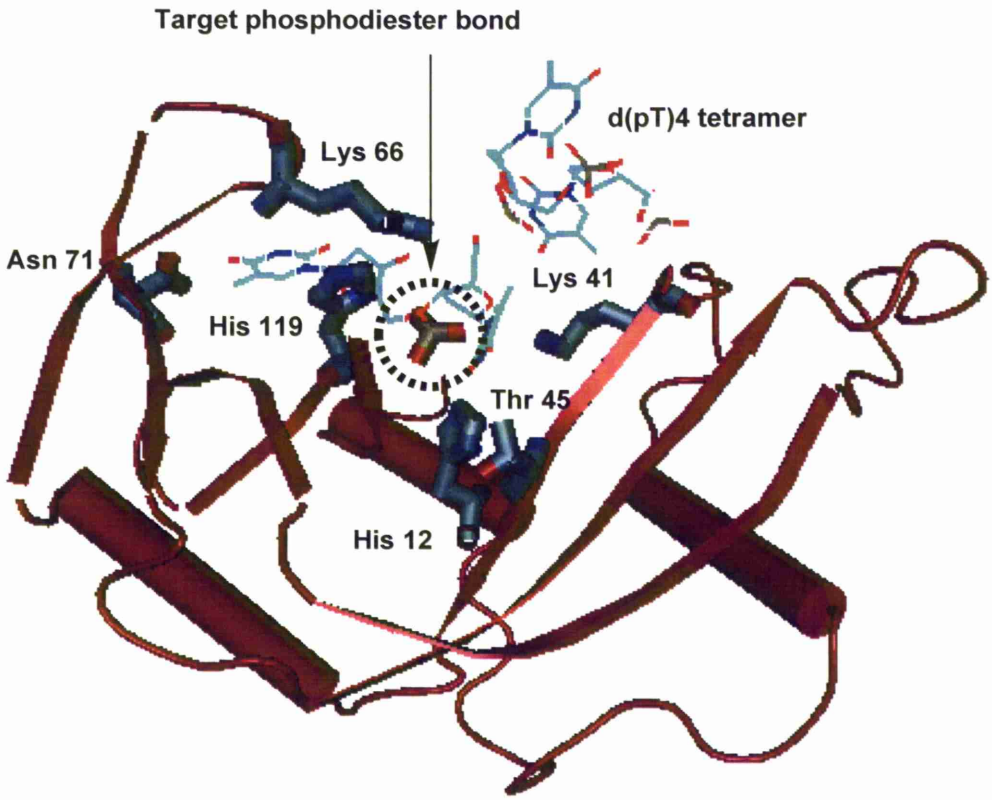

The detailed structural information of natural RNases now available from X-ray and NMR analysis provides a platform for further improvement in the structure-based design of artificial ribonucleases (see for example Figure 1.6 for crystal structure of ribonuclease A).

Several enzymes (RNase H, RNase V, *etc.*) require metal cofactors in their active sites for efficient RNA hydrolysis. This has prompted development in the second

large group of artificial ribonucleases: inorganic ribonucleases, which subsequently incorporate inorganic metal ion complexes for RNA hydrolysis.

1.8.1. Mechanism of phosphodiester cleavage

Synthetic molecules which cleave RNA sequence specifically by biomimetic catalytic reactions are thought to do so by transesterification of the 2′-OH as a nucleophile and subsequent cleavage (or hydrolysis) of the 3′,5′-phosphodiester linkage with departure of the 5′ group [64, 110]. The kinetics and mechanisms of RNA cleavage have been reviewed by Oivanen, M [111].

RNase A contains two histidine residues (His 12 and His 119) and lysine 41 in its catalytical centre [4], which provide the acid/base catalytic residues for phosphodiester bond cleavage. The phosphodiester bond cleavage mechanism involves two steps and is summarised below (Figures 1.7, 1.8). The first step is a phosphate ester translocation, where the basic N1 of His 12 abstracts a proton from the 2′ OH group to form an anionic 2′ oxygen species, which attacks the phosphate bond. His 119 donates a proton to the departing 5′-oxygen atom to leave a 2′, 3′-cyclic phosphate. Lys 41 has the role of charge stabilization of the non-bridging phosphoryl oxygens in the transition state. In the second step this 2′, 3′-cyclic phosphate is hydrolysed, leaving a 3′ phosphate monoester and a 2′-hydroxyl group [4].

Anslyn *et al* [7, 112-115] have proposed an alternative mechanism (see Fig 1.9) which proceeds via a phosphorane intermediate [112, 116]. The phosphate ester is protonated and consequently activated by the imidazolium cation of His 119, followed by cyclization of the phospodiester via 2′-hydroxyl proton abstraction by the His 12 unprotonated imidazole [110]. Then, the unprotonated nitrogen of the imidazole (base form, His 119) catalyzes the rupture of that intermediate by proton abstraction and possibly by delivering the proton to the leaving 5′-oxygen atom. In the last step the 2′, 3′-cyclic phosphate is hydrolyzed in the standard way to produce the 2′-mono ester (not shown).

Figure 1.7. Putative mechanism for the cleavage of poly(A) by RNase A [4].

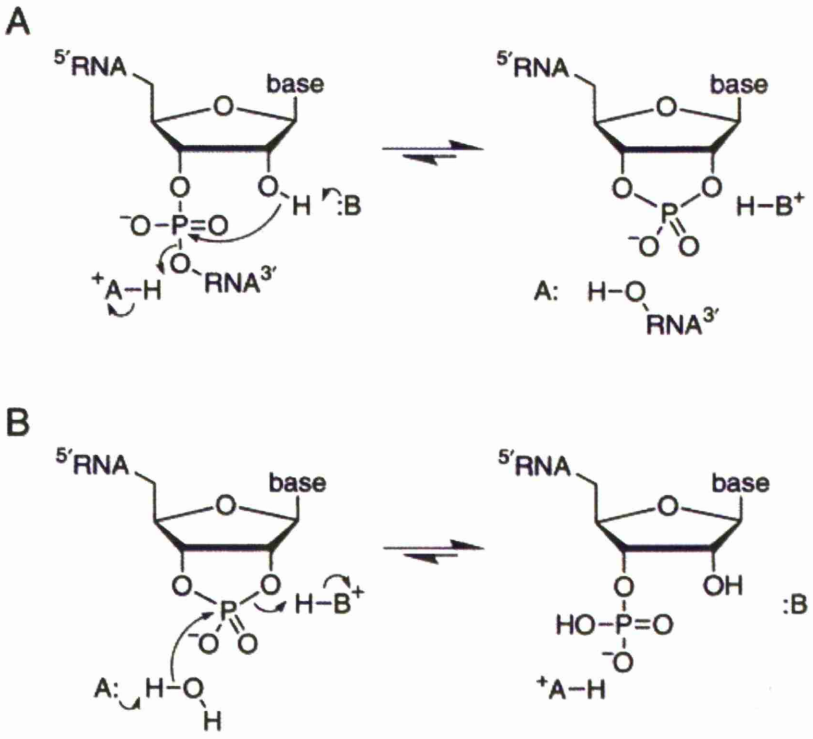

The residues found to be most important for the phosphodiester bond cleavage are His 12, Lys 41 and His 119 [4]. Figure 1.7 shows the classic mechanism of catalysis by RNase A that is consistent with all data available for this enzyme [4, 117, 118].

Figure 1.8. Schematic representation of the classic mechanism of action of ribonuclease A (adapted from [4], taken from [6]).

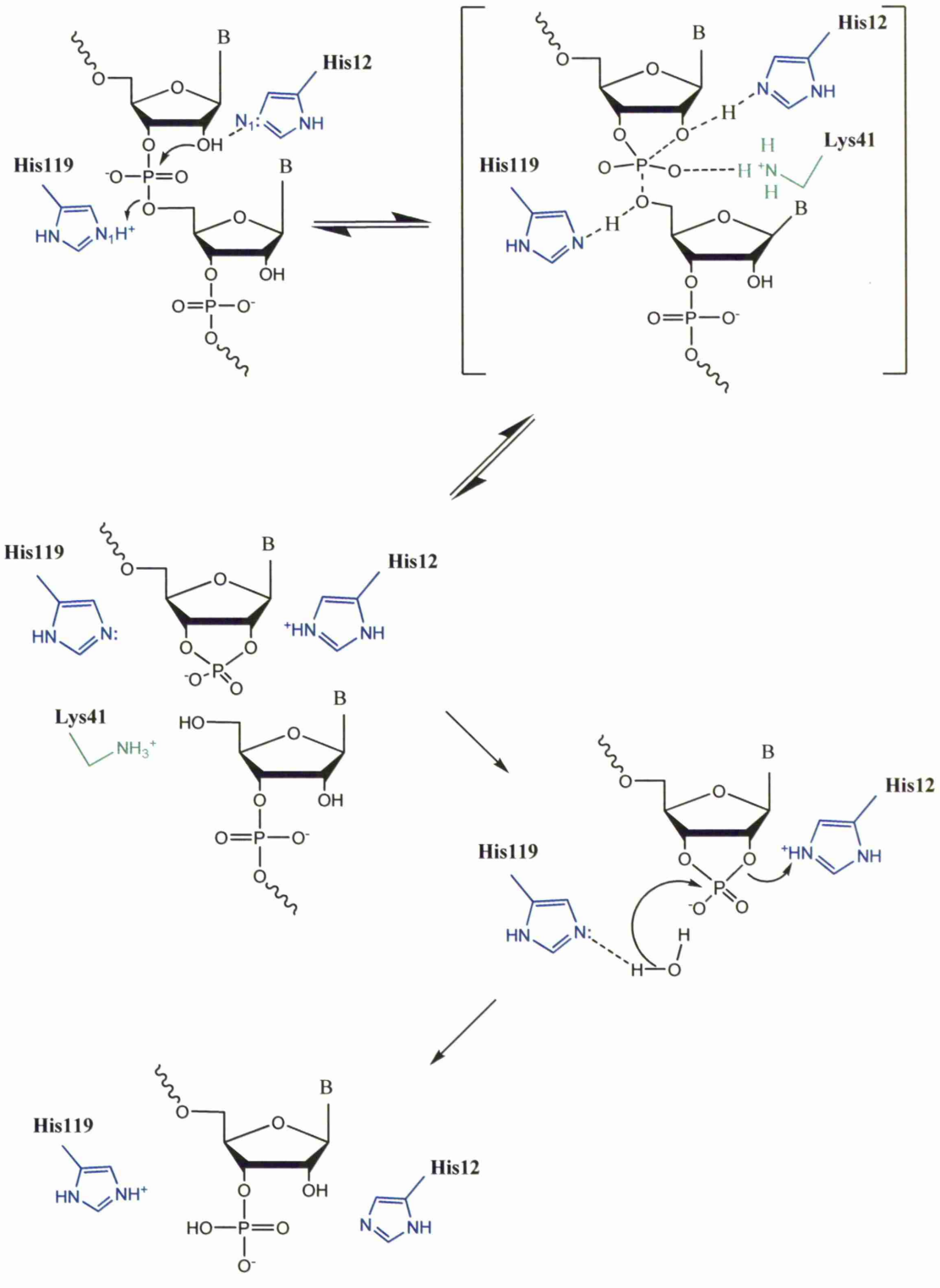

Figure 1.9. Schematic representation of an alternative mechanism for RNA cleavage by RNase A. The mechanism goes through a phosphorane intermediate and is based on the initial protonation of a non-bridging oxygen by His 119 (adapted from [7]).

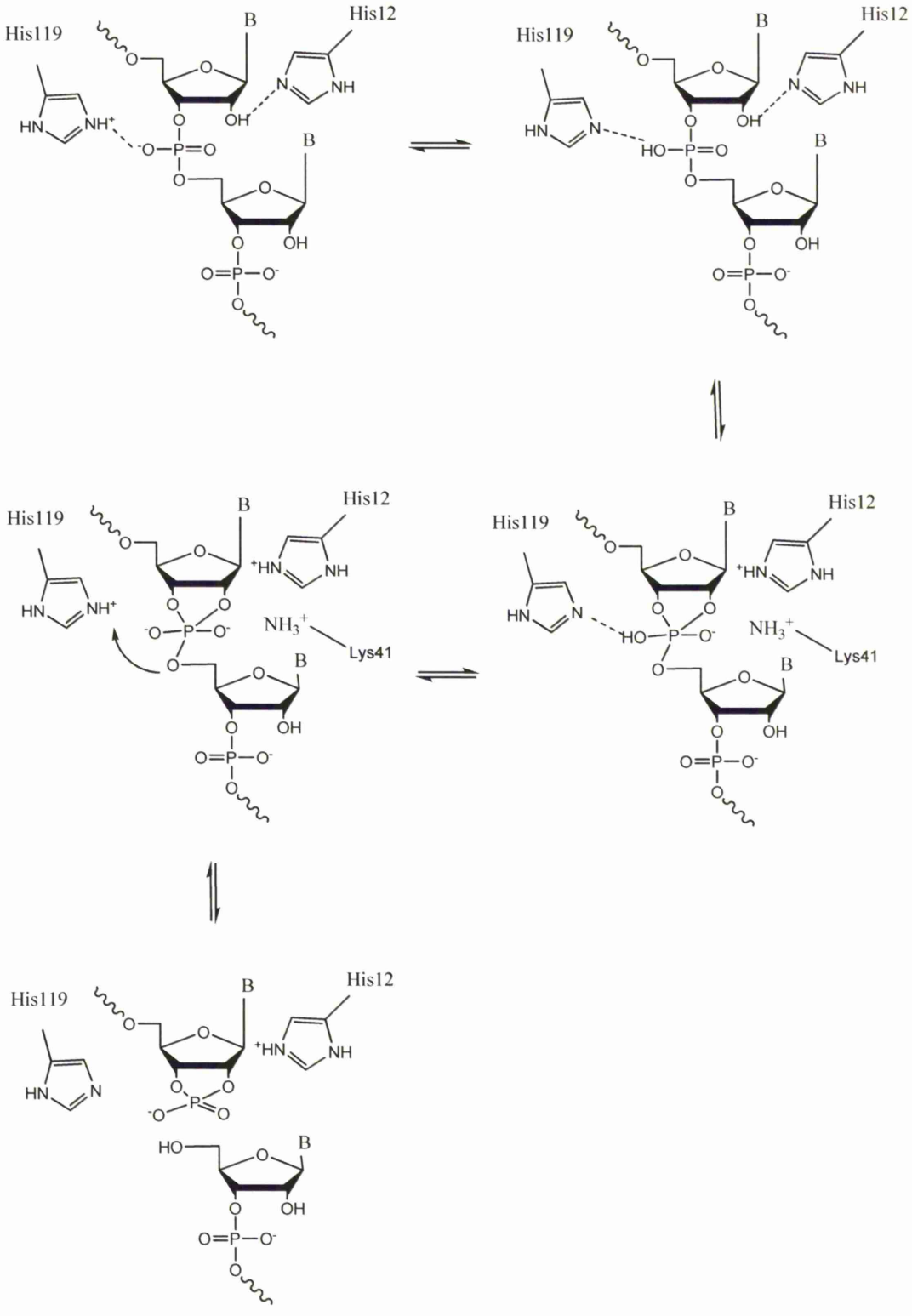

1.8.2. Organic ribonuclease mimics

The most popular approach to AR design has been to mimic the active centre of RNases, particularly RNase A [119, 120]. RNase A has been a popular model for AR design, originally chosen for its well studied structure resulting from its accessible source (bovine pancreas), ease of purification and small size [4, 101]. More importantly, for structure-based design, it has a very high catalytical, RNA phosphodiester bond cleaving activity as well as a well characterised three-dimensional structure; including the amino acid residue orientation of its active site (see Figures 1.5, 1.6) [121, 122]

RNase A contains two histidine residues (His 12 and His 119) and lysine 41 in its catalytic centre[4]. Therefore, the most common types of AR have RNA-binding domains and low molecular weight cleaving moieties consisting of functional groups found in the active centre of RNases [123].

The presence of two histidine residues has led to the popular use of imidazole groups or imidazole-based compounds [21] in the design of ARs. Other reactive groups that are common constituents of the active centres of nucleases include guanidinium (from arginine), carboxyl, and amino groups mimicked in the form of peptides and oligoamines. This has resulted in many teams synthesising imidazole or multi-imidazole groups, often combined with carboxylic acids and amine groups, short peptides and (poly)amine structures. Structures containing short peptides or peptide-like oligomers are especially attractive as they usually involve simple peptide chemistry.

Common organic RNase mimics include several types of organic cleaving domains including: single imidazole groups able to cleave RNA at reasonable levels [8, 21, 25, 124], as well as *bis*-imidazole constructs [9, 25, 26, 119, 125] including various combinations of imidazole(s) with carboxylic acids [25], amine groups [9, 10, 126, 127], various short peptides [128-131] and simple amine or polyamine moieties [9, 132-134]. The design based on RNase A has lead to many reports of di- and tripeptides or similar peptide-like molcules containing histidine (or its derivative histamine) and lysine which are capable of successfully cleaving RNA targets [95, 120].

Figure 1.10. Examples of organic RNase mimics. (A) *mono*-imidazole containing groups [8], (B) polyamine constructs [9], (C) *bis*-imidazole containing group and (D) combination of imidazole and amine groups [10]. Note: R represents RNA binding domains.

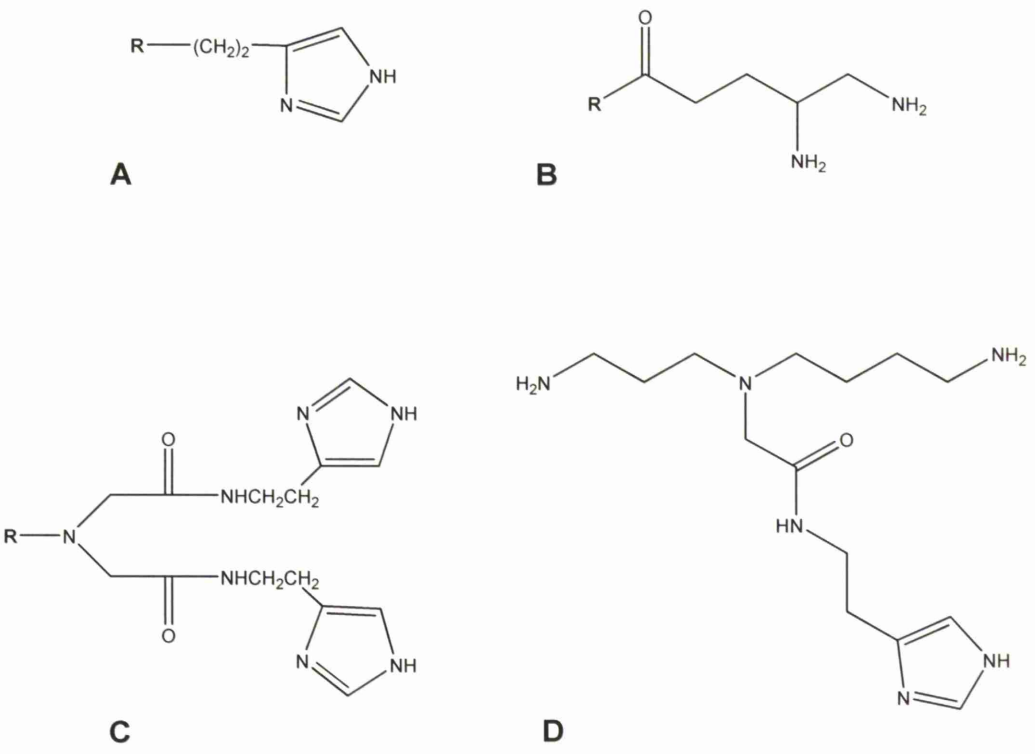

The staphylococcal nuclease (SNase) active centre has also been used as a structural model for AR design, albeit less commonly. The amino acids most important for RNA (and DNA) cleavage catalysis by SNase are Glu 43, Arg 35 and Arg 87 [135, 136]. The residues Arg 35 and Arg 87 of the SNase active site of have been mimicked using constructs of simple alkyl or acyl guanidinium groups. Such constructs have shown that the combination of guanidinium groups is sufficient to produce phosphodiester cleavage of model RNA-like substrates [11, 137]

Figure 1.11. A simple organic mimic of SNase active site. The guanidinium groups mimic amino acids Arg 35 and Arg 87 on the SNase active centre [11].

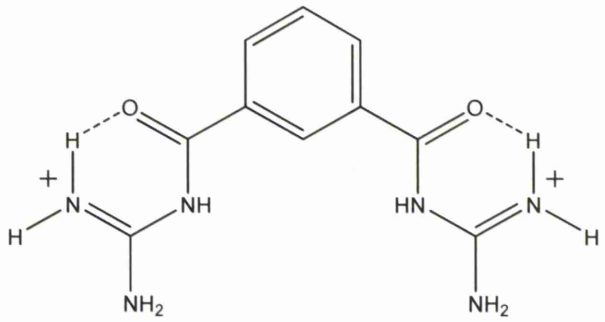

However, with the exception of few recent examples [25, 119], their hydrolytic activity tends to be less than that of their inorganic counterparts, so there is scope for improvement in the rational approach to their design.

1.8.3. Inorganic ribonuclease mimics

Metallocomplexes (*e.g.* complexes of metal ions such as lanthanides, copper, zinc ions [13, 15, 138]) have been designed as ARs based on the fact that many ribonucleases (e.g. RNase H, RNase V, Ribonuclease P, Staphylococcal nuclease, *etc*) possess metal ions as essential cofactors in their active sites [139, 140]. All the the following metal ions have been reported to be able to cleave RNA even in the absence of any other catalytic group: Zn^{2+}, $Ni^{2+,}$ Ca^{2+}, Co^{2+}, Cu^{2+}, Mg^{2+}, Mn^{2+}, Fe^{3+}, Pb^{2+}, Al^{3+} and Ln^{3+} [64, 123]. So far, among all the different metal ions, the design of inorganic ribonuclease mimics containing metallic complexes of lanthanides appears to be the most promising due to their high ribonuclease activity [12, 15, 140-145].

Similarly, Cu^{2+} and Zn^{2+} complexes of aromatic nitrogen bases have also been shown to produce acceptable levels of ribonuclease activity [138, 140, 146, 147]. The development of inorganic ribonuclease mimics had had some success with regards to high hydrolytic rates (although usually for simple RNA-like model targets e.g. HPNP). Meanwhile, many questions concerning cleavage reaction mechanisms and other aspects related to *in vivo* applications remain unresolved. As examples of their limitations, selective scission is obtained only in the case where free metal ions are absent from the reaction mixture, organic co-solvents may be required for dissolution problems and there may be uncontrollable

leakage of the ions from the complex leading to random cleavage [138, 140, 148].

Figure 1.12. Metal-dependent oligonucleotide-based artificial ribonuclease: macrocyclic lanthanide (Eu^{3+}) complex covalently attached to the 5'- phosphate of an antisense oligonucleotide [12].

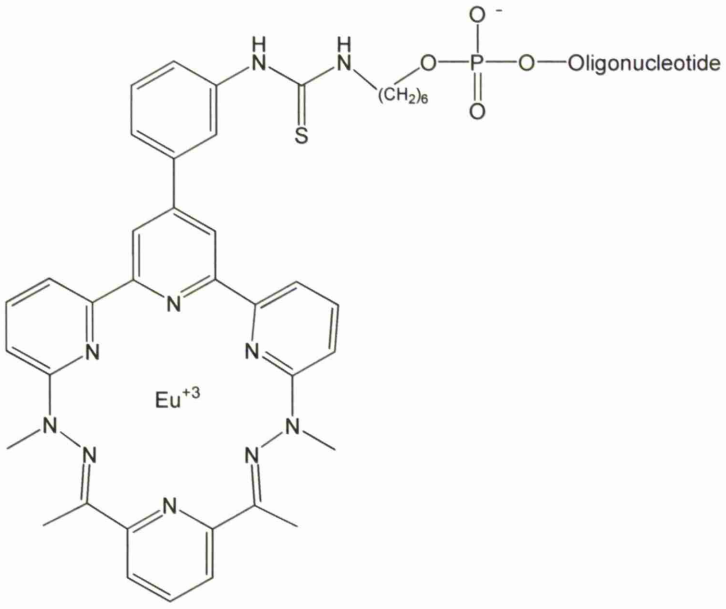

Figure. 1.13. A metal-dependent oligonucleotide-based artificial ribonuclease featuring a serinol-terpyridine(Cu^{2+})-containing artificial ribonuclease at the mid point of an antisense oligonucleotide [13, 14].

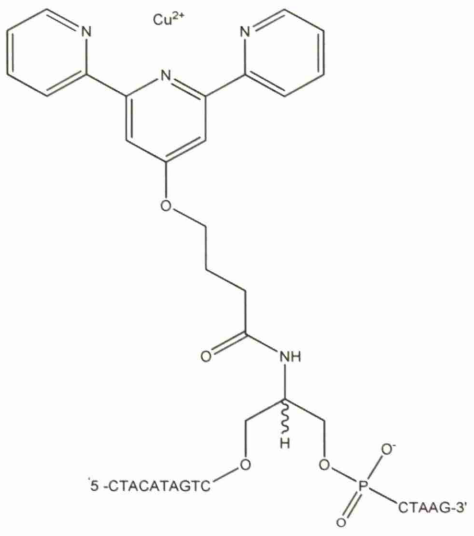

Overall, the reduced specificity of metal-dependent artificial ribonucleases, derived from difficulties in controlling the hydrolytic activity, appears to be the most significant drawback for using such complexes. These observations have made organic ribonuclease mimics appear the more attractive option, especially as they are easier to control and don't require additional external cofactors, simplifying their design and increasing their appeal.

1.8.4. Combined organic/inorganic ribonuclease mimics

Despite the fact that many natural ribonuclease active centres incorporate a combination of both metal ions and amino acids (e.g. staphylococcal nuclease and nuclease S1) [148], investigations concerning the development of AR with both organic and inorganic catalysts remains low [15, 149]. This area of development is still in its infancy where only very simple compounds have been studied and their activity has only been reported against very simple RNA-like molecules (e.g. 2-hydroxypropyl *p*-nitrophenyl phosphate, HPNP) [15].

Figure 1.14. Combined organic/inorganic-based ribonuclease mimic with a macrocyclic lanthanide ion and Gly-Gly cofactors conjugated as pendant arms [15]. Note: Ln = La (III), Ce (III), Pr (III), Nd (III), Eu (III), Lu (III).

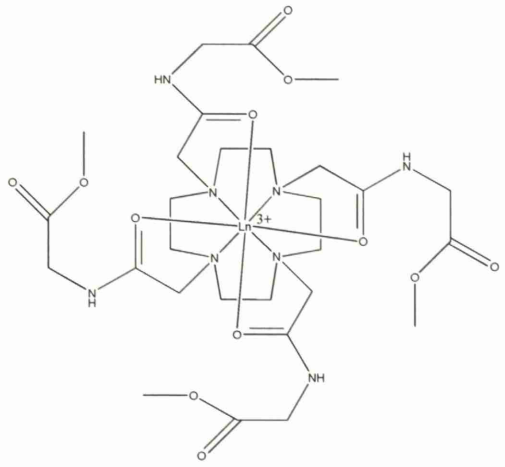

In a similar vein to inorganic AR complexes, for *in vivo* applications it would probably be requisite to use ARs which do not need additional cofactors such as oxygen, redox reagents or metal ions.

On balance of their advantages and disadvantages, organic-based ribonuclease mimics appear to be the most suitable candidates for development into potential drugs [9, 150].

1.8.5. Peptide based ARs as a particular class of AR

1.8.5.1. Natural representatives

Zinc finger proteins are members of a large super family of nucleic-acid-binding proteins in eukaryotes [151-154]. They are generally thought of as DNA-binding transcription factors. However, certain classes of zinc finger proteins, including the common C_2H_2 (Cys-Cys-His-His motif) zinc fingers, function as RNA-binding proteins. Each finger consists of a self-contained domain stabilized by a zinc ion ligated to a pair of cysteines and a pair of histidines, and by an inner structural hydrophobic core. These proteins are also being developed for their therapeutic potential as gene targeting agents [151, 155, 156].

1.8.5.2. Synthetic peptides

Some long synthetic polypeptides (*e.g.* poly(Leu-Lys), poly(Ala-Lys), poly(Arg-Leu), containing alternating hydrophobic (Ala, Leu) and basic (Lys, Arg) amino acids were shown to accelerate hydrolysis of the phosphodiester bonds in RNA, while short oligopeptides with similar alternating amino acid sequence displayed negligible RNase activity [157, 158]. These basic amino acids are not involved in phosphodiester cleavage but stabilise the pentacoordinated phosphorus state of the intermediates formed during cleavage, playing a similar role to Lys 41 residue in RNase A. Regular peptides containing lysine and (or) arginine can accelerate hydrolysis of phosphodiester bonds in ApAp and poly(A) [157]. Hydrophobic leucine is more active than the less hydrophobic alanine.

The efficacy of RNA cleavage with Arg- and His-containing tripeptides depends on their structure and correlates with the overall positive charge of these compounds. Of the tripeptides considered, compounds bearing the overall charge of +4 exhibited the highest ribonuclease activity [130].

1.8.5.3. Peptide-oligonucleotide conjugates

Conjugates of non-complementary (to target RNA) oligonucleotides and peptides represent a particular class of ARs: peptidyloligonucleotides (PCN). The presence of the oligonucleotide in PCNs is thought to 'activate' the peptide for cleavage [129, 159]. Only peptidyloligonucleotides (PCN) with short peptides with

alternating arginine and leucine amino acids have been found to hydrolyse RNA phosphodiester bonds [159].

Key aspects of peptide-oligonucleotide conjugates are that they:

1. Efficiently cleave single-stranded regions of target RNA.

2. Show either G-X>>Pyr-A or Pyr-A>>G-X cleavage specificity.

3. Show specificity that depends on the sequence and length of the oligonucleotide.

4. Have a catalytic turnover with up to 175 reactions for 24 hrs and maximum yield reaching 72% for 24 hrs (37° C, 10^{-5} M).

5. Do NOT have an oligonucleotide component which is complementary to the target RNA regions.

6. Achieve efficient cleavage with poorly or non-complementary oligonucleotides.

7. Have neither a free peptide nor unconjugated *peptide and oligonucleotide* mixture which possesses hydrolytic activity, suggesting the hybrid oligonucleotide-peptide promotes catalysis.

8. Show efficient cleavage of RNA, suggesting an important role of the oligonucleotide-moiety for catalysis.

9. Both the efficiency of cleavage and the RNA cleavage patterns depend on the sequences and secondary structure of the peptide and oligonucleotide units, providing artificial enzymes with aptamer-like properties [108]

Target RNA molecules used in this study [108, 160] included the synthetic linear oligonucleotide 5'-UUCAUGUAAA-3', *in vitro* transcripts of human tRNA3Lys and 96 nucleotide (nt) long fragment of HIV-1 RNA (123-218 nt) comprising the primer binding site (PBS) [129]. It was suggested from this study that the oligonucleotide component induces an `*active*` conformation of the peptide. This conformation is stabilised by intramolecular interactions (*e.g.* electrostatic or

hydrophobic interactions). The peptide component seems to be responsible for substrate affinity and catalytic activity.

1.9. Binding domains (binders) in artificial ribonucleases

The AR binding domain is designed to deliver the cleaving groups by binding exactly to the desired region of the target RNA. Binding domains can be classified based on their RNA target interacting specificity and can be as either non-specific or specific. For specific antisense binding see section 1.5.

1.9.1. Non-specific anchor groups used for nucleic acid binding

Types of non-specific, non-covalent (*i.e.* reversible) interactions, which potentially could be exploited in this approach, may include: electrostatic interactions, groove-binding and intercalation (Figures 1.15, A, B and C, respectively).

Figure 1.15. Illustration of the different types of non-covalent interactions with nucleic acids: (A) electrostatic (B) surface or groove binding and (C) intercalation (taken from [16])

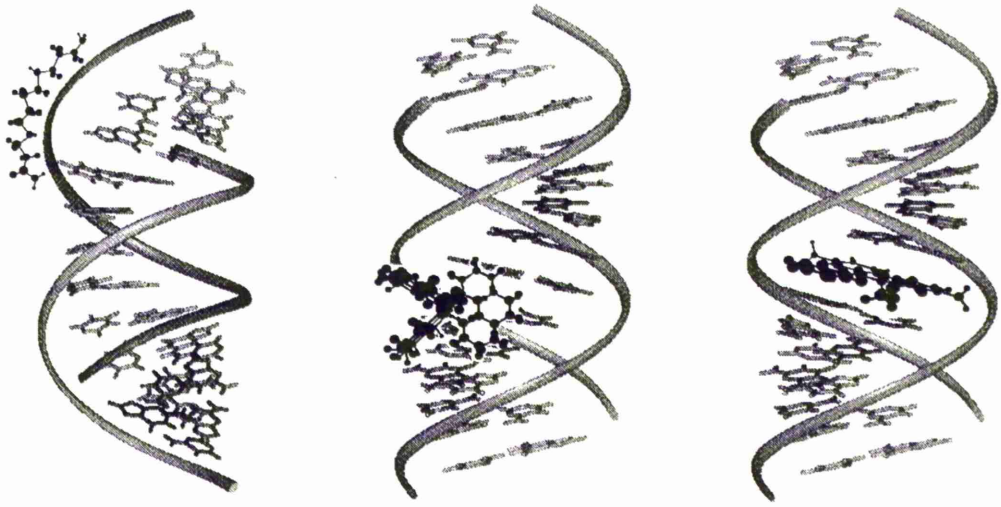

A. B. C.

The simplest representatives of known non-specific binding groups are positively charged (often polycationic) constructs and intercalating groups (and sometimes ligands with elements of both).

These non-specific binders (or ligands) do not interact with nucleic acids *via* Watson-Crick hydrogen-bonding (i.e. with complementary target oligonucleotide sequences) and therefore bind to these biomolecules in a non-sequence specific manner. Aside from their lack of sequence specificity, another potential disadvantage of using intercalating and polycationic anchor groups includes off-target binding to either charged or hydrophobic regions of other, possibly important macromolecules. This increases the likelihood of possible non-specific side-effects.

1.9.2. Polycationic groups and electrostatic interactions

Such binding domains include cationic structures (*e.g.* polycationic structures such as 1,4-diazobicyclo(2,2,2)octane, spermine, other polyamines and their derivatives) [161] which serve to increase binding affinity due to their interactions with the negatively charged phosphodieser backbone of the target RNA. They are used as a type of 'anchor group', forming reversible electrostatic interactions with the negatively charged phosphate backbone of the target RNA, thus increasing binding affinity due to their interactions.

In terms of RNA targeting, electrostatic interactions can be expected between the cationic functional groups of ligands and the anionic phosphodiester backbone of RNA. They can be both useful and important for enhancing binding, usually along the exterior of a nucleic acid helix or along the ssRNA phosphodiester backbone (see Fig 1.15, A).

Their electrostatic interactions advantageously enable them to associate with both double-stranded and single-stranded RNA regions (more vulnerable to cleavage). These non-specific, positively charged groups can be used as anchors in combination with antisense oligonucleotide recognition elements to enhance affinity of ON-ARs to the target RNA.

Figure 1.16. Spermine (A) and polycationic spermine (B) as binding domains used in imidazole-based artificial ribonuclease [17].

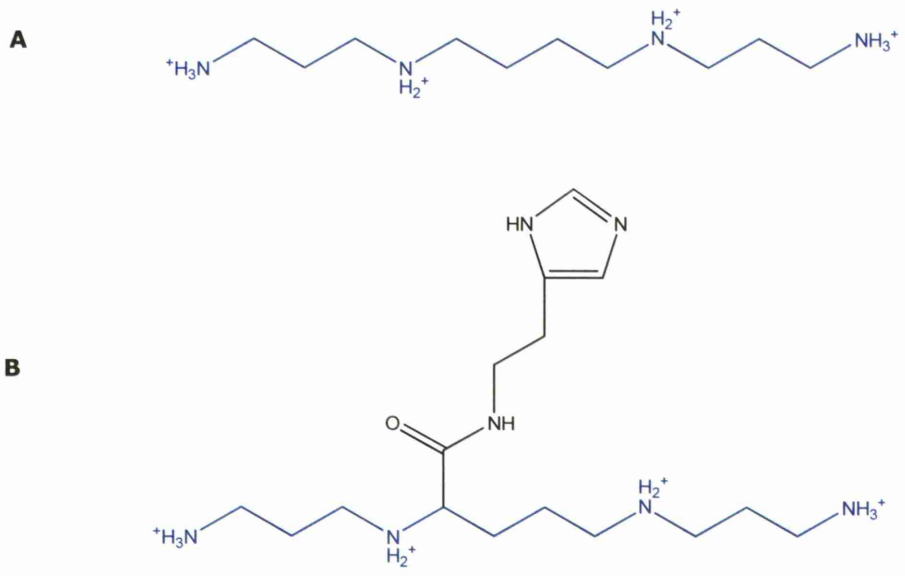

Figure 1.17. Imidazole and carboxylic acid-based AR with a cationic 1,4-diazabicyclo[2,2,2]octane binding domain [18].

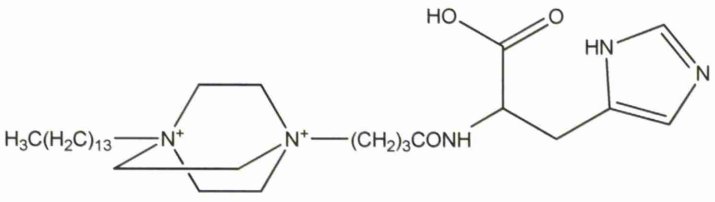

1.9.3. Groove-binding associations

This area of DNA targeting has been reviewed by Bailly *et al* [162] and more recently in terms of agents with potential antitumour and antimicrobial properties by Baraldi *et al* [163].

Groove binding involves either non-covalent hydrogen bonding or van der Waals interactions in the deep minor groove (e.g., distamycin A, Hoechst 33258, and pentamidine) or wide shallow minor groove of the DNA helix or DNA-binding compounds which cause cleavages in the DNA backbone (see Fig 1.15, B) [16, 164].

Minor groove binders are one of the most widely studied class of agents characterised by a high level of sequence specificity. They are still an interesting class of DNA binding ligands which possess several desirable biological properties including antiprotozoal, antiviral [165], and antibacterial [166].

Minor groove binding compounds which exhibit antitumour activity can be divided into two classes:

A) The first class comprises the compounds which are able to induce permanent DNA damage through a direct or indirect irreversible interaction with DNA nucleotides (e.g. mitomycin C, anthramycin, bleomycins).

B) The second class of compounds interacts only physically with DNA and causes only reversible inhibition of DNA-dependent functions. This group includes distamycin A (and analogues such as lexitropsins [166]), diarylamidines (e.g. DAPI, berenil, and pentamidine), and bis-benzimidazoles such as Hoechst 33258 [163, 167-169].

Figure 1.18. Examples of minor groove binders. (A) Pentamidine, a diarylamidine used second line in the treatment of *Pneumocystis jiroveci (P. carinii)* pneumonia [19]. (B) Dye Hoechst 33258, a bis-benzimidazole. (C) Mitomycin C, a potent DNA cross linker used in upper GI and breast cancers and by bladder irrigation for superficial bladder tumours [19].

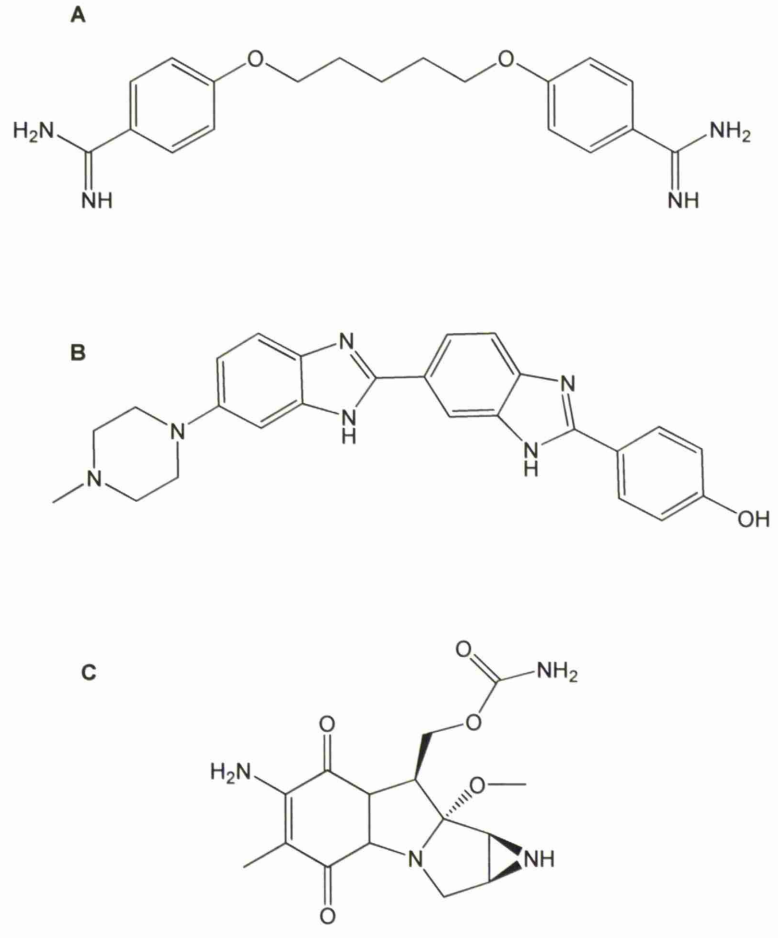

Important lessons may be learned from the base and sequence specificity which can be achieved for binding with specific nucleobases. This information may be exploited in RNA targeting where specific sequences of groups may be able to read specific nucleic acid bases [166].

1.9.4. Intercalating binding groups

Stacking interactions between hydrophobic RNA bases and hydrophobic aromatic ligands are important for intercalation. Another group of non-specific binding constructs, which can potentially be used as an anchor group for ON-ARs, consists of intercalators (for example phenazine, acridine [170], ethidium [171]) which bind to NA targets by the hydrophobic π- π stacking interactions with the nucleotide bases.

Intercalator ligands are usually planar, heteroaromatic moieties, which can slide between NA base pairs, binding perpendicular to the helix axis (see Fig 1.15, C).

Intercalating 'anchor groups' (consisting of polyaromatic planar groups such as acridine [20], phenazine, ethidium [21] *etc.* (see Figures 1.19, 1.20, 1.21)) have been used to increase the affinity of cleaving constructs with the target RNA molecule due to stacking (π- π) interactions with the nucleotide bases. When able to intercalate within double stranded RNA regions, the delivery of the AR cleaving domain to the RNA is greatly facilitated. Compared to unmodified oligonucleotides, those covalently linked to intercalating dyes have greater affinity for complementary targets [20, 21, 172].

Figure 1.19. (A) Acridine. (B) Acridine used as a binding domain in a mono-imidazole/amine artificial ribonuclease [20].

A

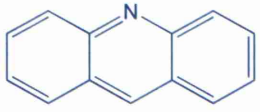

B

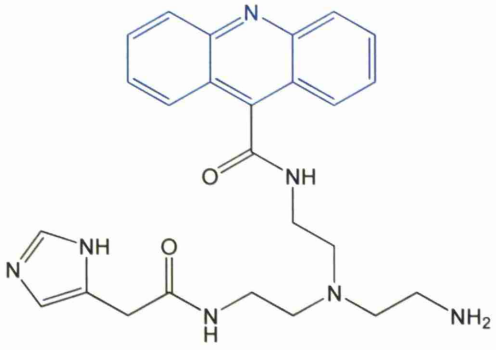

Figure 1.20. (A) *N*-methylphenazinium (B) *N*-methylphenazinium binding domain incorporated in a mono-imidazole artificial ribonuclease [21].

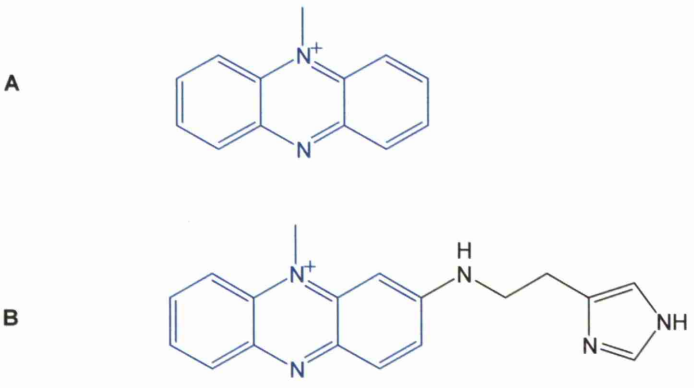

Figure 1.21. (A) Ethidium. (B) Ethidium binding domain conjugated to an oligopeptide containing glycine as the cleaving domain of the AR [22].

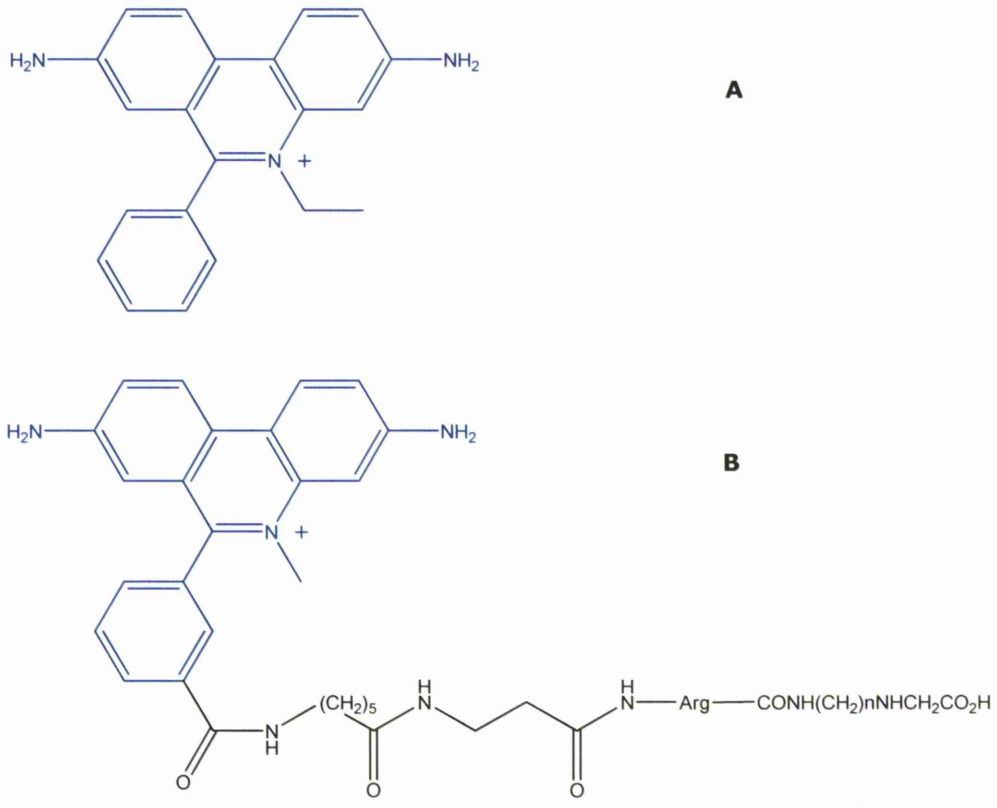

The availability of many experimental techniques suitable for the determination of NA-binding mode has advanced the understanding of NA–agent interactions and the nature of the chemical reactions effected on NA by such agents. For example, footprinting [173], affinity cleavage, coupled with high resolution definition of structural detail of binding by X-ray crystallography, detailed NMR studies [174, 175] and molecular modelling [176] with fluorescence and UV-visible spectroscopy and melting temperature determinations allow many perspectives for the analysis of such interactions.

1.10. Linker groups in artificial ribonucleases

In general, the function of the linker domain is to hold the cleaving and binding domains in the ideal spatial orientation, in relation to the target site to effect cleavage. Therefore structures and chemical compositions of linker groups may vary depending on their application within the structure of the other domains.

In nature, enzymes including ribonucleases have evolved over millions of years to achieve a very specific spatial and structural orientation of amino acids in their active site which explains their highly efficient catalytic properties [123]. To imitate nature's fine tuning, it would be expected that the linker size, composition and structure would need to be exact for the cleaver and binder to effect their roles efficiently.

However, literature data shows little emphasis on the design of linkers to date, suggesting a need and its importance as a possible variable in the approach to maximise the hydrolytic capabilities of the different RNase mimics. It has been shown that small changes in linker length and/or organisation in inorganic RNase mimics can greatly affect and play a crucial role in RNase activity [177].

1.11. Desired properties for artificial ribonucleases

In order to be effective as therapeutic agents they must fulfil the following requirements for ARs:

(i) be efficient in cleaving the target RNA
(ii) show high sequence-specificity in targeting particular RNA regions
(iii) exhibit a high level of catalytic turnover
(iv) be stable in biological fluids

(v) be deliverable through the cell membrane

1.11.1. Efficient cleavage

Firstly, efficient cleavage of the phosphodiester backbone is essential to overcome the short lifetimes of cellular mRNA targets [147]. Other important requirements include ease of preparation and chemical and physical stability.

1.11.2. High sequence-specificity in targeting particular RNA regions

ARs must specifically recognize and bind target RNA sequences to ensure selectivity and eliminate toxicity. For example, the AR must not affect other macromolecules, such as DNA, to prevent possible mutagenesis or carcinogenesis.

1.11.3. Catalytic turnover mechanism: binding affinity versus turnover

Catalytic turnover is an intrinsic property of a true enzyme. As in a natural enzyme, a catalytic method of binding and cleaving is much more attractive than a stoichiometric method. In practical terms, an AR with catalytic turnover means that more work is done with a lower quantity of the AR. In the area of molecular therapeutics this would mean a lower dose and fewer side effects.

An AR bound too strongly to the target RNA would not undergo catalytic turnover. Therefore a compromise in the binding strength is required if turnover is to be enabled. Therefore, the main challenge would be to combine sequence specificity with catalytic control. One approach to reduce binding strength and increase the capacity for turnover is to place the cleaving site in the middle of the binding site [178]. This method splits the length of the binding oligonucleotide, reducing the strength of binding of the shorter cleaved products.

1.11.4. Stability in biological fluids

Unmodified RNA and DNA oligonucleotides are unstable *in vivo* due to metabolism by nucleases (and other degradation pathways). In recent years, progress has been made through the development of novel chemical modifications to stabilise oligonucleotides against nucleolytic degradation and enhance their target affinity [23].

In general, three types of modifications of ribonucleotides can be distinguished: analogues with unnatural bases, modified sugars (especially at the 2' position of the ribose) or altered phosphate backbones [23].

Figure 1.22. Sites for chemical modifications of ribonucleotides taken from [23].

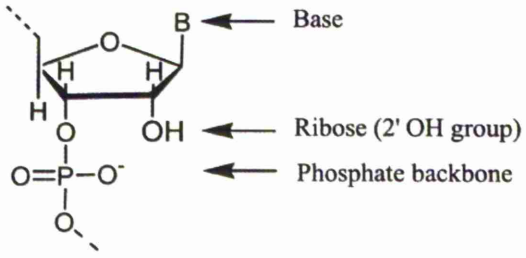

A review dealing with base-modified oligonucleotides was published previously by Herdewijn [24]. However, little is known about the potential of base-modified oligonucleotides as antisense molecules and their possible toxic side-effects.

Figure 1.23. Nucleic acid analogues adapted from [24].

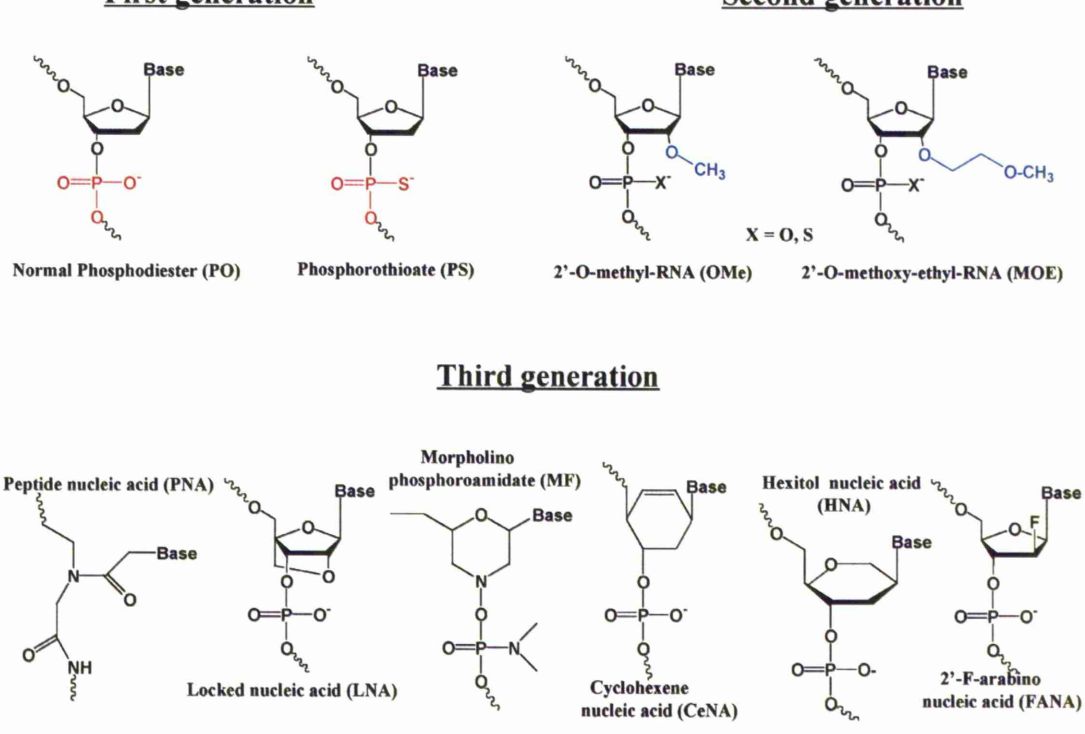

Considered as first-generation antisense oligonucleotides, phosphorothioate (PS) oligodeoxynucleotides have one of the nonbridging oxygen atoms in the phophodiester bond replaced by sulfur to give more nuclease-resistant analogues [179] (Fig 1.23). Phosphorothioate oligonucleotides are water soluble and elicit a RNase H response. Antisense PS oligonucleotides have shown promising results in animal experiments and several compounds are currently being tested in the clinics against a variety of diseases [180, 181]. However, the major disadvantage of PS oligonucleotides is their binding to certain proteins, particularly those that interact with polyanions such as heparin-binding proteins [182]. Reasons for this nonspecific interaction is not yet fully understood, but it may cause cellular toxicity [183].

'Second generation' nucleotides have alkyl modifications at the 2' position of the ribose. These modifications make DNA more RNA-like; increasing their ability to hybridise with RNA while making them more nuclease resistant. The most important members of this class are 2'-*O*-methyl and 2'-*O*-methoxy-ethyl RNA. Unlike phosphorothioates, however, most second-generation modifications do not induce degradation of messenger RNA by an RNase H-based mechanism, which in most cases is an essential component of antisense activity [181, 184]. Thus their efficacy becomes significantly reduced. However, success of second generation antisense in terms of greater target affinity and better uptake has translated to increased success therapeutically, as seen with ISIS301012 (see 1.4.4).

All antisense modifications, which are not recognised by RNase H, may benefit from the incorporation of an additional cleaver into the structure.

The major third generation antisense oligonucleotides represent novel chemically modified nucleotides with improved properties such as enhanced serum stability, higher target affinity and low toxicity [23]. They include peptide nucleic acids (PNA), locked nucleic acids (LNA) and other chemically modified oligonucleotides including morpholino oligonucleotides (MO) which have been reviewed by Kurreck [23].

In PNA, the deoxyribose phosphate backbone is replaced by polyamide linkages to give non-ionic DNA mimics composed of repeating *N*-(2-aminoethyl) glycine units. The polyamide backbone has secondary amino atoms anchored through methylenecarbonyl linkers to natural nucleobases (see Fig 1.23) [185]. PNA are

highly stable to nucleases (due to their unnatural backbone) and proteases in biological environments, and bind to complementary DNA and RNA targets with very high affinity and specificity. However, limited uptake of PNA into mammalian cells has been the major obstacle for applying PNA as an antisense agent in cell cultures and *in vivo* [186]. In principle, membrane permeability of PNA may be increased by attachment of lipophilic groups such as adamantyl or phosphonium cations to the PNA or conjugation with membrane permeable peptides [185]. PNA do not recruit RNase H, however, due to lack of charge.

Locked nucleic acids (LNA) [187] represent a novel oligonucleotide analogue in which 2'-O and 4'-C positions in the β-D-ribofuranosyl ring are joined via an O-methylene, S-methylene or amino-methylene moiety, locked in a puckered C3'-endo (N-type) furanose conformation (see Figure 1.23). LNA has high RNA affinity, is nuclease-resistant and has minimal toxicity [81]. LNAs at selected binding sites have been shown to be very potent inhibitors of HIV-1 expression in cell culture at concentrations as low as 4nM, showing potential for antiviral drug therapy [188].

Backbone modifications also alter cell uptake, distribution, metabolism, and excretion.

1.11.5. Transport through cellular membrane

Difficulties in targeting RNA include challenges in drug delivery across a hydrophobic cell membrane, which is difficult for charged oligonucleotides (ON).

For ON-based molecules to carry out their role they require drug delivery to the correct intracellular regions *i.e.* nuclear localisation for binding to the target RNA with sufficient affinity to inhibit translation into its corresponding protein.

These molecules have little or no ability to diffuse across cell membranes and are mostly taken into cells by energy-dependent mechanisms such as endocytosis. This results in oligonucleotides ending up in endosomes or lysosomes where they are usually degraded.
Continuing advances in drug delivery and in the medicinal chemistry of nucleic acid analogues may help to enhance ON abilty to enter cells.

One method of overcoming these delivery problems is with conjugation to cell penetrating peptides (CPPs), also known as protein transduction domains (PTDs), to enhance cell membrane penetration. P. M. Fischer, *et al* discuss the use of CPPs to vectorise molecules not actively imported by living cells, or which are impermeable to cell membranes due to their size or physicochemical properties [189, 190]. Well known CPPs include Penetratin [191], HIV-1 Tat (residues 48–60) [192, 193] and Transportan [194]. Conjugation of macromolecules such as antisense with some short highly basic peptides, such as TAT, antennapedia and Transportan results in their rapid translocation into cells [195]. As a common feature, these peptides appear to be amphipathic and net positively charged. The mechanism of cell translocation is not known but is thought to be receptor and energy independent although, in certain cases, translocation can be partially mediated by endocytosis. Other cationic polymers *e.g.* polyethylenimine (PEI) may be used to neutralise ON negative charge to help with intracellular delivery. However, non-specific reactions with blood components have limited use of such polymers [196, 197] although research into the development of more non-toxic derivatives is ongoing.

$(KFF)_3K$ is another cationic peptide which has previously been shown to permeate bacterial cell membranes for improved cell delivery [185]. Petersen *et al*. have synthesised a trifunctional PNA-peptide-DETA artificial ribonucleases. This AR is composed of a 10-mer RNA-recognising PNA oligonucleotide conjugated to a diethylenetriamine (DETA) cleaving domain and a cellular delivery peptide connected to the PNA *via* a linker [185]. However, no *in vivo* results have yet been reported although PNA-conjugated CPPs appear to have had more success *in vitro* than their more natural ON counterparts [198].

Fischer *et al.* [199] conclude that as pharmacological applications are possible, therapy seems more feasible. However, despite the promise of these peptides, their absorption, distribution, metabolism, immunogenicity, and cellular fate in conjugation with oligonucleotides will need to be studied in depth before these agents can be used for therapeutic applications [189, 199].

1.12. Aims

The main goal of the project is to develop robust and facile synthetic strategies to produce and characterise a number of oligonucleotide-based ARs containing an additional phenazinium anchor group (see Figures 1.24 - 1.30). The anchor group and oligonucleotide recognition element will vary in their location relative to the catalytic domain. These oligonucleotide-based ARs can be seen in Figures 1.24 - 1.30. Different synthetic strategies will be compared in terms of (i) robustness and simplicity (ii) efficiency (in terms of final reaction yield) and (iii) cost-efficiency in terms of time and resources spent.

The next challenge will be to determine physico-chemical aspects and the modes of interactions between synthesised ARs and the target RNA molecules, which may influence their performance and ability to irreversibly damage RNA molecules in a sequence-specific manner.

An additional aspect to be evaluated in our collaboration with the Russian collaborative group (Prof. Marina Zenkova, Novosibirk, Russia) will include estimation of hydrolytic activity and site-specificity of the synthesised ARs from their ability to cleave $tRNA^{Phe}$ as a model target.

The objectives of the project are:

(a) The design and synthesis of novel oligonucleotide-based ribonuclease mimics containing a *bis*-imidazole catalytic centre and an *N*-hydroxyethylphenazinium anchor group using varied synthetic routes (see Figures xx- xx).

(b) To fully characterise synthesised compounds using NMR, MS, IR, UV, m.p., TLC or HPLC.

(c) To contrast the different synthetic strategies in terms of (i) the highest reaction yield, (i) simplicity and robustness and (iii) site-efficiency.

(d) To determine hybridisation properties and binding affinity (T_m values) of synthesised conjugates with target 23-mer RNA.

(e) To study and determine the type of interaction between the *N*-hydroxyethylphenazinium anchor group and RNA target.

(f) To assess the hydrolytic activity and site specificity of these artificial ribonucleases in terms of their cleaving potential against RNA phosphodiester bonds (practical laboratory work to be conducted by project collaborators, Prof. Vlassov's group, Novosibirsk, Russia).

(g) To evaluate the impact of the phenazinium anchor group on performance of *bis*-imidazole containing artificial ribonucleases in terms of (i) their ability to enhance affinity of cleaving groups to RNA target and (ii) to improve their hybridisation properties *via* additional stacking interactions with nucleotide residues.

(h) Study the mode of interaction of the *N*-methylphenazinium anchor with the oligonucleotide part of the *DNA:RNA* hybrid using UV-visible spectroscopy.

The following questions are to be addressed:

1. N-hydroxyethylphenazinium-containing artificial ribonucleases.

- Does the Phn affect the RNA binding capabilities of the designed conjugates?
- Are the conjugates still able to specifically cleave the RNA target in the presence of a bulky phenazinium group linked in very close proximity to the cleaving domain?
- Do the varied postions of the non-specific *N*-hydroxyethylphenazinium anchor group and oligonucleotide binding domain affect the cleavage potential of the conjugates?

Figure 1.24. Synthetic pathway for preparation of intermediate tripeptide precursor **6** and tetrapeptide **7.1**.

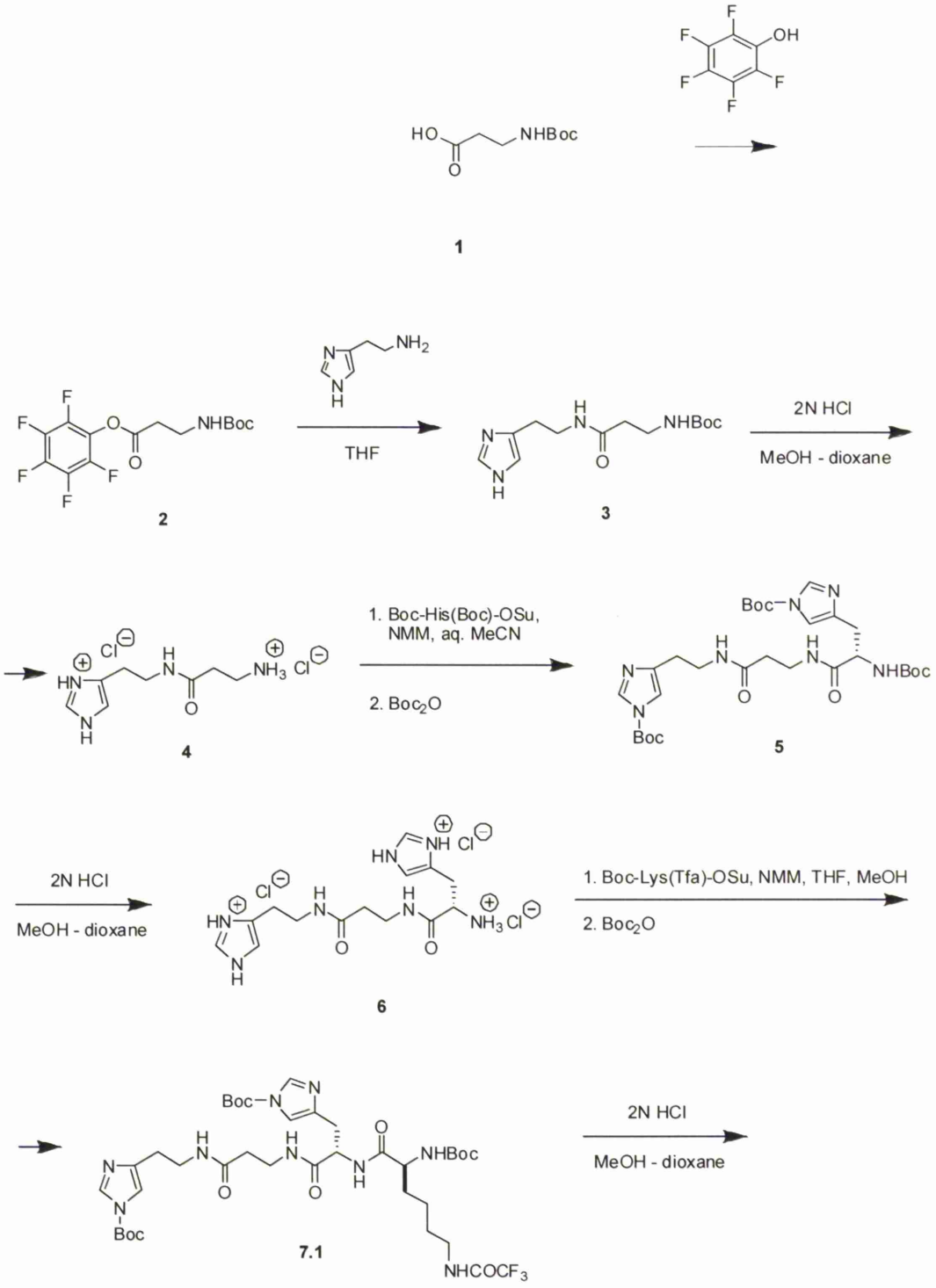

Figure 1.25. Synthetic pathway for preparation of **11.1**.

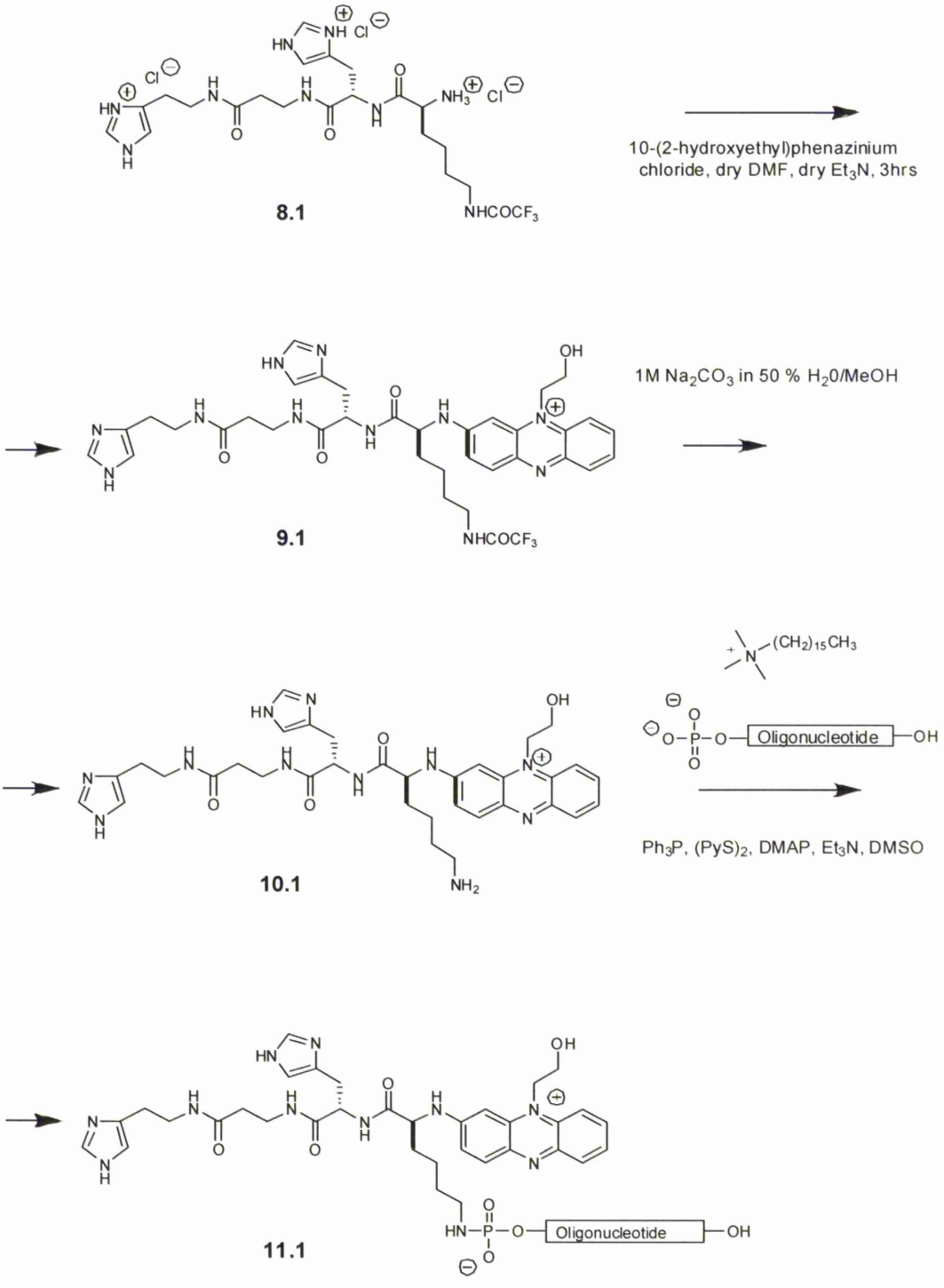

Figure 1.26. Synthetic pathway for the preparation of cleaving constructs **13.2**.

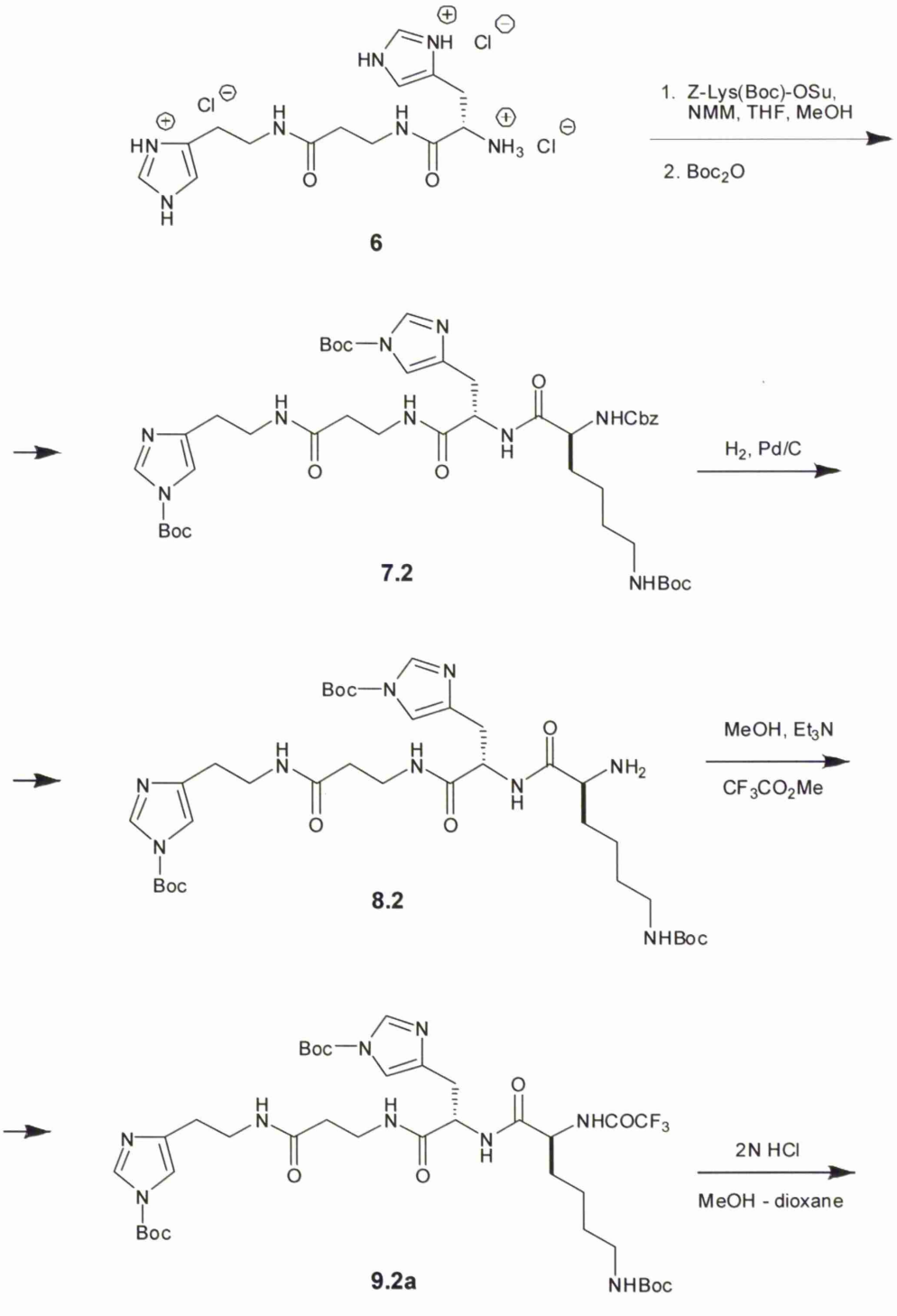

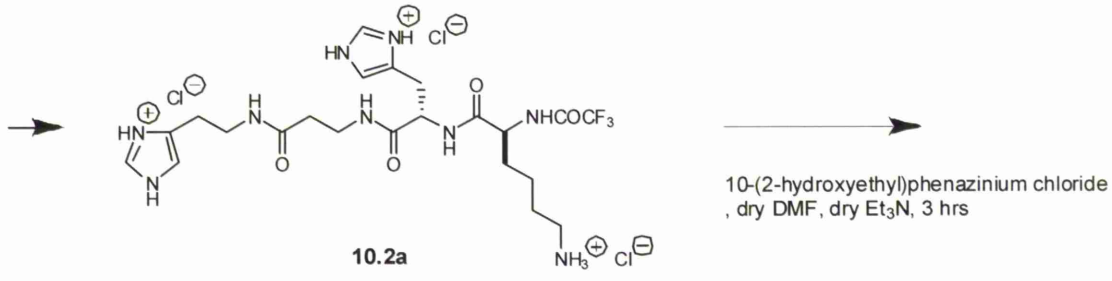

10.2a

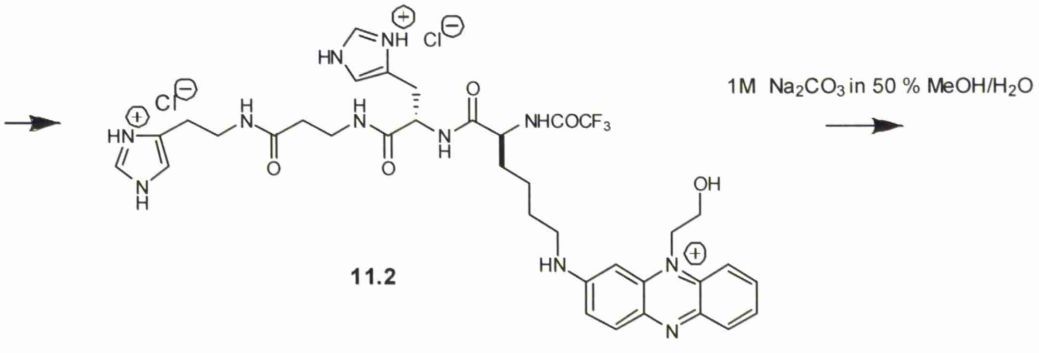

11.2

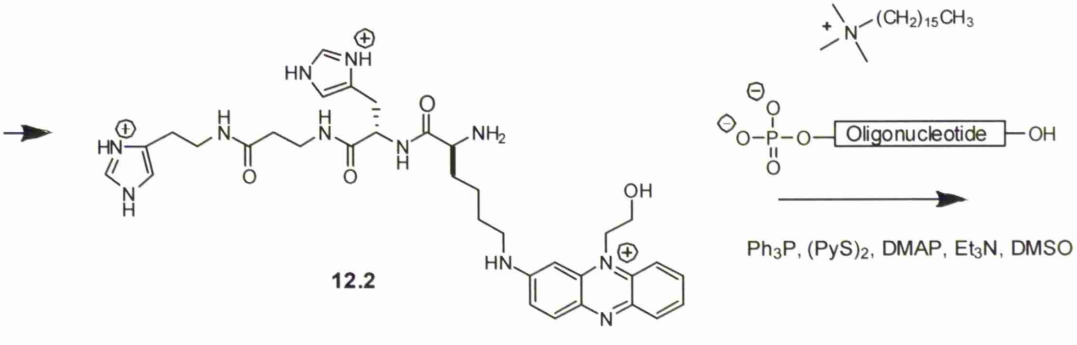

12.2

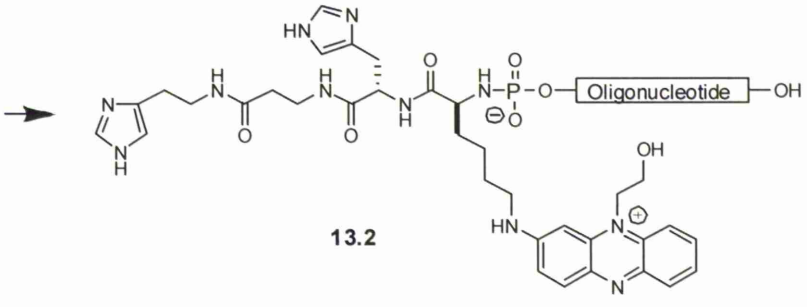

13.2

Figure 1.27. Alternative synthetic pathway for the preparation of compound **13.2** renamed as compound **10.2**.

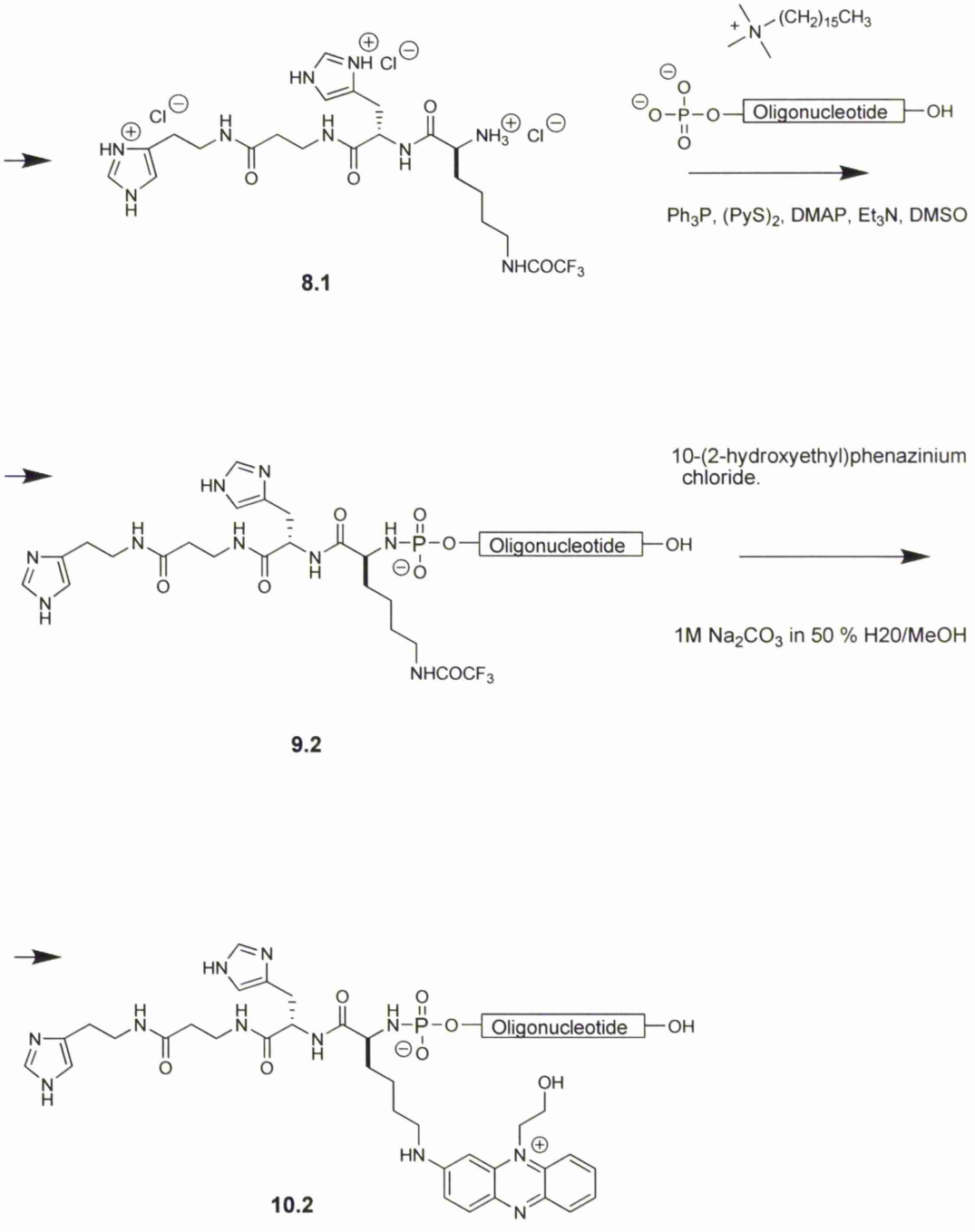

Figure 1.28. Synthetic pathway for the preparation of **10.3**.

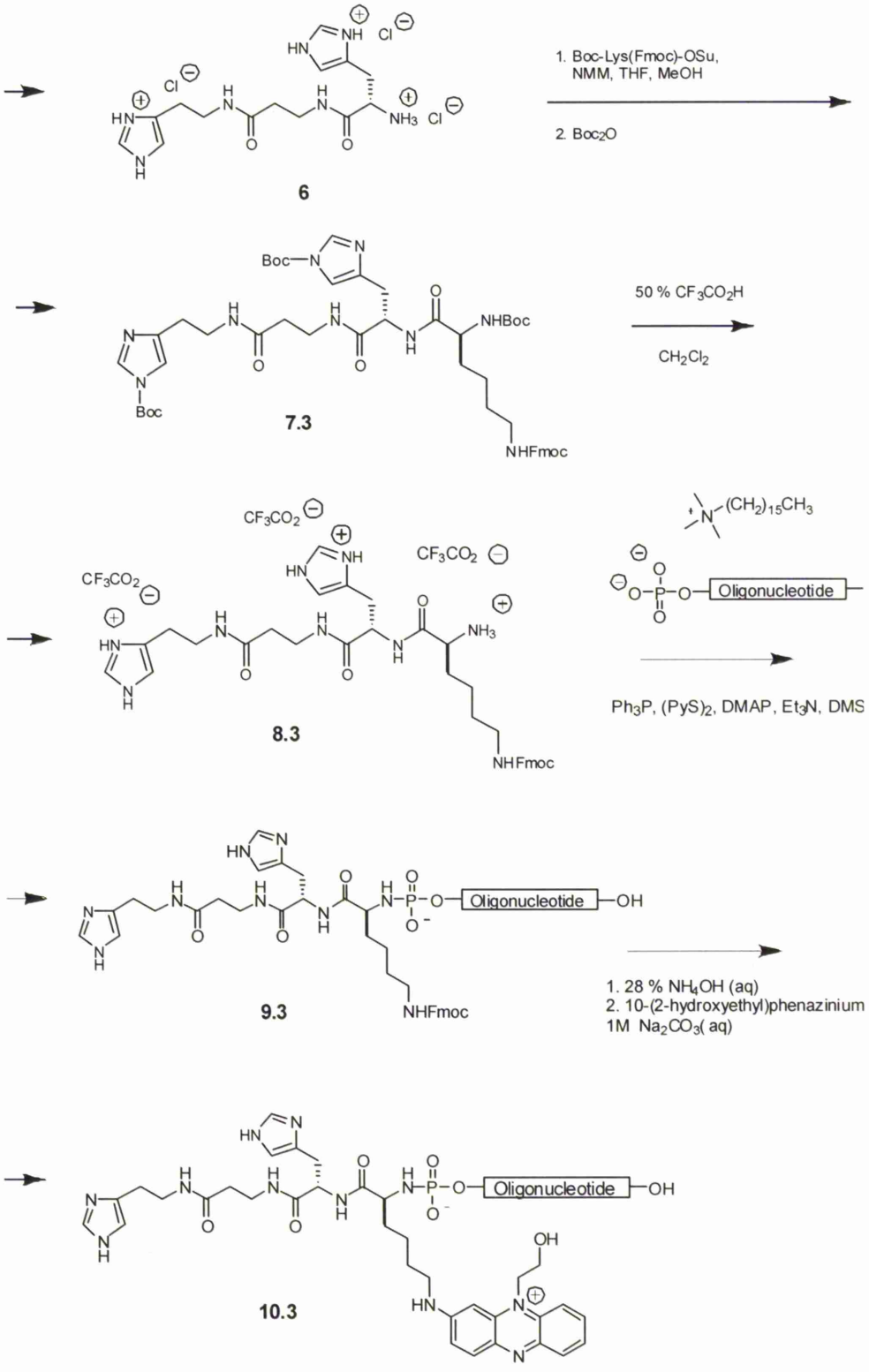

Figure 1.29. Synthetic pathway for the preparation of cleaving constructs **10.4**.

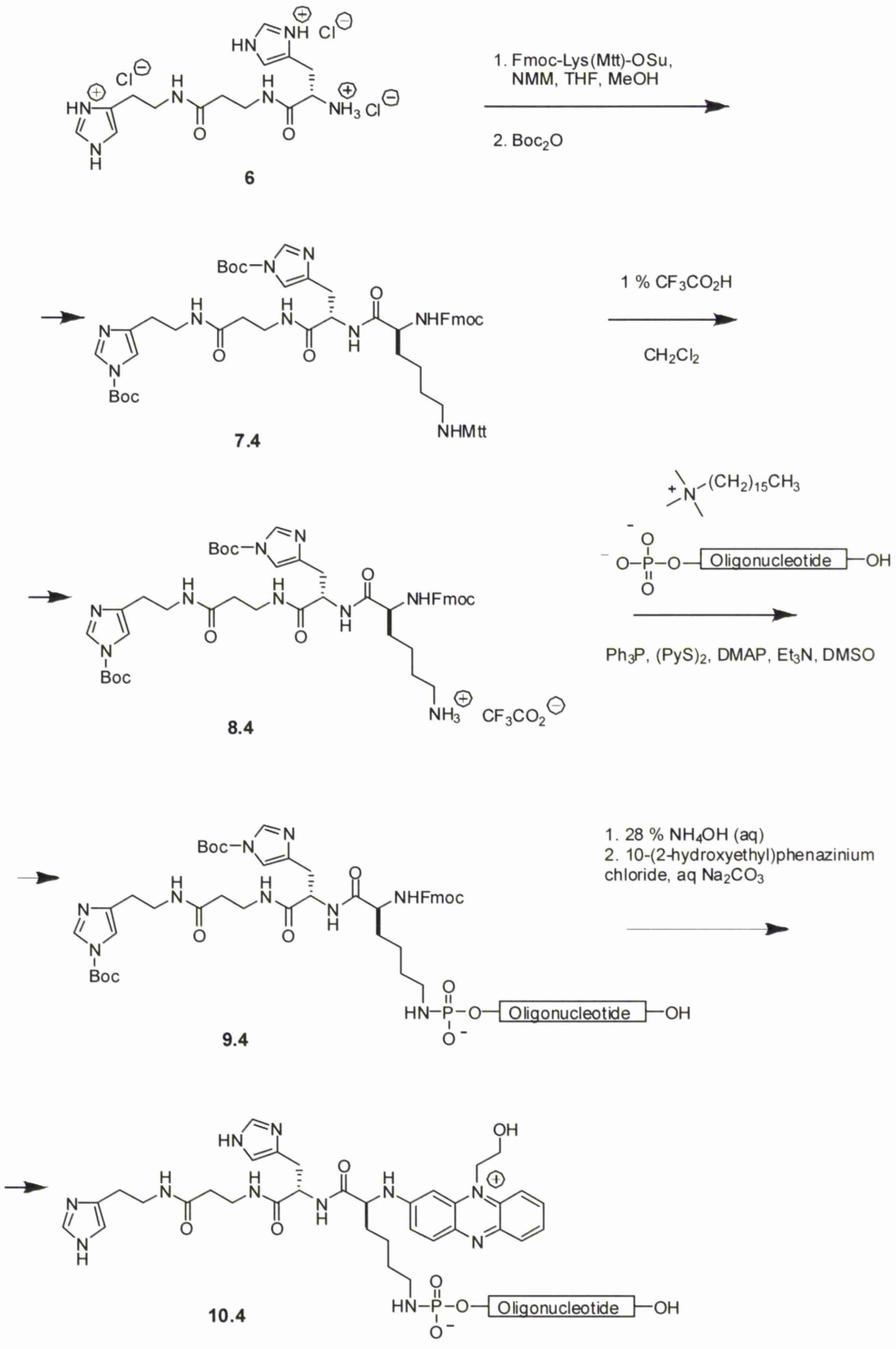

Figure 1.30. Alternative synthetic pathway for the preparation of **10.4.**

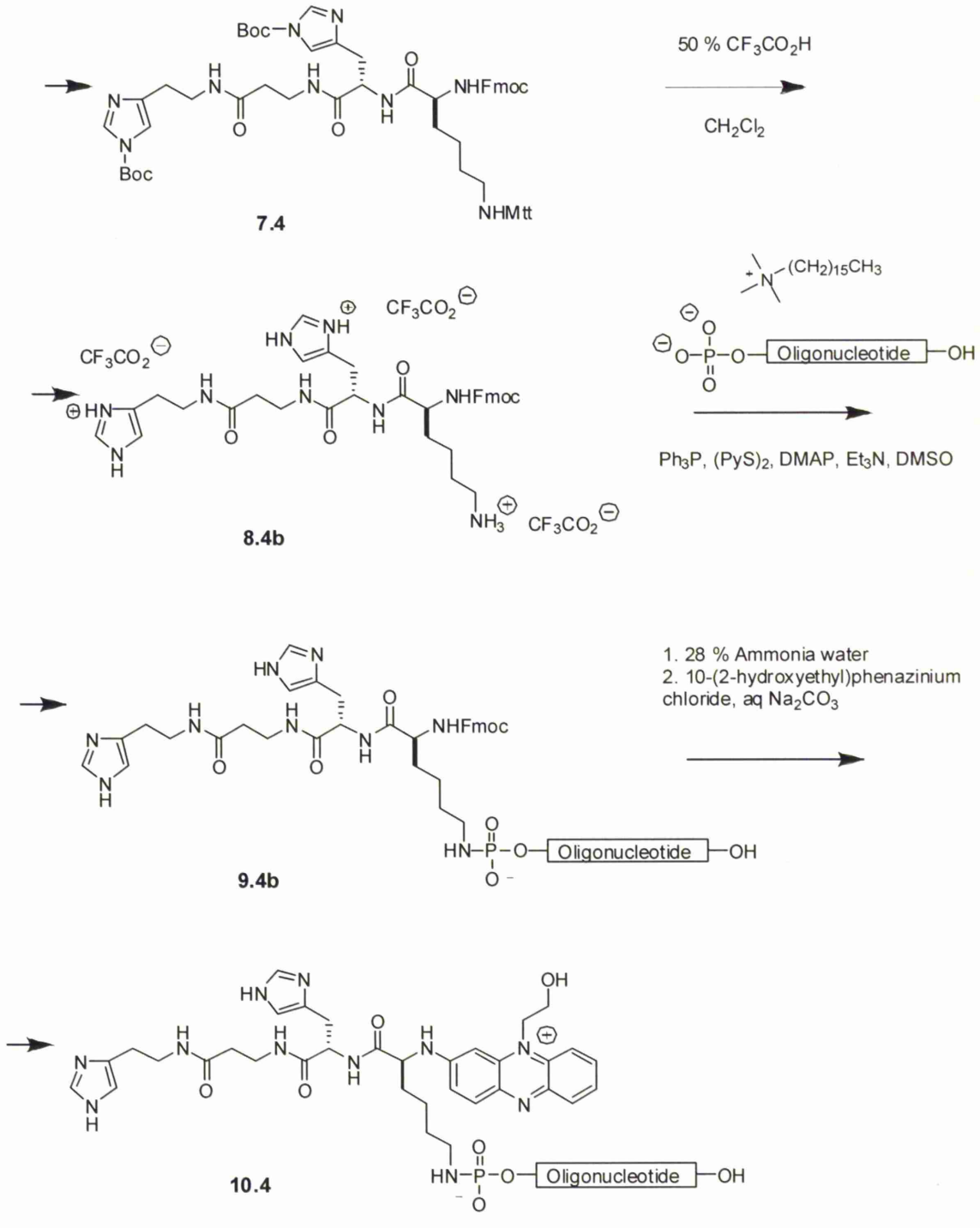

1.13. Numerical Nomenclature of synthesised compounds

Each different fourth amino-acid (*i.e.* natively protected lysine derivative) added to the tripeptide **6** is numbered using decimals from 0.1 to 0.4. These decimals are used to distinguish the different protecting groups used to protect lysine amino groups, resulting in four different derivatives of lysine.

For example, the decimal 0.1 represents the lysine derivative: Boc-lys-(Tfa)-OH and all further derivatives of this tetrapeptide **7.1** are numbered **8.1**, **9.1**, **10.1**, etc, accordingly (see Figures 3.3 and 3.4). The decimal annotations 0.2, 0.3 and 0.4 represent the alternative lysine derivatives: Z-lys(Boc)-OH, Boc-lys(Fmoc)-OH and Fmoc-Lys(Mtt)-OH, respectively (see Figures 3.5- 3.9).

Figures 3.4 and 3.5 represent synthetic schemes involving conjugation of a phenazinium anchor moiety to the tetrapeptide construct before oligonucleotide addition. Conversely, Figures 3.6- 3.9 represent conjugation of an oligonucleotide moiety to the tetrapeptide prior to the phenazinium anchor conjugation.

Figures 3.10 and 3.11 show numbering of the protons within the tetra-peptide moiety and the whole cleaving construct, respectively, used for the assignment of ^{1}H NMR signals.

Figure 1.31. Numbering system used for the assignment of ^{1}H NMR signals.

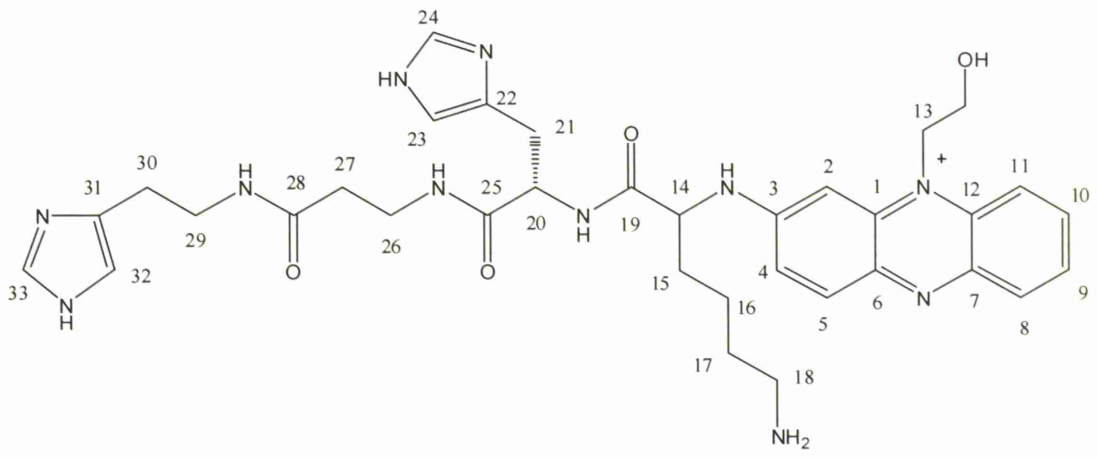

Figure 1.32. Numbering system used for the assignment of ^{1}H NMR signals for the core tetra-peptide structure.

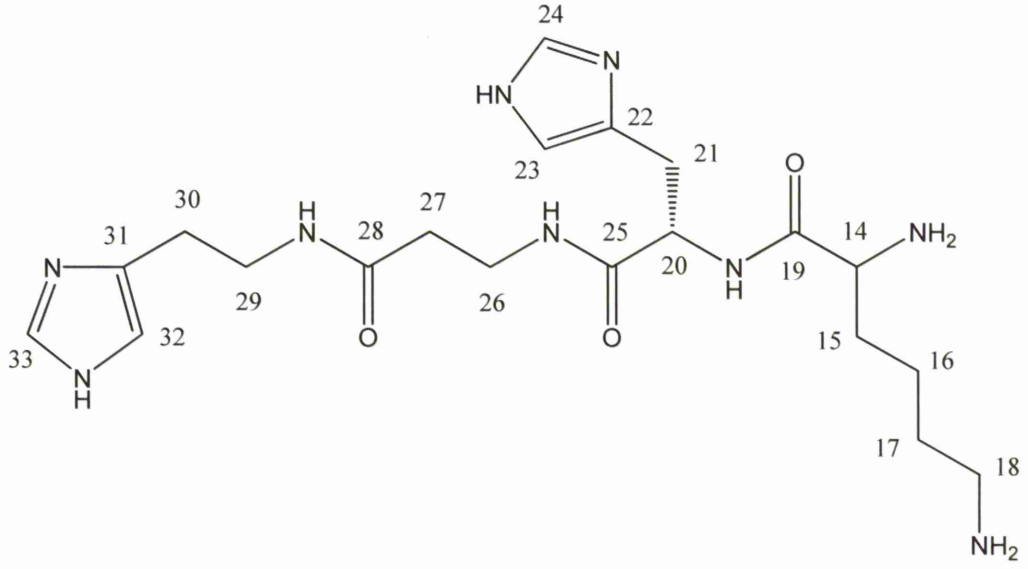

2. Materials and Methods

2.1. Instrumentation and Methods

2.1.1. UV-Visible Spectroscopy

UV and visible spectra were measured at 20 °C on a Cary-Varian 1E 4000 UV-Visible spectrophotometer, operating under Varian Cary WinUV software and equipped with a Peltier temperature controlled cuvette holder. The wavelength range was from 200 to 900 nm and quartz cuvettes of 1 cm path-length were used.

2.1.1.1. UV-Visible Spectral Measurements

The UV-visible spectra of phenazinium derivatives **9.1**, **11.1**, **10.2**, **10.3** and **10.4** (5 μM in water) were measured in 1 cm path length quartz cuvettes at 20 °C using a Cary-Varian 1E 4000 UV-visible spectrophotometer.

To determine the molar extinction coefficients for the *free* cleaving construct **9.1** and **11.1**, **10.2**, **10.3** and **10.4**, small quantities of them were weighed and dissolved in 1 ml water. Small aliquots were subsequently diluted and UV-visible spectra measured in 1 cm path length quartz cuvettes. Extinction coefficients were determined from plots of absorbance *versus* concentration, using the following equation:

$$A_{\lambda max} = \varepsilon_{\lambda max} \times C \times l \qquad (\mathbf{1})$$

where $A_{\lambda max}$ is the absorbance at λ_{max}, C is the concentration in moles/litre, l is the path length in cm and $\varepsilon_{\lambda max}$ is the molar extinction coefficient at that wavelength (λ_{max}).

Hybridisation of the oligonucleotide conjugates **11.1**, **10.2**, **10.3** and **10.4** with a complementary 2'-O-methyl 23-mer RNA oligonucleotide (5'-rAGGUCCUGUGUUCGAUCCACAGA) were studied in 50 mM Tris-HCl buffer, pH 7.6, 200 mM KCl, 0.5 mM EDTA.

To assess any change to their UV-visible characteristics in response to hybridisation with target RNA, UV-visible spectra of the *free* (i.e. without RNA

target) oligonucleotide conjugates **11.1**, **10.2**, **10.3** and **10.4** (5 μM) were measured in buffer at 20 °C, followed by the addition of 2'-O-methyl target 23-mer oligoribonucleotide to achieve a final concentration of 5 μM, and spectra were recorded until no further change occurred.

2.1.1.2. Melting Curve Experiments

Melting curve experiments were performed in a Peltier temperature controlled cuvette holder in Cary-Varian 1E UV-Visible spectrophotometer, which plotted absorbance against temperature. Melting denaturation temperature experiments involve slowly heating hybridised complementary oligonucleotides beyond a temperature where the two strands separate and then slowly allowing them to cool to the starting temperature. This typically produces a sigmoidal UV-vis spectrum when plotting UV-visible absorption against temperature at the absorption wavelengths specific to oligonucleotides and phenazinium derivatives, 260 nm and 520 nm, respectively. Hence, melting temperature (T_m) profiles were obtained by detection at 260 nm and 520 nm wavelengths. The melting temperature, T_m, is defined as the temperature corresponding to the half-transition of the dehybridisation process (temperature at which 50% of the oligonucleotide and its perfect complement are in duplex) which is represented by the halfway point in the sigmoid curve with two plateaus. A heating and cooling rate of 0.1 °C/ min was applied for a temperature range from 20 °C to 90 °C with a data interval of 0.1 °C.

Methods of calculating T_m

T_m values were calculated using both techniques below:

1) Taking the absorbance reading halfway between the plateaus of a melting temperature (temperature vs. absorbance) S-shaped curve.

2) Using the first derivative method (using Cary software). The T_m value is the maximal value of the first derivative: the greatest rate of inflection on the raw data curve, which is the point of greatest change in absorbance in unit time.

2.1.2. Fluorescence Spectroscopy

Fluorescence excitation and emission spectra were recorded using a Cary Eclipse fluorescence spectrophotometer (Varian Inc., Australia), operating under the Cary Eclipse Bio Package software (Varian Inc., Australia). The instrument was fitted with a Peltier 4-position multiple stirred cell holder capable of maintaining a constant temperature (± 0.1 °C) in the range -10 °C to 100 °C. It was connected with a nitrogen purging system to avoid condensation at low temperatures. It was equipped with a 15W pulse Xenon Flash Lamp, Czerny-Turner excitation and emission grating monochromators (1200 lines/mm) and a 2X photomultiplier tube for the 190 – 900 nm range. Fluorescence measurements were performed at 5 °C in a Peltier temperature controlled cuvette holder either in water or Tris buffer (50 mM Tris, 200 mM KCl, pH 7.6, 0.5 mM EDTA) on a Varian Eclipse Fluorescence spectrophotometer, operated with Cary Eclipse software for Windows.

The excitation wavelengths (λ_{EX}) used were 394 and 525 nm and the emission spectra were recorded between 507- 800 nm, using 1 cm path-length quartz cuvettes. Setting parameters included: excitation slit, 5 nm; emission slit, 10 nm;
Excitation spectra, emission spectra and slit-width (5 or 10 nm) were optimized for each experiment and recorded at 20 °C unless otherwise stated with a scan rate of 120 nm/ min.

2.1.2.1. Fluorescence-based experiments

Hybridisation of **9.1** or **15** with complementary 2'OMe 23-mer RNA oligonucleotide (5'-rAGGUCCUGUGUUCGAUCCACAGA) was studied in 50 mM Tris-HCl, pH 7.6, 200 mM KCl, 0.5 mM EDTA. Initially, the emission spectrum of **9.1** or **15** (5 μM) was measured in buffer at 20 °C with the excitation λ_{EX} of 394 nm or 525 nm. Then, target 23-mer oligoribonucleotide was added (final concentration, 5 μM) and emission spectra taken until no further change occurred.

2.1.3. Nuclear Magnetic Resonance (NMR) Spectroscopy

NMR spectra were recorded using a Bruker 300 MHz (7.05 T) spectrometer (Avance-300) equipped with a 5 mm single-axis Z-gradient quattro nucleus probe.

The NMR spectrometer allows observation of four specific nuclei (^{1}H, ^{19}F, ^{31}P, and ^{13}C), operating at 300 MHz, 282 MHz, 121 MHz and 75 MHz, respectively, at 20 °C. The spectrometer was equipped with Microsoft Windows NT workstation (Version 4.0) running XWIN-NMR and XWIN-Icon NMR software (Version 3.0). The software used to obtain and analyse the spectra was Topspin v2.0 or Topspin v2.1. Chemical shifts (δ) are reported in parts per million (ppm) with peak positions reported relative to TMS (0.00) as an internal standard. Data are reported using the following convention: chemical shift (splitting patterns, integrated intensity, assignment). Abbreviations used for splitting patterns are: s (singlet), d (doublet), t (triplet), q (quartet), m (multiplet), dd (doublet of doublets), dt (doublet of triplets), br (broad), obs (obscured).

Some ^{1}H NMR spectra were also recorded with Bruker Avance II+ 400 MHz (9.4 T) and 500 MHz (11.75 T) spectrometers, operating at 400 MHz and 500 MHz for protons, respectively. The software used to obtain and analyse the spectra was Topspin v2.0 or Topspin v2.1.

2.1.3.1. One- and two-dimensional NMR spectroscopy

One- and two-dimensional NMR spectra of samples were acquired in deuterated methanol (or when necessary in D_2O or DMSO-d_6) at 20 °C at concentrations of approximately 5 mg in 600 µl.

^{1}H NMR

For one-dimensional ^{1}H NMR, data were collected into 64 K data points over a spectral width of 6172.84 Hz giving a final resolution of 0.096 Hz/point. For each spectrum at least 16 transients were acquired with 2 s recycle delay.

^{13}C and DEPT 45 and 135

One-dimensional ^{13}C and DEPT 45, 135 NMR data were collected into 64 K data points over a spectral width of 17985.61 Hz giving a final resolution of 0.281 Hz/point. For each spectrum 6144-12288 transients were acquired with 2 s recycle delay.

^{31}P NMR

Oligonucleotide samples of 1.6 μM concentration in D_2O were analysed by one-dimensional ^{31}P NMR using proton decoupling. Data were collected into 64 K data points over a spectral width of 4866.80 Hz giving a final resolution of 0.076 Hz/point. For each spectrum 20 K transients were acquired with 2 s recycle delay.

^{19}F NMR

For one-dimensional ^{19}F NMR data were collected into 64 K data points over a spectral width of 6172.84 Hz giving a final resolution of 0.096 Hz/point. For each spectrum at least 16 transients were acquired with 2 s recycle delay.

COSY

Two-dimensional ^{1}H-^{1}H COSY NMR (Aue W.P. 1976) data were collected with quadrature detection into 2048 complex data points for $2x256t_1$ increments with 8 transients being acquired for each t_1 increment. Data were acquired over 3086.42 Hz spectral width (final F_2 resolution was 1.507 Hz/point) with 2 s relaxation delay.

2.1.4. Mass Spectrometry

Molecular weights of peptide precursors and oligonucleotide conjugates have been verified by mass spectrometry techniques.

Electrospray ionisation mass spectra (EI) were taken using a Waters Platform II instrument and Accurate mass determinations were carried out using a Thermo Finnigan Mat95XP instrument or Waters QTOF instrument in the Chemistry Department, Manchester University.

Matrix Assisted Laser Desorption Ionisation- Time of Flight-/Time of flight (MALDI-Tof/Tof) mass spectra were taken using a MALDI-ToF/ToF Instrument (Ultraflex II®) with pulsed nitrogen laser of wavelength 337 nm and

Voyager software in the Manchester Interdisciplinary Biocentre (MIB), Manchester
University. Samples of all oligonucleotide conjugates were also sent to the EPSRC Mass Spectrometry Centre, Swansea University.

Samples were initially prepared in solvent (usually water) at concentrations of 1 µg/ µl. Gel matrix solution (10 mg/ ml of solvent) was made of gel matrix dissolved in: MeCN, Water, TFA (50:50:1). Gel matrix: α-cyano-4-hydroxycinnamic acid (10 mg/ ml of solvent) was used for oligonucleotide-peptide conjugates. Gel matrix: 2,5-dihydroxybenzoic acid (10 mg/ ml of solvent) was used for peptides. Samples were pipetted (0.5 µl) onto a MALDI sample plate and allowed to dry. Pipetted sample spots were then covered with 0.5 µl of matrix solution.

2.1.5. Elemental Analysis

Elemental analyses were recorded on an EA 1108-Elemental Analyser (Carlo Erba Instruments) in the Chemistry Department, London Metropolitan University.

2.1.6. Infrared Spectroscopy

Infrared spectra were recorded on a Fourier Transform Infrared Spectrometer (Jasco® FT/IR- 4100) using Specta Manager (version 2) software.

2.1.7. Thin Layer Chromatography

Reactions were monitored by TLC on silica gel (precoated F254, Merck 1.05554) or RP-18 (precoated F254, Merck 1.05560) and visualized under UV light with a UV GL-58 Mineral-Light lamp. Additional staining was done by exposure to iodine vapor, permanganate immersion, or treatment with a 1:1 mixture of 1 % sulphanilic acid in 1 M HCl and 5 % $NaNO_2$ (Pauly reagent, specific test for imidazole-containing compounds [200]) and ninhydrin test to test for free amine groups.

Use of Pauly reagent. TLC plates were sprayed with equal volumes of refrigerated 1 % sulphanilic acid in 1 N HCl and 5 % aq $NaNO_2$ (mixed 5 mins before use) followed by treatment with 15 % $NaCO_3$ (aq). Spots containing imidazole groups give a red/orange colour immediately [200].

Solvent mixtures used are indicated in experimental procedure descriptions.

2.1.8. Determination of pH

Measurements of pH were made using a digital pH meter (HANNA Instruments) calibrated with standard buffers (Sigma Chemical Co.) at 20 °C.

2.1.9. Preparation of Tris Buffer

Tris buffer contained 50 mM Tris.HCl, 200 mM KCl, 0.5 mM EDTA, pH 7.6. Water used for the buffer preparation was distilled, deionised and treated by ion-exchange and charcoal filtration using a MilliQ System (Millipore Ltd). The buffer was prepared following standard procedures using analytical grade reagents and stored below 4 °C prior to use. The pH value was adjusted using a pH meter (HANNA Instruments) at 20 °C.

2.1.10. Preparation of Stock Solutions

Desired concentrations of stock and sample solutions were prepared either by dilution of a concentrated stock solution or by lyophilisation and subsequent reconstitution in Milli-Q water.

To calculate both the concentrations of the test samples in the cuvette and consequently the concentration of original stock solution the Beer-Lambert Law was used:

$$A_{\lambda max} = \varepsilon_{\lambda max} \times c \times l \qquad (1)$$

A= absorption
ε= molar extinction coefficient (M^{-1} cm^{-1})
l= path length of cuvette (cm)
c= concentration of sample (mol/L)

Rearrangement of the equation (**1**) allow calculations of the sample's concentration in the cuvette:

$$c = A / \varepsilon \times l \quad (2)$$

In all experiments cuvettes with a path length of 1 cm were used; therefore, l was equal to 1 cm for all calculations.

The molar extinction coefficient (or molar absorptivity) is a constant specific to a wavelength; usually at the peak of each chromophoric band (λ_{max}). For example, ε_{260} is the molar extinction coefficient at the λ_{260} for oligonucleotides (see Fig. 3.29). It can therefore be calculated using equation (3) and by empirically recording the absorbance of a known concentration of compound. UV-visible spectra were used to identify the chromophoric bands and their λ_{max} for which absorbance was recorded empirically (and ε calculated using Beer-Lambert law (equation 2) when unknown).

The millimolar extinction coefficient (ε) values used in the calculations are shown below:

17-mer oligodeoxyribonucleotide, ε_{260nm}= 169 $mM^{-1}\,cm^{-1}$;
23-mer 2′ OMe oligoribonucleotide, ε_{260nm}= 222.4 $mM^{-1}\,cm^{-1}$.

Phn has a chromophore which produces UV-visible spectral bands at 395 nm and 520 nm. Calculation of molar extinction coefficients at 395 nm and 520 nm for Phn containing tetrapeptide construct was achived by rearranged equation (1):

$$\varepsilon = A / b \times c \quad (3)$$

For oligonucleotide conjugates containing Phn, where the quantity or concentration was unknown, the contribution of absorptivity from the Phn chromophore at 260 nm had to be taken into account. To achieve this, the extinction coefficient of Phn at 260 nm was evaluated for the Phn incorporating tetrapeptide **9.1** using equation (3) and measuring UV absorption at 260nm:

Molar extinction coefficient (ε_{260}) of **9.1**: = 6.7 $mM^{-1}cm^{-1}$

Subsequently, the extinction coefficients at 260 nm for the oligonucleotide conjugates containing phenazinium chromophore was determined by adding the contribution at 260 nm from both oligonucleotide part (169 $mM^{-1}\,cm^{-}1$) and Phn incorporating tetrapeptide **9.1** (ε_{260} = 6.7 $mM^{-1}cm^{-1}$). For example, ε_{260} for Phn

incorporating oligonucleotide conjugate **11.1** was calculated as 169 + 6.7 = 175.7 ± 0.13 $mM^{-1}cm^{-1}$.

Molar extinction coefficient (ε_{260}) of 17-mer oligonucleotide (DNA: 5'-pdGATCGAACACAGGACCT): 169 $mM^{-1}cm^{-1}$

Molar extinction coefficient (ε_{260}) of oligonucleotide conjugates (**11.1**, **10.2**, **10.3**, **10.4**): 169 + 6.7= 175.7 $mM^{-1}cm^{-1}$

To determine the concentrations of unknown stock solutions of each oligonucleotide or oligonucleotide conjugates, a 10 µl sample of stock was taken and diluted to 1000 µl (1 ml). The measured absorbance at 260 nm (A_{260}) by UV-visible spectroscopy was used to calculate the concentration of the test sample using Beer-Lambert's law, equation (2). The concentration of the original stock solution was recalculated using the 100-fold dilution factor.

Initial quantities of oligonucleotide conjugates were determined and 1 mM stock solutions were prepared in Milli-Q water and stored at -80 °C untill required.

2.1.11. Reverse- Phase HPLC

HPLC purifications were performed on an Agilent 1100 system, consisting of a quaternary pump with solvent degasser, diode-array module for multi-wavelength signal detection and a fluorescence detector for on-line acquisition of excitation/ emission spectra. The system had a manual injector, temperature controlled column compartment with two heat exchangers for solvent pre-heating and was operated through a PC running Agilent HPLC 2D ChemStation Software. The following reverse-phase columns were used (depending on the purification protocol): semi-prep Zorbax Eclipse XDB-C18, 5 micron, (9.4 mm x 25 cm), semi-prep VYDAC Protein & Peptide C18, 5 micron, (9.4 mm x 25 cm), semi-prep Phenomenex Luna, 10 micron, C18 (250 x 21.2 mm), or analytical Phenomenex Luna, 5 micron, C18 (250 x 4.6 mm). Elution protocols are reported in experimental procedure descriptions.

2.1.12. Ion-Exchange Column Chromatography

Dowex 550 Å OH anion exchange resin packed in a 2 x 10 cm plastic column was used for ion-exchange chromatography. The column was equilibrated with repeated washing with H_2O until neutral pH was achieved. The sample (dissolved in H_2O) was then loaded. The elution gradient was initiated with H_2O and gradually changed to H_2O/ methanol 1:1 (v/v). For each experiment the eluate was checked regularly by TLC and the pH was measured. Fractions were collected whilst the pH remained basic. Fractions containing the desired compounds were evaporated *in vacuo* and stored at -20 °C.

2.1.13. Silica Gel Column Chromatography

Silica gel column (normal phase) chromatography was carried out using silica gel packed in a 2 x 15 cm glass column. The column was washed with cold, filtered, degassed, non-polar solvent, followed by sample-loading in the same solvent. Elution was performed using an increasingly polar solvent gradient. Eluates were analysed by TLC. Fractions containing expected compounds were evaporated *in vacuo* and stored at -20 °C. Elution solvent gradients are reported in experimental procedure descriptions.

2.2. Chemical Reagents

Chemicals were chosen based on the highest purity available.

Proligo Primers and Probes, France:

23-mer RNA: 5′-AGGTCCTGTGTTCGATCCACAGA.

17-mer DNA: 5′-pdGATCGAACACAGGACCT.

ATDBio, Southampton, UK:

23-mer 2′-*O*-methyl RNA: 5′-AGGUCCUGUGUUCGAUCCACAGA.

17-mer DNA: 5′-pdGATCGAACACAGGACCT.

Lancaster Synthesis UK, Morecambe: Histamine dihydrochloride, phenazine methosulphate, N-hydroxysuccinimide, Di-tert- butyl- dicarbonate.

Novabiochem, Nottingham, UK: Boc-Lys-(Fmoc)-OH (L-isomer), Boc-β-Ala-OSu (L-isomer), HObt (N-hydroxybenzotriazole), N-Fmoc-histamine 4 methoxytrityl resin.

Bachem, St. Helens, UK: Boc-His-(1-Boc)-OSu (L-isomer), Boc-β-Ala-OH, Z-lys (Boc)-OSu, Boc-lys (Tfa)-OSu, Phenazine.

Fisher Scientific UK, Loughborough: Phenazine methosulphate, n-butanol, N, N, N′, N′,- tetramethyl (succinimido) uronium tetrafluoroborate (TSTU)

Sigma-Aldrich, Dorset, UK: 4M Hydrochloric acid solution in 1, 4 dioxane, 3N methanolic HCl, sulphanilic acid (4-aminobenzenesulphonic acid) 99%, sodium nitrite, histamine, 2, 3, 4, 5, 6-pentafluorophenol, *N, N′*-dicyclohexylcarbodiimide.

Cambridge Isotope Laboratories, Andover, USA: Deuterated chloroform ($CDCl_3$), acetone (C_3D_6O), methanol (d_4-MeOD).

Goss Scientific Instruments Ltd: deuterium oxide, tetramethylsilane.

Senn Chemicals: O- (Cyano(ethoxycarbonyl)methylenamino)- 1,1,3,3-tetramethyluronium tetrafluoroborate (TOTU)

2.3. Synthetic Procedures

Chemical structures of synthesised compounds along with their nomenclature numbers are given in Figures 1.24 - 1.30. The synthetic chemistry routes are presented and discussed in the 'Results and Discussions' chapter (see section 3.1).

2.3.1. Synthesis of 3-tert-Butoxycarbonylamino-propionic acid pentafluorophenyl ester (2)

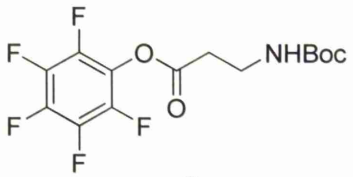

2

A solution of pentafluorophenol (9 g, 49 mmol; 1.1 eq) in EtOAc (30 ml) was added to a solution of Boc-β-ala-OH (**1**) (8.4 g, 44 mmol; 1 eq) in EtOAc (70 ml). A solution of DCC (10.1 g, 49 mmol; 1.1 eq) (DANGER, harmful if swallowed or inhaled, toxic in contact with skin, may cause serious eye damage and may act as a sensitizer) in EtOAc (20 ml) and DCM (20 ml) was added dropwise to the mixture over 1 hr, stirred for 30 mins at 4 °C and then kept overnight at room temperature. The insoluble dicyclohexylurea (DCU) side product was filtered off and EtOAc and DCM were evaporated *in vacuo.* The product (**2**) was re-dissolved in hexane and refrigerated overnight to assist crystallisation. The crystals were filtered while still cold and dried *in vacuo* (97 % yield; 15.3 g).

2.3.2. Synthesis of {2-[2-(1*H*-Imidazol-4-yl)-ethylcarbamoyl]-ethyl}-carbamic acid tert-butyl ester (3).

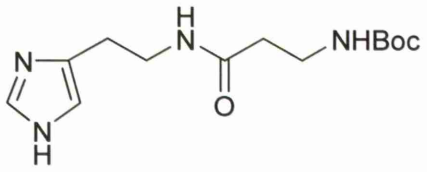

3

A solution of Boc-β-alanine pentafluorophenyl ester (Boc-β-ala-OPFP) (6.75 g; 19 mmol; 1 eq) and histamine (2.22 g; 20 mmol; 1.05 eq) was stirred in THF (20 ml) at room temperature for 1 hr. THF was evaporated and the mixture was extracted with 0.1 N HCl and EtOAc. Organic fractions were combined and solvent removed *in vacuo* to yield a yellow solid **3** (yield: 93 %; 4.98 g).

2.3.3. Synthesis of 3-Amino-N-[2-(1*H*-imidazol-4-yl)-ethyl]-propionamide dihydrochloride (4)

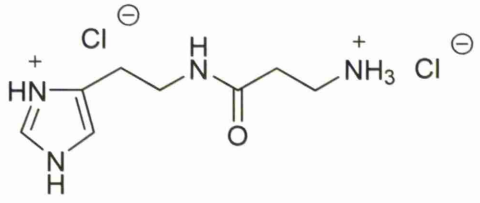

4

A mixture of HCl in 1, 4- dioxane (20 ml) and MeOH (20 ml) was added to **3** (2.82 g; 10 mmol) and stirred for 1 hr at room temperature. A change in colour was noticed from a brown solution to a cream coloured suspension. Evaporation of solvent gave cream coloured crystals of **4** (2.49 g; yield 97 %).

2.3.4. Synthesis of 3-[(*S*)-2-tert-Butoxycarbonylamino-3-(1-tert-butoxycarbonyl-1*H*-imidazol-4-yl)-propionyl]-amino-N-[2-(1-tert-butoxycarbonyl-1*H*-imidazol-4-yl)-ethyl]-propionamide (5)

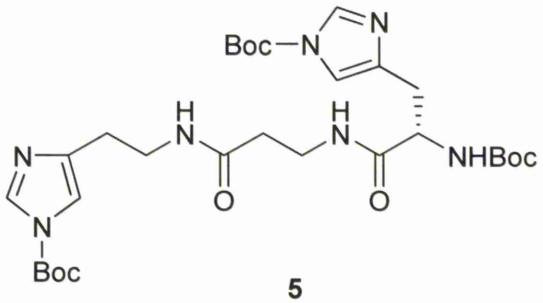

5

NMM (5.4 ml; 49 mmol; 2.5 eq) was added to a solution of **4** (5 g; 19.6 mmol; 1 eq) and Boc-His-(Boc)-OSu (10.6 g; 24 mmol; 1.2 eq) in 50 % MeCN (aq) (50 ml) and stirred for 1 hr. The reaction was monitored by TLC using Pauly reagent as a stain. Di-tert-butyl-dicarbonate (8.6 g; 39 mmol; 2 eq) was added once the starting material disappeared. The reaction mixture was stirred at room temperature for 1 hr, then after evaporating solvent *in vacuo*, extracted using $NaHCO_3$ and EtOAc. Solvent from the organic phase was evaporated *in vacuo* to leave a light brown residue (yield: 66 %).

2.3.5. Synthesis of 3-[(*S*)-2-Amino-3-(1*H*-imidazol-4-yl)-propionyl]-amino-N-[2-(1*H*-imidazol-4-yl)-ethyl]-propionamide trihydrochloride (6)

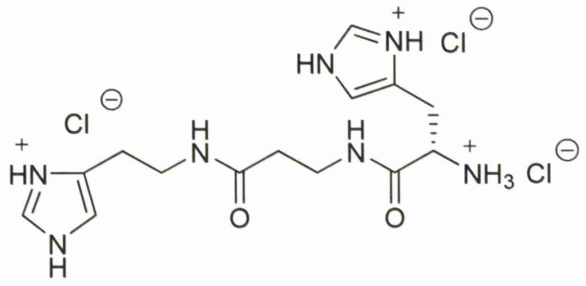

6

A solution of MeOH (10 ml) and HCl in 1, 4 -dioxane (10 ml) was added to **5** (1.7 g; 2.7 mmol) and stirred for 1 hr at room temperature. The reaction was monitored by TLC until completion and the solvent removed *in vacuo*. Product was purified by ion exchange chromatography using Dowex 550A OH anion exchange resin packed in a 2 x 10 cm plastic column (yield: 64 %).

The column was equilibrated with H_2O until a neutral pH was achieved. Elution was with H_2O and gradually changed to H_2O/ methanol 1:1 (v/v) for as long as the eluate pH was basic. Eluates were checked by TLC and their pH values measured. Desired fractions were evaporated *in vacuo* which produced a pink viscous liquid.

2.3.6. Synthesis of 3-{(*S*)-2-[(*S*)-2-tert-Butoxycarbonylamino-6-(2,2,2-trifluoroacetylamino)-hexanoyl]-amino-3-(1-tert-butoxycarbonyl-1*H*-imidazol-4-yl)-propionyl}-amino-N-[2-(1-tert-butoxycarbonyl-1*H*-imidazol-4-yl)-ethyl]-propionamide (7.1)

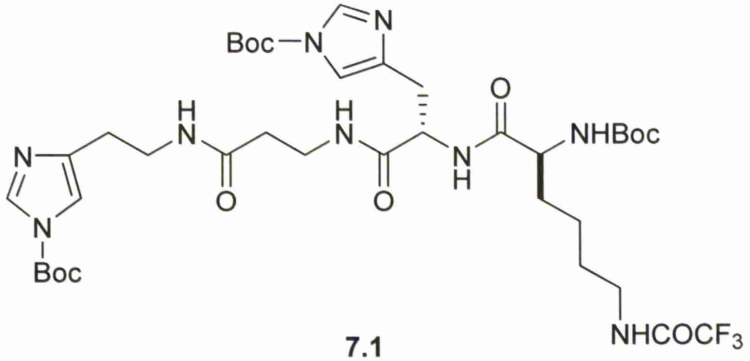

7.1

THF and methanol mixture (3:1 v/v) (4 ml) was added to **6** (335 mg; 780 mmoles; 1 eq) and Boc-Lys-(Tfa)-OSu (411 mg; 936 mmol; 1.2 eq), followed by NMM (214 μL; 2.5 eq) and stirred for 1 hr. The reaction mixture was monitored by TLC until the disappearance of the active ester and then Boc_2O (0.426 mg; 448 μl; 2.5 eq) was added and the mixture stirred overnight at room temperature. The reaction mixture was extracted using 5 % $NaHCO_3$ (aq) and EtOAc. The organic fractions were combined and solvent removed *in vacuo* to yield a brown gum (yield: 61 %).

2.3.7. Synthesis of 3-{(*S*)-2-[(*S*)-2-Amino-6-(2,2,2-trifluoroacetylamino)-hexanoyl]-amino-3-(1*H*-imidazol-4-yl)-propionyl}-amino-N-[2-(1*H*-imidazol-4-yl)-ethyl]-propionamide trihydrochloride (8.1)

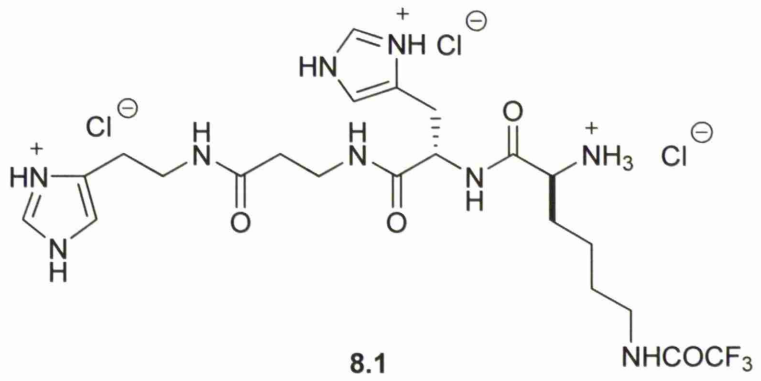

8.1

MeOH (3 ml) and 4 M HCl in dioxane (4 ml) was added to **7.1** (800 mg: 948 mmol) and the mixture stirred, with reaction monitored by TLC over 3 hrs. Once reaction was complete the solvent was evaporated *in vacuo* to yield a translucent brown gum (yield: 96 %).

The residue was extracted with H_2O and EtOAc, washed with EtOAc (~ 10 x 10 ml). The H_2O fraction (light brown coloured) was retained and dried *in vacuo* (yield: 84 %). The reaction mixture was further purified by preparative HPLC to give a translucent pink gum (yield: 68 %).

HPLC solvent A (0.1 % TFA in MeCN) and solvent B (0.1 % TFA in H_20).
HPLC solvent gradient: 0-40% A over 60 mins (0-15 % A from 0 – 20 mins; 15 – 40 % MeCN from 20- 60 mins).

2.3.8. Synthesis of 3-{(*S*)-2-[(*S*)-2-{(2-Hydroxyethyl)-phenazinium-5-yl}-amino-6-(2,2,2-trifluoro-acetylamino)-hexanoyl]-amino-3-(1*H*-imidazol-4-yl)-propionyl}-amino-N-[2-(1*H*-imidazol-4-yl)-ethyl]-propionamide (9.1)

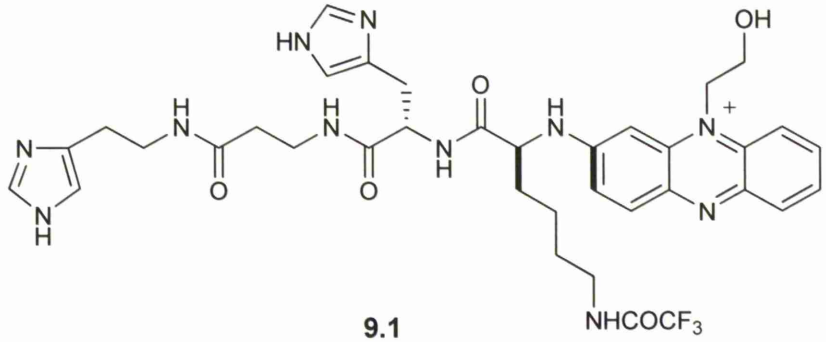

9.1

Phenazinium oxidative addition

The following reaction was performed in dry conditions to prevent alkaline hydrolysis of the trifluoroacetamide protecting group.

Dry DMF (2 ml) was used to dissolve **8.1** (1 eq; 4.6 mmol; 300 mg) together with 10-(2-hydroxyethyl) phenazinium chloride (1.1 eq; 5 mmol; 114 mg) and dry Et_3N (4 eq; 1.8 mmol; 182 mg; 250 µl). The reaction mixture was stirred for 3 hours at room temperature.
The reaction was monitored by UV-visible spectroscopy (until characteristic bands of product (at 390 and 520 nm) stopped increasing).
Solvent was evaporated, and then the minimal amount of MeOH was added dropwise to the reaction mixture until dissolution. Diethyl ether (50 ml) was added to form a precipitate which was filtered, dried *in vacuo* and then redissolved in H_20 for HPLC purification (yield: 8.5 %).

HPLC solvent A (0.1 % TFA in MeCN) and solvent B (0.1 % TFA in H_2O).
HPLC solvent gradient: (0-30% A over 60 mins: 0-10 % A from 0 – 10 mins; 10 – 30 % MeCN from 10- 60 mins).

2.3.9. Synthesis of 3-{(*S*)-2-[(*S*)-2-{(2-Hydroxyethyl)-phenazinium-5-yl}-amino-6-aminohexanoyl]-amino-3-(1*H*-imidazol-4-yl)-propionyl}-amino-N-[2-(1*H*-imidazol-4-yl)-ethyl]-propionamide (10.1)

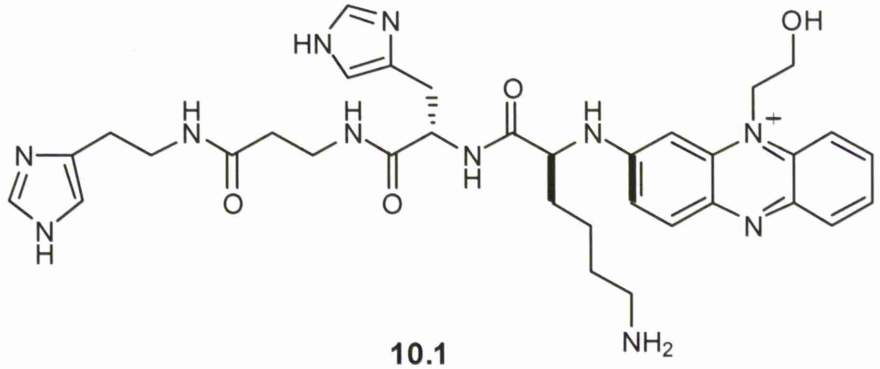

10.1

Deprotection trifluoroacetyl protecting group (Tfa) with aqueous Na_2CO_3 in MeOH

A 0.5 ml aliquot of 0.75 M Na_2CO_3 in H_2O/ MeOH (2:1) was added to **9.1** (7.2 mg; 9.4 x 10^{-6} moles) and the solution stirred at room temperature (whilst protected from light) for 24 hours. The product mixture was purified by HPLC (Yield: 61 %).

HPLC solvent A (0.1 % TFA in MeCN) and solvent B (0.1 % TFA in H_2O).
HPLC solvent gradient: (0-50% A over 60 mins: 0-10 % A from 0 – 10 mins; 10 – 50 % MeCN from 10- 60 mins).

2.3.10. Synthesis of oligonucleotide conjugate (11.1)

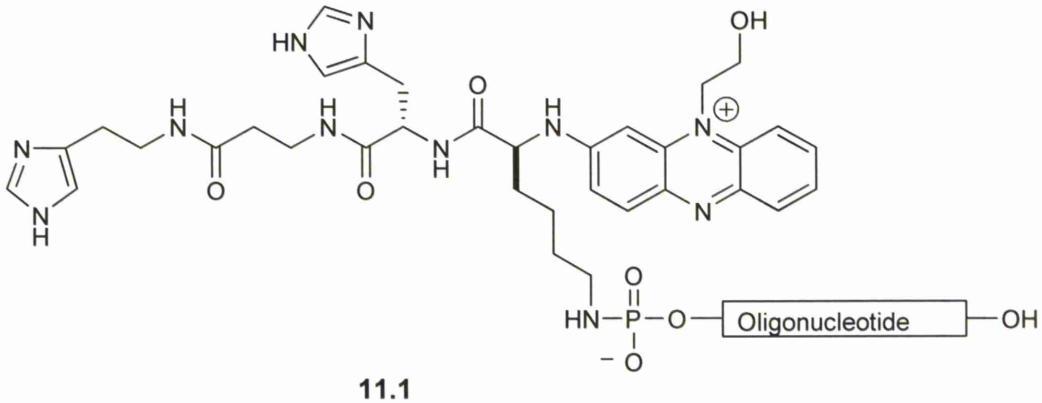

11.1

The free aliphatic ε- amine of **10.1** was coupled to the 5'-terminal phosphate group of pdGATCGAACACAGGACCT (17-mer) oligonucleotide via a phosphoramidate bond, using Godovikova's method, to yield **11.1** (22 %) [201].

2.3.10.1. Preparation of N-cetyl- N,N,N-trimethylammonium salts of oligonucleotides

Polyanionic oligonucleotides are highly insoluble in the organic solvents (*e.g.* DMSO or DMF) in which the coupling reactions are normally performed. To increase the solubility of the oligonucleotide it was converted to the *N*-cetyl-*N,N,N*-trimethylammonium salt as follows:

1. Oligonucleotide was dissolved in distilled water at a concentration of 200 ou_{260}/ml (*e.g.* dissolved 20 ou_{260} in 100 µl of water) and precipitated by the addition of 4 % aqueous *N*-cetyl-*N,N,N*-trimethylammonium bromide (CTAB) (10 µl) and centrifuged for 5 min at 10 000 rpm. The addition of 4 % CTAB (aq) (10 µl) followed by centrifugation was repeated several times until there was no apparent precipitation seen after the CTAB addition.

2. After oligonucleotide precipitation was complete, the supernatant was carefully removed, and the centrifuged pellet washed using 1 ml of water and lyophilised overnight for the following (conjugation) step.

2.3.10.2. Conjugation of (10.1) to 5'-terminal phosphate group of (N-cetyl-N,N,N-trimethylammonium salt of) 17-mer pdGATCGAACACAGGACCT oligonucleotide, via a phosphoramidate bond, using Godovikova's method [201]

1. The oligonucleotide *N*-cetyl-*N,N,N*-trimethylammonium salt (~ 0.12- 0.18 μmol, 20-30 ou_{260}) was completely dissolved (achieved by heating the reaction mixture up to 60-80 °C, followed by vigorous shaking when necessary) in the minimal volume of anhydrous DMSO (60 μl), then centrifuged (1 min, 10 000 rpm). (Optimal volume of DMSO for this amount of oligonucleotide was 60 μl).

2. The oligonucleotide was dissolved in DMSO (100 μl) then treated with an excess of the activating agents: 2,2'-dipyridyl disulfide (9.9 mg, 45 μmol) and triphenylphosphine (11.8 mg, 45 μmol) for 5 mins at room temperature, followed by treatment with dimethylaminopyridine (5.49 mg, 45 μmol) for another 5 mins.

3. The peptide construct **10.1** (1 mg) to be coupled to the oligonucleotide was separately prepared with approximately 4 μl of dry triethylamine in 60 μl DMSO and centrifuged (1 min, 10 000 rpm).

4. The peptide solution with **10.1** was transferred into the reaction mixture containing activated oligonucleotide and shaken vigorously followed by centrifugation (1 min, 10 000 rpm).

5. The reaction mixture was incubated at 40 °C overnight.

Fig 2.1. Mechanism of phosphoramidate formation (using Godovikova's method)

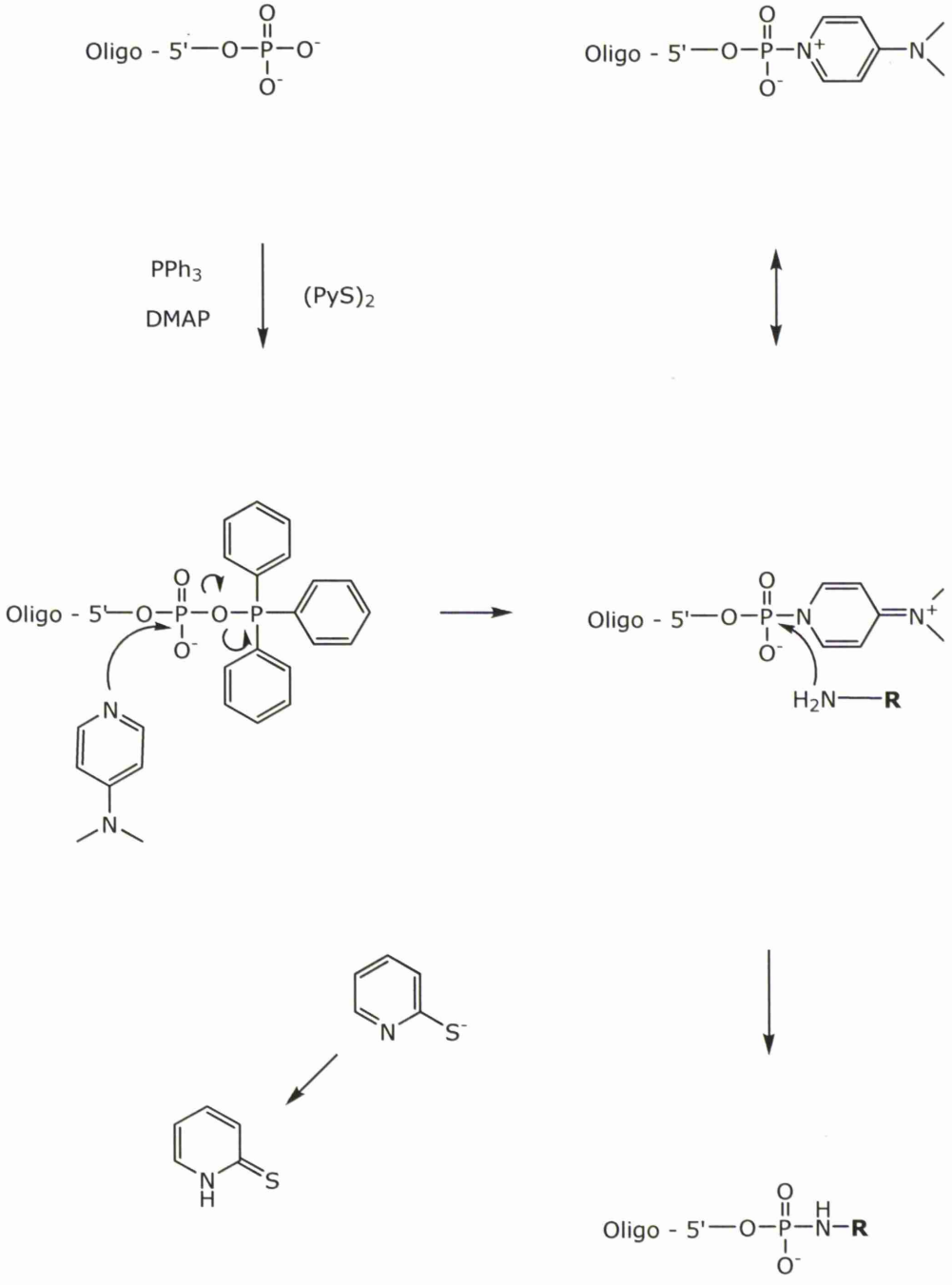

PPh_3 = triphenylphosphine

$(PyS)_2$ = 2, 2' -dipyridyl disulfide

DMAP = 4 -N', N' -Dimethylaminopyridine

2.3.10.3. Precipitation and purification of oligonucleotide after conjugation.

1. When the reaction was complete, the oligonucleotide-containing compounds were precipitated with 2 ml of 2 % $LiClO_4$ in acetone. This procedure converts oligonucleotide to the lithium salt form, thus reducing the solubility of oligonucleotides in the organic phase and resulting in oligonucleotide precipitation. To ensure complete oligonucleotide precipitation this mixture was stored at -25 ^oC for 2- 3 hours followed by centrifugation (5 min, 10 000 rpm). After centrifugation, the supernatant was removed and the oligonucleotide precipitate dried for 10- 15 minutes under atmospheric air to remove any acetone still present.

2. The dried oligonucleotide precipitate was re-dissolved in Milli-Q water (100 µl) and centrifuged to remove any activating agents still present. The supernatant containing oligonucleotide material was collected and the oligonucleotides were precipitated with 2 ml of 2 % $LiClO_4$ in acetone at -25 ^oC for 2- 3 hours followed by centrifugation (5 min, 10 000 rpm). The oligonucleotide precipitate was dried for 10- 15 minutes under atmospheric air to remove any acetone still present.

3. The dry oligonucleotide precipitate was re-dissolved in 500µl aqueous 1M $LiClO_4$ and the oligonucleotide conjugates were purified from non-reacted precursors by reverse-phase HPLC. Purification of the oligonucleotide conjugates was achieved using a linear gradient of acetonitrile (from 0 to 60%) in 0.05 M $LiClO_4$. The UV-visible detection during HPLC purification was at 260 nm (to monitor oligonucleotide components) and at 395 nm and 520 nm (to detect oligonucleotide derivatives with the covalently attached 10-hydroxyethyl-phenazinium group). Oligonucleotide conjugates are characterised by higher retention time (32 mins) compared to the starting (non-modified) oligonucleotide (30 mins).

HPLC solvent gradient: a mobile phase consisting of an increasing proportion with respect to time of component **B** in component **A**. Component **A** was 0.05 M $LiClO_4$ in *water : acetonitrile* (99 : 1) and component **B** was 0.05 M $LiClO_4$ in *water : acetonitrile* (1 : 99). Following a 5-minute wash with component **A** only, a typical (linear) gradient used to elute the conjugates was: 0-30% solvent A over 60 mins (0-10 % from 0 – 10 mins; 10 – 30% from 10- 60 minutes).

Fig 2.2. Chemical structure of 17-mer oligonucleotide conjugate **11.1**.

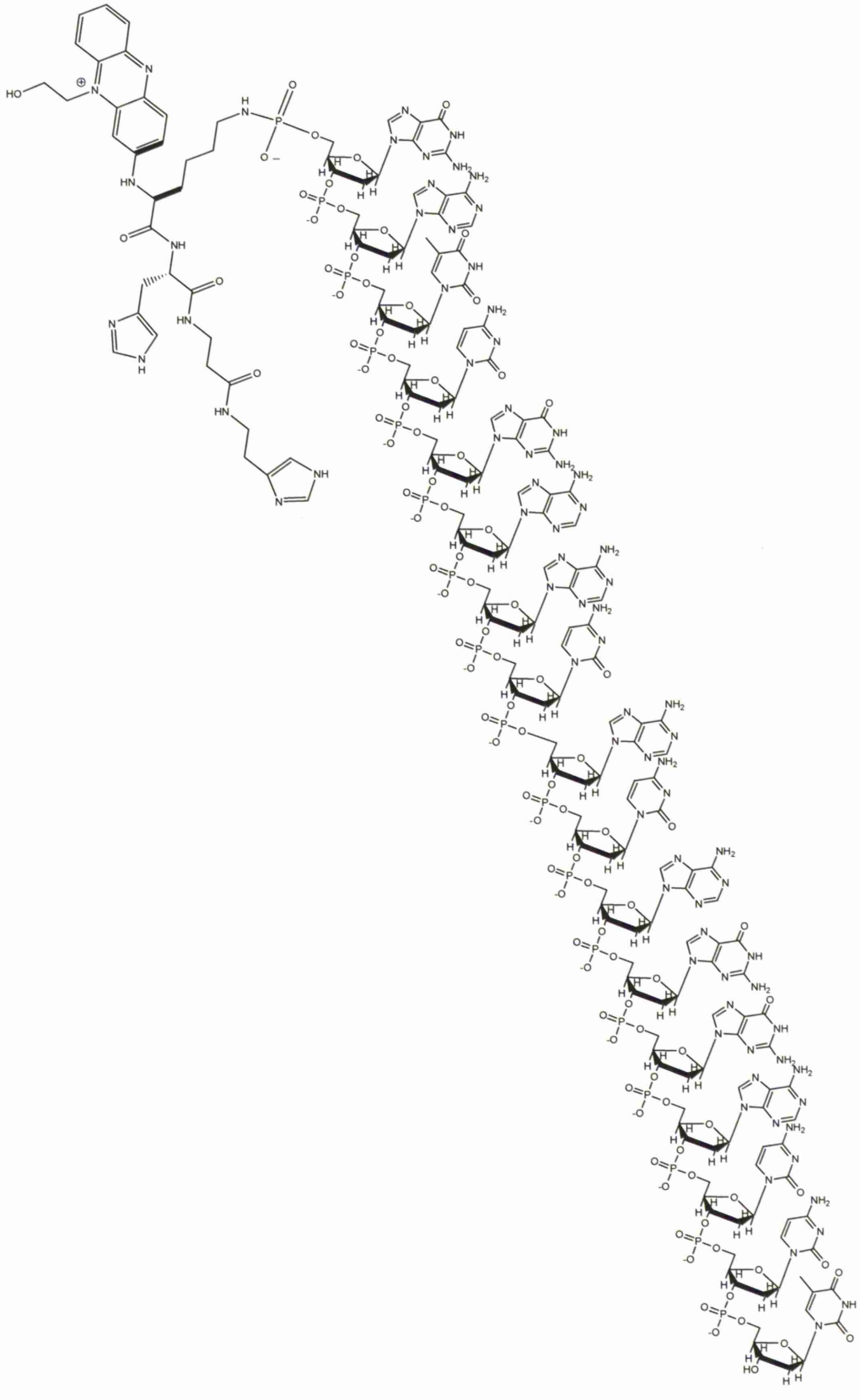

2.3.11. Synthesis of 17-mer oligonucleotide conjugate (9.2)

The free aliphatic α- amine of **8.1** was coupled to the 5'-terminal phosphate group of pdGATCGAACACAGGACCT (17-mer) oligonucleotide via a phosphoramidate bond, using Godovikova's method, to yield **9.2** (24 %) [201].

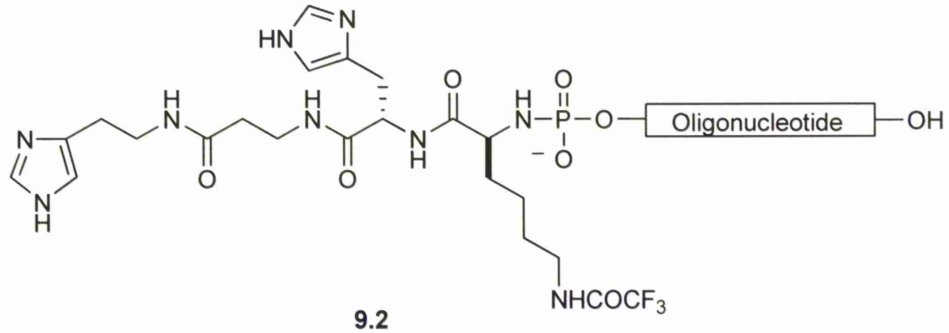

9.2

Synthesis of the oligonucleotide conjugate 9.2 was performed in the same manner as that of oligonucleotide conjugate 11.1 (see 2.3.10.1- 2.3.10.3 sections for full details of the conjugation process).

HPLC solvent gradient: a mobile phase consisting of an increasing proportion with respect to time of component **B** in component **A**. Component **A** was 0.05 M $LiClO_4$ in *water: acetonitrile* (99 : 1) and component **B** was 0.05 M $LiClO_4$ in *water : acetonitrile* (1 : 99). Following a 5 minute wash with component **A** only, a typical (linear) gradient used to elute the conjugates was: 0-30% solvent A over 60 mins (0-10 % from 0 – 10 mins; 10 – 30% from 10- 60 minutes).

2.3.12. Synthesis of oligonucleotide conjugate (10.2)

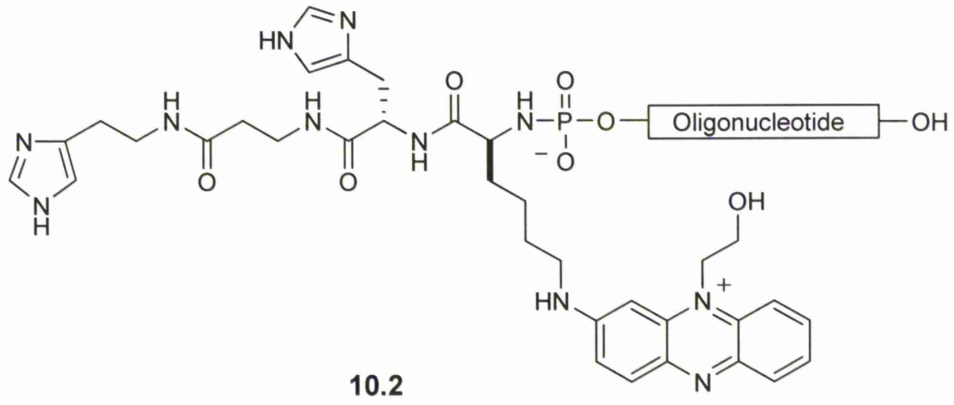

10.2

Deprotection of trifluoroacetyl (Tfa) protecting group with aqueous Na_2CO_3

A solution of 0.5 M Na_2CO_3 (aq) (0.2 ml) was added to **9.2** (~ 10 OU) and stirred at room temperature for 2 hours.

Phenazinium oxidative addition

10-(2-Hydroxyethyl)phenazinium chloride (13 mg; 0.1 M) was added with 0.3 ml of water to make a 0.2 M Na_2CO_3 (aq) solution and stirred at RT for 10 mins. The expected product **10.2** was precipitated with 2 % $LiClO_4$ in acetone and air dried before HPLC purification (yield: 61 %).

HPLC solvent gradient: a mobile phase consisting of an increasing proportion with respect to time of component **B** in component **A**. Component **A** was 0.05 M $LiClO_4$ in *water: acetonitrile* (99: 1) and component **B** was 0.05 M $LiClO_4$ in *water: acetonitrile* (1: 99). Following a 5-minute wash with component **A** only, a typical (linear) gradient used to elute the conjugates was: 0-30% solvent A over 60 mins (0-10 % from 0 – 10 mins; 10 – 30% from 10- 60 minutes).

Fig 2.3. Chemical structure of 17-mer oligonucleotide conjugate **10.2.**

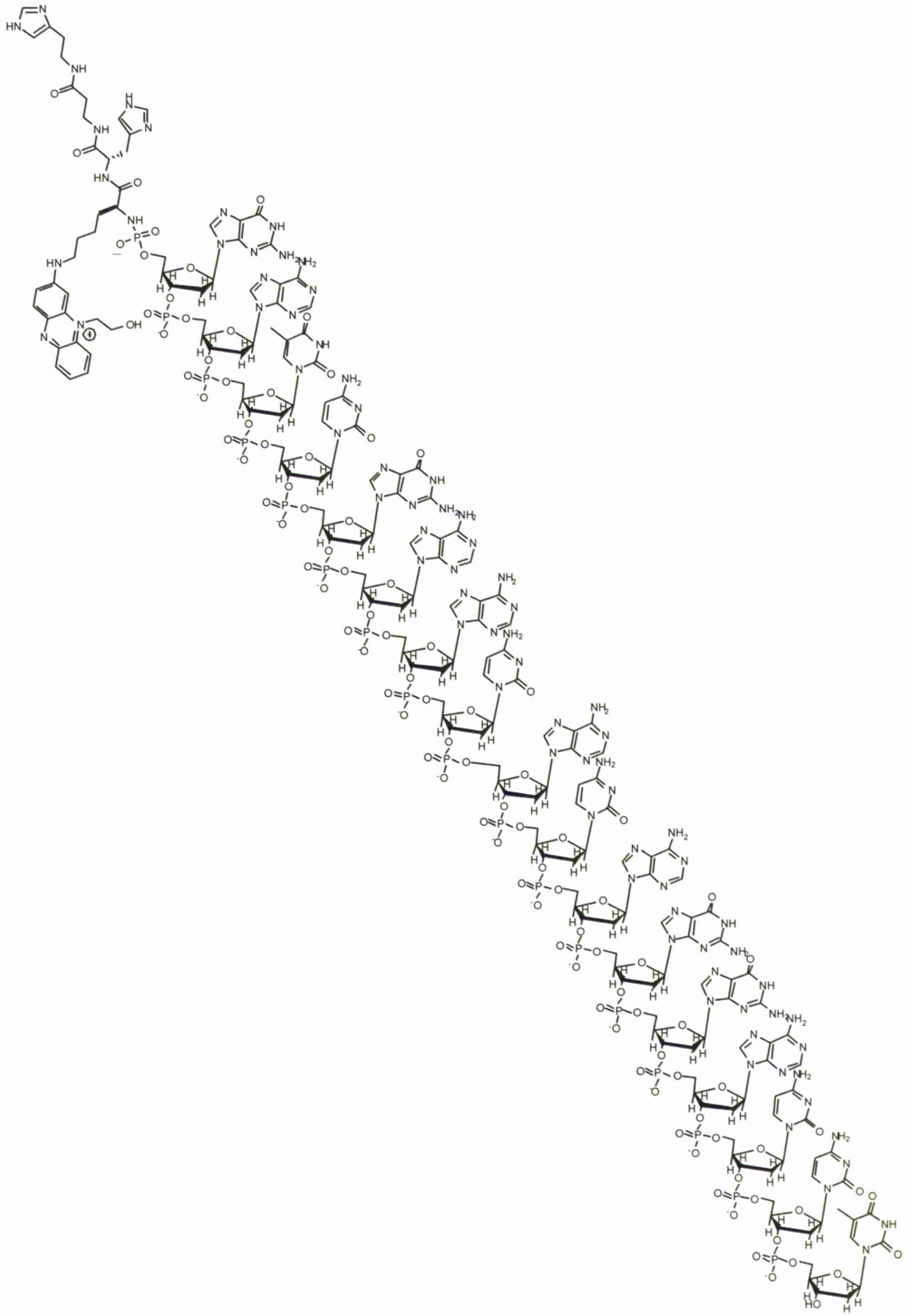

2.3.13. Synthesis of 2-(tert-butoxycarbonylamino)-6-(9*H*-fluoren-9-ylmethoxycarbonylamino)-hexanoic acid succinimide ester (Boc-Lys-(Fmoc)-OSu)

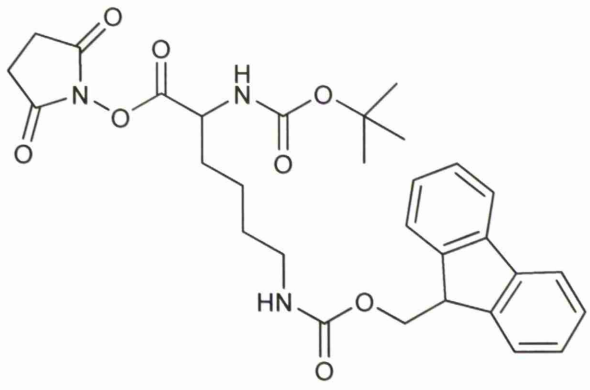

Boc-Lys-(Fmoc)-OSu

Boc-Lys-(Fmoc)-OH (5 g; 1 eq; 10.7 mmol) was added to NHS (1.48 g; 1.1 eq; 13 mmol) in anhydrous EtOAc (60 ml) with DCC (2.68 g; 1.1 eq; 13 mmol) and stirred for 1 hr at 0 °C and then at 25 °C for 1 hr. The product mixture was filtered and washed with EtOAc. The filtrate was evaporated and then heated at reflux in EtOAc for 10 mins and then allowed to cool for crystallisation. Crystals were filtered and discarded to leave filtrate which was evaporated *in vacuo* to yield a white, solid residue (yield 46 %).

2.3.14. Synthesis of 3-{(*S*)-2-[(*S*)-2-tert-butoxycarbonylamino-6-(9*H*-fluoren-9-ylmethoxycarbonylamino)-hexanoyl]-amino-3-(1-tert-butoxycarbonyl-1*H*-imidazol-4-yl)-propionyl}-amino-N-[2-(1-tert-butoxycarbonyl-1*H*-imidazol-4-yl)-ethyl]-propionamide (7.3)

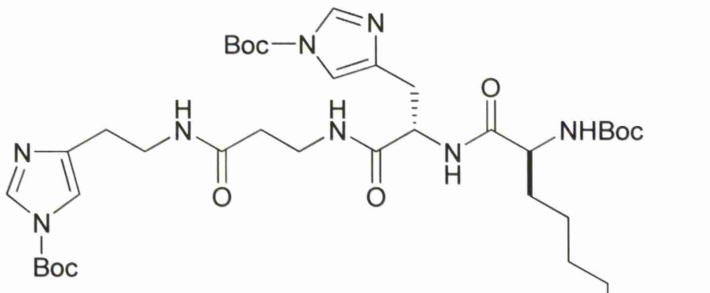

7.3

THF and methanol (3:1 v/v, 4 ml) were added to (**6**) (0.7 g; 2.19 mmol; 1 eq) and Boc-lys-(Fmoc)-OSu (1.48 g; 2.62 mmol; 1.2 eq) followed by NMM (0.71 ml; 3 eq) and the reaction mixture stirred for 24 hours. The reaction mixture was monitored by TLC until the active ester disappeared. Boc_2O (2.12 g; 4.38 mmol; 2 eq;) was then added and the mixture stirred for 2 hrs.

The solvent from the reaction mixture was evaporated *in vacuo*. EtOAc (6 ml) was added, followed by the dropwise addition of methanol untill dissolution, and then heated at reflux for 10 minutes. The reaction mixture was allowed to cool to room temperature, then stored at -20 °C for 1 hour. Insoluble impurities were discarded. The soluble product mixture was extracted using $NaHCO_3$ and $CHCl_3$. Solvent from organic phase was removed *in vacuo* to yield a light brown gum (yield 54 %).

2.3.15. Synthesis of 3-{(S)-2-[(S)-2-amino-6-(9H-fluoren-9-ylmethoxycarbonylamino)-hexanoyl]-amino-3-(1H-imidazol-4-yl)-propionyl}-amino-N-[2-(1H-imidazol-4-yl)-ethyl]-propionamide trifluoroacetate (8.3)

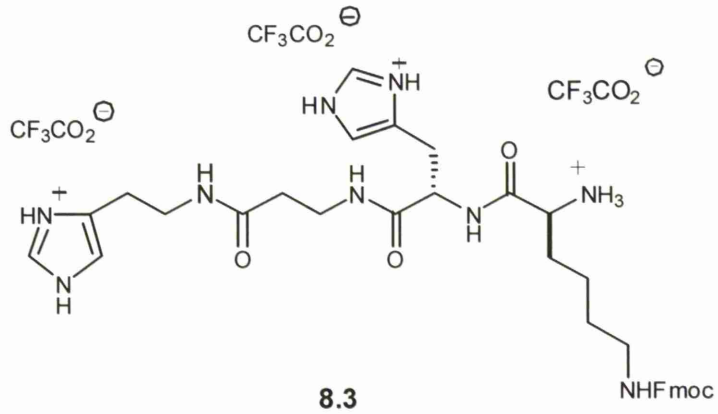

8.3

Deprotection of Boc groups

A solution of 50 % (v/v) CF_3CO_2H in DCM (1 ml) was added to **7.3** (115 mg; 0.12 mmol) and the mixture stirred for 30 minutes at RT and monitored by TLC. The reaction mixture was washed with DCM, with ethanol and then with toluene. The solvent was evaporated *in vacuo* overnight (yield: 97 %).

2.3.16. Synthesis of 17-mer oligonucleotide conjugate (9.3)

The free aliphatic amine of **8.3** was coupled to the 5'-terminal phosphate group of pdGATCGAACACAGGACCT (17-mer) oligonucleotide via a phosphoramidate bond, using Godovikova's method, to yield **9.3** (27 %) [201].

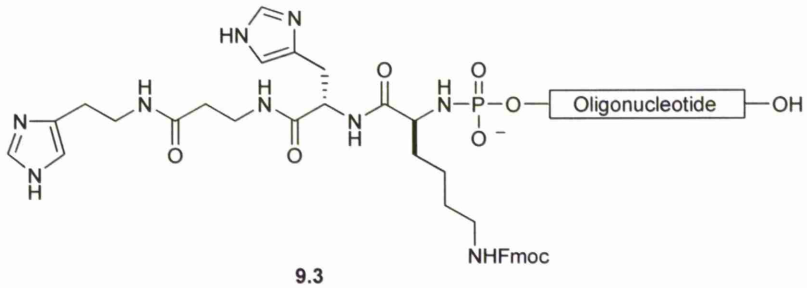

9.3

Synthesis of the oligonucleotide conjugate 9.3 was performed in the same manner as that of oligonucleotide conjugate 11.1, (see 2.3.10.1- 2.3.10.3 sections for full details of the conjugation process).

Oligonucleotide conjugates are characterised by higher retention time compared to the starting (non-modified) oligonucleotide.

HPLC solvent gradient: a mobile phase consisting of an increasing proportion with respect to time of component **B** in component **A**. Component **A** was 0.05 M $LiClO_4$ in *water : acetonitrile* (99 : 1) and component **B** was 0.05 M $LiClO_4$ in *water : acetonitrile* (1 : 99). Following a 5-minute wash with component **A** only, a typical (linear) gradient used to elute the conjugates was: 0-30% Solvent A over 60 mins: 0-10 % from 0 – 10 mins; 10 – 30% from 10- 60 mins.

2.3.17. Synthesis of oligonucleotide conjugate (10.3)

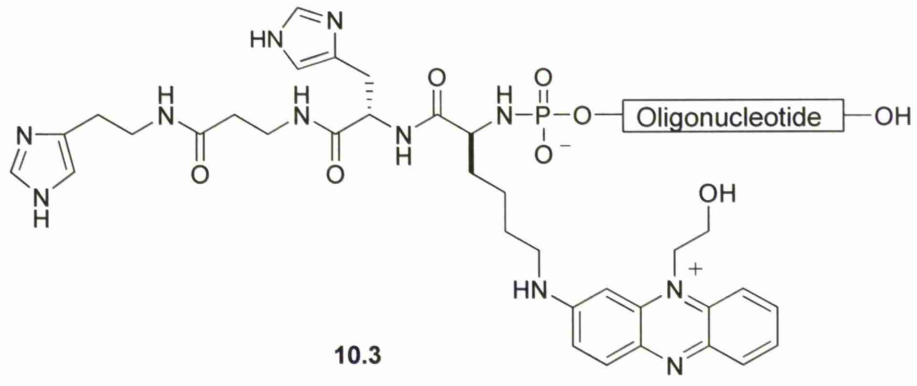

10.3

Fmoc deprotection

Compound **9.3** (~ 10 OD) was dissolved in 0.5 ml of 28 % ammonium hydroxide (aq) and the solution stirred for 12 hrs at RT.

The reaction mixture was centrifuged and the supernatant was decanted and retained to discard any precipitated dibenzofulvene. The supernatant was evaporated and dried *in vacuo* (to remove aqueous ammonia) before adding 100 µl of water followed by 1.8 ml of 2 % $LiClO_4$ in acetone to convert the oligonucleotide conjugate to its Li^{2+} salt form for precipitation (and further remove any traces of aqueous ammonia). The supernatant was discarded and the precipitate dried (yield: 70 %).

Phenazinium oxidative addition

10-(2-Hydroxyethyl)phenazinium chloride (13 mg; 0.1 M) in 0.2 M Na_2CO_3 (aq) (0.5 ml) was added to the dry precipitate and the mixture stirred at RT for 10 minutes. The reaction mixture was precipitated using 2 ml of 2 % $LiClO_4$ in acetone and dried before HPLC purification (yield: 76 %).

HPLC solvent gradient: a mobile phase consisting of an increasing proportion with respect to time of component **B** in component **A**. Component **A** was 0.05 M $LiClO_4$ in *water: acetonitrile* (99: 1) and component **B** was 0.05 M $LiClO_4$ in *water: acetonitrile* (1: 99). Following a 5-minute wash with component **A** only, a typical (linear) gradient used to elute the conjugates was: 0- 30% solvent A over 60 mins (0- 10 % from 0 – 10 mins; 10 – 30 % from 10- 60 mins).

2.3.18. Synthesis of 2-(9*H*-Fluoren-9-ylmethoxycarbonylamino)-6-(diphenyl-p-tolyl-methylamino)-hexanoic acid succinimide ester (Fmoc-Lys-(Mtt)-OSu)

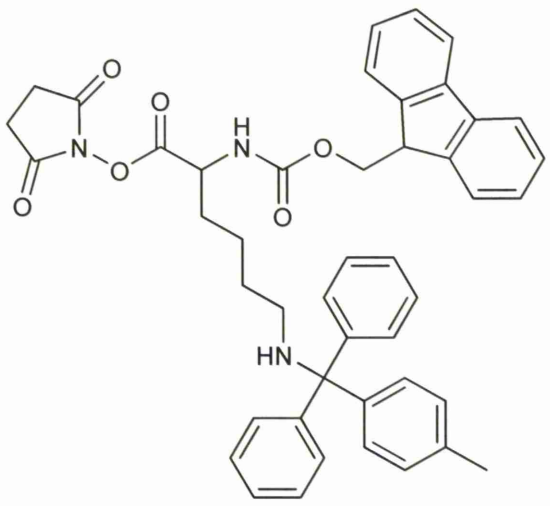

Fmoc-Lys-(Mtt)-OSu

Fmoc-Lys-(Mtt)-OH (5 g; 1 eq; 8 mmol) was added to NHS (1.01 g; 1.1 eq; 9 mmol) in anhydrous EtOAc (60 ml) with DCC (1.82 g; 1.1 eq; 9 mmol) and stirred for 1 hr at 0 °C and then at 25 °C for 1 hr. The reaction mixture was filtered and washed with EtOAc. The filtrate was evaporated and then heated at reflux in EtOAc for 10 mins and then allowed to cool for crystallisation. Crystals were filtered and discarded to leave the filtrate which was evaporated *in vacuo* to yield a yellow, viscous, translucent gum, then a white foam (yield: 53 %).

2.3.19. Synthesis of 3-{(*S*)-2-[(*S*)-2-(9*H*-fluoren-9-ylmethoxycarbonyl)-amino-6-(diphenyl-p-tolyl-methylamino)-hexanoyl]-amino-3-(1-tert-butoxycarbonyl-1*H*-imidazol-4-yl)-propionyl}-amino-N-[2-(1-tert-butoxycarbonyl-1*H*-imidazol-4-yl)-ethyl]-propionamide (7.4).

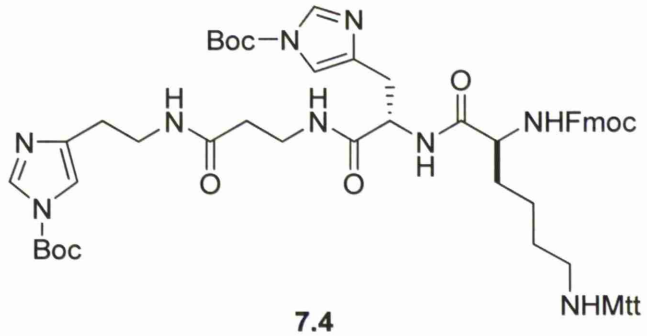

7.4

THF and methanol (3:1 v/v) was added to **6** (0.73 g; 2.27 mol; 1 eq) and Fmoc-lys-(Mtt)-OSu (1.96 g; 2.72 mol; 1.2 eq) followed by NMM (0.73 ml; 3 eq) and the mixture stirred for 24 hours. The reaction mixture was monitored by TLC untill the active ester disappeared and then Boc_2O (0.99 g; 2 eq) was added and stirred overnight.

The solvents were evaporated *in vacuo* and the product was then extracted using $NaHCO_3$ and $CHCl_3$. Organic fractions were combined and solvent removed *in vacuo*. The product was purified by column chromatography using 50 % hexane/diethyl ether (200 ml) to elute more hydrophobic impurities and 15 % MeOH, 85 % $CHCl_3$ (100 ml) to elute the remaining desired **7.4** (yield: 36 %).

2.3.20. Synthesis of 3-{(*S*)-2-[(*S*)-2-(9*H*-fluoren-9-ylmethoxycarbonyl)-amino-6-aminohexanoyl]-amino-3-(1*H*-imidazol-4-yl)-propionyl}-amino-N-[2-(1*H*-imidazol-4-yl)-ethyl]-propionamide tris-(trifluoroacetate) (8.4b)

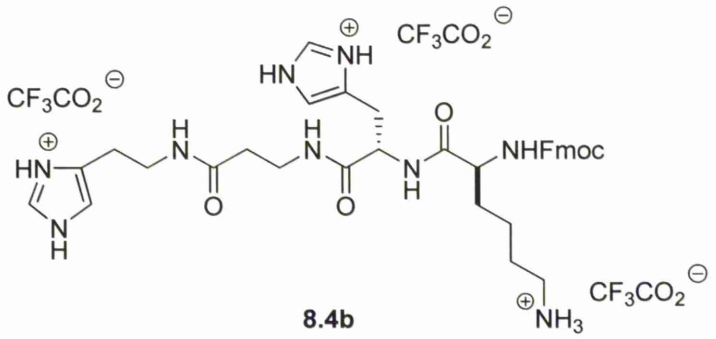

8.4b

Deprotection of Mtt and Boc groups

A portion of 50 % CF_3CO_2H in DCM (9.5 ml) was added to **7.4** (0.2 g; 0.229 mmol) with 5 % TES (0.5 ml), and the solution stirred for 2 hrs and monitored by TLC. Solvent was evaporated *in vacuo* and the product purified by HPLC (yield 72 %)

HPLC solvent A (0.1 % TFA in MeCN) and solvent B (0.1 % TFA in H_20).
HPLC solvent gradient: (0-50% A over 50 mins: 0-10 % A from 0 – 10 mins; 10 – 50 % MeCN from 10- 50 mins).

2.3.21. Synthesis of 17-mer oligonucleotide conjugate (9.4b)

The free aliphatic amine of **8.4b** was coupled to the 5'-terminal phosphate group of pdGATCGAACACAGGACCT (17-mer) oligonucleotide via a phosphoramidate bond using Godovikova's method (31 %) [201].

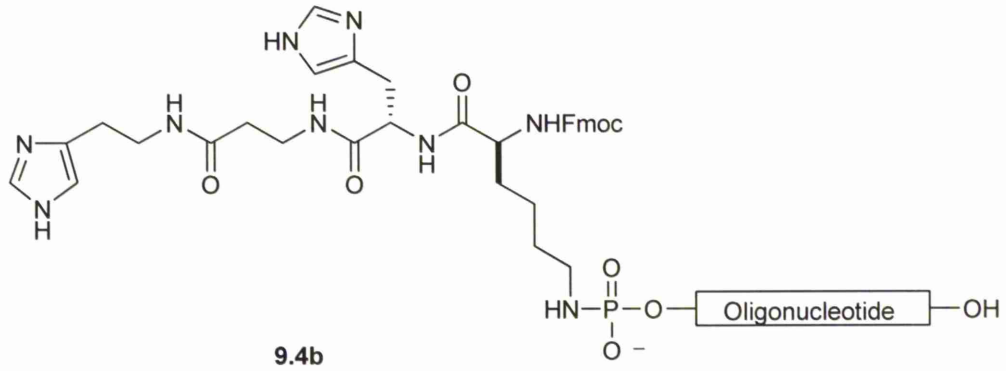

9.4b

Synthesis of the oligonucleotide conjugate **9.4b** was performed in the same manner as that of oligonucleotide conjugate **11.1** (see **2.3.10.1- 2.3.10.3** sections for full details of the conjugation protocol).

HPLC solvent gradient: a mobile phase consisting of an increasing proportion with respect to time of component **B** in component **A**. Component **A** was 0.05 M $LiClO_4$ in *water: acetonitrile* (99: 1) and component **B** was 0.05 M $LiClO_4$ in *water: acetonitrile* (1 : 99). Following a 5-minute wash with component **A** only, a typical (linear) gradient used to elute the conjugates was: 0-30% solvent A over 60 mins (0-10 % from 0 – 10 mins; 10 – 30 % from 10- 60 minutes).

Retention time: 34.2- 34.6 minutes.

Free oligonucleotide retention time: 30 minutes.

2.3.22. Synthesis of oligonucleotide conjugate (10.4)

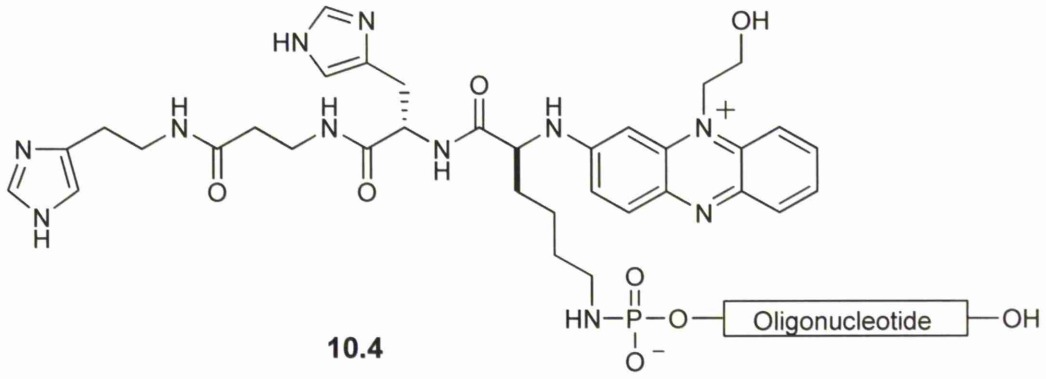

10.4

Fmoc deprotection

Compound **9.4b** (~ 10 OD) was dissolved in 0.5 ml of 28 % ammonium hydroxide (aq) (ammonia water) and stirred for 12 hrs at RT.
The reaction mixture was centrifuged and supernatant was decanted to remove the precipitated insoluble side product dibenzofulvene. The supernatant was evaporated and dried *in vacuo* (to remove ammonia water) before adding 100 µl of water followed by 1.8 ml of 2 % $LiClO_4$ in acetone to convert oligonucleotide conjugate to its Li^{2+} salt form for precipitation (and further remove any traces of ammonia water). The supernatant was discarded and the precipitate dried.

Phenazinium oxidative addition

10-(2-Hydroxyethyl)phenazinium chloride (13 mg; 0.1 M) in 0.2 M Na_2CO_3 (aq) (0.5 ml) was added to the dry precipitate and stirred at RT for 10 minutes. Precipitated with 2 % $LiClO_4$ in acetone and dried before HPLC purification (yield 62 %).

HPLC solvent gradient: a mobile phase consisting of an increasing proportion with respect to time of component **B** in component **A**. Component **A** was 0.05 M $LiClO_4$ in *water : acetonitrile* (99 : 1) and component **B** was 0.05 M $LiClO_4$ in *water : acetonitrile* (1 : 99). Following a 5-minute wash with component **A** only, a typical (linear) gradient used to elute the conjugates was: 0-30% solvent A over 60 mins (0-10 % from 0 – 10 mins; 10 – 30% from 10- 60 minutes).

2.3.23. Synthesis of *N*-(2-Hydroxyethyl)phenazinium Chloride

Ethylene oxide (50 ml)(DANGER: highly inflammable and toxic by inhalation, ingestion and through skin contact) was added dropwise to a solution of phenazinium chloride (10 g; 44 mmol) in 100 ml glacial acetic acid at 10 °C. After 6 days of incubation in a closed flask at 20 °C, 10 ml of concentrated HCl was added and the reaction mixture was evaporated *in vacuo*. The dark brown gum was treated twice with a mixture of toluene-heptane (1:1) and evaporated. Diethyl ether was added to form a suspension and to precipitate the product over 12 hr. The precipitate was washed and filtered using acetone and diethyl ether (yield: 57 %).

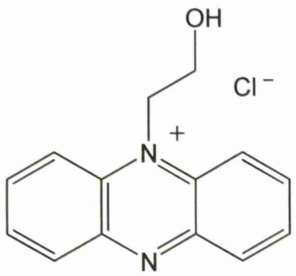

N-(2-Hydroxyethyl)phenazinium Chloride

3. Results and Discussion

3.1. Chemical Synthesis

3.1.1. Molecular design and synthetic strategy

This thesis presents the rational design, synthesis and study of *sequence-specific* oligonucleotide-based artificial ribonucleases incorporating the three major structural elements: recognition domain, cleaving construct and anchor group.

The antisense oligonucleotide used to deliver the catalytic groups to a specific target single-stranded RNA sequence *via* Watson-Crick hydrogen bonding is the specific antisense recognition domain. A hydrolytically active *bis*-imidazole group known to have ribonuclease activity [25] represents the cleaving domain. The third domain is an *N*-hydroxyethylphenazinium anchor group, which was incorporated with the aim to increase the binding association and stability of the complex formed with RNA.

Sequence specificity of studied artificial ribonucleases was attained by a specifically designed 17-mer oligonucleotide (5′-pdGATCGAACACAGGACCT), which was complementary to the region (44–60 nt) of the TΨC loop of yeast $tRNA^{Phe}$. This 17-mer oligonucleotide would be responsible for delivering both anchor group and hydrolytically active imidazole rings to the selected region of the $tRNA^{Phe}$ structure, when these groups are covalently attached to the terminal 5′-phosphate of the oligonucleotide fragment.

The cleaving domain used consisted of a tripeptide with two catalytically active imidazole rings (Figure 3.1). This structure has already been shown to provide substantial ribonuclease activity when conjugated to an intercalator [26, 202] or to an oligonucleotide moiety through a suitable linker [25].

Figure 3.1. Schematic representation of the *bis*-imidazole cleaving domain of the artificial ribonucleases designed and studied. **R** may represent various substituents, according to references [25, 26].

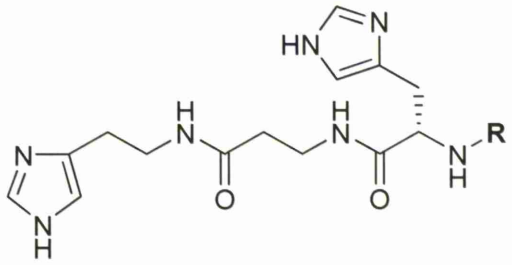

The function of the *N*-(2-hydroxyethyl)-phenazinium anchor group is to increase the affinity of the designed artificial ribonucleases to the RNA target and improve stability of the corresponding *RNA:DNA* hybrid. This may (potentially) enhance the probability of the cleaving group(s) being located near the RNA cleavage site and thus improve their hydrolytic performance [203-208]. In the structures designed, the *N*-(2-hydroxyethyl)-phenazinium group was connected either proximally to the cleaving domain (*via* conjugation with the α-amino group of lysine residue) or remote from the cleaving domain (*via* conjugation with the ε-amino group of lysine residue, see Figure 3.2).

Figure 3.2. Schematic representation of the tetra-peptide cleaving construct showing α-amino group and ε-amino group of the lysine residue (indicated by arrows) available for conjugation with either the oligonucleotide recognition domain or with an *N*-hydroxyethylphenazinium anchor group.

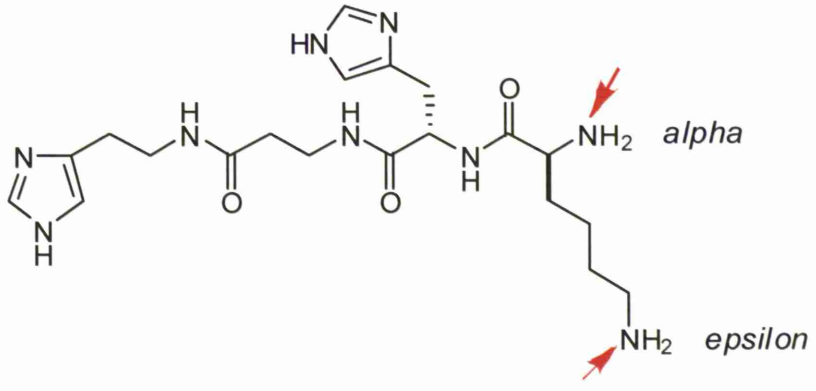

The aim of the *synthetic part* of the presented research was to obtain *bis*-imidazole cleaving constructs containing *N*-(2-hydroxyethyl)-phenazinium anchors that differed in the dispositions of the phenazinium anchor group and the oligonucleotide recognition element relative to tetra-peptide cleaving construct. The synthetic strategy was based on standard peptide chemistry [209]. Synthetic routes for the preparation of conjugates **10.2**, **10.3**, **10.4** and **11.1** and their precursors are summarised in Figures 1.24– 1.30.

The additional aim of this part of work was to contrast different synthetic strategies and identify synthetic route(s) with the most appropriate balance between robustness, simplicity, efficiency (in terms of final reaction yield) and cost-efficiency (in terms of time and resources spent).

The synthetic strategy to construct these AR constructs was based on the successive nucleophilic addition elimination reactions of activated (pentafluorophenyl and *N*-hydroxysuccinimide) esters of the necessary amino acids to form the desired cleaving (tripeptide) construct **6**, bearing two hydrolytically-active imidazole rings. In the following stage this tripeptide construct, **6**, was reacted with one of various *bis*-protected lysine amino acids, each containing a different combination of orthogonal protecting groups (Boc, Fmoc, TFA, Cbz or Mtt) at the α and ε- amino groups of the lysine (linker) residue. The resulting tetrapeptide structures (**7.1, 7.3, 7.4**) were deprotected in specific conditions (see Figures 1.24– 1.30) leaving either the ε-amino group or α-amino group of lysine residue available to be conjugated to either *N*-(2-hydroxyethyl)-phenazinium (Figures 1.25, 1.26) or the oligonucleotide recognition element (Figures 1.27, 1.28, 1.29, 1.30). This was followed by the final modification step to produce conjugates **10.2**, **10.3**, **10.4**, and **11.1** (Figures 1.25 – 1.30). Characterization of constructs **10.2**, **10.3**, **10.4**, and **11.1** as well as all intermediates were performed by NMR spectroscopy, IR, mass spectrometry and elemental analysis. ^{1}H and ^{13}C NMR signal assignment was carried out by using a series of ^{1}H, ^{13}C, DEPT135, COSY NMR experiments (using Bruker Avance 300 MHz, 400 MHz and 500 MHz instruments).

3.2. Characterisation of Synthetic Intermediates

3.2.1. Characterisation of 3-tert-Butoxycarbonylamino-propionic acid pentafluorophenyl ester (2)

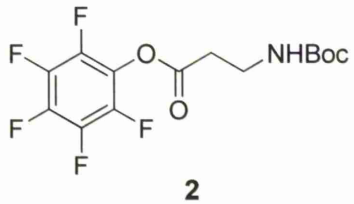

2

^{1}H-NMR (300 MHz, [d_4]-MeOD): δ_H 1.44 (s, 9H, CH_3), 2.92 (t, *J*= 6.5 Hz, 2H, CH_2), 3.43 (t, *J*= 6.5 Hz, 2H, CH_2).

^{1}H-NMR (300 MHz, [d_6]-DMSO): δ_H 1.38 (s, 9H, CH_3), 3.31-3.28 (m, 4H, CH_2) 7.02 (1H, -NH).

^{13}C NMR (75 MHz, [d_4]-MeOD): δ_C 27.73 (CH_3), 34.48 (CH_2), 37.09 (CH_2).

Quaternary carbons: δ_C 80.72, 126.78, 137.99, 141.31, 144.64, 158.36, 169.29.

NMR data do not incorporate ^{13}C-^{19}F coupling asignments.

^{19}F-NMR (282 MHz, [d_4]-MeOD): δ_F -155.73 - 155.79 (d, *J*= 17.5 Hz, 1F, Ar-F), -161.78 - 161.93 (t, *J* = 20.7 Hz, 2F, Ar-F), 166.19 - 166.32 (t, *J*= 19.6 Hz, 2F, Ar-F).

$C_{14}H_{14}N_1O_4F_5$ monoisotopic mass requires 355.08428

MS (ES$^+$) *m/z* 378.1 ([M+Na]$^+$, 50%).

MS (Accurate mass) *m/z* 378.0741 ([M+Na]$^+$, 30%).

378.0741- 22.9898= 355.0843

Elemental analysis (CHN):

$C_{14}H_{14}N_1O_4F_5$ requires: C, 47.33; H, 3.97; N, 3.94; O, 18.01%

Found: C, 47.36; H, 3.95; N, 3.99%.

V_{max}/cm^{-1} 3383 (N-H amide stretch), 2992 (CH), 1784 (C=O ester stretch), 1682 (C=O stretch of the amide group), 1518 (aromatic C=C stretch), 1092 (C-O), 989 (C-O).

Presence of two carbonyls (one carbamate (Boc) and one ester)

TLC: R_f = 0.77 (5% MeOH, $CHCl_3$).

m.p: 48-50°C (from hexane), white crystals.

Yield: 97 %

3.2.2. Characterisation of {2-[2-(1H-Imidazol-4-yl)-ethylcarbamoyl]-ethyl}-carbamic acid tert-butyl ester (3).

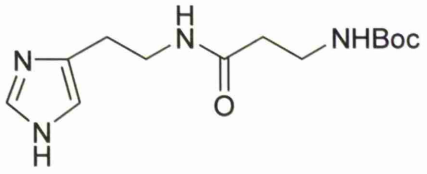

3

^{1}H-NMR (300 MHz, [d_4]-MeOD): δ_H 1.43 (s, 9H, C $(CH_3)_3$), 2.34 (t, *J*= 6.6 Hz, 2H, CH_2), 2.81 (t, *J*= 6.6 Hz, 2H, CH_2), 3.28 (t, *J*= 6.6 Hz, 2H, CH_2), 3.43 (t, *J*= 6.6 Hz, 2H, CH_2), 6.98 (s, 1H, Ar-H, imidazole: H-32), 7.91 (s, 1H, Ar-H, imidazole: H-33).

^{13}C NMR (75 MHz, [d_4]-MeOD): δ_C 28.76 (CH_3), 30.73 (CH_2), 37.37 (CH_2), 38.10 (CH_2), 40.13 (CH_2), 117.86 (imidazole- C-32-H), 135.74 (imidazole- C-33-H) Quaternary carbons: δ_C 68.90 (C $(CH_3)_3$) 135.14 (imidazole: C), 158.37 (R_2**C**=O), 173.98 (R_2**C**=O).

$C_{13}H_{22}N_4O_3$ monoisotopic mass requires 282.1692
MS (ES^+) *m/z* 283.2 ($[M+H]^+$, 100%). $C_{13}H_{22}N_4O_3$ average mass: 282.3427
MS (Accurate mass) *m/z* 283.1767 ($[M+H]^+$, 100%).
283.1767- 1.0078= 282.1689

Elemental analysis (CHN):

$C_{13}H_{22}N_4O_3$ requires: C, 55.30; H, 7.85; N, 19.84%; O, 17.00.

Found: C, 44.40; H, 7.41; N, 15.35

The presence of 1 H_2O (1 water of hydration) $C_{13}H_{24}N_4O_4$ and traces of HCl (1.53) and THF (C_4H_8O; 0.12) gives C, 44.40; H, 7.32; N, 15.35.

Presence of two carbonyls (one amide and one carbamate (Boc)):

V_{max}/cm^{-1} 3375 (N-H amide stretch), 3128 (=C-H aromatic), 3025 (=C-H aromatic), 1674 (C=O stretch of the amide), 1641 (C=O stretch of the carbamate), 1150 (C-O strech).

UV-visible spectroscopy: λ_{max}: 210 nm (ε_{210}= 4.23 $mM^{-1}cm^{-1}$) (solvent: methanol).

TLC: R_f = 0.45 (5% MeOH, $CHCl_3$).

m.p. 130 - 132°C (from EtOAc) off-white crystals.

Yield: 93 %.

3.2.3. Characterisation of 3-Amino-N-[2-(1H-imidazol-4-yl)-ethyl]-propionamide dihydrochloride (4)

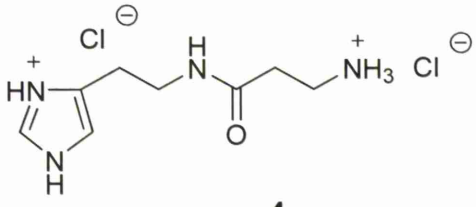

4

^{1}H-NMR (300 MHz, [d_4]-MeOD): δ_H 2.63 (m, 2H, CH_2-27), 2.94 (m, J = 6.8 Hz 2H, CH_2-30), 3.19 (m, 2H, CH_2-26), 3.52 (m, 2H, CH_2-29), 7.43 (s, 1H, Ar-H, imidazole: H-32), 8.86 (s, 1H, Ar-H, imidazole: H-33).

^{13}C NMR and CDEPT (75 MHz, [d_4]-MeOD): δ_C 25.71 (CH_2-27), 32.85 (CH_2-30), 37.08 (CH_2-26), 39.15 (CH_2-29), 117.67 (imidazole-C-32-H), 134.96 (imidazole-C-33-H).

Quaternary carbons: δ_C 132.85 (imidazole- C-31), 172.42 (R<u>C</u>=ONHR'-28).

$C_8H_{14}N_4O$ monoisotopic mass requires 182.1168

MS (ES^+) *m/z* 183.1 ($[M+H]^+$, 100%).

MS (Accurate mass) *m/z* 183.1247 ($[M+H]^+$, 100%).

182.11675 – 1.0078 = 182.1089

($C_8H_{14}N_4O$ average mass is 182.2254)

Elemental analysis (CHN):

$C_8H_{14}N_4O$ requires: C, 52.73; H, 7.74; N, 30.75; O, 8.78%.

Found: C, 35.81; H, 7.36; N, 17.62%.

The presence of 2 HCl and 1 H_2O ($C_8H_{18}N_4O_2Cl_2$) with small impurities of 1,4-dioxane ($C_4H_8O_2$; 0.07) and methanol (CH_3OH; 1.22) gives C, 35.81; H, 7.42; N, 17.62.

V_{max}/cm^{-1} 3391, 3385, 3379 (N-H amide stretch and overlapping N-H stretch of primary NH_2), 3249 (N-H aromatic), 1617 (C=O amide stretch).

UV-visible spectroscopy: λ_{max}: 209 nm (ε_{209}= 2.58 $mM^{-1}cm^{-1}$) (solvent: methanol).

TLC: R_f = 0.11 (n-BuOH, H_2O, AcOH (3:2:1)).

m.p. 60-64°C (chloride salt from 1,4- dioxane) cream coloured crystals.

Yield: 97 %.

3.2.4. Characterisation of 3-[(S)-2-tert-butoxycarbonylamino-3-(1-tert-butoxycarbonyl-1H-imidazol-4-yl)-propionyl]-amino-N-[2-(1-tert-butoxycarbonyl-1H-imidazol-4-yl)-ethyl]-propionamide (5)

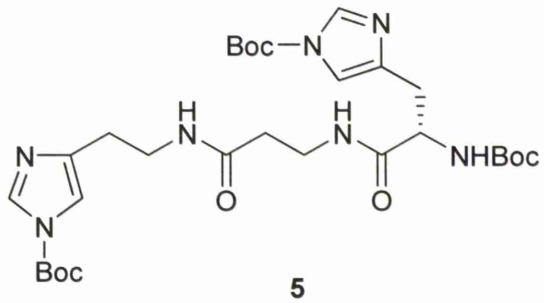

5

^{1}H-NMR (300 MHz, [d_4]-MeOD): δ_H 1.38 (bs, 9H, CH_3), 1.61- 1.63 (bs, 18H, 2x $(CH_3)_3$), 2.34 (m, 2H, CH_2-27), 2.72 (m, 2H, CH_2-30), 2.76 (m, 2H, CH_2-21), 3.29 (m, 2H, CH_2-26), 3.45 (m, 2H, CH_2-29), 4.20- 4.29 (m, 1H, C<u>H</u>, H-20), 6.81 (s, 1H, imidazole-H-32), 6.85 (s, 1H, imidazole-H-23), 8.11 (s, 1H, imidazole-H-33), 8.12 (s, 1H, imidazole-H-24).

^{13}C NMR and CDEPT (75 MHz, [d_4]-MeOD): δ_C 28.02 (6xCH_3), 28.86 (3xCH_3), 31.67 (CH_2-27), 34.78 (CH_2-30), 39.98 (CH_2-21), 40.82 (CH_2-26), 55.62 (CH_2-29), 136.07 (imidazole-<u>C</u>-32-H), 136.22 (imidazole-<u>C</u>-23-H), 140.06 (imidazole-<u>C</u>-33-H), 141.77 (imidazole-<u>C</u>-24-H).
Quaternary carbons: δ_C 138.28 (imidazole-C-31), 138.24 (imidazole-C-22), 148.19 (Boc <u>C</u>=O), 157.59 (Boc <u>C</u>=O), 173.72 (Boc <u>C</u>=O), 174.03 (C-28), 174.32 (C-25).

$C_{29}H_{45}N_7O_8$ monoisotopic mass requires 619.33293
MS (ES^+) *m/z* 620.6 ($[M+H]^+$ 100%).
Found: MS (Accurate mass) *m/z* 620.3388 ($[M+H^+$, 100%).
620.3388 - 1.0078 = 619.331 (error: - 2.2 ppm)
($C_{29}H_{45}N_7O_8$ average mass is 619.7184)

V_{max}/cm^{-1} 3354 (N-H amide stretch), 3279 (N-H aromatic), 3234 (N-H aromatic), 1752 (C=O amide stretch), 1710 (C=O amide stretch), 1678 (C=O amide stretch), 1646 (C=O amide stretch), 1151 (C-O).

UV-visible spectroscopy: λ_{max}: 206 nm (ε_{206}= 7.02 $mM^{-1}cm^{-1}$), 235 nm (ε_{235}= 3.66 $mM^{-1}cm^{-1}$) (solvent: methanol).

TLC: R_f = 0.4 (5% MeOH, $CHCl_3$).
m.p. 56-58°C (from H_20) light brown crystal flakes.
Yield: 66 %.

3.2.5. Characterisation of 3-[(S)-2-Amino-3-(1H-imidazol-4-yl)-propionyl]-amino-N-[2-(1H-imidazol-4-yl)-ethyl]-propionamide trihydrochloride (6)

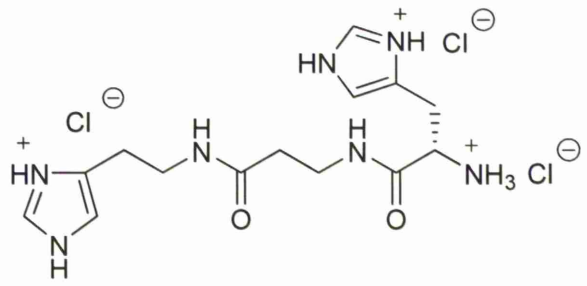

6

^{1}H-NMR (300 MHz, [d_4]-MeOD): δ_H 2.44 (d, 2H, *J* = 5.8 Hz, CH_2-27), 2.95 (d, 2H, *J* = 6.8 Hz, CH_2-30), 3.30 (d, 2H, *J* = 6.8 Hz, CH_2-21), 3.36 (d, 2H, *J*= 6.8 Hz, CH_2-26), 3.51 (d, 2H, *J*= Hz, CH_2-29), 7.43 (s, 1H, imidazole-H-32), 7.53 (s, 1H, imidazole-H-23), 8.84 (s, 1H, imidazole-H-33), 8.95 (s, 1H, imidazole-H-24).

^{13}C NMR (75 MHz, [d_4]-MeOD): δ_C 25.67 (CH_2-27), 27.67 (CH_2-30), 36.15 (CH_2-21), 37.57 (CH_2- 26), 39.38 (CH_2-29), 53.33 (CH-20), 117.80 (CH-32), 120.10 (CH-23), 134.96 (CH-33), 136.01 (CH-24).

Quaternary carbons: δ_C 128.02 (imidazole-C-31), 132.96 (imidazole-C-22), 168.51 (RC=ONHR'-28), 174.22 (RC=ONHR'-26).

$C_{14}H_{21}N_7O_2$ monoisotopic mass requires 319.1757
MS (ES^+) *m/z* 320 ($[M+H]^+$,100%).
MS (Accurate mass) *m/z* 320.1838 ($[M+H]^+$, 100%).
320.1838 - 1.0078 = 319.1760

($C_{14}H_{21}N_7O_2$ average mass is 319.3664)

V_{max}/cm^{-1} 3392, 3381, 3369 (N-H amide stretches and overlapping N-H stretch of primary NH_2), 3241 (N-H aromatic), 1617 (C=O amide stretch), 1678 (C=O amide stretch).

UV-visible spectroscopy: λ_{max}: 210 nm (ε_{210}= 4.93 $mM^{-1}cm^{-1}$) (solvent: methanol).

TLC: R_f = 0.10 (50% MeOH, 50% $CHCl_3$, few drops of Et_3N).
m.p. 84-95°C (choride salt from 1,4 dioxane) light brown residue.

Free base after ion exchange

$C_{14}H_{21}N_7O_2$ monoisotopic mass requires 319.1757
MS (ES^-) *m/z* 318.4 ($[M-H]^+$,100%).

Yield: 64 %.

3.2.6. Characterisation of 3-{(S)-2-[(S)-2-tert-butoxycarbonylamino-6-(2,2,2-trifluoroacetylamino)-hexanoyl]-amino-3-(1-tert-butoxycarbonyl-1H-imidazol-4-yl)-propionyl}-amino-N-[2-(1-tert-butoxycarbonyl-1H-imidazol-4-yl)-ethyl]-propionamide (7.1)

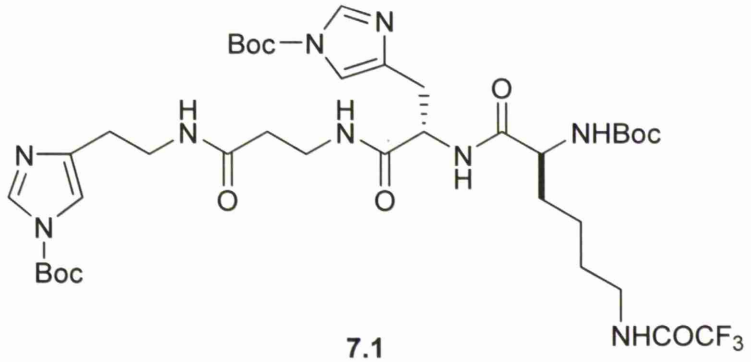

7.1

^{1}H-NMR (300 MHz, [d_4]-MeOD) δ_H 1.43 (bs, 27H, 3 x $C(CH_3)_3$), 1.50- 1.68 (m, 6H, CH_2-16, 17, 15), 2.33 (t, 2H, *J* = 6.7 Hz, CH_2-27), 2.86 (t, 2H, *J* = 6.8 Hz, CH_2-30), 3.16 (obs, 2H, CH_2-21), 3.23 (t, 2H, *J*= 6.4 Hz, CH_2-18), 3.30 (obs, 2H, CH_2-26) 3.44 (t, 2H, *J*= 6.5 Hz CH_2-29), 4.02 (t, 1H, *J*= 4.7 Hz, C<u>H</u>-14), 4.56 (t, 1H, *J*= 4.2 Hz, C<u>H</u>-20), 7.08 (s, 1H, imidazole-H-32, *pros*), 7.19 (s, 1H,

imidazole-H-23, *pros*), 8.09 (s, 1H, imidazole-H-33, *tele*), 8.38 (s, 1H, imidazole-H-24, *tele*).

^{13}C NMR (75 MHz, [d_4]-MeOD): δ_C 24.13 (CH_2), 28.70 (CH_3), 28.77 (CH_3), 29.54 (CH_2), 30.18 (CH_2), 30.86 (CH_2), 32.47 (CH_2), 36.77 (CH_2), 37.30 (CH_2), 39.84 (CH_2), 40.47 (CH_2), 54.19 (CH), 56.50 (CH).
Quaternary carbons: δ_C 80.83, 87.03, 87.15, 115.71 (CF_3), 138.34 (2 x imidazole-C), 139.77 (imidazole-CH), 141.79 (imidazole-CH), 148.11 (ROC=ONHR'), 148.22 (ROC=ONHR'), 158.28 (ROC=ONHR'), 159.17 (CF_3OC=ONHR'), 172.95 (RC=ONHR'), 173.60 (RC=ONHR'-28), 175.09 (RC=ONHR'- 25).

^{19}F-NMR (282 MHz, [d_4]-MeOD): δ_F -99.4 (s, 3F, CF_3)

$C_{37}H_{56}F_3N_9O_{10}$ monoisotopic mass requires 843.41018
MS (ES^+) *m/z* 844.7 ($[M+H]^+$, 100%).
MS (ES^+) *m/z* 866.6 ($[M+Na]^+$, 100%).
MS (Accurate mass) *m/z* 844.4180 ($[M+H]^+$, 100%).
844.4180 - 1.0078 = 843.4102 (error: 1.8 ppm)
($C_{37}H_{56}F_3N_9O_{10}$ average mass is 843.9015)

V_{max}/cm^{-1} 3287 (N-H amide stretches), 3081 (=C-H aromatic ring stretch), 2979 (C-H alkyl stretch), 2937 (C-H alkyl stretch), 1752 (C=O amide stretch), 1709 (C=O amide stretch), 1652 (C=O amide stretch), 1150 (C-O).

UV-visible spectroscopy: λ_{max}: 206 nm (ε_{206}= 10.85 $mM^{-1}cm^{-1}$) 234 nm (ε_{234}= 4.24 $mM^{-1}cm^{-1}$) (solvent: methanol).

TLC: R_f = 0.74 (50 % MeOH, 50 % $CHCl_3$).
m.p. = 75-83 °C (from EtOAc), white residue.
Yield: 61 %

3.2.7. Characterisation of 3-{(S)-2-[(S)-2-Amino-6-(2,2,2-trifluoroacetylamino)-hexanoyl]-amino-3-(1H-imidazol-4-yl)-propionyl}-amino-N-[2-(1H-imidazol-4-yl)-ethyl]-propionamide trihydrochloride (8.1)

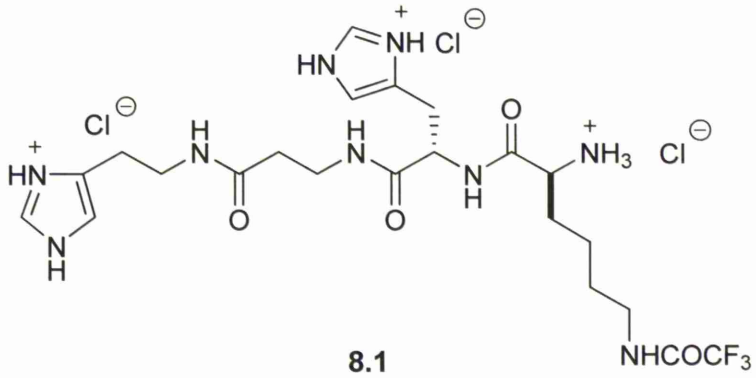

8.1

^{1}H-NMR and COSY NMR (300 MHz, [d_4]-MeOD) 1.40 (bs, 2H, CH_2-16), 1.60 (bs, 2H, CH_2-17), 1.89 (m, 2H, CH_2-15), 2.41 (s, 2H, CH_2-27), 2.94 (m, 2H, CH_2-30), 3.30 (m, 2H, CH_2-18), 3.36 (obs, 2H, CH_2-21), 3.44 (t, 2H, *J*= 6.5 Hz CH_2-26) 3.49 (obs, m, 4H, CH_2-29), 3.97 (t, 1H, *J* = 4.6 Hz, C<u>H</u>-14), 4.70- 4.89 (t, 1H, *J* = 4.8 Hz, C<u>H</u>-20), 7.41 (s, 1H, imidazole-H-32, *pros*), 7.46 (s, 1H, imidazole-H-23, *pros*), 8.83 (s, 1H, imidazole- H-33, *tele*), 8.85 (s, 1H, imidazole- H-24, *tele*).

^{19}F-NMR (282 MHz, [d_4]-MeOD): δ_F -73.75 (s, 3F, Tfa)

$C_{22}H_{32}N_9O_4F_3$ monoisotopic mass requires 543.25291
MS (ES^+) *m/z* 544.3 ($[M+H]^+$, 100%).
MS (Accurate mass) *m/z* 544.2580 ($[M+H]^+$, 100%).
543.2580- 1.0078 = 544.2502 (error: - 4.1 ppm)
($C_{22}H_{32}N_9O_4F_3$ average mass is 543.2529)

V_{max}/cm^{-1} 3389, 3381, 3372 (N-H amide stretches and overlapping N-H stretch of primary NH_2), 3069 (=C-H aromatic ring stretch), 2959 (C-H alkyl stretch), 2936 (C-H alkyl stretch), 1757 (C=O amide stretch), 1721 (C=O amide stretch), 1682 (C=O amide stretch).

UV-visible spectroscopy: λ_{max}: 210 (ε_{210}= 8.22 $mM^{-1}cm^{-1}$)

TLC: R_f = 0.1 (50% MeOH, 50% $CHCl_3$).

Solvent A (0.1 % TFA in MeCN) and solvent B (0.1 % TFA in H_20)
HPLC solvent gradient: 0-40% A over 60 mins (0-15 % A from 0 – 20 mins; 15 – 40 % MeCN from 20- 60 mins).
Retention time: 18.25- 18.75 minutes.

Yield: 68 %.

3.2.8. Characterisation of 3-{(S)-2-[(S)-2-{(2-Hydroxyethyl)-phenazinium-5-yl}-amino-6-(2,2,2-trifluoro-acetylamino)-hexanoyl]-amino-3-(1H-imidazol-4-yl)-propionyl}-amino-N-[2-(1H-imidazol-4-yl)-ethyl]-propionamide (9.1)

Precursor **9.1** was synthesised *via* covalent attachment of 10-(2-hydroxyethyl) phenazinium group at the α- amino group of the lysine residue of **8.1** as described in the 'Material and Methods' Chapter.

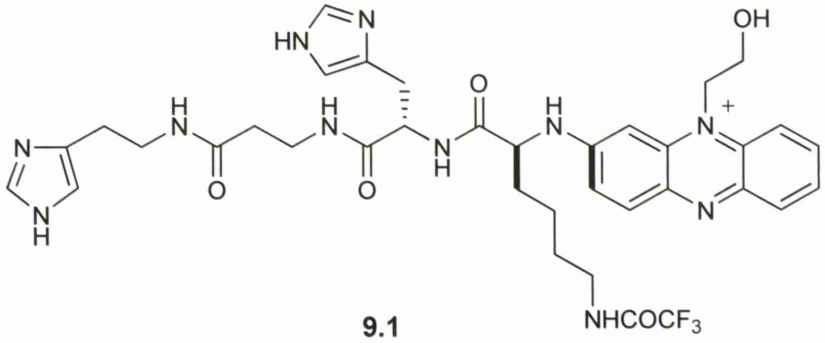

9.1

The reaction scheme for the attachment of *N*-(2-hydroxyethyl)phenazinium to the α-amino group of the lysine residue of the tetrapeptide construct **8.1** to produce **9.1** is shown in Figure 3.13.

Figure 3.3. Reaction of *N*-(2-hydroxyethyl)phenazinium with tetrapeptide construct **8.1** to produce **9.1**.

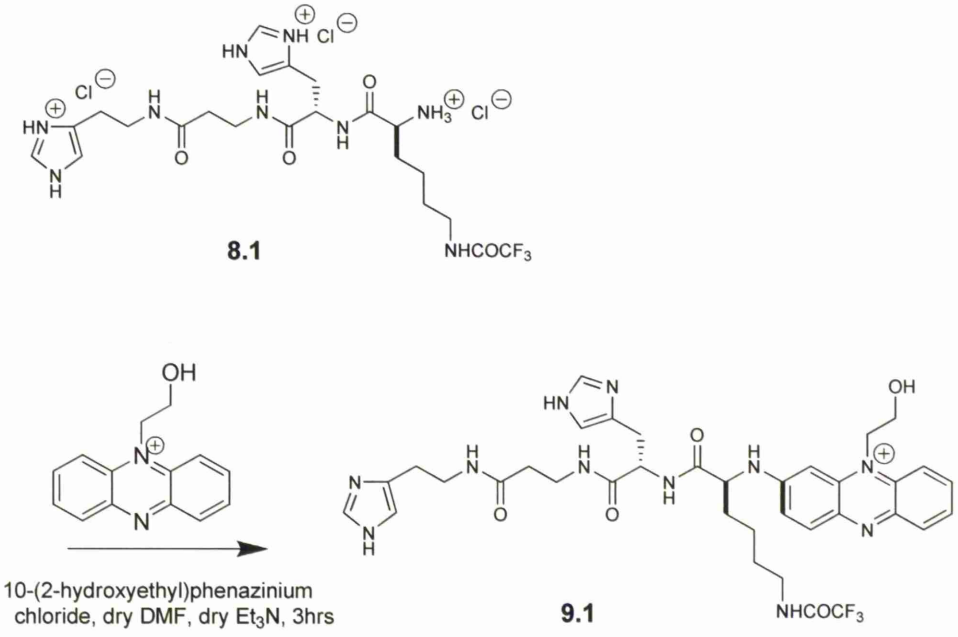

The reaction of the attachment of *N*-(2-hydroxyethyl)phenazinium anchor group to the tetrapeptide construct **8.1** has been monitored by UV-visible spectroscopy, following appearance of the new absorption bands at 283 nm and 520 nm as well as change in the shape and intensity of the absorption band at 387 nm (see Figure 3.3). 2 μl reaction aliquots were taking from the reaction mixture at certain time intervals and diluted with 998 μl of water followed by recording UV-visible spectra. Only 3 data points are presented for simplicity.

Figure 3.4. UV-visible spectra of the reaction aliquots (2 μl) taken from the reaction mixture containing *N*-(2-hydroxyethyl)phenazinium (5.5 x 10^{-5} moles) and tetrapeptide construct **8.1** (6.05 x 10^{-5} moles) in the presence of dry Et_3N (2.2 x10^{-5} moles) in anhydrous DMF at 20°C (Blue: 0 mins; Grey: 50 mins; Red: 180 mins).

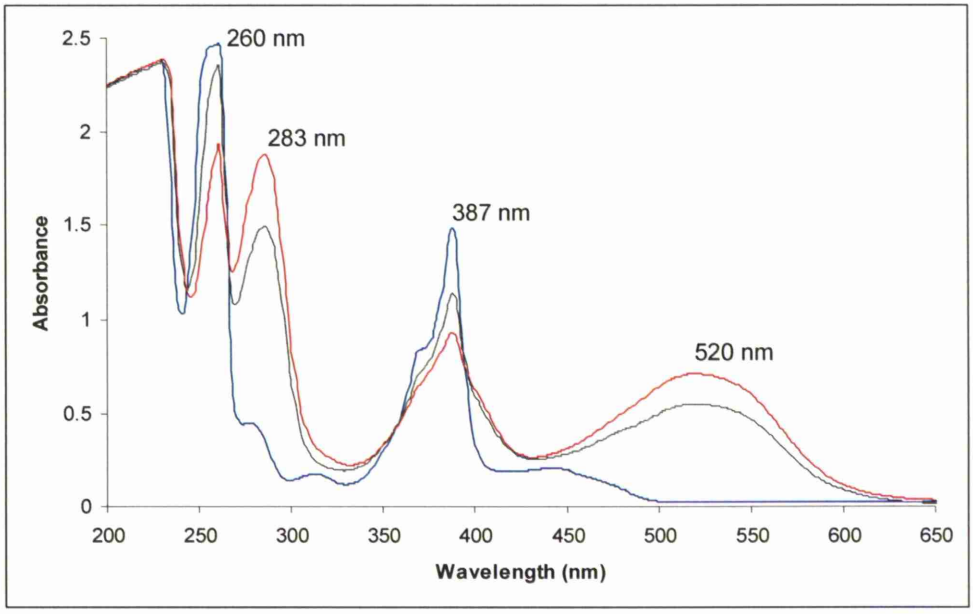

A change of absorption bands is seen as the reaction nears completion at 180 minutes. The band at *circa* 387 nm changed shape and diminished giving a new band with absorption maximum at 395 nm. Also, new absorption bands appeared at *circa* 283 nm and 520 nm (Figure 3.4), characteristic for phenazinium derivatives containing -NH-R substituting group in the aromatic ring [205].

^{1}H-NMR (300 MHz, [d_4]-MeOD): δ_H

^{1}H-NMR (300 MHz, [d_4]-MeOD): δ_H 1.50 (s, 2H, CH_2-16), 1.63 (bs, 2H, CH_2-17), 1.98 (m, 2H, CH_2-15), 2.86 (dd, 2H, *J* = 6.5 Hz, *J* = 6.5 Hz CH_2-27), 2.88 (dd, 2H, *J* = 6.7 Hz, *J* = 6.7 Hz, CH_2-30), 3.32 (m, 2H, CH_2-18), 3.44 (dd, 4H, *J* = 5.0 Hz, *J* = 5.0 Hz, CH_2-26,29), 4.20 (s, 2H, CH_2-15), 4.67 (dd, 2H, *J* = 6.2 Hz, *J* = 6.2 Hz, C<u>H</u>-14, 20), 5.16 (bs, 2H, CH_2-13), 6.98 (s, 1H, Ar-H, phenazinium-H-2), 7.32 (s, 2H, imidazole- H-23, imidazole- H-32, *pros*), 7.74 (d, 1H, *J* = 9.5 Hz, Ar-H, phenazinium-H-4), 7.9 (t, 1H, *J* = 7.6 Hz, Ar-H, phenazinium-H-9), 8.15 (dd, 2H, *J* = 6.2 Hz, *J* = 6.2 Hz, Ar-H, phenazinium-H-5,10), 8.34 (s, 1H, Ar-H, phenazinium-H-11), 8.37 (s, 1H, Ar-H, phenazinium-H-8), 8.73 (s, 1H, imidazole- H-33, *tele*), 8.80 (s, imidazole- H-24, *tele*).

^{19}F-NMR (282 MHz, [d_4]-MeOD): δ_F -75.65 (bs, 3F, CF_3)

$C_{36}H_{43}F_3N_{11}O_5$ monoisotopic mass requires 766.34004
MS (ES^+) *m/z* 766.5 ($[M]^+$ 100%).
MS (ES^+) *m/z* 767.6 ($[M+H]^+$ 40%).
MS (MALDI-TOF/TOF) *m/z* 766.314 ($[M]^+$ 100%)
($C_{36}H_{43}F_3N_{11}O_5$ average mass is 766.8038)

V_{max}/cm^{-1} 3275 (O-H stretch), 3093, 3027 (=C-H aromatic ring stretches), 2942 (C-H alkyl stretch), 2864 (C-H alkyl stretch), 1624 (C=O amide stretch), 1632 (C=O amide stretch), 1604 (C=C stretch), 1552 (C=N stretch).

UV-visible spectroscopy: λ_{max}: 230, 260, 395 and 520 nm (see Fig. 3.19).

HPLC solvent A (0.1 % TFA in MeCN) and solvent B (0.1 % TFA in H_20)
HPLC solvent gradient: 0-30% A over 60 mins (0-10 % A from 0 – 10 mins; 10 – 30 % MeCN from 10- 60 mins).

Retention time: 20.1- 20.6 minutes.

m.p. (unable to crystallise pink liquid).

Yield: 8.5%

3.2.9. Characterisation of 3-{(S)-2-[(S)-2-{(2-hydroxyethyl)-phenazinium-5-yl}-amino-6-aminohexanoyl]-amino-3-(1H-imidazol-4-yl)-propionyl}-amino-N-[2-(1H-imidazol-4-yl)-ethyl]-propionamide (10.1)

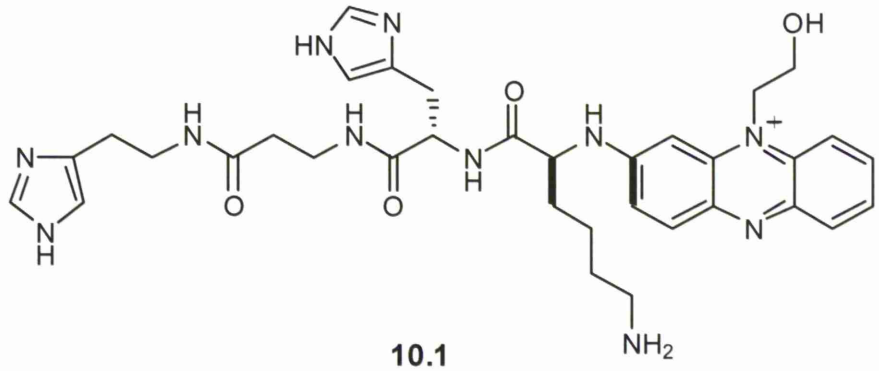

10.1

Compound **10.1** was produced from **9.1** by removal of the trifluoroacetyl protecting group from the ε-amino group of its lysine residue using aqueous Na_2CO_3 in MeOH as described in the 'Materials & methods' (2.2.2.9).

^{1}H-NMR (300 MHz, [d4]-MeOD): δ_H 1.59 (bm, obs, 2H, CH_2-16), 1.72 (dd, 2H, *J* = 7.5 Hz, *J* = 7.5 Hz, CH_2-17), 2.04- 2.06 (bs, obs, 2H, CH_2-15), 2.30 (dd, 2H, *J* = 6.6 Hz, *J* = 6.6 Hz, CH_2-27), 2.86 (dd, 2H, *J* = 5.7 Hz, *J* = 5.7 Hz, CH_2), 2.96 (dd, 2H, *J* = 7.6 Hz, *J* = 7.6 Hz, CH_2-30), 4.2 (s, 2H, CH_2-15), 4.67 (bs, obs, 2H, CH-14, 20), 5.16 (bs, 2H, CH_2-13), 6.96 (s, 1H, Ar-H, phenazinium-H-2), 7.26 (s, 1H, Ar-H, imidazole-H-32, *pros*), 7.33 (s, 1H, Ar-H, imidazole-H-23, *pros*), 7.70- 7.78 (d, 1H, *J* = 3.5 Hz, Ar-H, phenazinium-H-4), 7.91 (t, 1H, *J* = 3.5 Hz, Ar-H, phenazinium-H-9), 8.09 (d, 1H, *J* = 9.4 Hz, Ar-H, phenazinium-H-5), 8.13 (t, 1H, *J* = 8.5 Hz, 8.7 Hz, Ar-H, phenazinium-H-10), 8.34- 8.35 (d, 1H, *J* = 4.9 Hz, Ar-H, phenazinium-H-11), 8.36- 8.37 (d, 1H, *J* = 3.6 Hz, Ar-H, phenazinium-H-8), 8.67 (s, 1H, Ar-H, imidazole-H-33, *tele*), 8.77 (s, 1H, Ar-H, imidazole-H-24, *tele*).

$C_{34}H_{44}N_{11}O_4$ monoisotopic mass requires 670.35775
MS (ES^+) *m/z* 671.4 ($[M+H]^+$).
MALDI-TOF/TOF *m/z* 670.329 ($[M]^+$ 100%)

($C_{34}H_{44}N_{11}O_4$ average mass is 670.7947)

UV-visible spectroscopy: λ_{max}: 230, 290, 395 and 520 nm.

HPLC solvent gradient: (MeCN and H_2O) (0-50% MeCN over 60 mins: 0-10 % MeCN from 0 – 10 mins; 10 – 50 % MeCN from 10- 60 mins).
Retention time: 37.4- 38 minutes.

m.p. (unable to crystallise pink liquid).

Yield: 61 %

3.2.10. Characterisation of oligonucleotide conjugate 11.1

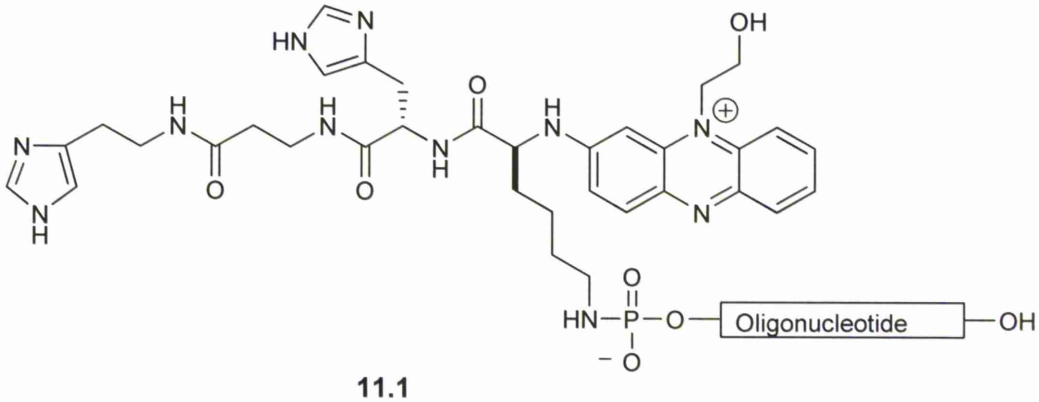

11.1

The oligonucleotide derivative **11.1** containing the *N*-(2-hydroxyethyl)-phenazinium anchor group at the α- amino group and recognition oligonucleotide element attached to the ε-amino group of the lysine residue was produced by conjugation of the free aliphatic ε- amine of **10.1** with the 5′-terminal phosphate group of pdGATCGAACACAGGACCT (17-mer) oligonucleotide [201] as described in the 'Material & Methods' section. The resulting compound **11.1** was purified by RP-HPLC (detected at 260 nm (oligonucleotide), 392 nm and 535 nm (*N*-(2-hydroxyethyl)-phenazinium group)) and characterised by ^{31}P NMR (to confirm conjugation), UV-visible spectroscopy and mass spectrometry.

^{31}P NMR (300 MHz, D_2O): δ_P 7.22 (s, 1P, -HN-$^{5'}$P-) ; δ_P -1.0- 1.0 ppm (s, 16×P, -$C^{5'}$-$O^{5'}$-P-$O^{3'}$-$C^{3'}$-).

The ^{31}P NMR spectrum of the oligonucleotide derivative **11.1** recorded in D_2O showed an appearance of a sharp downfield signal at 7.22 ppm of integral intensity 1P from ^{31}P of the phosphoramidate bond [210] in addition to the 16 signals around -1.0- 1.0 ppm from ^{31}P nuclei of the phosphodiester bonds. The appearance of this new band at 7.22 ppm indicated the presence of the phosphoramidate bond formed between the free aliphatic ε- amine of **10.1** and the 5′-terminal phosphate group of pdGATCGAACACAGGACCT (17-mer) oligonucleotide.

$C_{199}H_{233}N_{80}O_{102}P_{17}^{16-}$
(Mol. Wt.: 5904.01)
Monoisotopic mass: 5901.1

MALDI analysis showed a peak at 5188 which represents the 17-mer oligonucleotide without the tetra-peptide, phosphoramidate bond or phenazinium fragments, suggestive of **11.1** phosphoramidate bond degradation in the MALDI sample and/or during performing MALDI-TOF experiment.
The expected ion may not be detected if degradation products are preferentially ionised and dominate the spectrum or if there is suppression by factors such as ions in the sample.

Free 17-mer oligonucleotide **without** 5′ terminal phosphate: dGATCGAACACAGGACCT
Monoisotopic mass: 5187.
MALDI-TOF-TOF *m/z* 5188 ($[M+H]^+$ 100%).

Free 17-mer oligonucleotide **with** terminal phosphate: pdGATCGAACACAGGACCT (for comparison): Monoisotopic mass: 5247.75.

UV-visible spectroscopy: λ_{max}: 260, 392 and 535 nm.
Molar Extinction coefficient (ε_{260}): 175.7 $mM^{-1}cm^{-1}$ (solvent: water).

Figure 3.5. UV-visible spectrum of oligodeoxyribonucleotide conjugate **11.1** containing tetra-peptide cleaving group and phenazinium anchor. Spectrum was recorded in water at 20°C with 5μM sample concentration. λ_{max} values of the major absorption bands are indicated.

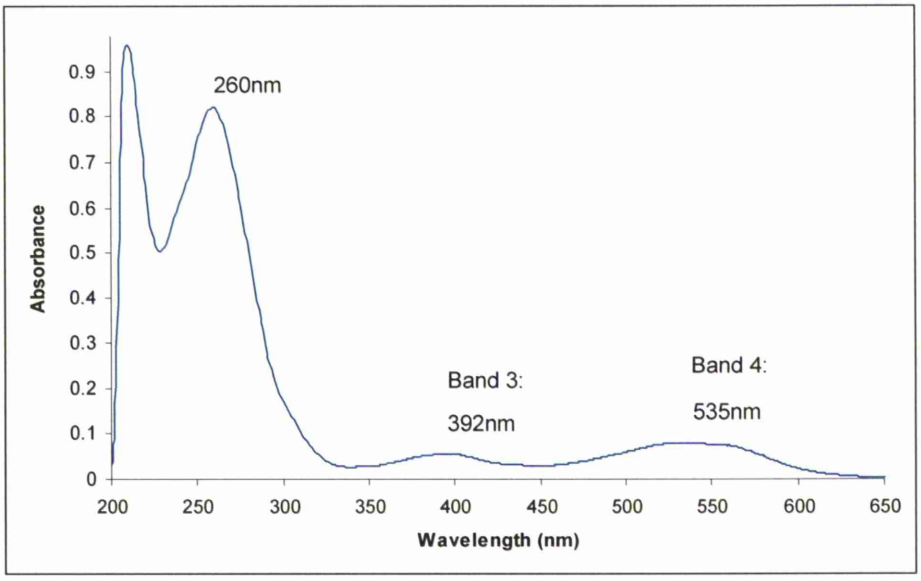

The appearance of bands 2 and 3 at 392nm and 535 nm, respectively, (Figure 3.14) provided additional confirmation of the incorporation of the *N*-(2-hydroxyethyl)-phenazinium anchor group into **11.1.**

HPLC solvent gradient: Solvent A (1% $LiClO_4$ and 0.1 % TFA in MeCN) and solvent B (1% $LiClO_4$ and 0.1 % TFA in H_20). Solvent gradient: 0-30% Solvent A over 60 mins: 0-10 % from 0 – 10 mins; 10 – 30% from 10- 60 mins.

Retention time: 32.2- 32.7 minutes.
Free oligonucleotide retention time: 30 minutes.
m.p. (unable to crystallise pink liquid).

Yield: 22 %

3.2.11. Characterisation of the 17-mer oligonucleotide conjugate (9.2)

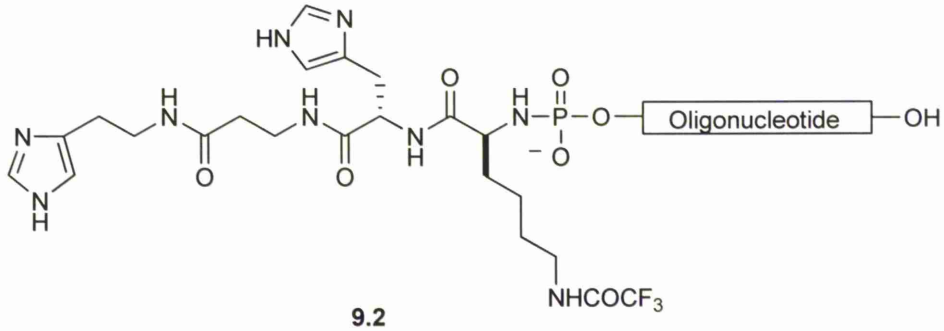

9.2

Synthesis of 17-mer oligonucleotide conjugate **9.2** was based on conjugation of the deprotected aliphatic α-amino group of **8.1** with the 5′-terminal phosphate group of pdGATCGAACACAGGACCT (17-mer) oligonucleotide as described in 'Material & Methods' section [201]. The resulting compound **9.2** was purified by RP-HPLC (detected at 260 nm for the oligonucleotide) and characterised by ^{31}P NMR (to confirm conjugation), UV-visible spectroscopy and mass spectrometry.

^{31}P NMR (300 MHz, D_2O): δ_P 7.19 (s, 1P, -HN-$^{5'}$P-) ; δ_P -1.0- 1.0ppm (s, 16×P, -$C^{5'}$-$O^{5'}$-P-$O^{3'}$-$C^{3'}$-).

The ^{31}P NMR spectrum of the oligonucleotide derivative **9.2** recorded in D_2O showed the appearance of a sharp downfield signal at 7.19 ppm of integral intensity 1P from ^{31}P of the phosphoramidate bond [210] in addition to the 16 signals around -1.0- 1.0ppm from ^{31}P nuclei of the phosphodiester bonds. The appearance of this new band at 7.19 ppm indicated the presence of the phosphoramidate bond formed between the free aliphatic ε- amine of **9.2** and the 5′-terminal phosphate group of pdGATCGAACACAGGACCT (17-mer) oligonucleotide.

$C_{187}H_{221}F_3N_{78}O_{102}P_{17}^{17-}$

Monoisotopic mass required: 5774. This expected ion was not detected, possibly because it was not efficiently ionised by the method used.

HPLC solvent gradient: Solvent A (1% $LiClO_4$ and 0.1 % TFA in MeCN) and solvent B (1% $LiClO_4$ and 0.1 % TFA in H_2O). Solvent gradient: 0-30% solvent A over 60 mins (0-10 % from 0 – 10 mins; 10 – 30% from 10- 60 minutes).
Retention time: 33- 33.4 minutes.

UV-visible spectroscopy: λ_{max}: 260 nm.
Molar Extinction coefficient (ε_{260}): 169 $mM^{-1}cm^{-1}$ (solvent: water).

Yield: 24 %

3.2.12. Characterisation of oligonucleotide conjugate (10.2)

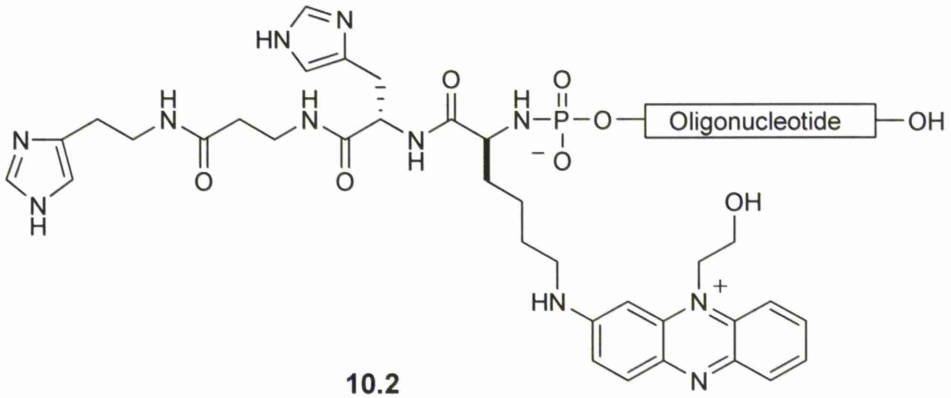

10.2

The resulting compound **10.2** was produced as described in the 'Material & Methods' chapter and purified by RP-HPLC (detected at 260 nm (oligonucleotide), 392 nm and 535 nm (*N*-(2-hydroxyethyl)-phenazinium group)) and characterised by ^{31}P NMR (to confirm conjugation) and UV-visible spectroscopy.

^{31}P NMR (300 MHz, D_2O): δ_P 7.29 (s, 1P, -HN-$^{5'}$P-) ; δ_P -1.0- 1.0ppm (s, 16×P, -$C^{5'}$-$O^{5'}$-P-$O^{3'}$-$C^{3'}$-).

$C_{199}H_{233}N_{80}O_{102}P_{17}^{16-}$ monoisotopic mass: 5901.
The expected ion was not detected possibly because it was not efficiently ionised by the method used.

UV-visible spectroscopy: λ_{max}: 260, 392 and 535 nm.
The presence of UV-visible absorption bands at 392 nm and 535 nm provided additional confirmation of incorporation of the *N*-(2-hydroxyethyl)-phenazinium anchor group into **10.2.**

Molar Extinction coefficient (ε_{260}): 175.7 $mM^{-1}cm^{-1}$ (solvent: water).

HPLC solvent gradient: Solvent A (1% $LiClO_4$ and 0.1 % TFA in MeCN) and solvent B (1% $LiClO_4$ and 0.1 % TFA in H_20). Solvent gradient: 0-30% Solvent A over 60 mins: 0-10 % from 0 – 10 mins; 10 – 30% from 10- 60 mins.

Retention time: 32.3- 32.5 minutes.
Free oligonucleotide retention time: 30 minutes.

m.p. (unable to crystallise pink liquid).

Yield: 61 %.

3.2.13. Characterisation of 2-(tert-butoxycarbonylamino)-6-(9H-fluoren-9-ylmethoxycarbonylamino)-hexanoic acid-N-hydroxy-succinimide ester (Boc-Lys-(Fmoc)-OSu).

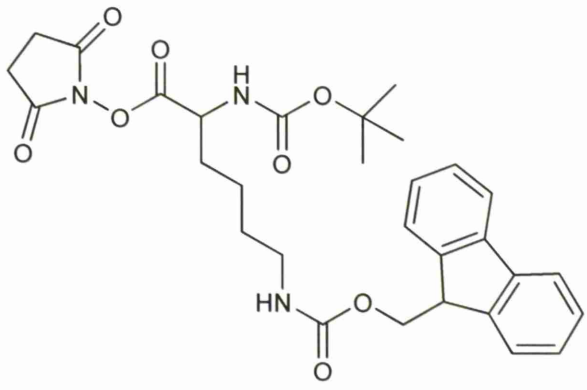

Boc-Lys-(Fmoc)-OSu

^{1}H-NMR (300 MHz, [d_4]-DMSO): δ_H 1.38 (s, 9H, $C(CH_3)_3$), 2.79 (bs, 4H, succinimide 2 x CH_2), 2.95 (bs, 2H, CH_2), 4.18 (s, 1H, CH), 4.20 (s, 1H, CH), 4.31 (bs, 2H, CH_2), 7.23 (dd, 2H, *J*= 7.3 Hz, *J*= 7.3 Hz, fluorene CH), 7.39 (dd, 2H, *J*= 7.3 Hz, *J*= 7.3 Hz, fluorene CH), 7.67 (s, 1H, fluorene CH), 7.69 (s, 1H, fluorene CH), 7.88 (s, 1H, fluorene CH), 7.90 (s, 1H, fluorene CH).

$C_{30}H_{35}N_3O_8$ monoisotopic mass requires: 565.24239

MS (ES^+) *m/z* 588.4 ($[M+Na]^+$ 100%).

($C_{30}H_{35}N_3O_8$ average mass: 565.614)

Elemental analysis (CHN): $C_{30}H_{35}N_3O_8$ requires: C, 63.70; H, 6.24; N, 7.43; O, 22.63. Found: C, 63.72; H, 6.22; N, 7.46.

TLC: R_f = 0.57 (5% MeOH, 95% $CHCl_3$).

Yield: 65 %

3.2.14. Characterisation of 3-{(S)-2-[(S)-2-tert-butoxycarbonylamino-6-(9H-fluoren-9-ylmethoxycarbonylamino)-hexanoyl]-amino-3-(1-tert-butoxycarbonyl-1H-imidazol-4-yl)-propionyl}-amino-N-[2-(1-tert-butoxycarbonyl-1H-imidazol-4-yl)-ethyl]-propionamide (7.3)

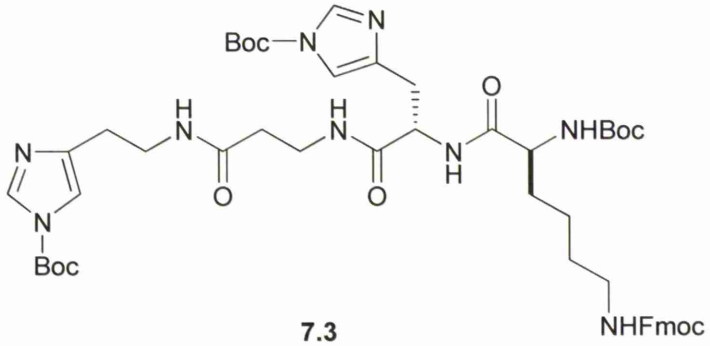

7.3

^{1}H-NMR (300 MHz, [d_4]-MeOD) δ_H 1.42 (bs, 9H, $C(CH_3)_3$), 1.60 (bs, 18H, 2 x $C(CH_3)_3$), 1.50- 1.68 (m, obs, 6H, CH_2-16, 17, 15), 2.33 (t, 2H, *J* = 6.7 Hz, CH_2-27), 2.72 (t, 2H, *J* = 6.8 Hz, CH_2-30), 3.10 (obs, 2H, CH_2-21), 3.33 (obs, 2H, CH_2-18), 3.30 (obs, 2H, CH_2-21) 3.45 (t, 4H, *J*= 6.5 Hz CH_2-26, 29), 3.91 (t,

1H, *J*= 5.2 Hz, C<u>H</u>-14), 4.20 (t, 1H, *J*= 6.2 Hz, C<u>H</u>-20), 4.34 (m, fluorene- C<u>H</u>), 4.61 ((bs, 2H, fluorene-C<u>H</u>$_2$)

7.29 (s, 2H, imidazole-H-32, 23, *pros*), 7.30 (t, 2H, *J*= 7.3 Hz, fluorene-H), 7.38 (t, 2H, *J*= 7.4 Hz, fluorene-H), 7.62- 7.64 (d, 2H, *J*= 7.6 Hz, fluorene-H), 7.77-7.80 (d, 2H, *J*= 7.3 Hz, fluorene-H), 8.09 (s, 2H, imidazole-H-33, 24, *tele*).

V_{max}/cm^{-1} 3304 (N-H amide stretch), 3081 (=C-H aromatic ring stretch), 3129 (=C-H aromatic ring stretch), 2978 (C-H alkyl stretch), 2933 (C-H alkyl stretch), 1752 (C=O amide stretch), 1704 (C=O amide stretch), 1651 (C=O amide stretch), 1152 (C-O).

$C_{50}H_{67}N_9O_{11}$ monoisotopic mass requires 969.49596
MS (ES^+) *m/z* 970.5 ($[M+H]^+$ 100%).
MS (Accurate mass) *m/z* 970.5038 ($[M+H^+$, 100%).
970.5038 - 1.0078 = 969.496

($C_{50}H_{67}N_9O_{11}$ average mass is 970.1357).

V_{max}/cm^{-1} 3304 (N-H amide stretches), 3128 (=C-H aromatic ring stretch), 3065 (=C-H aromatic ring stretch), 2977 (C-H alkyl stretch), 2933 (C-H alkyl stretch), 1152 (C-O).

TLC: R_f = 0.70 (50% MeOH, 50% $CHCl_3$).
m.p. (unable to crystallise gum).
Yield: 54 %.

3.2.15. Characterisation of 3-{(S)-2-[(S)-2-amino-6-(9H-fluoren-9-ylmethoxycarbonylamino)-hexanoyl]-amino-3-(1H-imidazol-4-yl)-propionyl}-amino-N-[2-(1H-imidazol-4-yl)-ethyl]-propionamide trifluoroacetate (8.3)

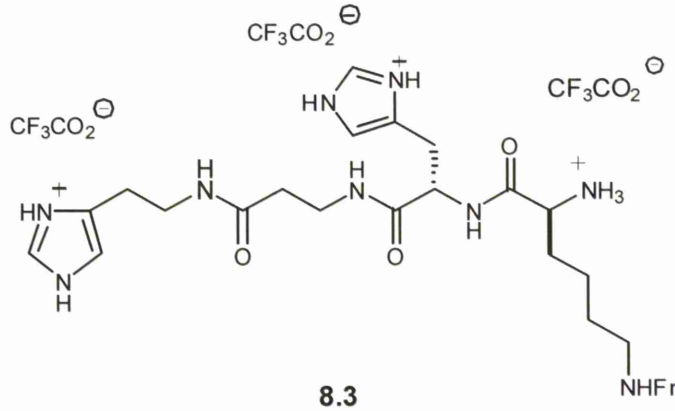

8.3

^{1}H-NMR (300 MHz, [d_4]-MeOD) δ_H 1.20- 2.0 (m, 6H, CH_2-16, 17, 15), 2.37 (t, 2H, *J* = 6.8 Hz, CH_2-27), 2.91 (m, 2H, CH_2-30), 3.10 (obs, 2H, CH_2-21), 3.33 (d, 2H, *J*= 6.4 Hz, CH_2-18), 3.45 (t, 4H, *J*= 6.5 Hz CH_2-26, 29), 3.82 (s, 1H, CH-14), 3.91 (t, 1H, *J*= 5.2 Hz, fluorene-C<u>H</u>), 4.34 (m, 1H, fluorene- C<u>H</u>), 4.33 ((d, 2H, *J*= 6.0 Hz, fluorene-C<u>H_2</u>), 4.70 (t, 1H, *J*= 6.2 Hz, C<u>H</u>-20), 7.27 (s, 1H, imidazole-H-32, *pros*), 7.29 (s, 1H, imidazole-H-23, *pros*), 7.32 (t, 2H, *J*= 6.9 Hz fluorene-H), 7.37 (t, 2H, *J*= 6.8 Hz fluorene-H), 7.61- 7.64 (d, 2H, *J*= 7.2 Hz, fluorene-H), 7.76- 7.78 (d, 2H, *J*= 7.3 Hz, fluorene-H), 8.76 (s, 1H, imidazole-H-33, *tele*), 8.79 (s, 1H, imidazole-H-24, *tele*).

$C_{35}H_{43}N_9O_5$ monoisotopic mass requires 669.33869
MS (ES$^+$) *m/z* 670.4 ([M+H]$^+$ 100%).
MS (MALDI-TOF/TOF) *m/z* 670.211 ([M]$^+$ 100%)

TLC: R_f = 0.3 (50 % MeOH, 50 % $CHCl_3$).

m.p. (unable to crystallise gum).

Yield: 97 %.

3.2.16. Characterisation of 17-mer oligonucleotide conjugate (9.3)

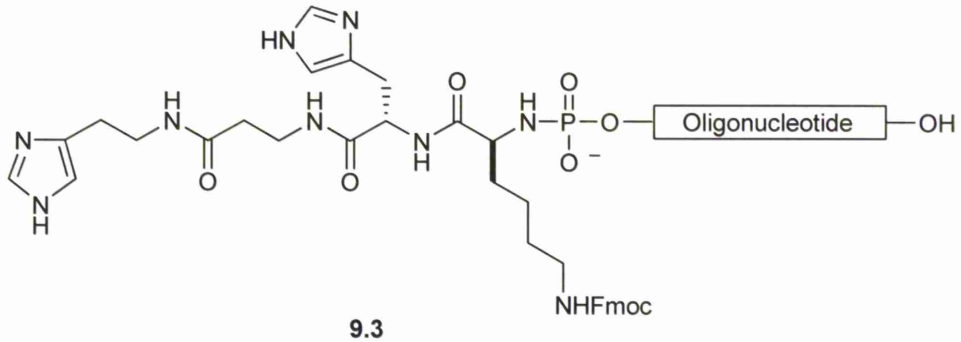

9.3

The synthesis of the 17-mer oligonucleotide conjugate **9.3** was based on conjugation of the deprotected aliphatic α-amine group of **8.3** with the 5′-terminal phosphate group of pdGATCGAACACAGGACCT (17-mer) oligonucleotide as described in the 'Material & Methods' section [201]. The resulting compound **9.3** was purified by RP-HPLC (detected at 260 nm for the oligonucleotide) and characterised by ^{31}P NMR (to confirm conjugation) and UV-visible spectroscopy.

^{31}P NMR (300 MHz, D_2O): δ_P 7.34 (s, 1P, -HN-$^{5'}$P-) ; δ_P -1.0- 1.0ppm (s, 16×P, -$C^{5'}$-$O^{5'}$-P-$O^{3'}$-$C^{3'}$-).

$C_{199}H_{233}N_{80}O_{103}P_{17}$

Monoisotopic mass: 5917.

The expected ion was not detected, possibly because it was not efficiently ionised by the method used.

UV-visible spectroscopy: λ_{max}: 260 nm.

Molar extinction coefficient (ε_{260}): 169 $mM^{-1}cm^{-1}$ (solvent: water).

HPLC solvent gradient: Solvent A (1% $LiClO_4$ and 0.1 % TFA in MeCN) and solvent B (1% $LiClO_4^-$ and 0.1 % TFA in H_2O). Solvent gradient: 0-30% Solvent A over 60 mins: 0-10 % from 0 – 10 mins; 10 – 30% from 10- 60 mins.

Retention time: 34.2- 34.8 minutes.

(Free oligonucleotide retention time: 30 minutes).

Yield: 27 %

3.2.17. Characterisation of 17-mer oligonucleotide conjugate (10.3)

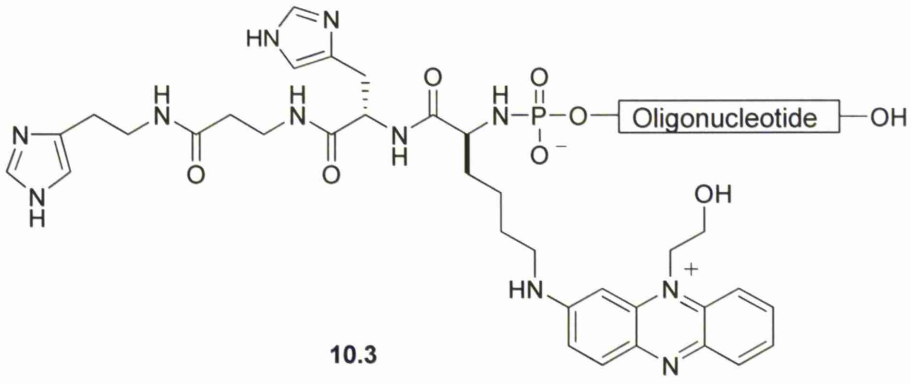

10.3

The resulting compound **10.3** was produced as described in 'Material & Methods' chapter and purified by RP-HPLC (detected at 260 nm (oligonucleotide), 392 nm and 535 nm (*N*-(2-hydroxyethyl)-phenazinium group)) and characterised by ^{31}P NMR (to confirm conjugation), UV-visible spectroscopy and mass spectrometry.

^{31}P NMR (300 MHz, D_2O): δ_P 7.37 (s, 1P, -HN-$^{5'}$P-) ; δ_P -1.0- 1.0ppm (s, 16×P, -$C^{5'}$-$O^{5'}$-P-$O^{3'}$-$C^{3'}$-).

Intermediate following Fmoc deprotection: $C_{184}H_{223}N_{80}O_{101}P_{17}$
Monoisotopic mass: 5695.
MALDI-TOF-TOF *m/z* 5695 ($[M+H]^+$ 100%)

Compound after Phn oxidative addition: $C_{199}H_{233}N_{80}O_{102}P_{17}^{16-}$
Monoisotopic mass: 5901.
The expected ion was not detected, possibly because it was not efficiently ionised by the method used.

UV-visible spectroscopy: λ_{max}: 260, 392 and 535 nm (see fig xx).
The presence of UV-visible absorption bands at 392 nm and 535 nm provided additional confirmation of incorporation of the *N*-(2-hydroxyethyl)-phenazinium anchor group into **10.3.**

Molar Extinction coefficient (ε_{260}): 175.7 $mM^{-1}cm^{-1}$ (solvent: water).

HPLC solvent gradient: Solvent A (1% $LiClO_4$ and 0.1 % TFA in MeCN) and solvent B (1% $LiClO_4$ and 0.1 % TFA in H_20). Solvent gradient: 0-30% Solvent A over 60 mins: 0-10 % from 0 – 10 mins; 10 – 30% from 10- 60 mins.

Retention time: 32- 32.5 minutes.

m.p. = unable to crystallise

Yield: 53 %

3.2.18. Characterisation of 2-(9H-fluoren-9-ylmethoxycarbonyl)-amino-6-(diphenyl-p-tolyl-methylamino)-hexanoic acid-N-hydroxy-succinimide ester (Fmoc-Lys-(Mtt)-OSu).

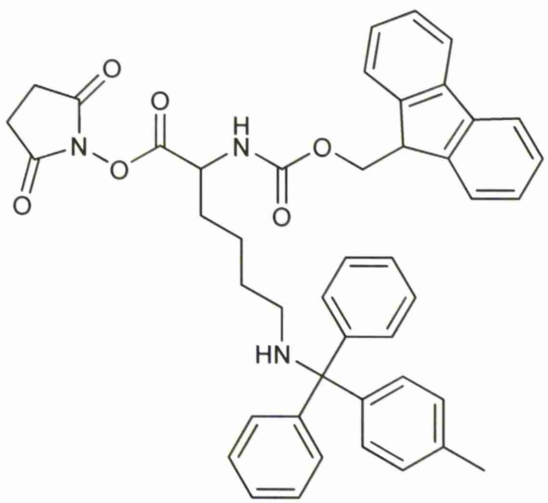

Fmoc-Lys-(Mtt)-OSu

^{1}H-NMR (300 MHz, [d_4]-Acetone): δ_H 1.59 (4H, bs, lysine 2 x CH_2), 1.84 (bs, 2H, lysine CH_2), 4.21 (d, 1H, *J*= 6.9 Hz, CH), 4.35 (d, 2H, *J*= 6.9 Hz, CH_2), 4.64 (1H, m, CH),
6.82 (s, 1H, Ar-H), 6.85 (s, 1H, Ar-H), 7.15 (t, 2H, *J*= 7.1 Hz, Ar-H), 7.24- 7.3 (obs, 8H, Ar-H), 7.39 (s, 4H, Ar-H), 7.42 (s, 2H, Ar-H), 7.71 (d, 1H, *J*= 2.8 Hz, Ar-H), 7.68 (d, 1H, *J*= 2.8 Hz, Ar-H), 7.87 (s, 1H, Ar-H), 7.89 (s, 1H, Ar-H).

$C_{45}H_{43}N_3O_6$ monoisotopic mass requires: 721.31516
MS (ES^+) *m/z* 744.7 ($[M+Na]^+$ 100%), 722.5 ($[M+H]^+$ 85%).

$C_{45}H_{43}N_3O_6$ requires 721.8529
(Mol. Wt.: 721.840)

TLC: R_f = 0.47 (20% MeOH, 80% $CHCl_3$).
Yield 55 %.

3.2.19. Characterisation of 3-{(S)-2-[(S)-2-(9H-fluoren-9-ylmethoxycarbonyl)-amino-6-(diphenyl-p-tolyl-methylamino)-hexanoyl]-amino-3-(1-tert-butoxycarbonyl-1H-imidazol-4-yl)-propionyl}-amino-N-[2-(1-tert-butoxycarbonyl-1H-imidazol-4-yl)-ethyl]-propionamide (7.4).

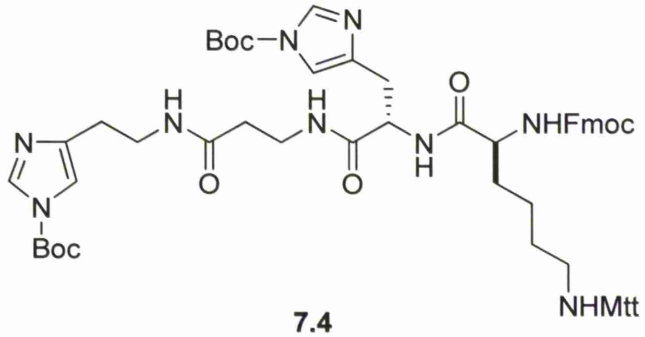

7.4

^{1}H-NMR (300 MHz, [d_4]-MeOD) δ_H 1.50 (bs, 9H, Boc $C(CH_3)_3$), 1.59 (bs, 9H, Boc $C(CH_3)_3$), 1.30- 1.72 (m, 6H, CH_2-16, 17, 15), 2.09 (s, 3H, 4-methyl trityl CH_3), 2.24 (t, 2H, *J* = 6.8 Hz, CH_2-27), 2.69 (m, 2H, CH_2-30), 3.04 (m, 2H, CH_2-21), 3.28 (m, 2H, *J*= 6.4 Hz, CH_2-18), 3.39 (t, 4H, *J*= 6.5 Hz, CH_2-26, 29), 4.00 (t, 1H, *J*= 5.2 Hz, fluorene-C<u>H</u>), 4.20 (s, 1H, CH-14), 4.25- 4.43 (m, 2H, *J*= 6.2 Hz, fluorene-C<u>H$_2$</u>), 4.59 (t, 1H, *J*= 6.2 Hz, C<u>H</u>-20), 7.03- 7.05 (d, 2H, 4-methyl benzene-H), 7.10- 7.15 (d, 2H, 4-methyl benzene-H), 7.20- 7.29 (m, obs, 8H, benzene-H), 7.26 (s, 2H, imidazole H-32, 23, *pros*), 7.34 (t, 2H, *J*= 7.2 Hz, benzene-H), 7.40- 7.42 (d, 4H, *J*= 7.5 Hz, fluorene-H), 7.63- 7.65 (d, 2H, *J*= 7.2 Hz, fluorene-H), 7.74- 7.77 (d, 2H, *J*= 7.2 Hz, fluorene-H), 7.93 (s, 1H, imidazole H-33, *tele*) 8.09 (s, 1H, imidazole-H-24, *tele*).

$C_{65}H_{75}N_9O_9$ monoisotopic mass requires: 1125.56873

MS (ES^+) *m/z* $C_{65}H_{75}N_9O_9$ requires 1125.6

MS (MALDI-TOF/TOF) *m/z* 1126.6 ($[M+H]^+$100%).

V_{max}/cm^{-1} 3292.9 (N-H amide stretch), 3005.5 (=C-H aromatic ring, stretch), 3129 (=C-H aromatic ring stretch), 2980 (C-H alkyl stretch), 2933 (C-H alkyl stretch), 1754 (C=O amide stretch), 1710 (C=O amide stretch), 1658 (C=O amide stretch), 1152 (C-O).

TLC: R_f = 0.85 (20% MeOH, 80% $CHCl_3$).

m.p. = 55- 59 °C (from $CHCl_3$), light yellow foam.

Yield: 36%.

3.2.20. Characterisation of 3-{(S)-2-[(S)-2-(9H-fluoren-9-ylmethoxycarbonyl)-amino-6-aminohexanoyl]-amino-3-(1H-imidazol-4-yl)-propionyl}-amino-N-[2-(1H-imidazol-4-yl)-ethyl]-propionamide tris-(trifluoroacetate) (8.4b)

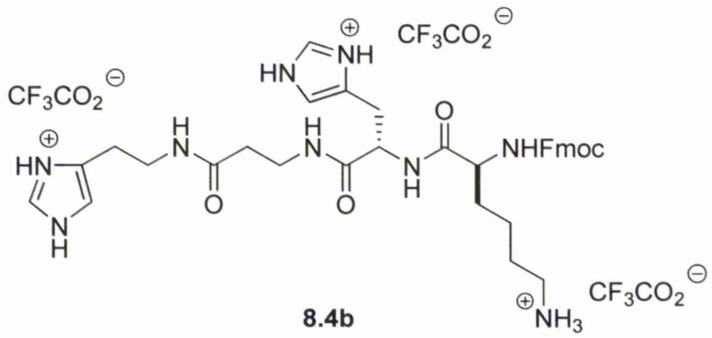

8.4b

^{1}H-NMR (300 MHz, [d_4]-MeOD) δ_H 1.43 (bs, 2H, CH_2-16), 1.69 (m, 4H, CH_2- 17, 15), 2.39 (t, 2H, *J* = 6.8 Hz, CH_2-27), 2.92 (m, 4H, CH_2-30, 21), 3.26 (m, 2H, CH_2-18), 3.46 (t, 4H, *J*= 6.5 Hz CH_2-26, 29), 4.34 (m, fluorene- C<u>H</u>),
4.00 (t, 1H, *J*= 5.2 Hz, fluorene-C<u>H</u>), 4.20 (s, 1H, CH-14), 4.35- 4.43 (m, 2H, fluorene-C<u>H_2</u>), 4.66 (t, 1H, *J*= 6.2 Hz, C<u>H</u>-20), 7.34 (s, 2H, imidazole H-32, 23, *pros*), 7.27- 7.44 (m, 4H, Ar-H, fluorene-H), 7.66 (d, 2H, *J*= 7.2 Hz, fluorene-H), 7.80 (d, 2H *J*= 7.2 Hz, fluorene-H), 8.72 (s, 1H, imidazole H-33, *tele*) 8.77 (s, 1H, imidazole-H-24, *tele*).

$C_{35}H_{43}N_9O_5$ Monoisotopic mass requires 669.33869

MS (ES^+) *m/z* 670.4 ($[M+H]^+$).

MS (Accurate mass) *m/z* 670.3391 ($[M+H^+$, 100%).

MS (MALDI-TOF/TOF) *m/z* 670.4 ($[M]^+$ 100%)

HPLC solvent A (0.1 % TFA in MeCN) and solvent B (0.1 % TFA in H_2O)
HPLC solvent gradient: (0-50% A over 50 mins: 0-10 % A from 0 – 10 mins; 10 – 50 % MeCN from 10- 50 mins).
Retention time: 29.7- 30.3 minutes.

TLC: R_f = 0.22 (10 % AcOH, 20 % MeOH, 70 % $CHCl_3$).
m.p. = 46- 48 °C (from H_2O), light yellow crystals.
Yield = 72 %.

3.2.21. Characterisation of 17-mer oligonucleotide conjugate (9.4b)

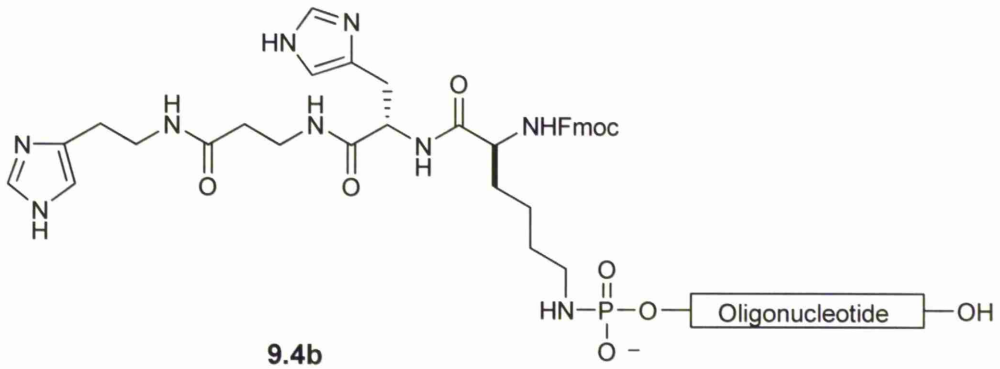

9.4b

Synthesis of the 17-mer oligonucleotide conjugate **9.4b** was achieved by conjugation of the deprotected aliphatic ε-amine group of **8.4b** with the 5′-terminal phosphate group of pdGATCGAACACAGGACCT (17-mer) oligonucleotide as described in 'Material & Methods' section [201]. The resulting compound **9.4b** was purified by RP-HPLC (detected at 260 nm for the oligonucleotide) and characterised by ^{31}P NMR (to confirm conjugation), UV-visible spectroscopy and mass spectrometry.

^{31}P NMR (300 MHz, D_2O): δ_P 7.23 (s, 1P, -HN-$^{5'}$P-) ; δ_P -1.0- 1.0ppm (s, 16×P, -$C^{5'}$-$O^{5'}$-P-$O^{3'}$-$C^{3'}$-).

$C_{199}H_{233}N_{80}O_{103}P_{17}$
Monoisotopic mass: 5917.
The expected ion was not detected, possibly because it was not efficiently ionised by the method used.

UV-visible spectroscopy: λ_{max}: 260 nm.
Molar Extinction coefficient (ε_{260}): 169 $mM^{-1}cm^{-1}$ (solvent: water).

HPLC solvent gradient: Solvent A (1% $LiClO_4$ and 0.1 % TFA in MeCN) and solvent B (1% $LiClO_4$ and 0.1 % TFA in H_2O). Solvent gradient: 0-30% solvent A over 60 mins (0-10 % from 0 – 10 mins; 10 – 30% from 10- 60 minutes).
Retention time: 34.2- 34.6 minutes.
Free oligonucleotide retention time: 30 minutes.

Yield: 31 %

3.2.22. Characterisation of 17-mer oligonucleotide conjugate (10.4)

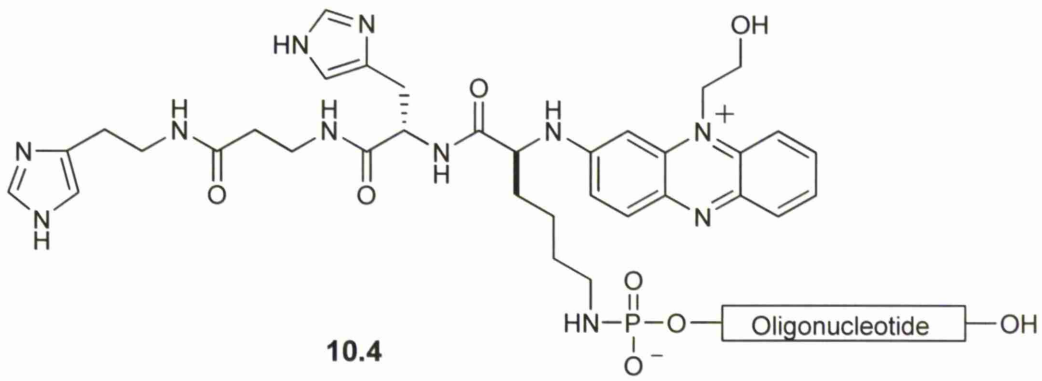

10.4

The resulting compound **10.4** was produced as described in the 'Material & Methods' chapter, purified by RP-HPLC (detected at 260 nm (oligonucleotide), 392 nm and 535 nm (*N*-(2-hydroxyethyl)-phenazinium group)) and characterised by ^{31}P NMR (to confirm conjugation), UV-visible spectroscopy and mass spectrometry.

^{31}P NMR (300 MHz, D_2O): δ_P 7.29 (s, 1P, -HN-$^{5'}$P-) ; δ_P -1.0- 1.0ppm (s, 16×P, -$C^{5'}$-$O^{5'}$-P-$O^{3'}$-$C^{3'}$-).

Intermediate following Fmoc deprotection: $C_{184}H_{223}N_{80}O_{101}P_{17}$ requires monoisotopic mass: 5695.
MALDI-TOF-TOF *m/z* 5695 ($[M+H]^+$ 100%)

Compound after Phn oxidative addition $C_{199}H_{233}N_{80}O_{102}P_{17}^{16-}$ requires monoisotopic mass: 5901.
The expected ion was not detected possibly because it was not efficiently ionised by the method used.

UV-visible spectroscopy: λ_{max}: 260, 392 and 535 nm (see Fig. 3.30).
Presence of the UV-visible absorption bands at 392 nm and 535 nm provided additional confirmation of incorporation of the *N*-(2-hydroxyethyl)-phenazinium anchor group into **10.4.**

Molar Extinction coefficient (ε_{260}): 175.7 $mM^{-1}cm^{-1}$ (solvent: water).

HPLC solvent gradient: Solvent A (1% $LiClO_4$ and 0.1 % TFA in MeCN) and solvent B (1% $LiClO_4$ and 0.1 % TFA in H_2O). Solvent gradient: 0-30% solvent A over 60 mins (0-10 % from 0 – 10 mins; 10 – 30% from 10- 60 minutes).

Retention time: 31.9- 32.6 minutes.
m.p. (unable to crystallise)
Yield: 62 %

3.2.23. Characterisation of N-(2-Hydroxyethyl)phenazinium Chloride

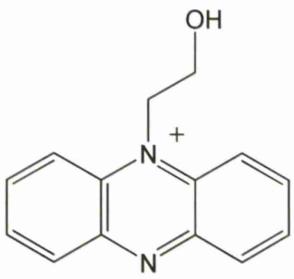

^{1}H-NMR (300 MHz, [d_4]-MeOD): δ_H 4.36 (dd, 2H, *J* = 5.1 Hz, *J* = 5.1 Hz, CH_2), 5.82 (dd, 2H, *J* = 5.0 Hz, *J* = 5.0 Hz, CH_2), 8.35 (dd, 2H, *J* = 6.0 Hz, *J* = 6.0 Hz, Ar-H), 8.53 (t, 2H, *J* = 7.1 Hz, Ar-H), 8.71 (s, 1H, Ar-H), 8.74 (s, 1H, Ar-H), 8.88 (s, 1H, Ar-H), 8.93 (s, 1H, Ar-H).

^{13}C NMR (75 MHz, [d_4]-MeOD): δ_C 54.89 (CH_2), 61.77 (CH_2), 120.83 (Ar-H), 133.77 (Ar-H), 141.07 (Ar-H).

$C_{14}H_{13}N_2O^+$ monoisotopic mass requires 225.10278
MS (ES^+) *m/z* 225.1 ([M] $^+$ 100%).
MS (Accurate mass) *m/z* 225.10228. ([M] $^+$ 100%).
($C_{14}H_{13}N_2O$ average mass requires: 225.27009)

Elemental analysis (CHN): requires: C, 74.65; H, 5.82; N, 12.44.
Found: C, 64.5; H, 5.1; N, 10.5.
Recalculated for $C_{14}H_{13}N_2OCl$ which requires C, 64.5; H, 5.0; N, 10.7.

m.p. = 340- 350°C

UV-visible spectroscopy: λ_{max}: 260, 370, 388nm (see Fig. 3.18).
Molar extinction coefficient (ε_{260}): 75.414 $mM^{-1}cm^{-1}$

V_{max}/cm^{-1} 3230-3400 (-OH), 3030 (=C-H), 2840, 2950 (C-H alkyl stretch (-CH_2-)), 1610 (C=C), 1560 (C=N).

Yield: 57 %

3.2.24. Characterisation of synthesised AR by HPLC

The *on-line* UV-visible spectral detection system of the HPLC instrument was very useful for identifying the different eluates during the HPLC purification at wavelengths of 260, 392 nm and 535 nm.

Typically the unmodified parent oligonucleotide would elute first with a retention time of approximately 30 min; recognisable from its characteristic single UV absorption band at 260 nm.

The ARs (oligonucleotide-phenazinium incorporating conjugates) would normally elute later (due to their increased hydrophobicity) with a peak of retention time of approximately 32 min, showing absorption bands at 260, 392 and 535 nm (ratio ~ 10_{260} : 0.4_{395} : 0.6_{530}) .These absorption bands and their shape (see Figure 3.13) were characteristic of the oligonucleotide and Phn-containing ARs.

3.2.25. Discussion of chemistry

Comparison of different chemistry routes

All chemistry routes summarised in the reaction schemes (Figures 1.25-1.30) share the same chemical precursor **6**, shown in Figure 1.24. Therefore, the comparison of cost-efficiency of the chemistry strategies was carried out starting from precursor **6**. Summary of the main criteria for success of the different synthetic routes generated from precursor **6** is presented in Table 3.1.

The synthetic route to making **10.4** in Figure 1.30 was more cost-effective than that used to make the same compound **11.1** in Figure 1.25 for several reasons:

It took ten steps to synthesise **11.1** and nine steps to synthesise **10.4**. This was based on the decision to add the oligonucleotide before the Phn group in the synthetic sequence which allowed deprotection and subsequent Phn addition to be combined *in situ* reducing the number of steps by one.

Adding the Phn first as in the synthesis of **11.1** (Figure 1.25) significantly reduced the yield of this step (yield of 8.5 % compared to approx 50-70 % when Phn was attached in the step following the oligonucleotide attachment). All routes involving oligonucleotide attachment before Phn attachment gave much higher yields.

It is also more difficult to add Phn in basic conditions while keeping trifluoroacetamide (Tfa) intact, which requires a reaction in dry conditions to prevent alkaline hydrolysis of the Tfa. This favours the synthesis of **10.4** (Figure 1.30) as a less precarious and more facile route.

The oligonucleotide moiety's large size and polarity greatly assisted purification as it was easily precipitated in 2 % $LiClO_4$ in acetone prior to HPLC. Further purification of **10.4** by HPLC was easier as the main peak was the desired compound. When **11.1** was purified there were multiple unwanted compounds making it difficult to find the correct compound without separating all the fractions and subjecting each of them to NMR analysis to find the correct one.

Routes to **10.3** (Figure 1.28) and **10.4** (Figure 1.30) allow comparison of the effectiveness of the two pairs of orthogonal protecting groups used (Mtt and Fmoc or Boc and Fmoc).

Fmoc and Mtt were initially selected to allow imidazoles to retain their Boc protection under very mild acidolysis, however imidazole protection with boc proved to be precarious and acid labile under even mildly acidic conditions. With this in mind it is more cost effective to use Boc instead of Mtt.

Comparing **10.2** (Figure 1.27) and **10.3** (Figure 1.28) allows comparison of using Fmoc or Tfa before conjugation to Phn. Both gave similar yields (53 % and 61 %, respectively) when used in this reaction.

In terms of the most cost effective protecting groups to use, Boc and Fmoc or Boc and Tfa were the best and similarly effective.

Synthetic routes to **10.2** and **10.3** were therefore the most robust and cost effective. The synthetic route to **10.4** would be similar in cost effectiveness if the Mtt is replaced with Boc and is more robust than the route to **11.1**.

Oligonucleotide introduction before Phn which was attached as the final step produced a much higher yield. This step was also easier to perform and precipitate and subsequently produced a single main fraction on HPLC which greatly simplified its purification. This method also doesn't require the extensive, time consuming HPLC purification of adding the Phn first which produces a series of impurities and makes identification of many of the eluates necessary by NMR to determine the correct fraction and results in a very low yield of approximately 8.5 %.
This realisation lead to abandoning synthesis of **13.2** (Figure 1.26) and instead using the alternate route in Figure 1.27 to make the same final product called **10.2**

The route to **13.2** was too long-winded and experience synthesising **11.1** lead to the conclusion that the adapted route to **10.2** would be more facile and cost-effective with fewer steps.

Although attempts were made to protect the imidazole groups throughout, unfortunately, it was not possible to deprotect mtt without deprotecting the acid-

labile Bocs on the imidazole groups which proved to be very good leaving groups even at low concentrations of acid at which the Boc on the ε amine of lysine remained intact. Hence the alternative route in Figure 1.30 was adopted. On this basis, the base-labile Fmoc was preferred as an orthogonal protecting group with Boc.

Table 3.1. Summary of main criteria for success of the different synthetic routes generated from precursor **6.**

Final compound of synthetic route	Number of steps	Final yield (from precursor **6**) (%)	Special care/conditions/ dangers
11.1	10	0.47	Difficult to add Phn in basic conditions while keeping trifluoroacetamide (Tfa) intact
10.2	9	8.57	NA
10.3	9	7.50	NA
10.4	9	4.98	NA

Safety considerations

Synthesis of the precursor **6** required the use of DCC. DANGER: harmful if swallowed or inhaled, toxic in contact with skin, may cause serious eye damage and may act as a sensitizer.

Synthesis of *N*-(2-Hydroxyethyl)phenazinium chloride required the use of ethylene oxide. DANGER: highly inflammable and toxic by inhalation, ingestion and through skin contact.

3.3. Biophysical studies

3.3.1. Introduction

This chapter focuses on the evaluation of the role of *N*-(2-hydroxyethyl)phenazinium as an anchor group. This anchor has been incorporated with the bis-imidazole catalytic domain of the studied oligonucleotide-based ribonuclease mimics (**11.1**, **10.2**, **10.3** and **10.4**) to enhance their overall affinity to target RNA molecules. The rationale behind this concept was based on the assumption that the strength of the sequence–specific binding of the studied ARs towards complementary RNA regions can be re-enforced by additional non-specific (*e.g.* hydrophobic and/or electrostatic) interactions between anchor groups and target RNA molecules. An additional synergistic effect expected from the incorporation of *N*-(2-hydroxyethyl)phenazinium anchor group could be an increase in attraction of the bis-imidazole cleaving constructs towards the RNA chain, which may promote superior cleaving potential.

3.3.2. Aim of this Chapter

The studied conjugates **11.1**, **10.2**, **10.3** and **10.4** consist of two pairs of structural isomers (**11.1** and **10.4** are a structurally identical pair of conjugates prepared by different synthetic routes (see Figures 1.25 and 1.30), and likewise **10.2** and **10.3** are an identical pair of conjugates also prepared by different synthetic routes (see Figures 1.27 and 1.28). The two pairs differ with a varied disposition of the cleaving construct, phenazinium anchor and oligonucleotide binding domains (Figure 3.6). The aim of this Chapter was therefore to assess:

(i) Whether the *N*-(2-Hydroxyethyl)phenazinium anchor group is capable of enhancing the hybridisation ability of the studied ribonuclease biomimetics.

(ii)The influence of *N*-(2-Hydroxyethyl)phenazinium anchor group on hydrolytic ability of this type of chemical nuclease.

(iii) Structural factors (*e.g.* mutual orientation of the anchor and cleaving groups towards oligonucleotide moiety) that might affect both affinity and hydrolytic potential.

The initial stage of this study was focused on evaluation of the nature and efficiency of non-specific RNA binding agents, here the *N*-(2-

hydroxyethyl)phenazinium anchor group without a specific oligonucleotide binding domain (section 3.4.6). This was followed by further assessment of the ability of the phenazinium anchor to promote binding affinity towards RNA at the level of oligonucleotide-based ARs (*i.e.* **11.1**, **10.2**, **10.3** and **10.4)**.

Figure 3.6. Schematic presentation of the two families of conjugates with different mutual orientation of cleaving groups, linker, anchor and oligonucleotide binder. Conjugates **11.1** and **10.4** (**A**) have Phn anchor group more closely attached to the cleaving group (on α-amine of lysine linker). Conjugates **10.2** and **10.3** (**B**) have oligonucleotide recognition element more closely attached to the cleaving group (on ε-amine of lysine linker).

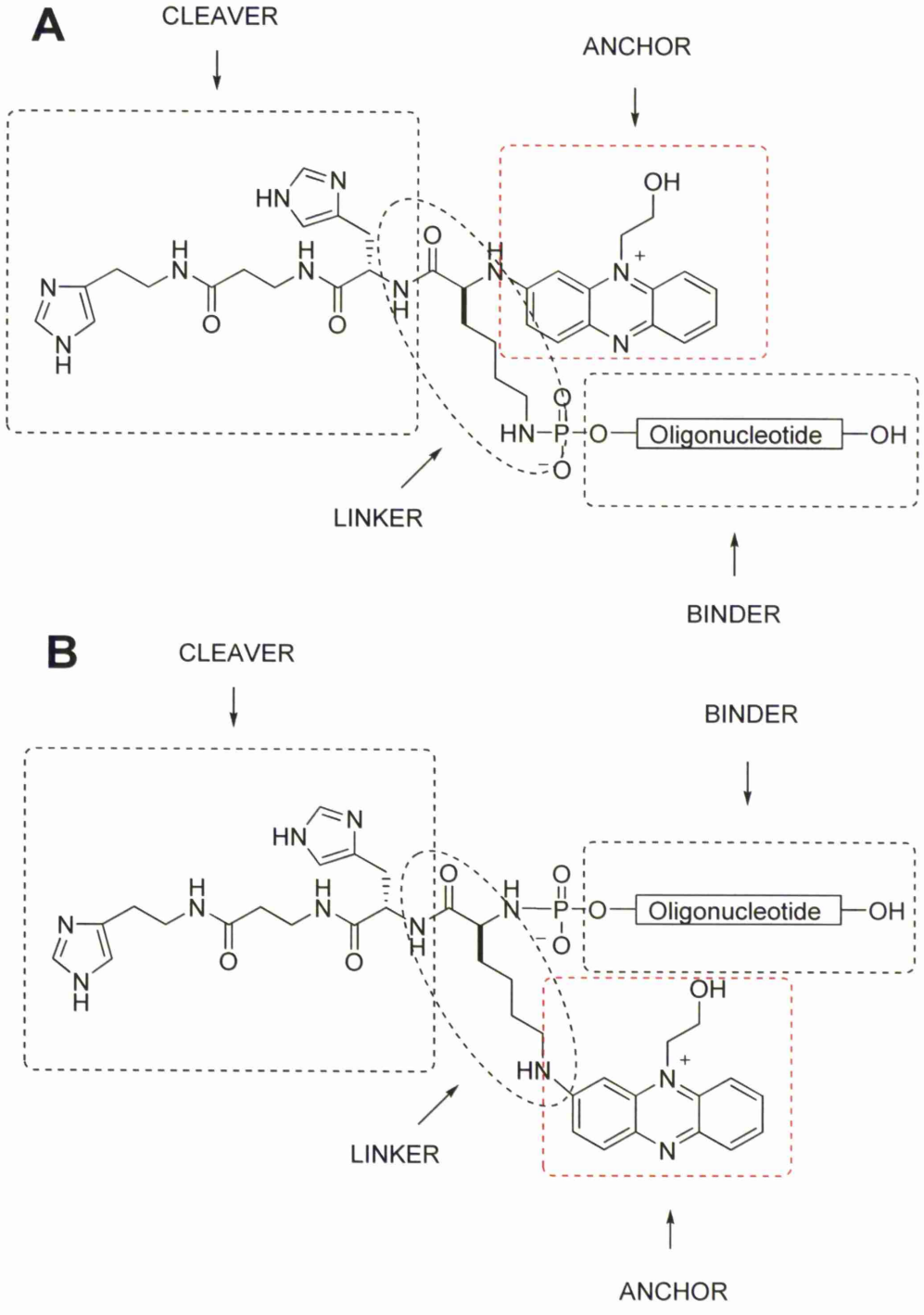

The 'anchor' group used in this study (10-(2-hydroxyethyl)phenazinium) is a well known intercalator [204] and is also a cationic (phenazinium quaternary salt) and polyaromatic compound (see Fig. 3.7).

Figure 3.7. Chemical structure of 10-(2-hydroxyethyl)phenazinium chloride (quaternary salt) used as the potential 'anchor' group for the studied conjugates.

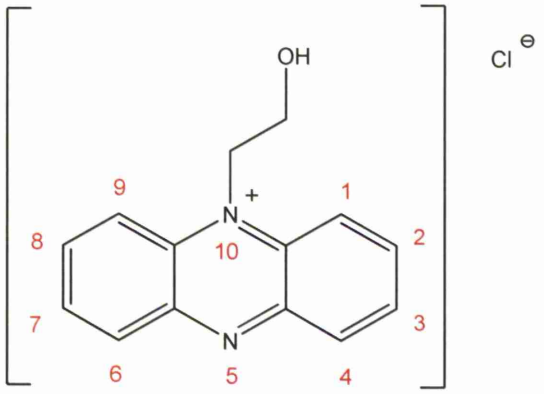

Based on the planar structure and positive charge of the cationic quaternary salt, *N*-(2-hydroxyethyl)phenazinium chloride might be expected to bind nucleic acids *via* intercalation (Denisov A. Yu, 2000) and/or electrostatic interactions with negatively charged sugar-phosphate backbone of target RNA sequence.

Therefore, this part of my research is focused on the biophysical evaluation of the RNA-interacting properties of this *N*-(2-hydroxyethyl)phenazinium anchor group. The aim is to assess the potential impact of these interactions upon binding and on the catalytic properties of the synthesised conjugates **11.1, 10.2, 10.3** and **10.4**. Better understanding of the modes of interactions between the phenazinium anchor group with RNA can lead to the superior design of novel classes of more efficient and potent artificial ribonucleases with higher affinity towards RNA.

3.3.3. Advantages of using phenazinium as an 'anchor' group

There are several advantages of using phenazinium-based ions as stabilising agents. Intercalating and cationic agents conjugated to oligodeoxyribonucleotides have been shown to produce better binding affinity (referred to as 'excess binding energy') to complementary strands [172, 211] whilst appearing to be less sensitive to cellular nucleases [212] and more readily taken up by cells compared to their respective unmodified oligodeoxyribonucleotide [204].

From an organic synthesis point of view, the enhanced reactivity of phenazinium at position 2 makes it suitable for easy conjugation with compounds containing a free primary aliphatic amine [213], as required for its incorporation into AR complexes.

Another important advantage of this anchor group could be stabilisation of the interactions between the recognition (oligonucleotide) component of ARs and RNA target. It has been shown in a previous study [203] that T_m values of the complementary complex formed by a 7-mer oligonucleotide conjugated to *N*-(2-hydroxyethyl)phenazinium and 12-mer oligonucleotide was up to 19 °C higher as compared to that found for the unmodified oligonucleotide analogues (See Table 3.2, taken from [203]). The degree of stabilisation was strongly dependent on the length of the linker separating the oligonucleotide moiety and the intercalating dye and stabilisation decreased linearly with increased linker length [203].

Table 3.2. T_m values of 7-mer oligonucleotides conjugated to *N*-hydroxyethyl phenazinium with various linker lengths in a duplex with a complementary 12-mer oligonucleotide (taken from [203]).

Intercalator	**Position**	**Duplex studied**	**Tm (°C)**
N-(2-hydroxyethyl)-phenazinium chloride (Pzn)	5'	5'-p(d(AACCTGTTTGGC))-3' + (Pzn)NH$(CH_2)_n$NH5'-p(d(CCAAAC)rA)- 3'	
n=2			47
n=3			45
n=4			44
n=5			43
n=6			43
n=7			41
5'-p(d(AACCTGTTTGGC))-3' + 5'-p(d(CCAAAC)rA)-3'			28
5'-p(d(AACCTGTTTGGC))-3' + $NH_2(CH_2)_n$NH5'-p(d(CCAAAC)rA)-3'			28

From previous research two possible arrangements which the phenazinium group can adopt in a duplex environment include (i) stacking on top of the neighbouring base-pair of the double-stranded part of the nucleic acid duplex [27], (ii) intercalation *between* the base pairs of the duplex, or (iii) binding to the major/minor grooves [207].

However, no previous research has been conducted on the evaluation of the contribution from the electrostatic interactions of this *positively charged* phenazinium group with the negatively charged phosphodiester backbone of oligonucleotides. The results in this area therefore represent my contribution to the field.

Both, circular dichroism and 2D NMR spectroscopy have been used to detect intercalation and groove binding [27, 203, 204, 207, 208, 214]. According to these studies the phenazinium group interacts with the neighbouring bases of the duplex structure by stacking on top of the terminal base-pair of the complex where the phenazinium is covalently bonded (Figure 3.7). This arrangement is adopted regardless of the specific base sequence of the complex.

Figure 3.8. Representation of the proposed interaction model between the *N*-(2-hydroxyethyl)phenazinium group covalently attached to the 7-mer oligonucleotide conjugate and a DNA duplex formed with the complementary 8-mer target. The model was based on 2D-NMR spectroscopy [27].

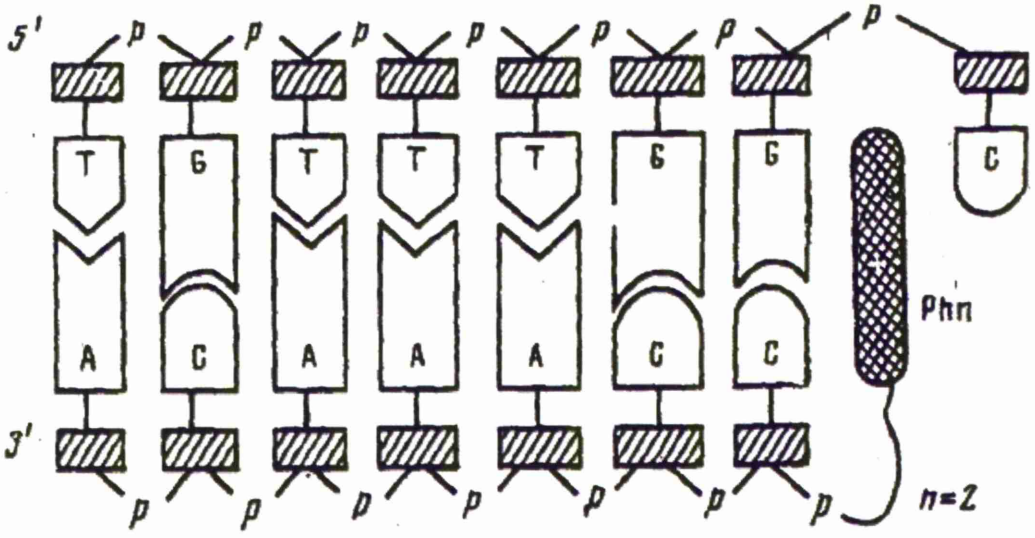

In this research, the *N*-(2-hydroxyethyl)phenazinium was integrated as part of a bulky bis-imidazole catalytic domain and linker (lysine residue) and, thus, the mode of its interaction with the target nucleic acid could be substantially different from the mechanism of interactions previously detected for the substantially simplified models [27, 203, 204, 207, 214]. Here we used UV-visible and fluorescence spectroscopy to evaluate any difference in the mode of action of the phenazinium anchor groups within the bis-imidazole catalytic construct, both free and attached to the oligonucleotide recognition element, towards the RNA molecule.

3.3.4. UV- visible and fluorescent properties of phenazinium

The presence of very distinctive absorption and fluorescence bands in the UV-visible and fluorescent spectra of *N*-(2-hydroxyethyl)phenazinium group provide a very robust and sensitive approach to monitor the behaviour of **9.1** (bis-imidazole tetrapeptide construct with covalently attached phenazinium anchor, but lacking oligonucleotide recognition element) and the oligonucleotide conjugates **11.1, 10.2, 10.3** and **10.4** with the model 23-mer RNA target. UV-visible spectroscopy and fluorescence spectroscopy were used to follow the change in absorption and fluorescence emission, respectively, as a result of any interactions with the RNA target.

UV-visible-based (T_m) profiles monitored by absorption at both oligonucleotide (260 nm) and phenazinium bands (395nm and 520nm, respectively) were used to assess the stability of the *AR:Target RNA* hybrid complexes.

The typical UV-visible absorption spectra of 2-substituted phenazinium derivatives show bands at *ca*. 237, 290, 390 and 530 nm [205], distinct from the spectrum of unmodified *N*-(2-hydroxyethyl)phenazinium (compare UV-visible spectra on Figure 3.3 for **9.1** and unconjugated *N*-(2-hydroxyethyl)phenazinium).

The typical fluorescence spectrum of Phn-labelled constructs produce emission bands at *ca*. 608 nm when excited at 395 nm and 525 nm (Figure 3.37).

3.3.5. General strategy and experimental design

To evaluate the effects of the *N*-hydroxyethylphenazinium anchor group incorporated into the bis-imidazole cleaving constructs of the AR molecules (**11.1, 10.2, 10.3** and **10.4)**, we initially monitored the interactions of the *oligonucleotide-free N*-hydroxyethylphenazinium-containing construct **9.1** (see Figure 3.12) with the 23-mer RNA sequence (5′-AGGUCCUGUGUUCGAUCCACAGA), using either UV-visible or fluorescence spectroscopy. The 17-mer oligodeoxyribonucleotide sequence of the conjugates was perfectly complementary to the target's 23-mer 2′ OMe RNA sequence (see Figure 3.29). Modified RNA (2′ OMe RNA) was used in all experiments due to its greater stability to cleavage.

Intermolecular interactions between *N*-(2-hydroxyethyl)phenazinium for each test compound and the RNA target were monitored by following the characteristic UV-visible bands of the *N*-(2-hydroxyethyl)phenazinium chromophore at *ca*: 395 nm and 525 nm, (band at 288nm was not used due to its overlap with the absorbance of RNA at 260nm).

Firstly, interactions of the *N*-(2-hydroxyethyl)phenazinium conjugated to the cleaving tetrapeptide construct (**9.1**, Figure 3.9) were monitored upon the interaction of **9.1** with the 23-mer RNA sequence. This construct lacks a specific recognition 17-mer oligonucleotide component and thus does not have the ability to form specific Watson-Crick hydrogen bonding with the RNA target.

Secondly, the interactions of the *N*-(2-hydroxyethyl)phenazinium incorporated into the structures of the ARs **11.1**, **10.2**, **10.3** and **10.4** were studied on hybridisation with the complementary 23-mer 2′ OMe RNA target (Figure 3.8). These conjugates **11.1**, **10.2**, **10.3** and **10.4** possess an additional oligonucleotide recognition element, designed to specifically hybridise to the complementary regions of the 23-mer 2′ OMe RNA target via Watson-Crick hydrogen bonding (see Figure 3.36).

Finally, the above data were compared with a control experiment using *N*-(2-hydroxyethyl)phenazinium conjugated to the terminal 5′ phosphate of the 17-mer oligonucleotide *via* an ethylene diamine linker (Fig. 3.9, (**15**)). Compound **15**, (which is a structural analogue of **11.1, 10.2, 10.3** and **10.4**, but lacking

the bis-imidazole containing tetrapeptide fragment) was used as a control compound to evaluate the influence that the cleaving groups may have on interaction with RNA.

The molecules incorporating *N*-(2-hydroxyethyl)phenazinium, which have been studied in this Chapter, are shown below:

Figure 3.9. The 3 different types of phenazinium- incorporated cleaving compounds.

1) **9.1**: *N*-(2-hydroxyethyl)phenazinium conjugated to the tetrapeptide construct.

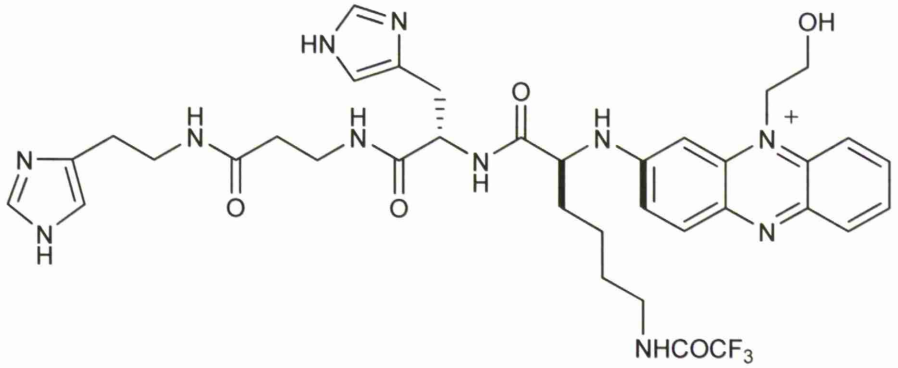

2) Control (**15**): *N*-(2-hydroxyethyl)phenazinium conjugated to the 5′ phosphate of a 17-mer oligonucleotide (5′-pdGATCGAACACAGGACCT) via an ethylene diamine linker i.e. without the bis-imidazole tetrapeptide.

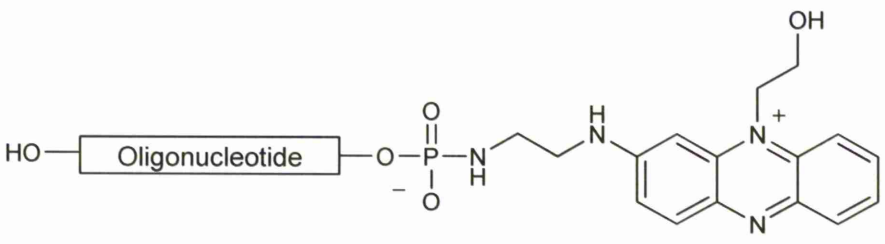

3) *N*-(2-hydroxyethyl)phenazinium coupled to the tetrapeptide construct which is conjugated to a 17-mer oligodeoxyribonucleotide (5'-pdGATCGAACACAGGACCT). These included **11.1** and **10.4**, which have the same chemical structures, but have been synthesised using two different synthetic routes (see Figures 1.25 and 1.30, and section 1.12 for details).

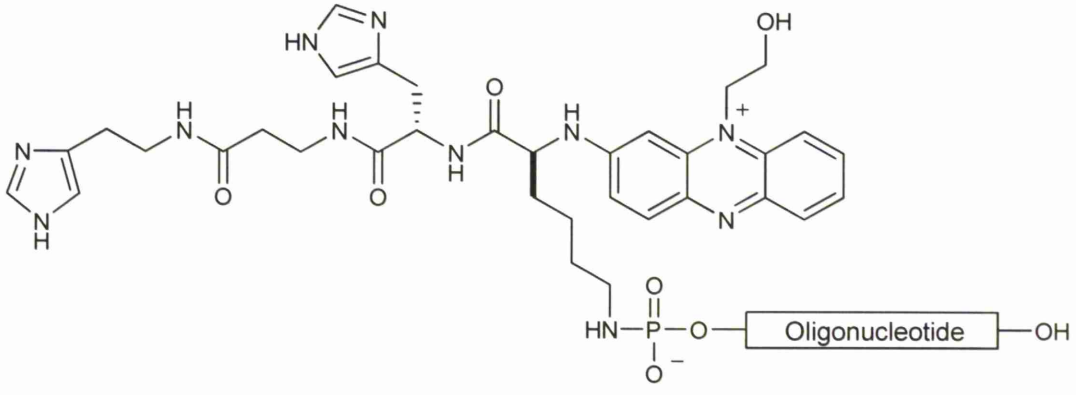

In addition, structurally different from **11.1** and **10.4**, compounds **10.2** and **10.3** (shown below) are also identical to each other but synthesised by different synthetic routes (see Figures 1.27 and 1.28).

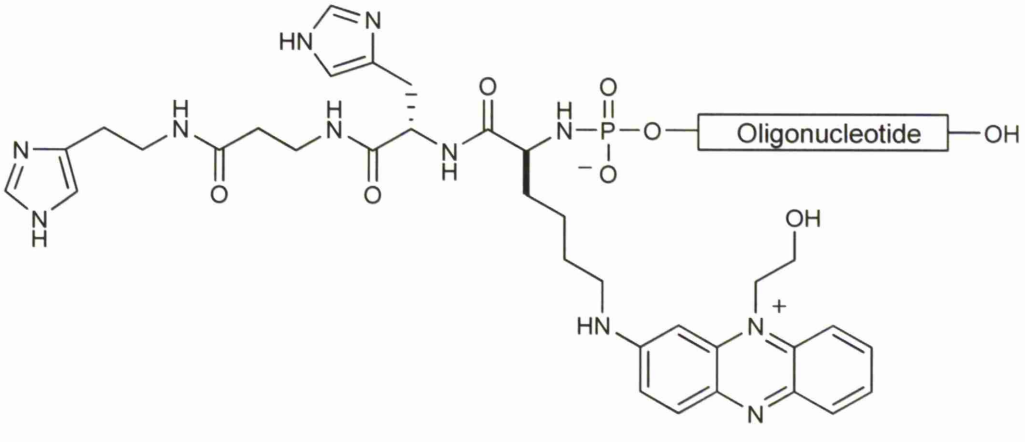

3.3.6. UV-visible spectroscopy

3.3.6.1. UV-visible spectroscopy of free N-(2-hydroxyethyl)phenazinium

UV-visible spectroscopy of free *N*-(2-hydroxyethyl)phenazinium in aqueous solutions showed two main absorption bands *circa* 260 and 390 nm. An aqueous solution of *N*-(2-hydroxyethyl)phenazinium has a yellow colour due to UV-visible absorption band at 390 nm.

Figure 3.10. UV-visible spectrum of *free* *N*-(2-hydroxyethyl)phenazinium recorded in water at 20°C. Chemical structure and absorption λ_{max} are also indicated.

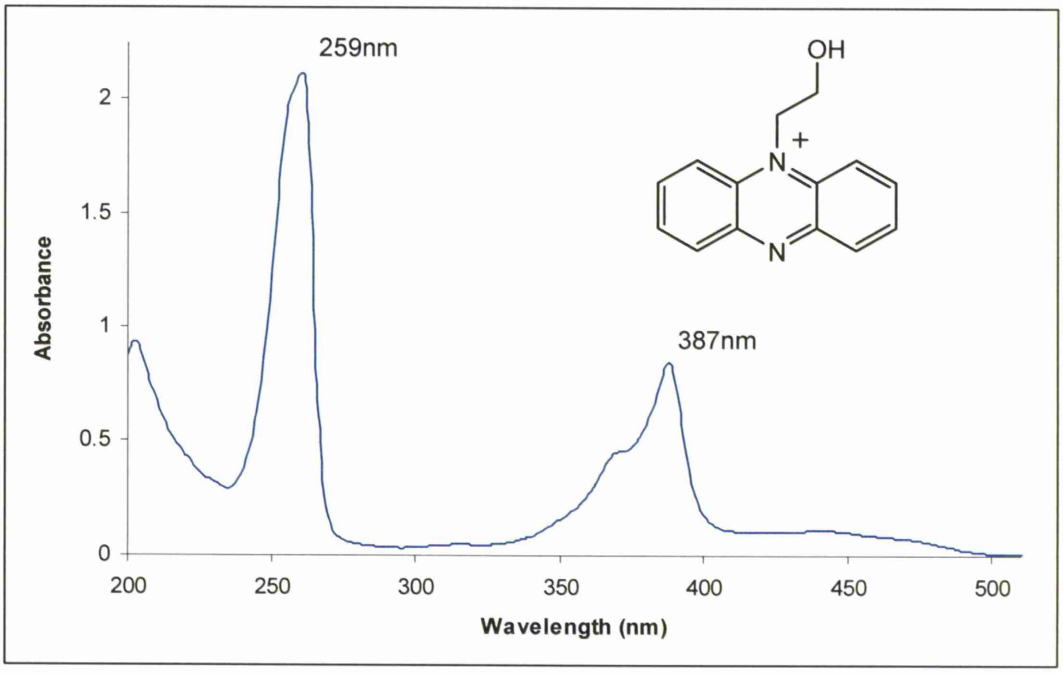

The molar extinction coefficient (ε_{260}) of *N*-(2-hydroxyethyl)phenazinium, measured in water, as described in the experimental section (see 'Material and Methods'), was found to be 75.4 $mM^{-1}cm^{-1}$.

3.3.6.2. UV-visible spectroscopy of construct 9.1.

Aqueous solutions of **9.1** showed a UV-visible absorption spectrum typical for a phenazinium derivative with an amino-alkyl substituting group at position 2 [213], Figure 3.11. It is seen that the substitution at position 2 (with the –NH-R group) of the heteroaromatic ring of *N*-(2-hydroxyethyl)phenazinium results in a major change of the visible region of the absorption spectrum with main absorption bands seen at 230, 290, 395 and 520 nm (Bands 1 - 4, respectively). The major indicative band of the above modification is the appearance of longer wavelength absorption at 520 nm, responsible for the red-purple colour of **9.1**.

Figure 3.11. UV-visible spectrum of *N*-(2-hydroxyethyl)phenazinium conjugated to tetrapeptide construct (**9.1**) recorded at 5 μM concentration in water at 20°C. UV-visible absorption λ_{max} values and designated band numbers are indicated.

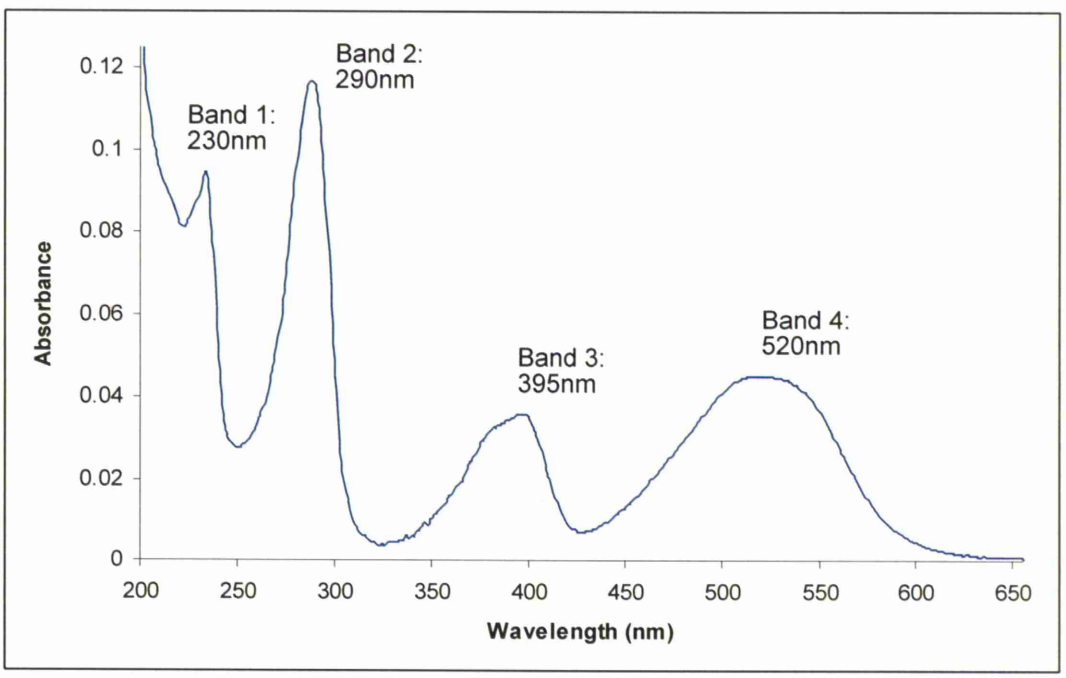

The molar extinction coefficient (ε_{260}) of **9.1** measured in water, as described in the experimental section (see 'Material and Methods'), was found to be 6.7 $mM^{-1}cm^{-1}$.

The addition of the target 23-mer ssRNA molecule (1: 1) in water (without any counter cations present) induced a substantial bathochromic (13 nm) and 12.7 % hypochromic shift of the absorption band at 520 nm and a bathochromic shift (2 nm) and 24.4% hypochromic shift of the absorption band at 394 nm (see Figure 3.12 **A** and **B** (expanded region of the spectrum), Table 3.3).

These substantial changes in the UV-visible spectrum of the *N*-(2-hydroxyethyl) phenazinium on addition of RNA clearly indicate strong interactions between the **9.1** construct and the ssRNA molecule.

A similar experiment was performed in Tris buffer (50 mM Tris-HCl, pH 7.6, 200 mM KCl, 0.5 mM EDTA) to assess any possible interactions between **9.1** and ssRNA in the presence of K^+ counter cations. However, as seen from Figure 3.13, the addition of RNA to **9.1** did not cause any significant detectable changes in the UV-visible spectrum of **9.1**, indicating a lack of interactions with ssRNA.

Figure 3.12. (**A**) UV-vis spectrum of **9.1** (5 μM) without 23-mer 2'OMe RNA (blue) and with 2'OMe 23-mer RNA (5 μM) (red) recorded in water at 20°C. (**B**) Expansion of spectrum to show bands 3 and 4.

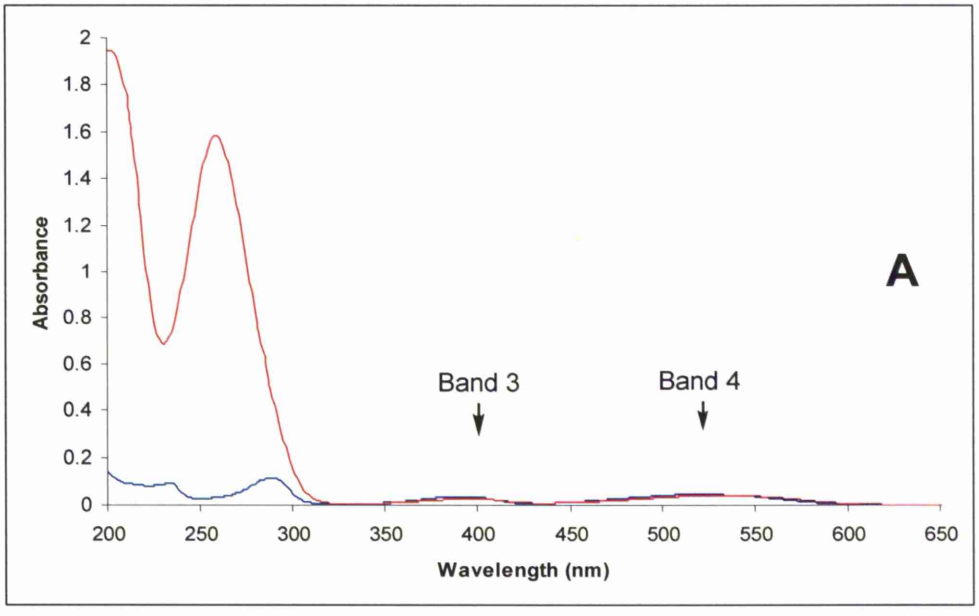

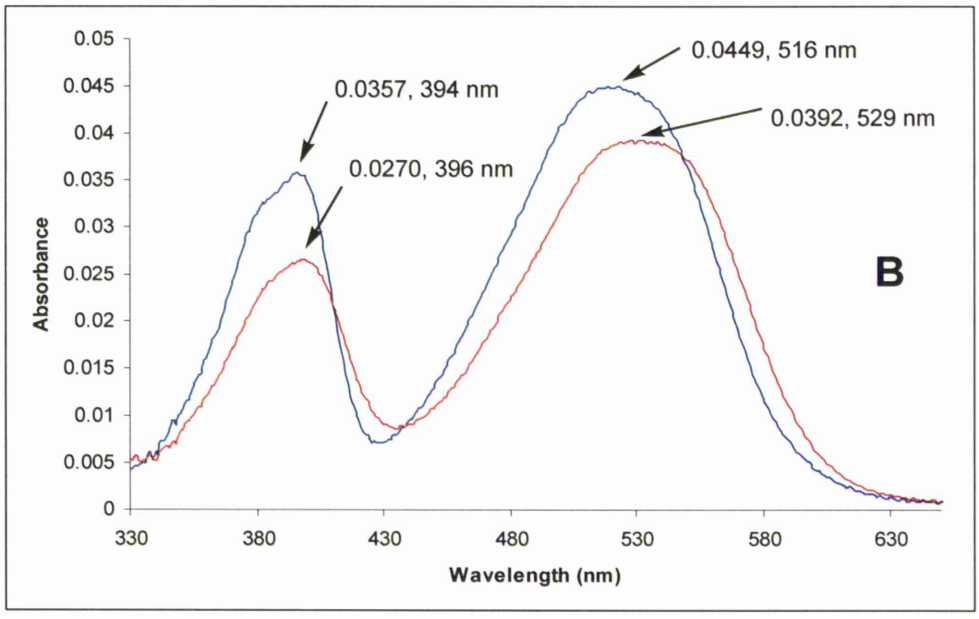

Table 3.3. Differences in absorbance and λ_{max} on addition of target RNA (5 μM) to **9.1** (5 μM) in water.

	Band 3 λ_{max} (nm)	Band 3 Absorbance	Band 4 λ_{max} (nm)	Band 4 Absorbance
9.1	394	0.0357	516	00.0449
9.1 + 23 mer	396	0.0270	529	00.0392
Difference	**2**	**0.0087 (24.4%)**	**13**	**00.0057 (12.7%)**

Figure 3.13. (**A**) UV-vis spectrum of **9.1** (5 μM) without 23-mer 2'OMe RNA (blue) and with 2'OMe 23-mer RNA (5 μM) (red) recorded in Tris buffer (50 mM Tris, 200 mM KCl, pH 7.6, 0.5 mM EDTA) at 20°C. (**B**) Expansion of spectrum to show bands 3 and 4.

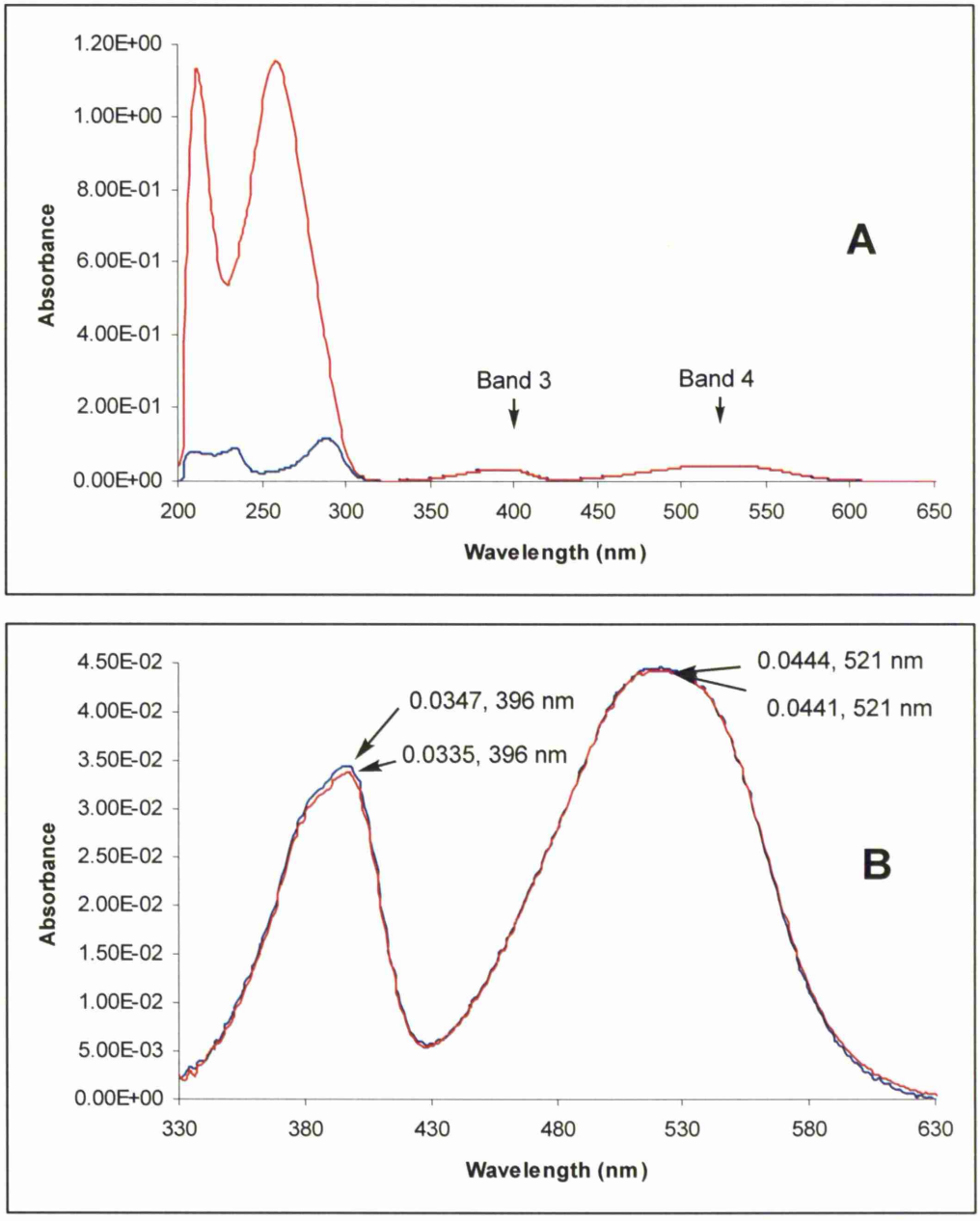

Table 3.4. Differences in absorbance and λ_{max} on addition of target RNA (5 μM) to **9.1** (5 μM) in buffer.

	Band 3 λ_{max} (nm)	Band 3 Absorbance	Band 4 λ_{max} (nm)	Band 4 Absorbance
9.1	396	0.0347	521	0.0444
9.1 + 23-mer	396	0.0335	521	0.0441
Difference	**0**	**0.0012 (3.45 %)**	**0**	**0.0003 (0.67 %)**

These findings indicated that the key 'driving forces' responsible for the interactions between Phn-containing molecules and ssRNA could be attributed to electrostatic interactions, especially as the presence of competitive K^+ counter cations at much higher concentrations (200 mM versus 5μM for **9.1**) completely blocked the binding of **9.1** to RNA. Counter cations (K^+) present in the buffer seem to compete with the positively charged Phn fragment, pushing it away from the negatively charged phosphate groups of the RNA target's phosphodiester backbone. This hypothesis has been tested in the section below.

3.3.6.3. Elucidation of the nature of interactions between 9.1 and ssRNA

To test the hypothesis above and confirm the predominance of electrostatic interactions, we repeated the experiment described in Section 3.4.6.2 (see Figure 3.12) involving the interaction of **9.1** with ssRNA in water. However, after detecting binding between **9.1** and ssRNA (see Figure 3.14, red curve), we added NaCl to achieve a 1M final concentration of NaCl (aq). This resulted in complete recovery of the absorption band (see Figure 3.14, grey curve). This experiment confirmed that excessive amount of positively charged counter cations can completely displace positively charged **9.1** from the negatively charged ssRNA phosphodiester backbone, indicating its predominant electrostatic nature of interaction.

Figure 3.14. UV-visible spectrum of **9.1** (blue), **9.1** with 23-mer 2'OMe RNA in water *before* (red) and *after* addition of 1M NaCl (grey). The concentrations of both **9.1** and 2'OMe RNA was 5 μM (1:1). Spectra were recorded at 20°C.

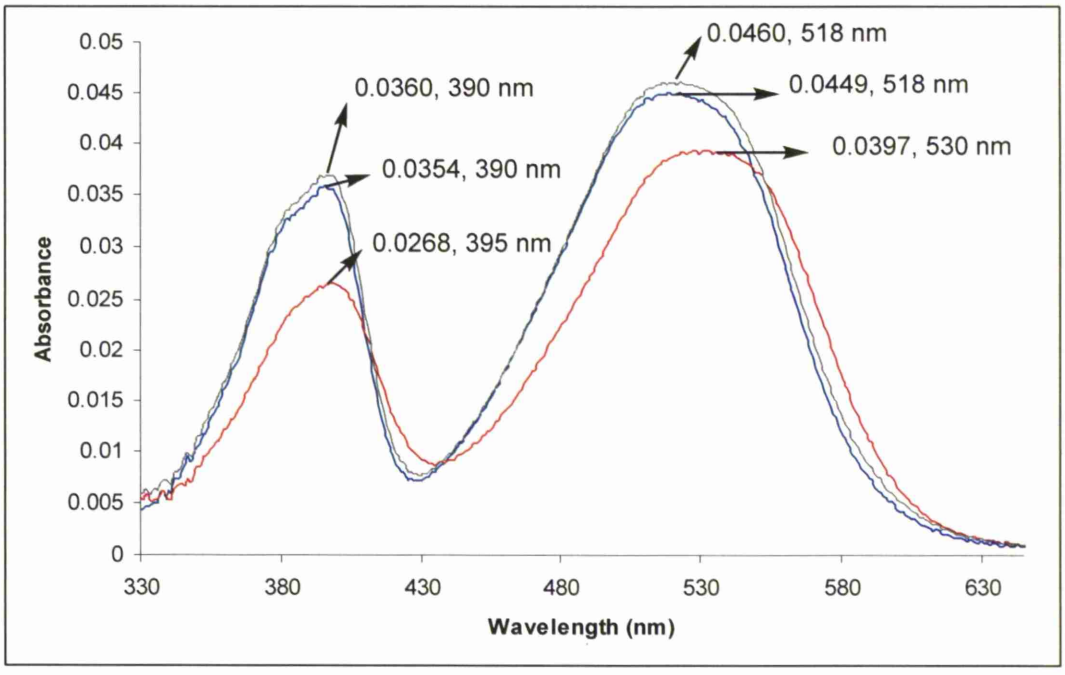

Table 3.5. Differences in absorbance and λ_{max} on addition of target RNA (5 μM) to **9.1** (5 μM) in water.

	Band 3 λ_{max} (nm)	Band 3 Absorbance	Band 4 λ_{max} (nm)	Band 4 Absorbance
9.1	390	0.0354	518	0.0449
9.1 + 23 mer	395	0.0268	530	0.0397
Difference	**5**	**0.0086 (24.2 %)**	**12**	**0.0052 (11.6 %)**
9.1 + 23 mer + 1M NaCl	390	0.0360	518	0.0460

These hypochromic and bathochromic shifts observed on addition of 23-mer target RNA were reversible on addition of (a high concentration) 1M NaCl (aq), demonstrating a predominant electrostatic nature of the interactions.

3.3.6.4. Interaction of 9.1 with complementary duplex

Comparison in 10 fold diluted buffer

The *N*-(2-hydroxyethyl)phenazinium of **9.1** (5 μM) has a similar mode of interaction with the double-stranded duplex of 23-mer *2'OMe RNA: 17mer DNA* (1:1; 5 μM) in 0.1-fold buffer (5 mM Tris, 20 mM KCl, pH 7.6, 0.05 mM EDTA).

Although the buffer concentration was 10 times lower in this experiment than in the normal hybridisation buffer (to avoid excessive amount of counter cations and thus decrease electrostatic 'shield' around the RNA target), a sufficient concentration of counter cations to allow hybridisation of the duplex was demonstrated by the T_m experiment (Figure 3.15, below), which showed a sigmoidal melting with a T_m of 49°C for the control system (*17-mer DNA: 23-mer* 2'OMe *RNA duplex)* in the absence of **9.1.**

Figure 3.15. Melting curve (cooling phase) of control system (*17-mer DNA: 23-mer* 2'OMe *RNA duplex* (5μM)) in the absence of **9.1.** monitored at 260 nm in 10 x diluted Tris buffer (5 mM Tris, 20 mM KCl, pH 7.6, 0.05 mM EDTA).

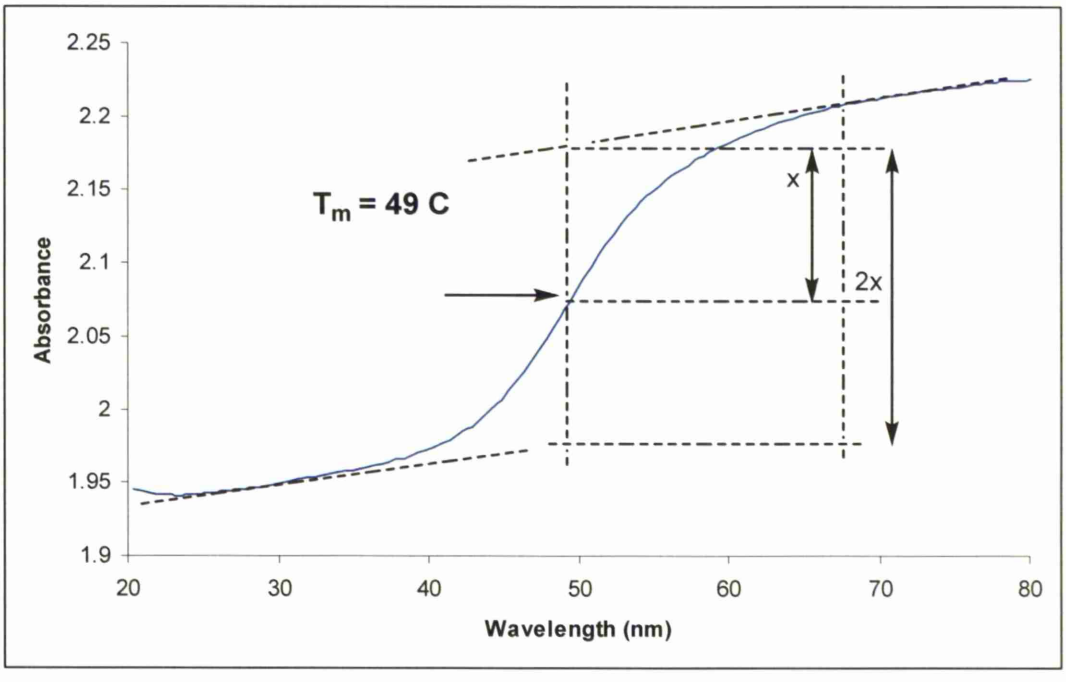

However, addition of the **9.1** to the pre-formed double-stranded duplex (17-mer DNA and 23-mer 2'OMe RNA) increased the T_m value (see Figure 3.16 below).

Figure 3.16. Melting curve (cooling phase) *17-mer DNA:23-mer RNA duplex* (5 μM) in the *presence* of **9.1** (5 μM), monitored at 260 nm in 10 x diluted Tris buffer (5 mM Tris, 20 mM KCl, pH 7.6, 0.05 mM EDTA).

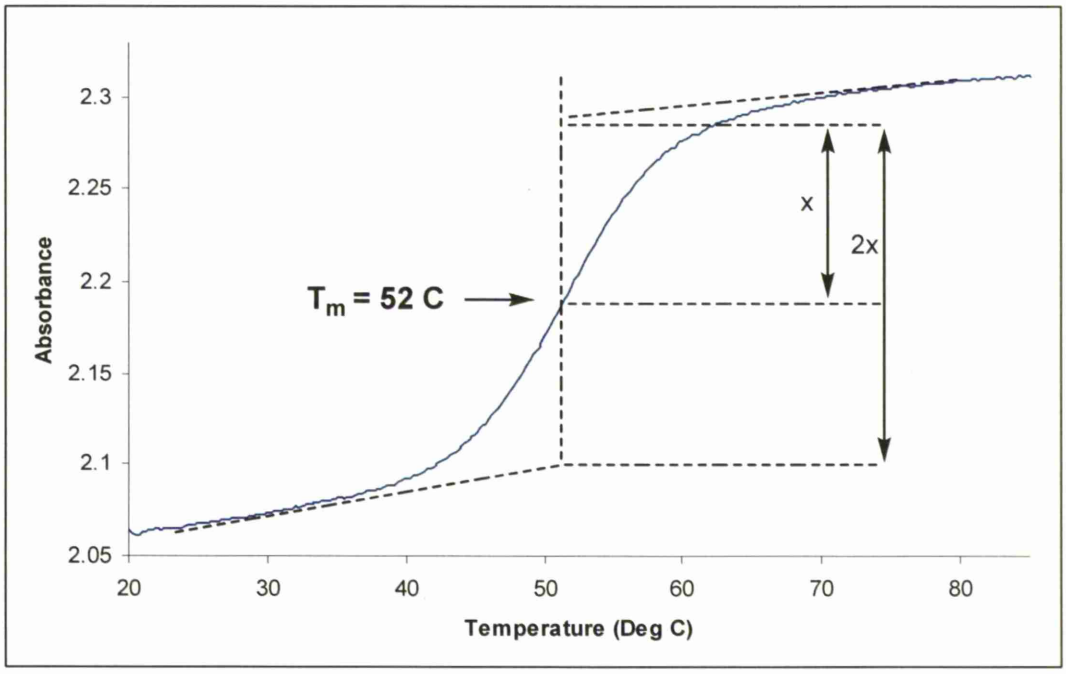

Melting temperature results: **9.1** with duplex (17-mer DNA and 23-mer 2'OMe RNA): 50 ± 1 °C, 51 ± 1 °C in 10 X diluted buffer.

Therefore, T_m of the *target 23-mer 2'OMe RNA* duplex in the *presence* of **9.1** (5 μM) was found to be 52 ± 1 °C (average from 3 results). This showed a stabilisation effect of 3 °C of the duplex, induced by **9.1**.

Moreover, the addition of double-stranded *2'OMe RNA: 17-mer DNA hybrid* (1:1) induced substantial bathochromic shifts of (5 nm and 13 nm) and 36 % and 20 % hypochromic shifts of the absorption bands at 395 nm and 520 nm, respectively (see Figure 3.17, Table 3.6).

Figure 3.17. UV-visible spectrum of **9.1** (5 μM)(blue) with (17-mer DNA + 23-mer 2'OMe RNA) duplex (5 μM)(red) recorded in (10 x diluted) Tris buffer (5 mM Tris, 20 mM KCl, pH 7.6, 0.05 mM EDTA) at 20°C.

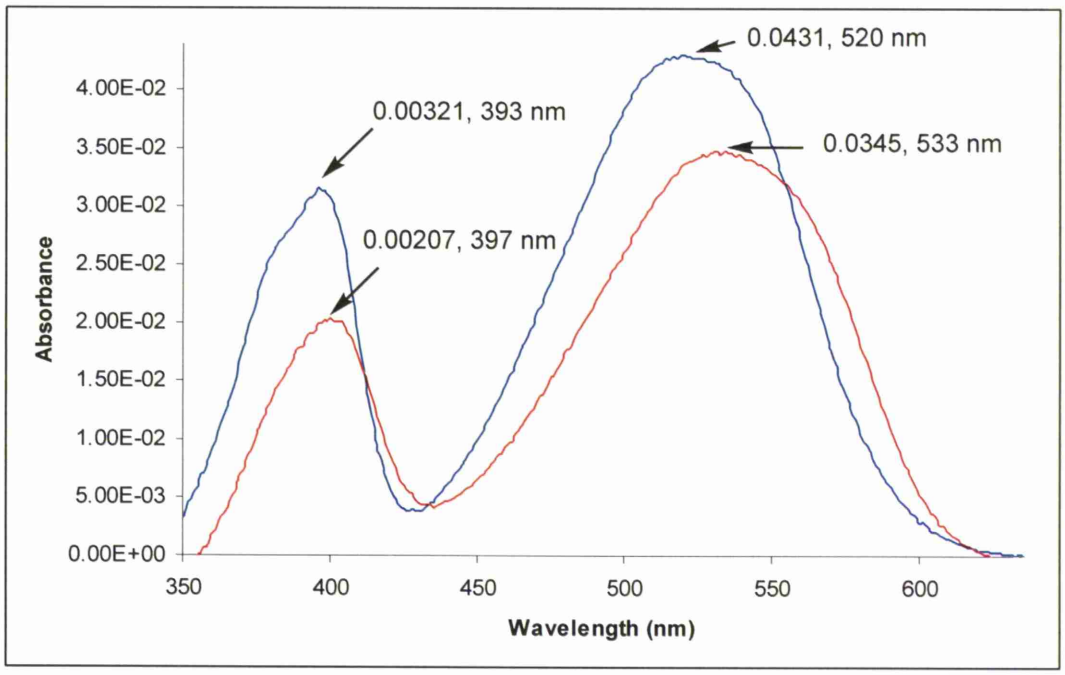

Table 3.6. Differences in absorbance and λ_{max} on addition of the (17-mer DNA + 23-mer 2'OMe RNA) duplex (5 μM) to **9.1** (5 μM).

	Band 3 λ_{max} (nm)	Band 3 Absorbance	Band 4 λ_{max} (nm)	Band 4 Absorbance
9.1	0.0321	393	520	0.0431
9.1 + (17 mer + 23 mer)	0.0207	397	533	0.0345
Difference	**0.0114 (36%)**	**4**	**13**	**0.0086 (20%)**

The results of **9.1** with the double stranded duplex were similar to those of **9.1** and ssRNA.

Therefore, the above experiment clearly indicates that *N*-(2-hydroxyethyl) phenazinium moiety of **9.1** strongly interacts with the *2'OMe RNA: 17mer DNA* in the 0.1-fold buffer.

3.3.6.5. Interaction of (15) with the target RNA

A 17-mer oligodeoxyribonucleotide attached to *N*-(2-hydroxyethyl)phenazinium via an ethylene diamine linker (lacking the bis-imidazole tetrapeptide construct) was used as a control compound (Figure 3.18).

Figure 3.18. Control compound: (**15**), *N*-(2-hydroxyethyl)phenazinium conjugated to a 17-mer oligonucleotide (5′-pdGATCGAACACAGGACCT) via an ethylene diamine linker on the 5′ phosphate.

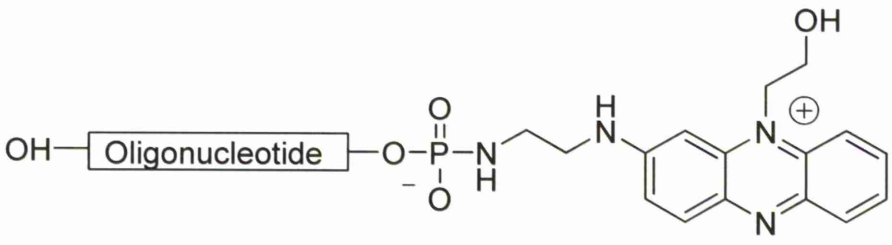

Figure 3.19. Expanded UV-visible spectrum of **15** (5 μM) without 23-mer 2′OMe RNA (blue) and with 23-mer 2′OMe RNA (red) (5 μM) recorded in Tris buffer (50 mM Tris, 200 mM KCl, pH 7.6, 0.5 mM EDTA) at 20°C.

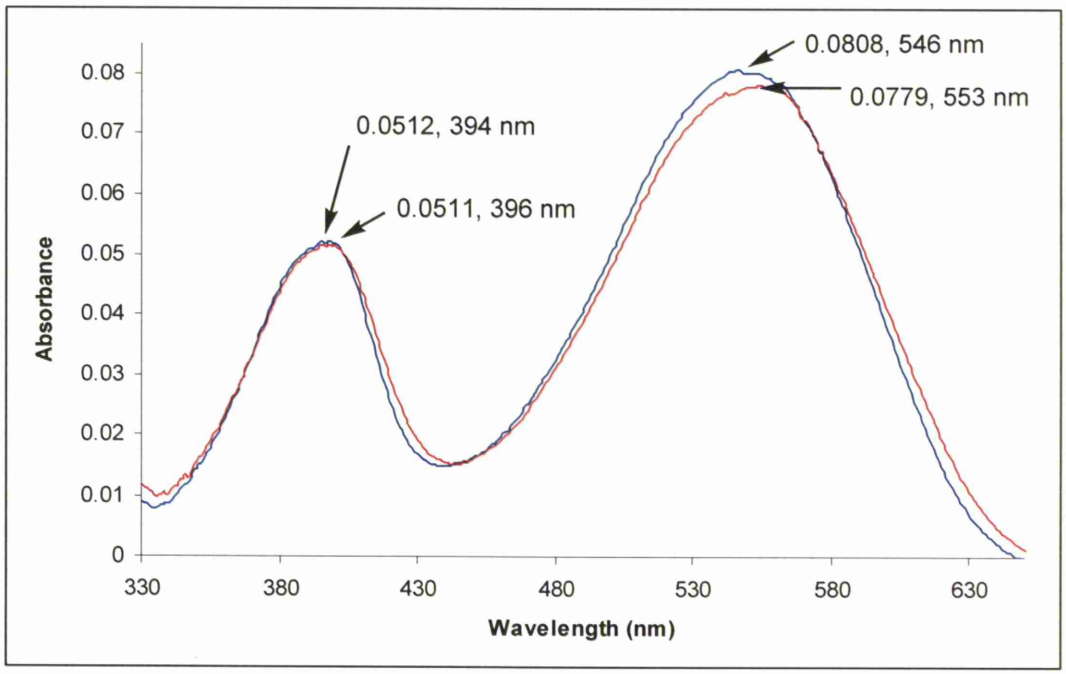

It is seen from Figure 3.19 that on addition of 23-mer 2'OMe RNA both bands at 394 nm and 546 nm show bathochromic shifts of 4 nm and 7 nm, respectively, see Table 3.7. The band at 546 nm also experienced a hypochromic shift of 3.6%. These spectral changes, (small, but reproducible), clearly indicate an interaction between the *N*-(2-hydroxyethyl)phenazinium and 23-mer 2'OMe RNA.

Table 3.7. Differences in absorbance intensities and λ_{max} values on addition of target (5 μM) RNA to **15** (5 μM).

	Band 3 λ_{max} (nm)	Band 3 Absorbance	Band 4 λ_{max} (nm)	Band 4 Absorbance
15	394	0.0512	546	0.0808
15 + 23-mer	396	0.0511	553	0.0779
Difference	**2**	**0.0001**	**7**	**0.0029 (3.6%)**

3.3.6.6. Interactions of oligonucleotide conjugates with the RNA target

The next stage of this research was to study the interactions between the oligonucleotide conjugates: **11.1, 10.2, 10.3** and **10.4** (Fig. 3.27, 3.28), each also containing both a covalently attached catalytic bis-imidazole tetrapeptide and a *N*-(2-hydroxyethyl)phenazinium anchor with linear, complementary ss 2′ OMe RNA targets**.** These conjugates were produced by the conjugation of the 5′ terminal phosphate of the 17-mer oligonucleotide (5′-pdGATCGAACACAGGACCT) with the free primary amine of either **10.1** or **9.4** construct (to generate conjugates **11.1** and **10.4**, respectively) or **9.2** and **9.3** construct (to generate conjugates **10.2** and **10.3**, respectively), see section 3.1.

Figure 3.20. The chemical structure of **11.1** and **10.4** produced by the attachment of constructs **10.1** and **9.4**, respectively, from different synthetic routes (see Figure 3.1.2 and Figure 3.1.7, respectively). Oligonucleotide sequence: GATCGAACACAGGACCT.

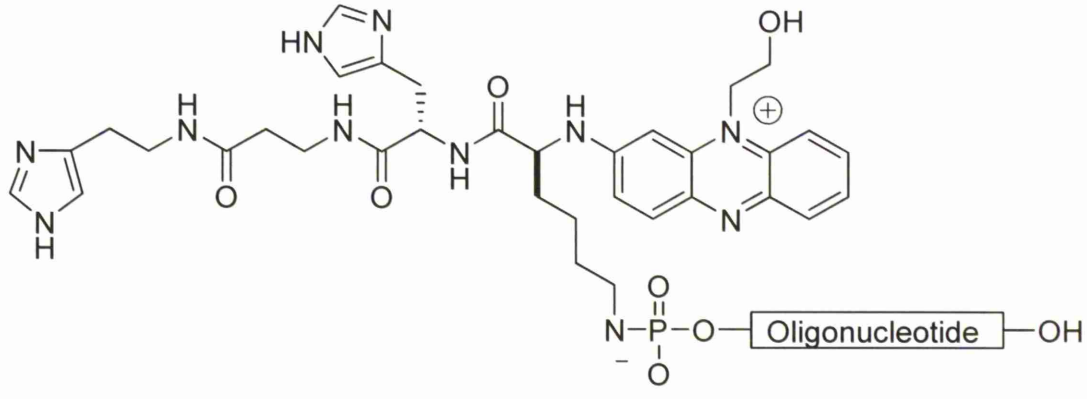

Figure 3.21. The chemical structure of **10.2** and **10.3**, produced by the attachment of constructs **9.2** and **9.3**, respectively, from different synthetic routes (see Figure 3.1.4 and Figure 3.1.5). The 17-mer oligonucleotide sequence was: dGATCGAACACAGGACCT.

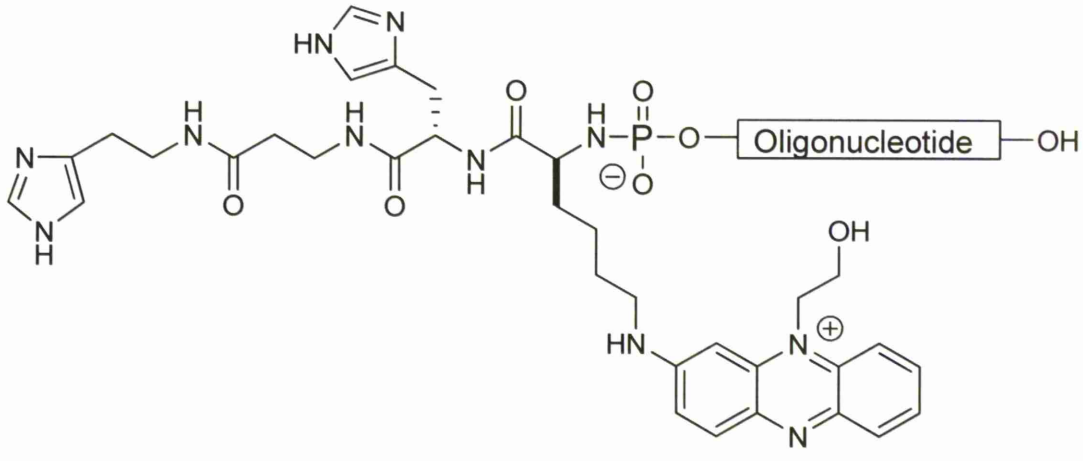

Both the above molecules have an orthogonally placed anchor group and oligonucleotide binding domain (on either α- amine or ε- amine of lysine linker) but have the positioning of the anchor and the recognition site alternatively arranged (into the two possible orientations e.g. the anchor group is on either the α- amine and oligonucleotide on the ε- amine of lysine linker or *vice versa*) for each molecule.

Using UV-visible spectrophotometry, we monitored the response of the *N*-(2-hydroxyethyl)phenazinium (incorporated into the conjugates **11.1**, **10.2**, **10.3** and **10.4**) on interaction with the complementary 23-mer 2'-OMe RNA sequence (1:1; 5uM) by following the phenazinium absorption bands 3 and 4 (see Figure 3.23).

The following figures (Figures 3.22 and 3.23) compare the UV-visible spectra of both a free 17-mer oligonucleotide and an example of a corresponding oligonucleotide conjugate (**10.4**).

Figure 3.22. UV-visible spectrum (with λ_{max}) of unmodified 17-mer (2 μM) oligodeoxyribonucleotide recorded in water at 20°C.

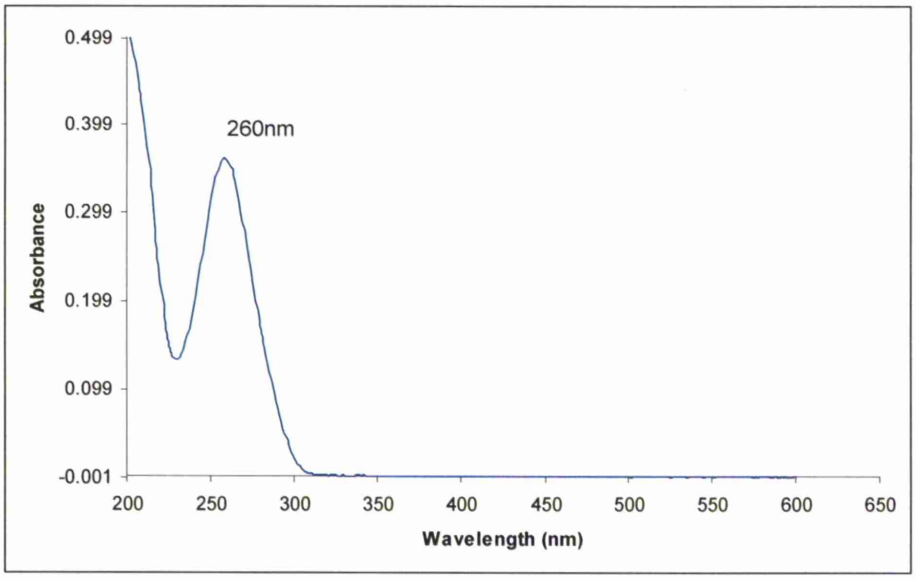

Figure 3.23. UV-visible spectrum (with λ_{max}) of oligodeoxyribonucleotide-tetrapeptide- phenazinium conjugates: **10.4** (5 μM) recorded in water at 20°C.

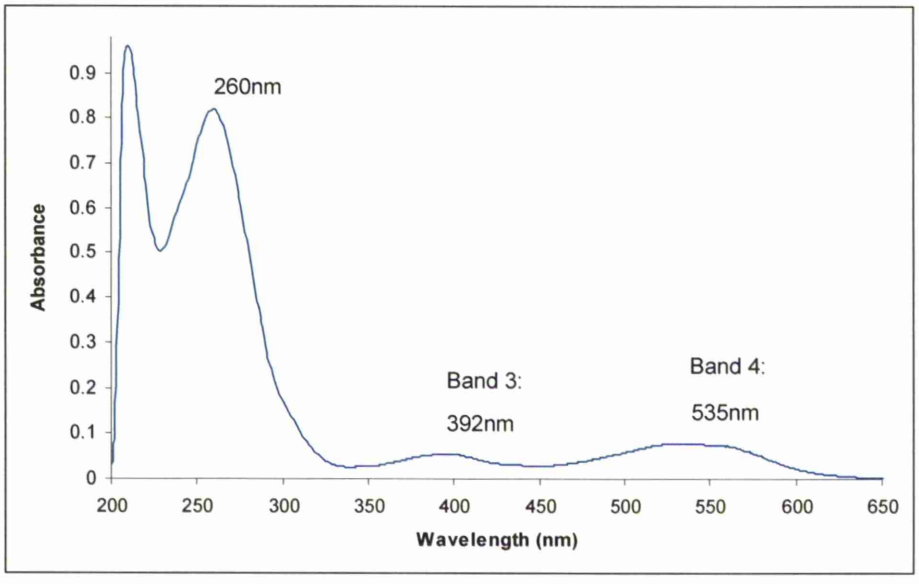

Figure 3.22 shows a typical absorption spectrum for a 17-mer oligonucleotide with a λ_{max} *circa* 260 nm. In comparison, Figure 3.23 shows a typical absorption spectrum for an oligonucleotide conjugated to the phenazinium incorporating tetrapeptide construct **10.4** with a λ_{max} *circa* 260, 390 and 535 nm.

Molar extinction coefficients for construct **9.1**, the 17-mer oligodeoxyribonucleotide and oligodeoxyribonucleotide conjugates (**15**, **11.1**, **10.2**, **10.3**, **10.4**) were evaluated as described in 'Material & and Methods (see Section 2.1.9) and summarised in Table 3.8 below.

Table 3.8. Molar extinction coefficients ($mM^{-1}cm^{-1}$) for compounds with corresponding wavelengths of maximum absorbance ((λ_{max} (nm)) indicated in parenthesis. Note, λ_{max} for **9.1** was at 290 nm but ε_{260} was calculated.

Compound	ε Band 2	ε Band 3 (λ_{max})	ε Band 4 (λ_{max})
9.1	6.7 (260)	7.1 (394)	8.8 (516)
17-mer DNA	169 (260)	-	-
15	175.7 (260)	10.2 (394)	16.2 (546)
11.1	175.7 (260)	21.8 (392)	23.7 (535)
10.2	175.7 (260)	11 (394)	15.4 (538)
10.3	175.7 (260)	12.6 (390)	15.8 (538)
10.4	175.7 (260)	23.6 (392)	25.6 (535)

Figure 3.24. Comparison of UV-visible spectra (with λ_{max}) of *N*-(2-hydroxyethyl)phenazinium alone (30 μM) (**A**), conjugated to tetrapeptide (17 μM) (**B**) and conjugated to oligonucleotide-tetrapeptide construct (5 μM) (**C**). Spectra were recorded in water at 20°C.

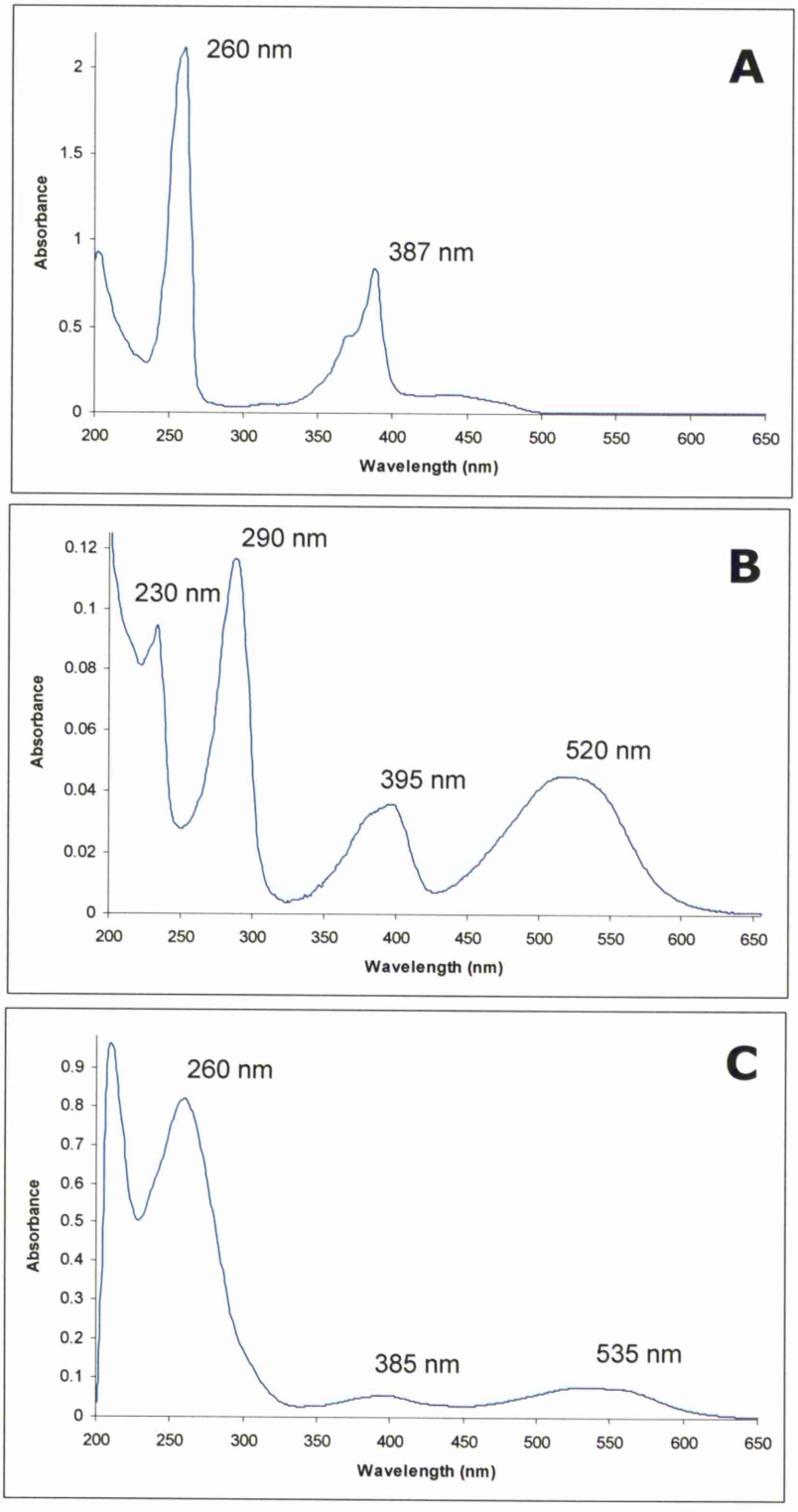

The spectral properties seen in UV-visible spectra of *N*-(2-hydroxyethyl)phenazinium are contrasted with those of **9.1**, and **10.4** and are summarised below:

i. The unconjugated (or *free*) *N*-(2-hydroxyethyl)phenazinium molecule has only two prominent peaks at 260 nm and *circa* 385 nm.

ii. A new band appears at 520 nm in the case of the *N*-(2-hydroxyethyl)phenazinium conjugated to the tetrapeptide **9.1**. The major band at 260 nm shifts to *ca.* 290 nm. The band at *ca.* 385 nm changes shape and extinction coefficient and shifts bathochromically to *ca.* 395nm.

iii. A new band appears at 535 nm for oligonucleotide conjugates: 11.1, 10.2, 10.3, 10.4 (see Fig 3.24, C). Band *ca.* 385 nm changes shape and extinction coefficient upon conjugation (see Table 3.8). The most prominent band is at 260 nm, which is attributed to the 17-mer oligonucleotide.

Figure 3.25. (A) UV-visible spectrum of **10.2** (5 μM) without 23-mer 2'OMe RNA (blue) and with 23-mer 2'OMe RNA (red) (5 μM) recorded in Tris buffer (50 mM Tris, 200 mM KCl, pH 7.6, 0.5 mM EDTA) at 20°C. (B) expansion of spectrum to show bands 3 and 4.

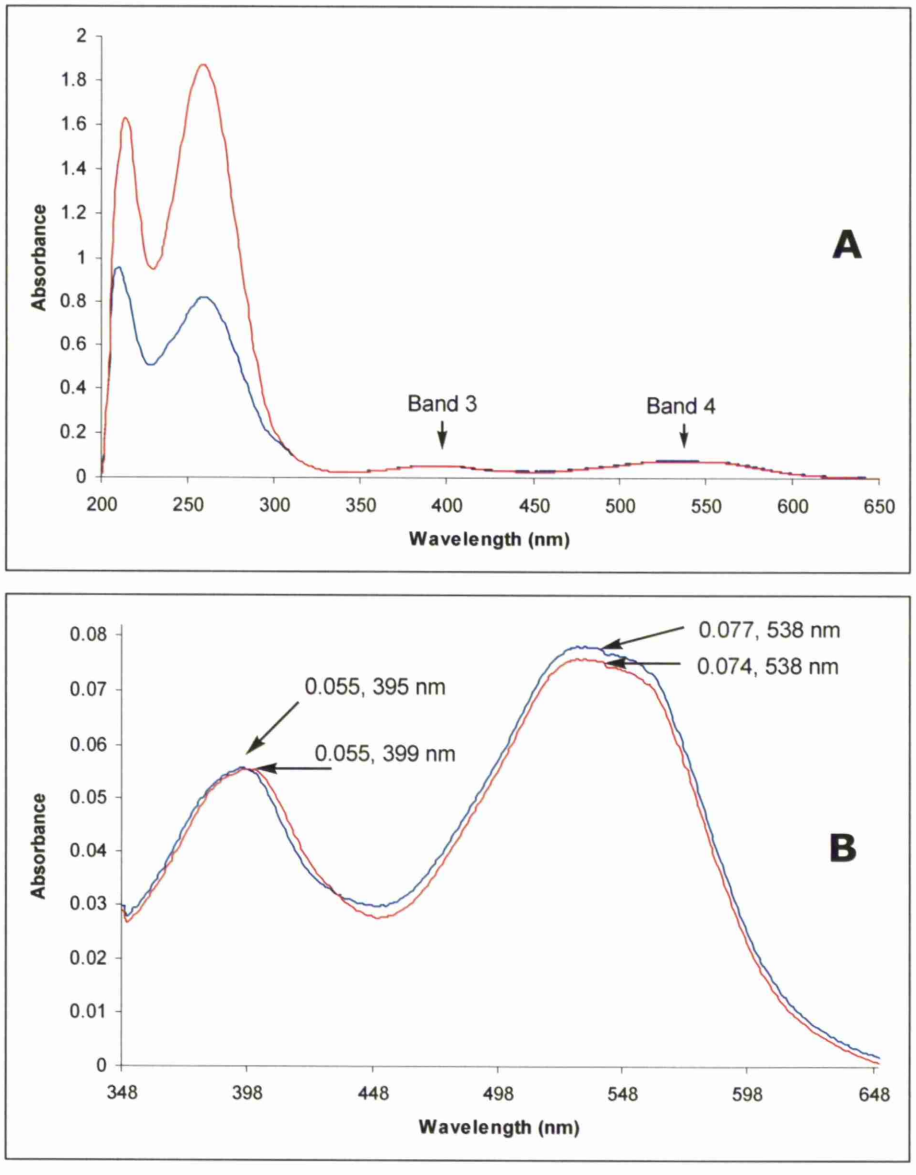

Table 3.9. Differences in absorbance and λ_{max} of **10.2** (5 μM) conjugate in response to addition of target RNA (5 μM).

	Band 3 λ_{max} (nm)	Band 3 Absorbance	Band 4 λ_{max} (nm)	Band 4 Absorbance
10.2	394	0.055	538	0.077
10.2 + 23-mer	399	0.055	538	0.074
Difference	**5**	**0**	**0**	**0.003 (3.9%)**

Addition of single-stranded RNA molecule (1:1) in Tris buffer induced a bathochromic shift of 5 nm at band 3 (394 nm) and 3.9 % hypochromic shift of the absorption band at 520 nm (see Figure 3.25, Table 3.9).

Figure 3.26. UV-visible spectrum of **10.3** (5 μM) without 23-mer 2'OMe RNA (blue) and with 23-mer 2'OMe RNA (red) (5 μM) recorded in Tris buffer (50 mM Tris, 200 mM KCl, pH 7.6, 0.5 mM EDTA) at 20°C.

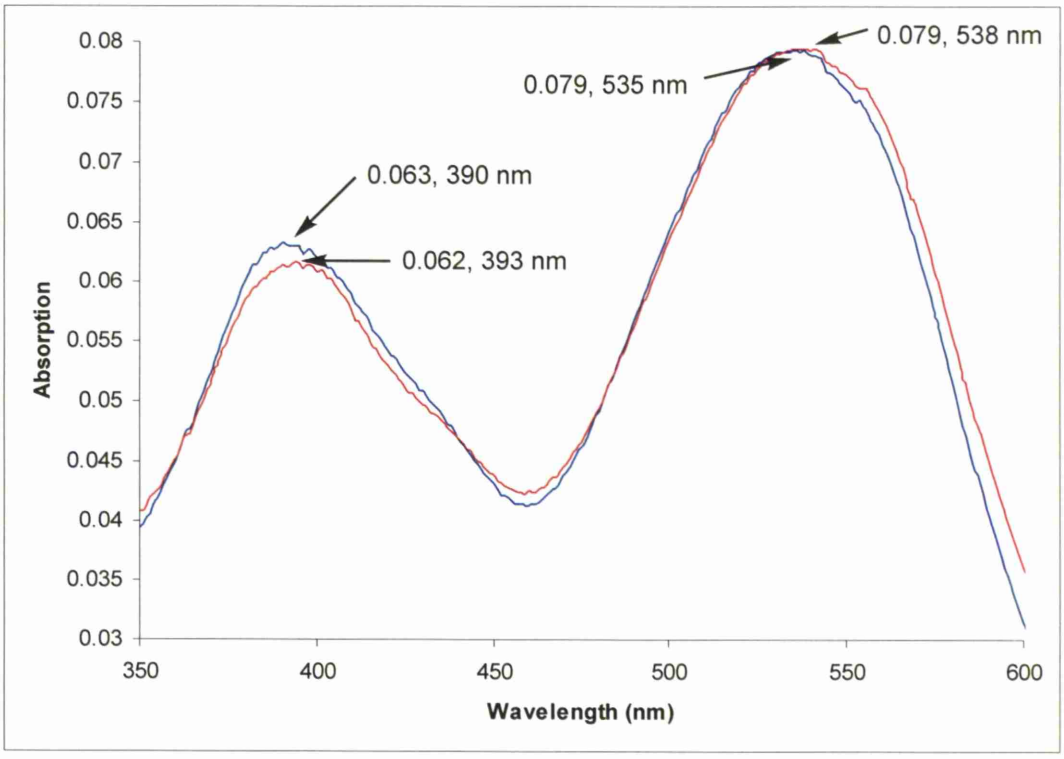

Table 3.10. Differences in absorbance and λ_{max} for **10.3** (5 μM) conjugate in response to the addition of target RNA (5 μM).

	Band 3 λ_{max} (nm)	Band 3 Absorbance	Band 4 λ_{max} (nm)	Band 4 Absorbance
10.3	390	0.063	538	0.079
10.3 + 23-mer	393	0.062	535	0.079
Difference	**3**	**0.001**	**3**	**0**

Addition of single-stranded RNA molecule (1:1) in Tris buffer induced a bathochromic shift of 3 nm at band 3 (390 nm), 3 nm at band 4 (537 nm) and 3.9% hypochromic shift of the absorption band at 538 nm (see Figure 3.26, Table 3.10).

Figure 3.27. Expanded region of UV-visible spectrum of **10.4** (5 μM) without 23-mer 2'OMe RNA (blue) and with 23-mer 2'OMe RNA (red) (5 μM) recorded in Tris buffer (50 mM Tris, 200 mM KCl, pH 7.6, 0.5 mM EDTA) at 20°C.

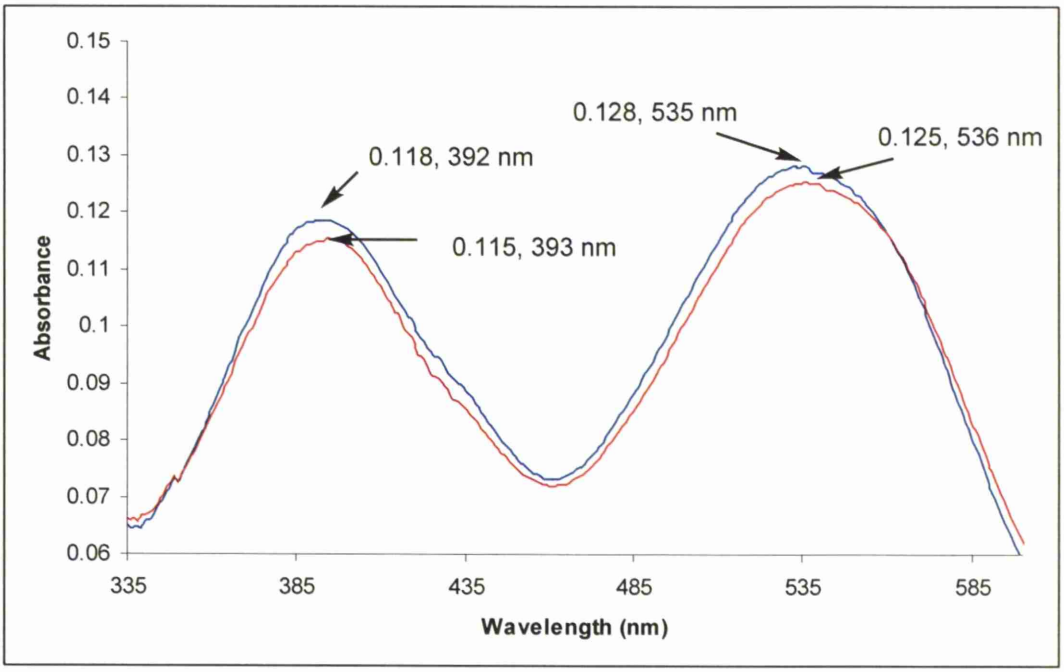

Table 3.11. Differences in absorbance and λ_{max} for **10.4** (5 μM) as response on addition of target RNA (5 μM).

	Band 3 λ_{max} (nm)	Band 3 Absorbance	Band 4 λ_{max} (nm)	Band 4 Absorbance
10.4	392	0.118	535	0.128
10.4 + 23 mer	393	0.115	536	0.125
Difference	**1**	**0.003 (2.5 %)**	**1**	**0.003 (2.3%)**

It is evident from the above experiments (see Figures 3.27 and Table 3.11) that hybridisation of the conjugates **10.2**, **10.3** and **10.4** with the complementary 23-mer 2'OMe RNA target results in a small, but reproducible change in λ_{max} values (mainly noticeable for band 3) and a decrease in absorbance. The detected bathochromic shift for the bands 3 and 4 ranges between 0 to 5 nm and the observed hypochromic shift for these bands range from 0% to 3.9%.

Such a small change induced by hybridisation with complementary 23-mer 2'OMe RNA target (as compared with unconjugated **9.1**, see Figure 3.11) could be explained by the fact that, even prior to the addition of the RNA target, *N*-(2-

hydroxyethyl)phenazinium anchor strongly interacts with nucleotide residues of the covalently attached 17-mer oligonucleotide recognition element (see Fig 3.28). The evidence of these interactions is seen from the substantial bathochromic shift of ~15 nm and decreased ε_{520} value observed for the band 4 induced by conjugation of **9.1** to the 17-mer to generate **11.1 10.2**, **10.3** or **10.4** (see Figure 3.23 and Table 3.8).

Figure 3.28. The interaction of the Phn anchor with the oligonucleotide moiety on the same compound can be envisioned from the following diagram.

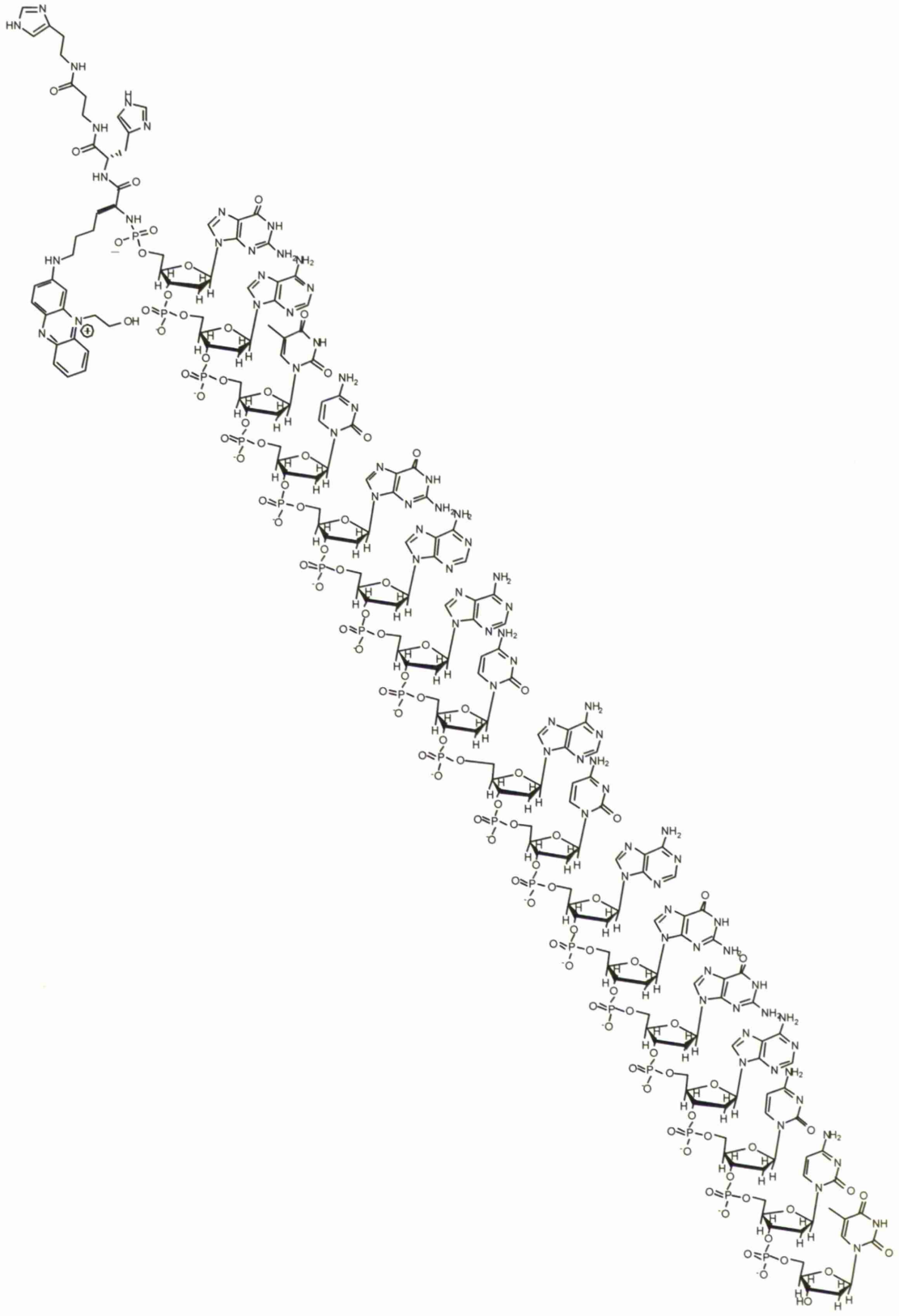

3.3.7. Induced thermal denaturation (melting temperature) experiments

T_m profiles of oligonucleotide conjugates (monitored at 260 nm and 390 nm) were studied to analyse any effects of the *N*-(2-hydroxyethyl)phenazinium anchor group on hybridization/annealing with the target RNA sequences. Higher melting denaturation temperatures suggest an increase in binding ability and hence a stabilising interaction. Lower melting temperatures suggest a disruption/perturbation/weakening in binding and hence a destabilising interaction.

3.3.7.1. Melting temperature control system

The hybridization of the unmodified 17-mer oligodeoxyribonucleotide (5′-pdGATCGAACACAGGACCT) with the target 23-mer 2′OMe RNA (5′-AGGTCCTGTGTTCGATCCACAGA) was used as a control system to which any changes in T_m due to the conjugation of additional groups (*e.g.* tetrapeptide and *N*-(2-hydroxyethyl)phenazinium or both) could be compared. For the complementary target strand of RNA, 2′OMe RNA was used in all melting temperature experiments as it is more stable than RNA towards cleaving activity of ARs and therefore less prone to degradation during the experiments.

Figure 3.29. Target 23-mer oligonucleotide 2′OMe RNA sequence (red) bound to complementary 17-mer oligonucleotide DNA (blue).

5′- AGGUCCUGUGUUCGAUCCACAGA- 3′
3′-TCCAGGACACAAGCTAG- 5′

T_m of the control hybrid: unmodified 17-mer DNA + target 23-mer 2′OMe RNA was found to be 67 ± 1 °C (average from 3 results). The T_m values for any other studied systems were compared to this T_m value to determine any effects on hybridisation binding.

Figure 3.30. Melting curve (cooling phase) of control system: *17-mer DNA:23-mer 2'-OMe RNA* duplex (5 μM), monitored at 260 nm in Tris buffer (50 mM Tris, 200 mM KCl, pH 7.6, 0.5 mM EDTA).

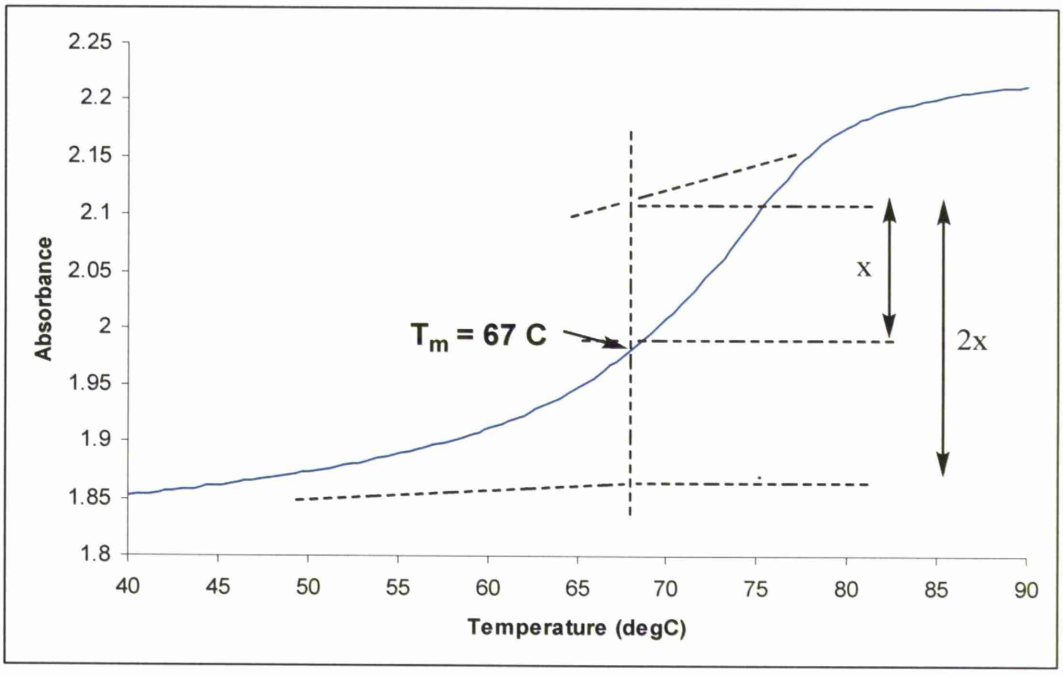

3.3.7.2. Interaction of (15) with the target RNA

To evaluate the stabilisation effect from the *N*-(2-hydroxyethyl)phenazinium anchor alone (without interference from cleaving tetrapeptide construct), a melting denaturation experiment was performed for the hybrid complex *2'OMe RNA:**15*** (1:1, 5 μM) in hybridisation buffer (50 mM Tris, 200 mM KCl, pH 7.6, 0.5 mM EDTA) and compared with that for the control complex *2'OMe RNA:17-mer* (under the same conditions but with an unmodified 17-mer oligodeoxyribonucleotide which lacks the Phn anchor group). Melting temperature profile is shown in Figure 3.31.

Figure 3.31. Melting curve (cooling phase) of **15** (5 μM) with target 23-mer 2'OMe RNA, monitored at 260 nm in Tris buffer (50 mM Tris, 200 mM KCl, pH 7.6, 0.5 mM EDTA). T_m at half point of curve is 73 °C ± 1 °C.

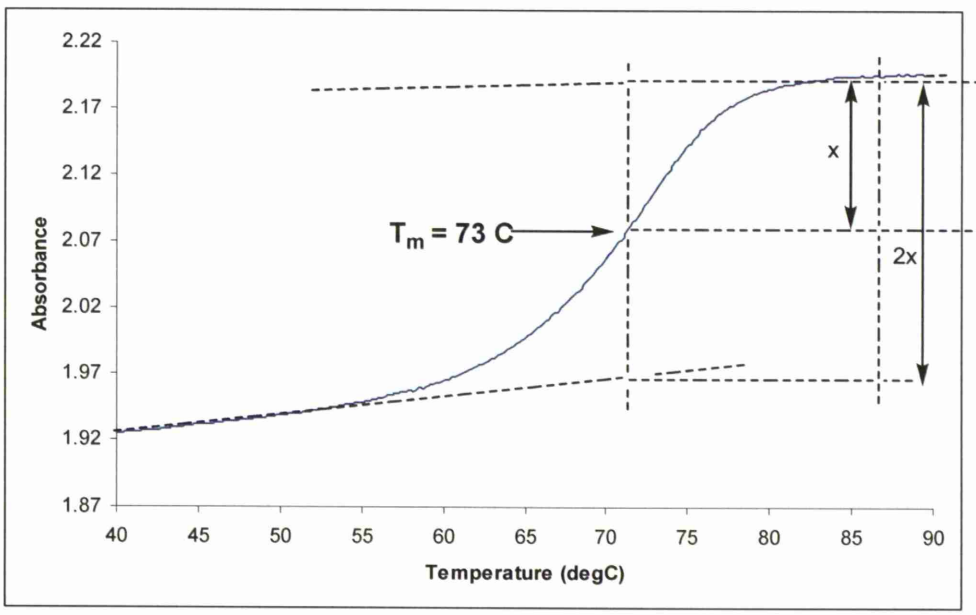

The T_m is calculated from the half way point on the curve as is shown in Fig. 3.31 and is given in Table 3.12.

T_m of **15** + target 23-mer 2'OMe RNA was found to be 73 ± 1 °C (average from 3 results). This is approximately 6 °C greater than the control T_m.

It is seen (Table 3.12) that incorporation of the Phn anchor group into the 17-mer recognition site substantially increases the melting temperature by about 6

°C, indicating enhanced stability of the hybrid complex. This is in accordance with the data reported previously.

3.3.7.3. Interaction of oligonucleotide conjugates with the target RNA

Figure 3.32. Melting curve (cooling phase) of **11.1** (5 μM) with 23-mer 2'OMe RNA, monitored at 260 nm in Tris buffer (50 mM Tris, 200 mM KCl, pH 7.6, 0.5 mM EDTA).

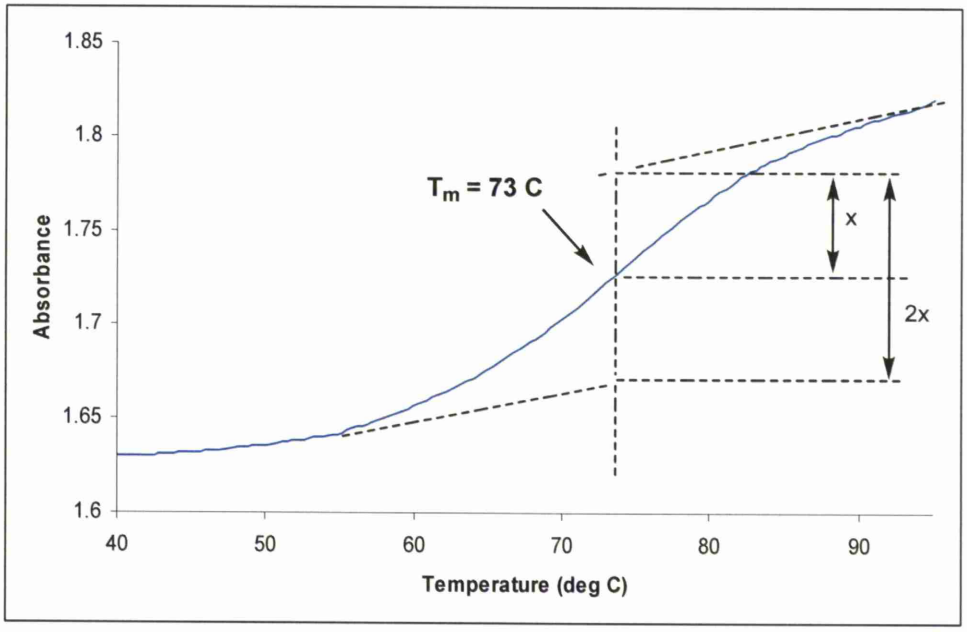

T_m of (**11.1**) + target 23mer RNA was found to be 73 ± 1 °C (average from 3 results). This is approximately 6 °C greater than control.

Figure 3.33. Melting curve (cooling phase) of **10.2** (5 μM) with 23-mer 2'OMe RNA, monitored at 260 nm in Tris buffer (50 mM Tris, 200 mM KCl, pH 7.6, 0.5 mM EDTA).

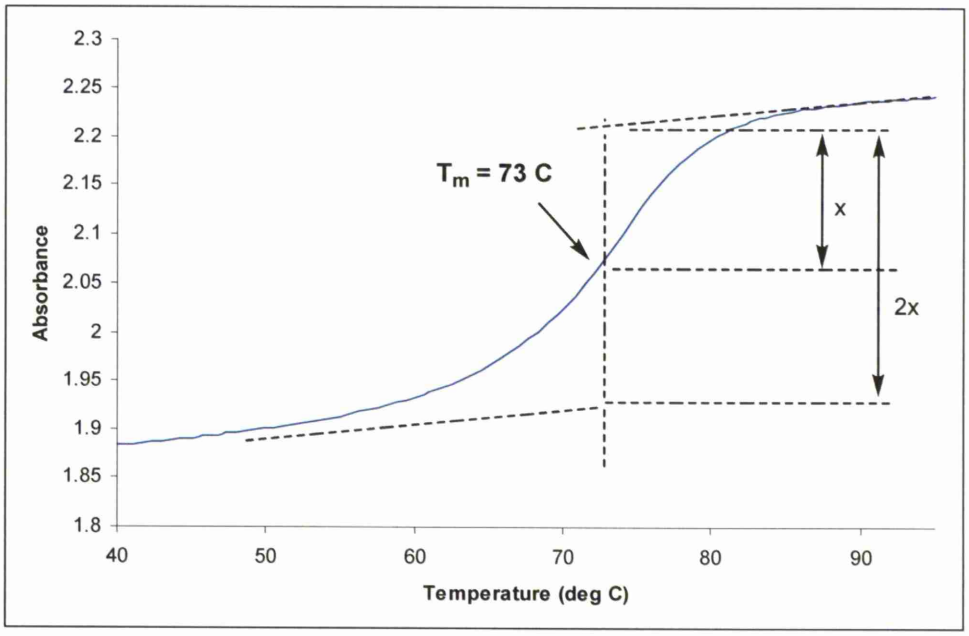

T_m of **10.2** + target 23-mer 2'OMe RNA was found to be 73 ± 1 °C (average from 3 results). This is approximately 6 °C greater than control.

Figure 3.34. Melting curve (cooling phase) of **10.3** (5 μM) with 23-mer 2'OMe RNA, monitored at 260 nm in Tris buffer (50 mM Tris, 200 mM KCl, pH 7.6, 0.5 mM EDTA).

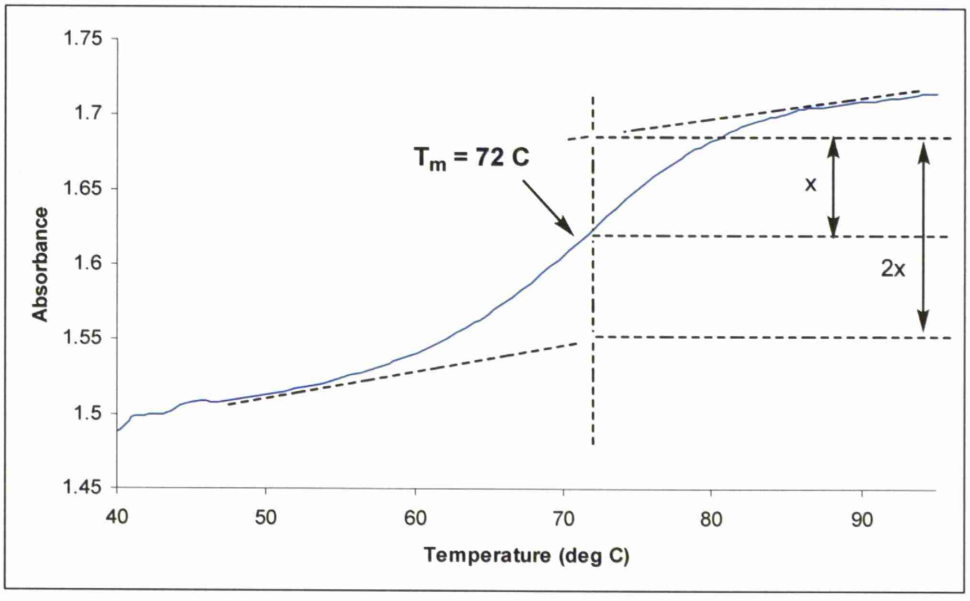

T_m of **10.3** + target 23-mer 2'OMe RNA was found to be 72 ± 1 °C (average from 3 results). This is approximately 5 °C greater than control.

Figure 3.35. Melting curve (cooling phase) of **10.4** (5 μM) with 23-mer 2'OMe RNA, monitored at 260 nm in Tris buffer (50 mM Tris, 200 mM KCl, pH 7.6, 0.5 mM EDTA).

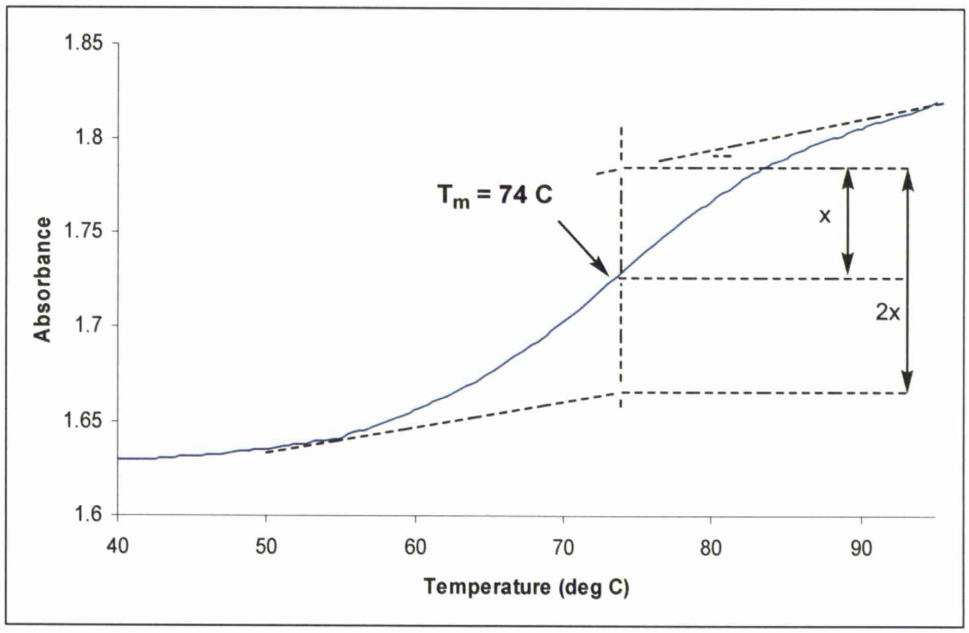

T_m of **10.4** + target 23-mer 2'OMe RNA was found to be 74 ± 1 °C (average from 3 results). This is approximately 7 °C greater than the control T_m.

Table 3.12. Comparison of T_m of test compounds with control (17-mer DNA and 23-mer 2'OMe RNA).

Compound hybridized with target 23-mer	Average T_m (°C) at 260 nm	Average T_m (°C) at 390 nm	Difference in T_m (°C) at 260 nm from control
Control: 17 mer	67	-	0
11.1	73	73	6
10.2	73	73	6
10.3	72	73	5
10.4	74	73	7
15	73	74	6

Table 3.13. T_m calculated by first derivative method (see Fig. 3.43).

Compound hybridized with target 23 mer	T_m (°C) at 260 nm	Difference in T_m (°C) from control
Control: 17 mer	69	0
11.1	74	5
10.2	73	4
10.3	73	4
10.4	74	5
15	74	5

Figure 3.36. (A) First derivatives of UV-visible spectroscopically measured melting curves (at 260 nm) of control (17-mer DNA and 23-mer 2'-O-Me RNA; thick red line) compared with oligonucleotide conjugates (**11.1** (blue), **10.2** (green), **10.3** (orange), **10.4** (brown), **15** (dark green)).

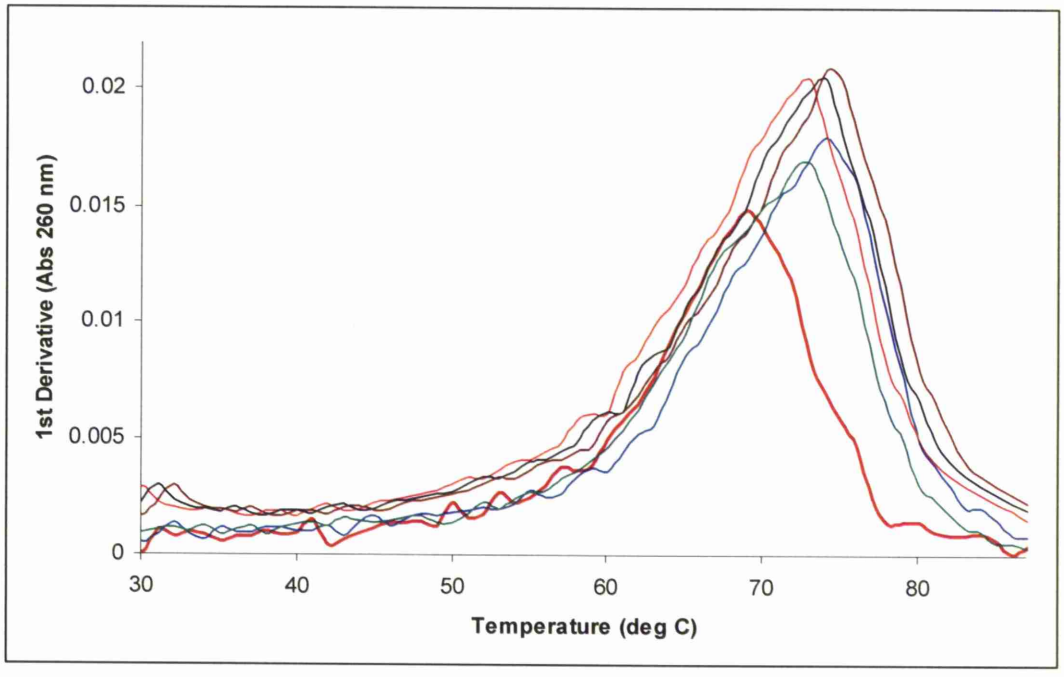

There is a reproducible stabilisation of 5 – 7 °C from phenazinium for each system. Repeated experiments produced an approximate error of experiment of ± 1 °C.

Melting temperature studies showed the Phn anchor increased the binding affinity of all ARs synthesised (compared to the parent antisense oligonucleotide), including the analogue without a catalytic domain (**15**).

11.1 and **10.4** which had Phn closer to the catalytic cleaving domain (on the α amine of lysine) showed a slightly higher T_m and stabilisation than **10.2** and **10.3**, but not by a significant difference.

These data are consistent and similar with Dr Martin Fabani's thesis data (Table 3.14). Comparing to similar but *N*-methylphenazinium containing compounds synthesised by Dr M Fabani, stabilisations of 4- 7 °C were found [6]. From Dr M Fabani's thesis compounds 35- 39 in Table 3.14 represent similar compounds but with decreasing linker length and an *N*-methylphenazinium as the anchor group.

Table 3.14. T_m values of similar compounds with *N*- methylphenazinium as the anchor group, synthesized by M Fabani (taken from [6])

Compound hybridized with target 23 mer	T_m (°C) at 260 nm	Difference in T_m (°C) from control
17 mer (Control)	62	0
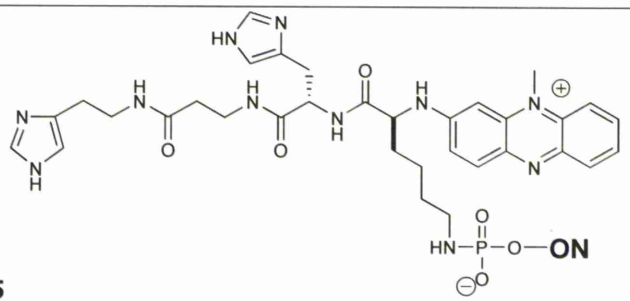 **35**	67	5
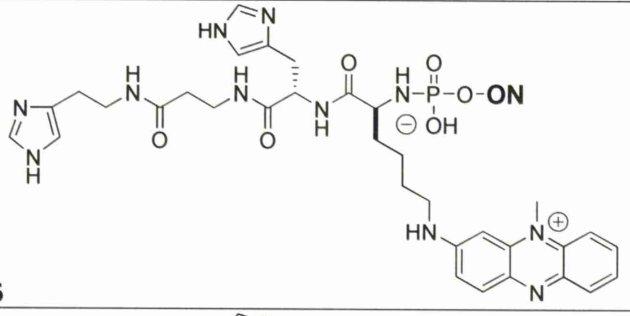 **36**	68	6
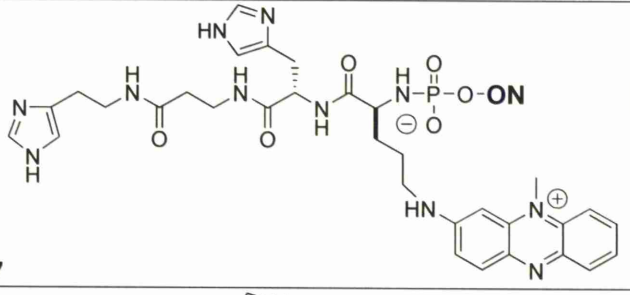 **37**	66	4
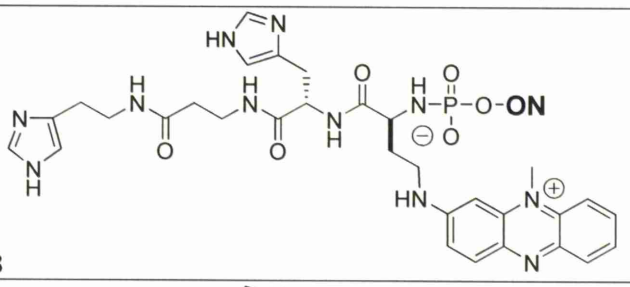 **38**	68	6
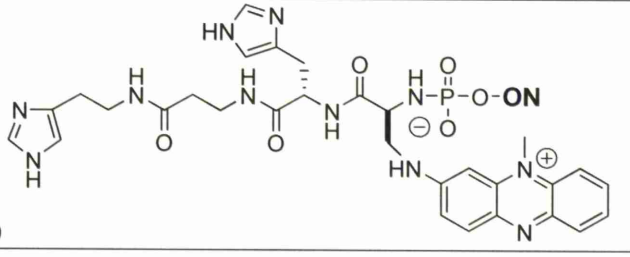 **39**	69	7

The partial positive charge on the substituted-nitrogen atom is higher for *N*-hydroxyethylphenazinium compared to *N*-methylphenazinium and, therefore should increase the interaction of the *N*-hydroxyethylphenazinium group with the negatively charged sugar-phosphate backbone. However, only a slight increase is observed.

Compared to literature data on stabilization effects of *N*-hydroxyethylphenazinium modified oligonucleotides [203-205, 215], it seems that the observed stabilization effect is not very strong, only 5 – 7 ^{o}C. However, the published data in this area is based on short Phn-containing oligos (6- 8-mers), for which the stabilization effect is expected to be more evident than for longer derivatives such as the 17-mer conjugates used in this study.

The observed stabilisation effect induced by the Phn anchor group can be attributed to the additional stacking interactions of the phenazinium groups with oligonucleotide residues. This may involve the intercalation of the Phn heterocycle group between the first base pair of the complex and the following nucleotide base of the complementary RNA strand, which is consistent with the previous NMR/molecular modelling studies of the DNA duplexes containing 5′-phenazinium-tethered oligonucleotide [27, 203, 204, 207, 214].

3.3.8. Fluorescence studies

3.3.8.1. Interaction of (9.1) or (15) with the target RNA

Fluorescence spectroscopy was also used to further consolidate the interaction of phenazinium with target RNA seen with UV-visible spectroscopy. Phn produces a broad fluorescence emission band at 500-700 nm when excited at 396 and 525 nm.

As seen in Figures 3.46- 3.50, the fluorescence emission spectrum of **9.1** or **15** in an equimolar mixture with the target 23-mer 2'OMe RNA shows both hypsochromic and hypochromic shifts which are evidence of an interaction.

Figure 3.37. Fluorescence spectrum of **9.1** (5 μM) without 23-mer 2'OMe RNA (blue) and with 23-mer RNA (red) (5 μM) recorded in Tris buffer (50 mM Tris, 200 mM KCl, pH 7.6, 0.5 mM EDTA), with 10 nm slit width, at 20°C. Excitation at 396 nm and 525 nm produced fluorescence emission at 608 nm.

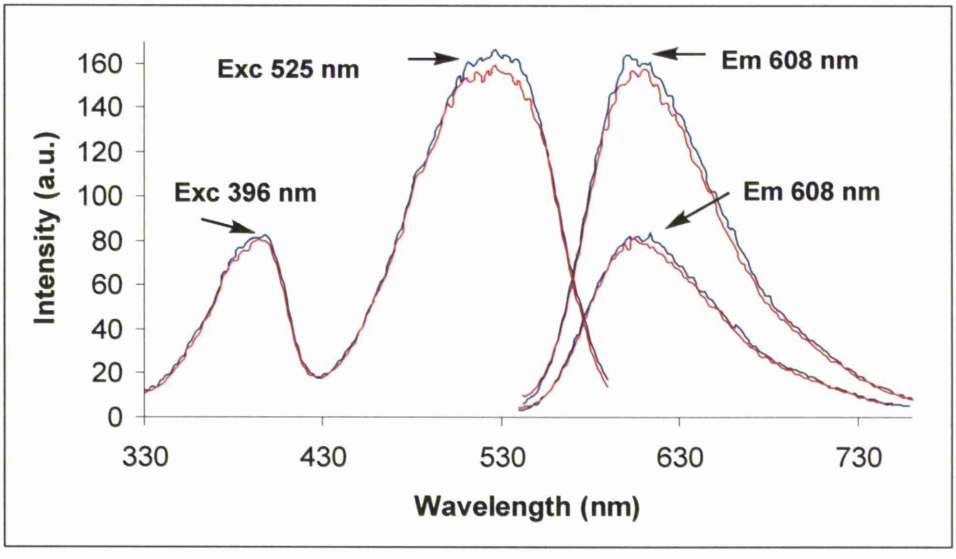

Excitation (λ_{EXC}) at 396 nm produces an emission at 608 nm (λ_{EM})

Figure 3.38. Fluorescence spectrum of **9.1** (5 μM) without 23-mer 2'OMe RNA (blue) and with 23-mer 2'OMe RNA (red) (5 μM) recorded in Tris buffer (50 mM Tris, 200 mM KCl, pH 7.6, 0.5 mM EDTA), with 10 nm slit width, at 20°C, at excitation 396 nm and emission 608 nm.

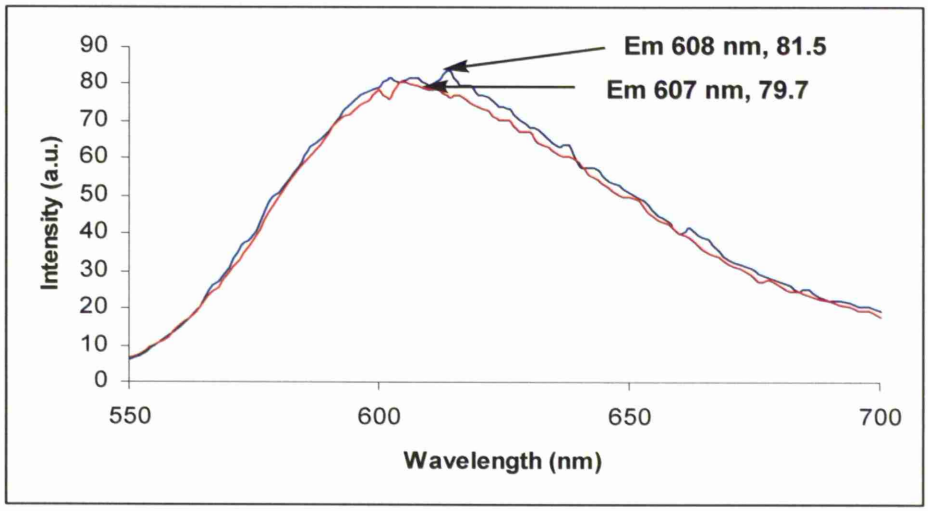

Excitation λ_{EX} at 525 nm produces an emission at 608 nm (λ_{EM})

Figure 3.39. Fluorescence spectrum of **9.1** (5 μM) without 23-mer 2'OMe RNA (blue) and with 23-mer 2'OMe RNA (red) (5 μM) recorded in Tris buffer (50 mM Tris, 200 mM KCl, pH 7.6, 0.5 mM EDTA), with 10 nm slit width, at 20°C, at excitation 525 nm and emission 608 nm.

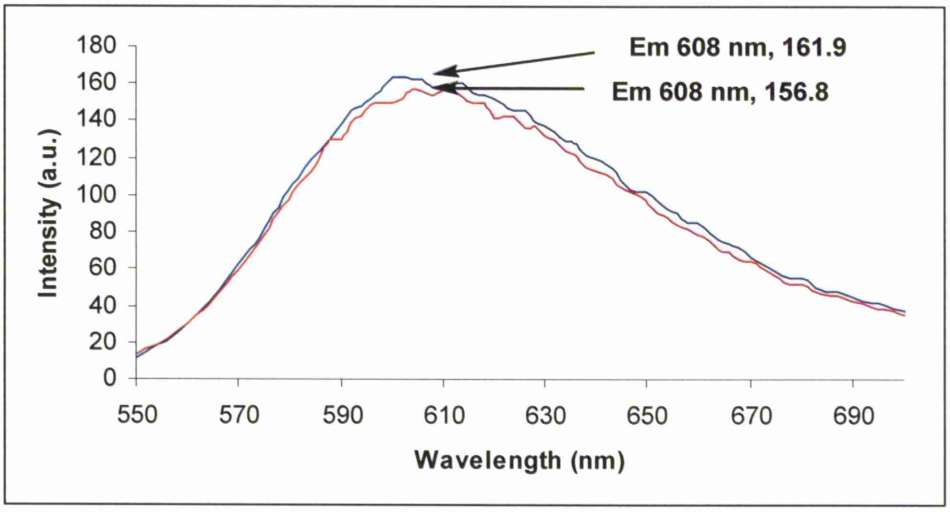

Addition of single-stranded RNA molecule (1:1) in Tris buffer induced a hypochromic shift of 2.9 % and 4.8 % at 394 nm and 528 nm, respectively (see Figure 3.48).

3.3.8.2. Interaction of (15) with the target RNA

Figure 3.40. Fluorescence spectrum of **15** (5 μM) without 23-mer 2'OMe RNA (blue) and with 23-mer 2'OMe RNA (red) (5 μM) recorded in Tris buffer (50 mM Tris, 200 mM KCl, pH 7.6, 0.5 mM EDTA) at 20°C, slit width 10 nm, at excitation 550 nm and emission 608 nm.

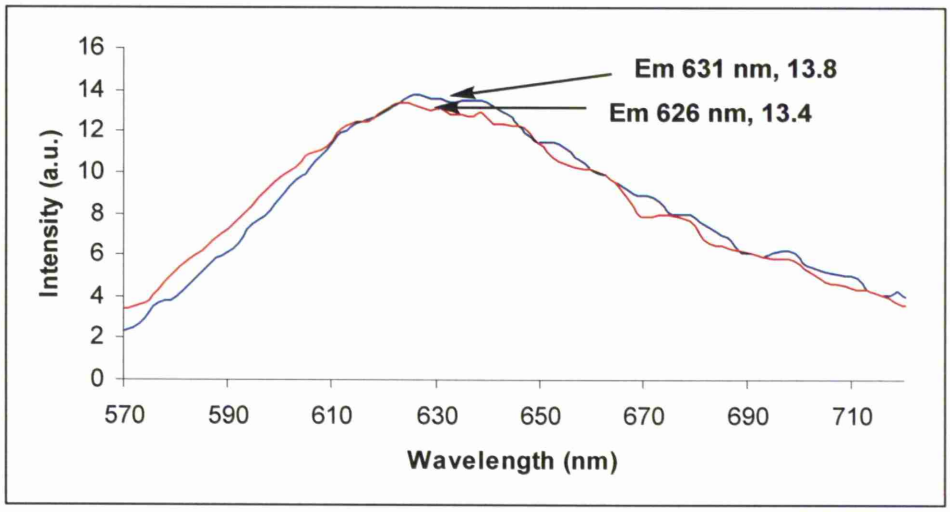

Figure 3.41. Fluorescence spectrum of **15** (5 μM) without 23-mer 2'OMe RNA (blue) and with 23-mer 2'OMe RNA (red) (5 μM) recorded in Tris buffer (50 mM Tris, 200 mM KCl, pH 7.6, 0.5 mM EDTA) at 20°C, slit width 10 nm, at excitation 395 nm and emission 608nm.

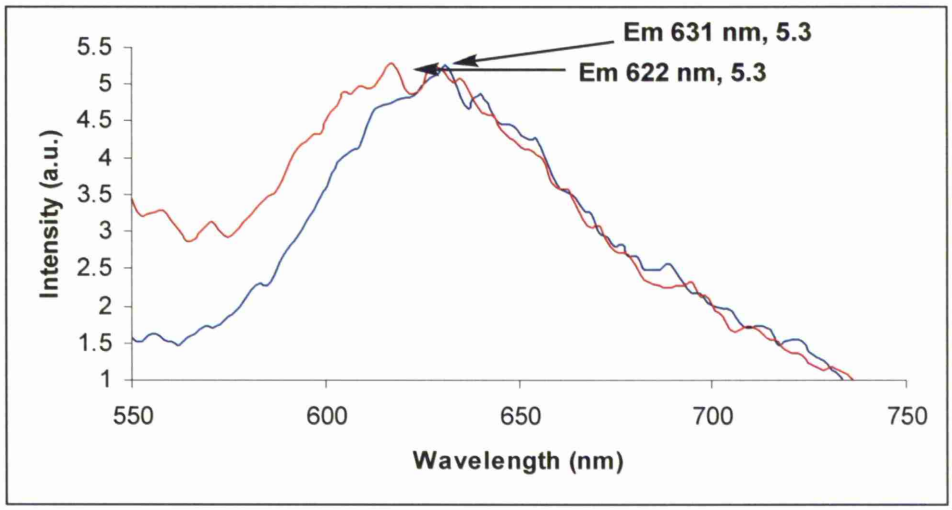

3.3.9. Assessment of the hydrolytic potential of the oligonucleotide conjugates

The hydrolytic activity of the oligonucleotide-conjugates **11.1** and **10.2** containing both oligonucleotide recognition element and phenazinium anchor group has been evaluated against 5'- [^{32}P] -tRNA^{Phe} target. The conjugates **11.1** and **10.2** have alternative locations for the *N*-(2-hydroxyethyl)phenazinium group and for the 17-mer oligonucleotide component relative to *bis*-imidazole cleaving construct (see Figure 3.9). In the structure of **11.1** the phenazinium anchor is directly attached to the cleaving construct, whereas oligonucleotide recognition component is separated from the above groups by the tetramethylene linker of the Lysine residue. In contrast, conjugate **10.2** has cleaving and oligonucleotide recognition elements in close proximity, whereas the phenazinium anchor is separated from them by the tetramethylene linker of the Lysine residue.

Figure 3.42. Cloverleaf structure of yeast $tRNA^{Phe}$ and schematic representation of 17-mer conjugate hybridised with TΨC loop of $tRNA^{Phe}$.

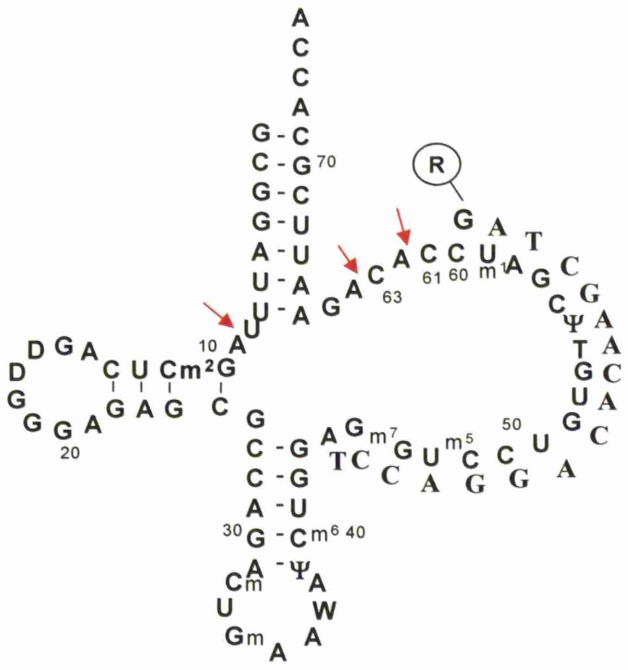

The aim of the cleavage experiments was to investigate whether the oligonucleotide conjugates were capable of unfolding and hydrolysing a structurally complex RNA target (here $tRNA^{Phe}$) in a sequence-specific manner. An additional the purpose of these experiments was to investigate whether the above structural variations within the engineered artificial ribonucleases would affect (i) the site specificity and (ii) the level of cleavage of the target RNA sequence.

As the target, $tRNA^{Phe}$ was chosen deliberately as a reference target for comparison to previous studies. It has been used by many other research groups [17, 25, 134, 216-218] to assess the performance of different types of oligonucleotide-based artificial ribonucleases due to its well known RNA structure.

Cleavage reactions were performed by Dr. N. Tamkovich (research group of Prof. M. Zenkova group, the Institute of Chemical Biology and Fundamental Medicine, Novosibirsk, Russia). 5′- [^{32}P] – $tRNA^{Phe}$ was incubated in the presence of 50 μM concentration of conjugate **11.1**, **10.2,** 17-mer-Phn (**15**) or unmodified 17-mer oligonucleotide in 50 mM imidazole buffer containing 200 mM KCl, 0.1 mM EDTA, 100 μg/ml RNA carrier at 37 °C.

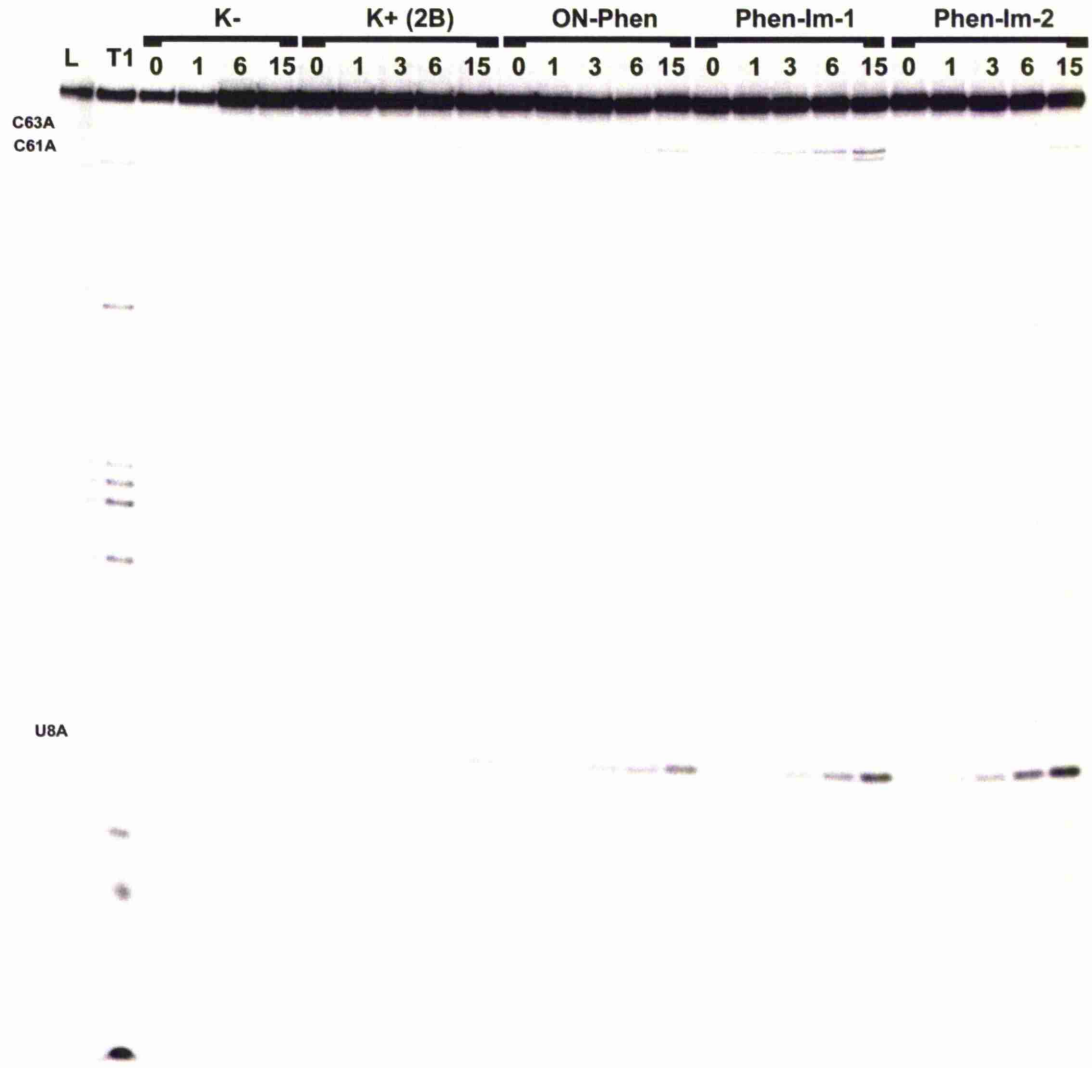

Figure 3.43. Autoradiograph of 12% polyacrylamide/8M urea gel containing tRNA cleavage products after the treatment of the 5'- [^{32}P] -tRNA^{Phe} with the conjugates **11.1**, **10.2**, **15** or unmodified 17-mer oligonucleotide in the presence of 100 μg/ml RNA carrier. Lanes: **K-**, tRNA^{Phe} incubated in the imidazole reaction buffer at 37° C for 0, 1, 5 and 15 hours, respectively, in the absence of the conjugates **11.1** and **10.2** or unconjugated 17-mer oligonucleotide; Lanes: **K+ (2B)**, tRNA^{Phe} incubated in the presence of unconjugated 17-mer oligonucleotide in the imidazole reaction buffer at 37° C for 0, 1, 5 and 15 hour, respectively; Lines **ON-Phen**, **Im-1** and **Phen-Im2**: tRNA^{Phe} incubated in the reaction buffer in the presence of the control oligonucleotide 17mer-Phn lacking the bis-imidazole cleaving groups, **11.1** or **10.2** at 37°C for 0, 1, 3, 6 and 15 hours, respectively. **L**, ladder produced by 2M imidazole buffer; **T**, partial digest with RNase T1. Concentration of the conjugates **11.1**, **10.2**, **15** and 17-mer oligonucleotides was 5×10^{-5} M in all experiments. Data has been kindly supplied by Prof. M. Zenkova.

Figure 3.43 above shows an autoradiograph of 12% polyacrylamide/8M urea gel containing tRNA cleavage products after the treatment of the 5′- [^{32}P] -tRNA^{Phe} with the conjugates **11.1**, **10.2**, control **(15)** lacking bis-imidazole cleaving groups or unmodified 17-mer oligonucleotide in the presence of 100 μg/ml RNA carrier.

Figure 3.44. Overall cleavage of the tRNA^{Phe} as a function of time induced by 11.1, 10.2 and 15. 5′- [^{32}P] – tRNA^{Phe} was incubated in the presence of 50 μM concentration of conjugate 11.1, 10.2 or 15 in 50 mM imidazole buffer containing 200 mM KCl, 0,1 mM EDTA, 100 μg/ml RNA carrier at 37°C. The overall tRNA cleavage was analyzed after incubation at 37°C for 0, 1, 3, 6 and 15 hours. Concentration of the conjugates 11.1, 10.2 and 15 was 5×10^{-5} M in all experiments. These data were kindly supplied by Prof. M. Zenkova.

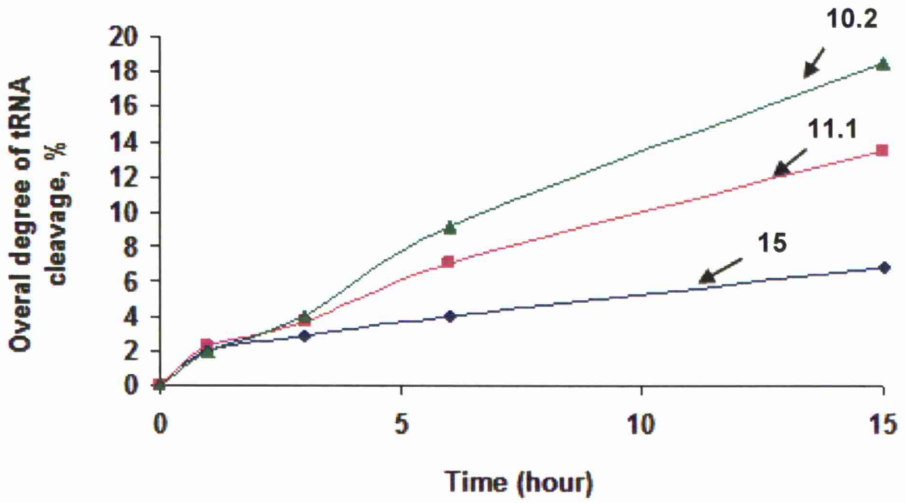

Figure 3.44 shows overall cleavage of the tRNA^{Phe} as a function of time indicated by **11.1**, **10.2** and **15** at a concentration of the conjugates **11.1**, **10.2**, **15** of 5×10^{-5} M in all experiments.

A control experiment performed in the absence of 17-mer oligonucleotide showed no evidence of cleavage (Line K-, Figure 3.43), demonstrating the catalytic role of the ARs. It is also seen from the autoradiograph that unmodified 17-mer lacking both phenazinium anchor and *bis*-imidazole cleaving groups did not produce any substantial cleavage of the tRNA^{Phe} target even at longer incubation times (Lanes: K+ (2B), Figure 3.43). In all cases the cleavage activity was dependent on incubation time.

However, incubation of the 5′- [^{32}P] -tRNA^{Phe} with the conjugates **11.1** and **10.2** resulted in detectable cleavage of the tRNA^{Phe} sequence at two consecutive CA sites, positions **C^{61}A**, **C^{63}A,** and especially at position **U^{8}A** (Lines: **Im-1** and **Phen-Im2;** see also cloverleaf structure of yeast tRNA^{Phe}, Figure 3.42).

It is well known that pancreatic RNase cleaves mainly at 5′-Py-A-3′ sequences. Therefore, these data correlate well with the previously obtained results that single-stranded *pyrimidine-purine* sequences are very susceptible to artificial ribonuclease cleavage [119, 219]. Another important issue was that the level of cleavage at the **C^{63}A** position was higher compared to the cleavage at position **C^{61}A**. A similar observation was obtained in various studies showing cleavage of tRNA^{Phe} by imidazole-based oligonucleotide conjugates [6, 25] designed for the same tRNA target. Marked cleavage of the **U^{8}A** site observed for the studied conjugate site is rather unusual for this type of artificial ribonucleases and could be explained by possible spatial proximity of this region to the **C^{61}A** and **C^{63}A** sites, presumably induced by stacking interaction of the Phn anchor group with the nearest nucleotide residues of tRNA.

Surprisingly, the cleavage of the above sites (*i.e.* **C^{61}A**, **C^{63}A** and **U^{8}A**) was also detected for oligonucleotide conjugate **15**, containing the phenazinium anchor group, but lacking the bis-imidazole cleaving construct. The question to address here was how **15**, which lacks any conventional catalytic groups, was capable of cleaving a phosphodiester bond in the vicinity of the tRNA clevage sites? One possibility could be that multipoint contacts formed between **15** (containing *positively charged* phenazinium group) and the tRNA nucleotide residues disrupt the stacking interactions within the tRNA molecule and thus change the conformation of the the sugar-phosphate backbones in the vicinity of cleavage site. This may induce a conformational stress of the sugar-phosphate backbones within tRNA in the vicinity of the cleavage sites leading to the to self-cleavage of the most vulnerable bonds. Similar effects have already been observed for small-molecule cationic compounds containing a benzene ring substituted with the bis-quaternary salt of diazabicyclo[2.2.2]octane (DABCO) and bearing a polymethylene fragment at the bridge positions [220, 221], but not containing traditional cleaving moieties.

Overall, it was found that the level of cleavage by conjugates **11.1** and **10.2** was 13.5% and 18.5%, respectively, at 37 °C after 15 h incubation, with conjugates at 50 μM concentration and RNA at 0.5 μM concentration. However, the cleavage potential of ARs studied in this research was found to be lower than the data

obtained for the other *bis*-imidazole-containing artificial ribonucleases without a phenazinium anchor group [25, 119].

One possible reason for these observations could be that intercalation of the phenazinium anchor group in the vicinity of the double-stranded region (C61-A62-C63-A64) of the target tRNA, may increase the rigidity of the helical structure. In turn, this might prevent the neighbouring 2'-OH group (which is normally involved in the cleavage mechanism) from adopting an 'in-line' conformation relative to the phosphorus atom and 5'- departing oxygen atoms and making this region to be less susceptible to cleavage [6, 222].

4. Conclusions

Novel oligonucleotide-based ribonuclease mimics containing a *bis*-imidazole catalytic centre and an *N*-hydroxyethylphenazinium anchor group were successfully synthesised using the variety of synthetic routes discussed in section 3.1. These AR and their intermediates were characterised using NMR and IR spectroscopes, MS spectrometry, UV-visible spectrophotometry, m.p. analysis, TLC and/or HPLC. The ability of these AR to hybridise with the single-stranded RNA target has been evaluated using biophysical studies. It was also demonstrated that the *N*-hydroxyethylphenazinium moiety provided a useful way to monitor oligonucleotide conjugate hybridization ability.

The impact of the *N*-hydroxyethylphenazinium anchor group on the performance of *bis*-imidazole containing artificial ribonucleases in terms of (i) their ability to enhance affinity of cleaving groups to RNA target and (ii) to improve their hybridisation properties *via* additional stacking and electrostatic interactions with nucleotide residues was evaluated and the following conclusions were made.

UV hybridisation studies showed *N-(2*-hydroxyethyl)phenazinium had definite electrostatic interactions with the RNA target. The different dispositions of the *N-(2*-hydroxyethyl)phenazinium appeared to have no significant impact on the magnitude of the interaction which is consistent with the predominant electrostatic nature of mode of interactions with RNA target.

The phenazinium-containing oligonucleotide conjugates were able to hybridize readily to the target 23-mer 2'-O-Me RNA. The hybridisation properties and binding affinity (T_m values) of synthesised conjugates with target 23-mer 2'-O-Me RNA showed definite and reproducible interactions, detected by both UV-visible spectrophotometry and fluorescence spectroscopy.

Melting temperature studies showed the *N-(2*-hydroxyethyl)phenazinium anchor increased the binding affinity of all ARs synthesised (compared to the parent antisense oligonucleotide), including the analogue without a catalytic domain (**15**). The *N-(2*-hydroxyethyl)phenazinium anchor increased the RNA binding capabilities of the designed conjugates by a modest degree of between 5- 7 °C.

The synthesised ARs **11.1** and **10.4**, which had a *N*-hydroxyethylphenazinium anchor closer to catalytic cleaving domain (located on the α amine of lysine

residue), overall showed a slightly higher T_m and stabilisation than **10.2** and **10.3**, but not by a significant amount. These effects on T_m are likely to be attributable to a contribution from stacking interactions (which increased binding affinity within the nitrogenous nucleotide bases).

The hydrolytic activity and site specificity of these artificial ribonucleases in terms of their cleaving potential against RNA phosphodiester bonds was assessed by project collaborators, Prof. Vlassov's and Prof M Zenkova's group, Institute of Chemical biology and Fundamental Medicine, Novosibirsk, Russia.

The conjugates **11.1** and **10.2** showed detectable cleavage of the $tRNA^{Phe}$ sequence at two consecutive CA sites, positions $C^{61}A$, $C^{63}A$, and especially at position $U^{8}A$. This demonstrated an ability of the synthesised ARs to cleave RNA target in a sequence-specific manner.

The results showed modest cleavage rates for these compounds but had less cleaving ability than the compounds *without* the Phn anchor reported by Belaglazova *et al* [25].

The cleavage rate of the studied conjugates **11.1** and **10.2** was 13.5 % and 18.5 %, respectively, at 37 °C after 15 h incubation, with conjugates at 50 μM concentration and RNA at 0.5 μM concentration.

Although the cleaving potential of the AR **11.1** with the close location of the phenazinium anchor to catalytic domain was lower that that seen for **10.2**, this conjugate was still able to specifically cleave the RNA target in the presence of the bulky *N*-(2-hydroxyethyl)phenazinium group linked in very close proximity to the cleaving domain.

The alternative attachment of the non-specific *N*-(2-hydroxyethyl)phenazinium anchor group and oligonucleotide binding domain affected the cleavage potential of the ARs. The AR **10.2** with the non-specific *N*-hydroxyethylphenazinium anchor further away from the cleaving domain appeared to have greater hydrolytic ability, presumably due to decreased sterical obstruction from the bulky anchor group.

5. Future work

The lack of an available 3D-structure of *AR:RNA* target complex (*e.g.* from high-field NMR) hinders the safe identification of possible interactions between the cleaving and anchor groups and the RNA target. Therefore, further structural studies are required to obtain reliable information about the structure and dynamics of some designed artificial ribonucleases comprising active ribonuclease mimics within their complexes with the RNA. This could be done by a combination of NMR spectroscopy and computer calculations.

Novel artificial ribonuclease constructs could be investigated further in living cells by screening *in vitro*.

Developments in the medicinal chemistry of antisense molecules has produced a number of modified nucleic acids which may be tried in place of DNA oligonucleotides as specific binders. For example, the incorporation of cleaving agents into peptide nucleic acids could be tried (using peptide chemistry), especially by placing the cleaver at different positions in the PNA strand to try to effect a turn-over mechanism.

6. References

1. Yao, Y., Wang, C., Varshney, R. R., Wang, D. A. *Antisense makes sense in engineered regenerative medicine.* Pharmaceutical Research, 2009. **26** (2). p. 263-275.
2. Patel, A. *Knocked Down or Out ???* Drug Discovery & Development. 2008 [cited 2009; Available from: http://www.dddmag.com/article-Antisense-technology-knocked-down-or-knocked-out.aspx.
3. Lee, J.E. and R.T. Raines, *Ribonucleases as novel chemotherapeutics: The ranpirnase example.* BioDrugs, 2008. **22** (1). p. 53-58.
4. Raines, R.T., *Ribonuclease A.* Chem Rev, 1998. **98** (3): p. 1045-1066.
5. Birdsall, D.L. and A. McPherson, *Crystal structure disposition of thymidylic acid tetramer in complex with ribonuclease A.* Journal of Biological Chemistry, 1992. **267** (31): p. 22230-22236.
6. Fabani, M.M., *Artificial Ribonucleases. Design, Synthesis and Investigation*, in *School of Pharmacy and Pharmaceutical Sciences*. 2004, University of Manchester.
7. Breslow, R., D.L. Huang, and E. Anslyn, *On the mechanism of action of ribonuclease: Dinucleotide cleavage catalyzed by imidazole and Zn2+.* Proceedings of the National Academy of Sciences of the United States of America, 1989. **86** (6): p. 1746-1750.
8. Hovinen, J., Guzaev, A., Azhayeva, E., Azhayev, A., Lonnberg, H. *Imidazole tethered oligodeoxyribonucleotides: Synthesis and RNA cleaving activity.* Journal of Organic Chemistry, 1995. **60** (7): p. 2205-2209.
9. Reynolds, M.A., Beck, T. A., Say, P. B., Schwartz, D. A., Dwyer, B. P., Daily, W. J., Vaghefi, M. M., Metzler, M. D., Klem, R. E., Arnold Jr, L. J. *Antisense oligonucleotides containing an internal, non-nucleotide-based linker promote site-specific cleavage of RNA.* Nucleic Acids Research, 1996. **24** (4): p. 760-765.
10. Fouace, S., Gaudin, C., Picard, S., Corvaisier, S., Renault, J., Carboni, B., Felden, B. *Polyamine derivatives as selective RNaseA mimics.* Nucleic Acids Research, 2004. **32** (1): p. 151-157.
11. Jubian, V., Veronese, A., Dixon, R. P., Hamilton, A. D. *Acceleration of a phosphate diester transesterification reaction by bis(alkylguanidinium) receptors containing an appended general base.* Angewandte Chemie (International Edition in English), 1995. **34** (11): p. 1237-1239.
12. Canaple, L., Husken, D., Hall, J., Haner, R. *Artificial ribonucleases: Efficient and specific in vitro cleavage of human c-raf-1 RNA.* Bioconjugate Chemistry, 2002. **13** (5): p. 945-951.
13. Putnam, W.C. and J.K. Bashkin, *De novo synthesis of artificial ribonucleases with benign metal catalysts.* Chemical Communications, 2000 (9): p. 767-768.
14. Daniher, A.T. and J.K. Bashkin, *Precise control of RNA cleavage by ribozyme mimics.* Chemical Communications, 1998 (10): p. 1077-1078.
15. Gunnlaugsson, T., Jeremy, R., Davies, H., Nieuwenhuyzen, M., Stevenson, C. S., Viguier, R., Mulready, S. *Rapid hydrolytic cleavage of the mRNA model compound HPNP by glycine based macrocyclic lanthanide ribonuclease mimics.* Chemical Communications, 2002 (18): p. 2136-2137.

16. Chow, C.S. and F.M. Bogdan, *A structural basis for RNA-ligand interactions.* Chemical Reviews, 1997. **97** (5): p. 1489-1513.
17. Silnikov, V., Zuber, G., Behr, J. P., Giege, R., Vlassov, V. *Design of ribonuclease mimics for sequence specific cleavage of RNA.* Phosphorus, Sulfur and Silicon and Related Elements, 1996. **109** (1-4): p. 277-280.
18. Konevetz D.A., B.I.E., Beloglazova N.G., Sulimenkov I.V., Silnikov V.N., Zenkova M.A., Shishkin G.V., Vlassov V.V., *Artificial ribonucleases: synthesis and RNA cleaving properties of cationic conjugates bearing imidazole residues.* Tetrahedron, 1999. **55**: p. 503-512.
19. *British National Formulary. 56. September 2008.* Vol. 56. 2008.
20. Shinozuka, K., Shimizu, K., Nakashima, Y., Sawai, H. *Synthesis and RNA cleaving activities of polyamine derived novel artificial ribonuclease.* Bioorganic and Medicinal Chemistry Letters, 1994. **4** (16): p. 1979-1982.
21. Podyminogin, M.A., V.V. Vlassov, and R. Giege, *Synthetic RNA-cleaving molecules mimicking ribonuclease A active center. Design and cleavage of tRNA transcripts.* Nucleic Acids Research, 1993. **21** (25): p. 5950-5956.
22. Patino, N., Di Giorgio, C., Dan-Covalciuc, C., Peytou, V., Terreux, R., Cabrol-Bass, D., Bailly, C., Condom, R. *Modelling, synthesis and biological evaluation of an ethidium-arginine conjugate linked to a ribonuclease mimic directed against TAR RNA of HIV-1.* European Journal of Medicinal Chemistry, 2002. **37** (7): p. 573-584.
23. Kurreck, J., *Antisense technologies: Improvement through novel chemical modifications.* European Journal of Biochemistry, 2003. **270** (8): p. 1628-1644.
24. Herdewijn, P., *Heterocyclic modifications of oligonucleotides and antisense technology.* Antisense and Nucleic Acid Drug Development, 2000. **10** (4): p. 297-310.
25. Beloglazova, N.G., Sil'Nikov, V. N., Zenkova, M. A., Vlassov, V. V. *Cleavage of yeast tRNA(Phe) with complementary oligonucleotide conjugated to a small ribonuclease mimic.* FEBS Letters, 2000. **481** (3): p. 277-280.
26. Vlassov, V.V., Zuber, G., Felden, B., Behr, J. P., Giege, R. *Cleavage of tRNA with imidazole and spermine imidazole constructs: A new approach for probing RNA structure.* Nucleic Acids Research, 1995. **23** (16): p. 3161-3167.
27. Bichenkova, E.V., Zarytova V.F., Ivanova E.M., Maltseva T.V., Sal'nikov G.E., Lebedev A.V. . *Study of the structure of the duplex (Phn-NH(CH2)2NH)pd(CCAAACA) .pd(TGTTTGGC) with covalently bound 10-(2-hydroxyethyl)phenazine in an aqueous solution by 2D-^{1}H-NMR spectroscopy.* Bioorganicheskaya Khimiya, 1992. **18** (3): p. 398-412.
28. *The World Health Report 1996 - Fighting disease, fostering development.* [cited 09/06/2009]; Available from: http://www.who.int/whr/1996/en/.
29. Kirschner, D., *Timebomb: The Global Epidemic of Multi-Drug Resistant Tuberculosis.* Nature Medicine, 2001. **7** (11): p. 1173.
30. Davies, J., *Inactivation of antibiotics and the dissemination of resistance genes.* Science, 1994. **264** (5157): p. 375-82.
31. Davies, J. and G.D. Wright, *Bacterial resistance to aminoglycoside antibiotics.* Trends Microbiol, 1997. **5** (6): p. 234-40.
32. Prasad, R., *Management of multi-drug resistant tuberculosis: practitioner's view point.* Indian J Tuberc, 2007. **54** (1): p. 3-11.
33. Mehta, S.R. and S. Das, *Management of malaria: recent trends.* J Commun Dis, 2006. **38** (2): p. 130-8.

34. Zaman, G.J., P.J. Michiels, and C.A. van Boeckel, *Targeting RNA: new opportunities to address drugless targets.* Drug Discov Today, 2003. **8** (7): p. 297-306.
35. Pearson, N.D. and C.D. Prescott, *RNA as a drug target.* Chem Biol, 1997. **4** (6): p. 409-14.
36. Hermann, T. and E. Westhof, *RNA as a drug target: chemical, modelling, and evolutionary tools.* Curr Opin Biotechnol, 1998. **9** (1): p. 66-73.
37. Xavier, K.A., P.S. Eder, and T. Giordano, *RNA as a drug target: methods for biophysical characterization and screening.* Trends Biotechnol, 2000. **18** (8): p. 349-56.
38. Gleave, M.E. and B.P. Monia, *Antisense therapy for cancer.* Nature Reviews Cancer, 2005. **5** (6): p. 468-479.
39. Sun, X., Kanwar, J. R., Leung, E., Lehnert, K., Wang, D., Krissansen, G. W. *Gene transfer of antisense hypoxia inducible factor-1α enhances the therapeutic efficacy of cancer immunotherapy.* Gene Therapy, 2001. **8** (8): p. 638-645.
40. Henke, E., Perk, J., Vider, J., De Candia, P., Chin, Y., Solit, D. B., Ponomarev, V., Cartegni, L., Manova, K., Rosen, N., Benezra, R. *Peptide-conjugated antisense oligonucleotides for targeted inhibition of a transcriptional regulator in vivo.* Nature Biotechnology, 2008. **26**(1): p. 91-100.
41. Stenvang, J. and S. Kauppinen, *MicroRNAs as targets for antisense-based therapeutics.* Expert Opinion on Biological Therapy, 2008. **8** (1): p. 59-81.
42. Sullenger, B.A. and E. Gilboa, *Emerging clinical applications of RNA.* Nature, 2002. **418**(6894): p. 252-258.
43. Gottesman, S., *Small RNAs shed some light.* Cell, 2004. **118** (1): p. 1-2.
44. Mattick, J.S., *The human genome and the future of medicine.* Med J Aust, 2003. **179** (4): p. 212-6.
45. Zamecnik, P.C. and M.L. Stephenson, *Inhibition of Rous sarcoma virus replication and cell transformation by a specific oligodeoxynucleotide.* Proceedings of the National Academy of Sciences of the United States of America, 1978. **75** (1): p. 280-284.
46. Schubert, S. and J. Kurreck, *Oligonucleotide-based antiviral strategies.* Handb Exp Pharmacol, 2006 (173): p. 261-87.
47. Von Ahsen, U., J. Davies, and R. Schroeder, *Antibiotic inhibition of group I ribozyme function.* Nature, 1991. **353** (6342): p. 368-370.
48. Rife, J.P., *Therapeutic Agents Acting on RNA Targets*, in *Burger's Medicinal Chemistry and Drug Discovery, Sixth Edition.*, D.J. Abraham., Editor. 2003, Wiley-Interscience. p. 168-198.
49. Melnikova, I., *RNA-based therapies.* Nature Reviews Drug Discovery, 2007. **6** (11): p. 863-864.
50. Bonetta, L., *RNA-Based Therapeutics: Ready for Delivery?* Cell, 2009. **136** (4): p. 581-584.
51. Schein, C.H., *From housekeeper to microsurgeon: The diagnostic and therapeutic potential of ribonucleases.* Nature Biotechnology, 1997. **15** (6): p. 529-536.
52. Zhang, Y.C., Taylor, M. M., Samson, W. K., Phillips, M. I. *Antisense inhibition: oligonucleotides, ribozymes, and siRNAs.* Methods Mol Med, 2005. **106**: p. 11-34.
53. Fedor, M.J. and J.R. Williamson, *The catalytic diversity of RNAs.* Nature Reviews Molecular Cell Biology, 2005. **6** (5): p. 399-412.

54. Schubert, S. and J. Kurreck, *Ribozyme- and deoxyribozyme-strategies for medical applications.* Current Drug Targets, 2004. **5**(8): p. 667-681.
55. Grimm, D., *Small silencing RNAs: State-of-the-art.* Advanced Drug Delivery Reviews, 2009. **61** (9): p. 672-703.
56. Masiero, M., Nardo, G., Indraccolo, S., Favaro, E. *RNA interference: Implications for cancer treatment.* Molecular Aspects of Medicine, 2007. **28** (1): p. 143-166.
57. Sioud, M., *Therapeutic siRNAs.* Trends in Pharmacological Sciences, 2004. **25** (1): p. 22-28.
58. Zhang, Y.C., Taylor, M. M., Samson, W. K., Phillips, M. I. *Antisense inhibition: oligonucleotides, ribozymes, and siRNAs.* Methods in molecular medicine, 2005. **106**: p. 11-34.
59. Phillips, M.I., S.M. Galli, and J.L. Mehta, *The potential role of antisense oligodeoxynucleotide therapy for cardiovascular disease.* Drugs, 2000. **60** (2): p. 239-248.
60. Phillips, M.I., *Antisense therapeutics: a promise waiting to be fulfilled.* Methods Mol Med, 2005. **106**: p. 3-10.
61. Crooke, S.T., *Progress in antisense therapeutics.* Medicinal Research Reviews, 1996. **16** (4): p. 319-344.
62. Crooke, S.T., *Molecular mechanisms of action of antisense drugs.* Biochimica et Biophysica Acta - Gene Structure and Expression, 1999. **1489** (1): p. 31-43.
63. Crooke, S.T., *Potential roles of antisense technology in cancer chemotherapy.* Oncogene, 2000. **19** (56): p. 6651-6659.
64. Trawick, B.N., A.T. Daniher, and J.K. Bashkin, *Inorganic mimics of ribonucleases and ribozymes: From random cleavage to sequence-specific chemistry to catalytic antisense drugs.* Chemical Reviews, 1998. **98** (3): p. 939-960.
65. Gautschi, O., Tschopp, S., Olie, R. A., Leech, S. H., Simoes-Wust, A. P., Ziegler, A., Baumann, B., Odermatt, B., Hall, J., Stahel, R. A., Zangemeister-Wittke, U. *Activity of a novel bcl-2/bcl-xL-bispecific antisense oligonucleotide against tumors of diverse histologic origins.* Journal of the National Cancer Institute, 2001. **93** (6): p. 463-471.
66. Sohail, M. and E.M. Southern, *Selecting optimal antisense reagents.* Advanced Drug Delivery Reviews, 2000. **44** (1): p. 23-34.
67. Sohail, M. and E.M. Southern, *Hybridization of antisense reagents to RNA.* Current Opinion in Molecular Therapeutics, 2000. **2** (3): p. 264-271.
68. Chaubey, B., Tripathi, S., Ganguly, S., Harris, D., Casale, R. A., Pandey, V. N. *A PNA-transportan conjugate targeted to the TAR region of the HIV-1 genome exhibits both antiviral and virucidal properties.* Virology, 2005. **331** (2): p. 418-428.
69. Greene, W.C., Debyser, Z., Ikeda, Y., Freed, E. O., Stephens, E., Yonemoto, W., Buckheit, R., W., Estel̀, J. A., Cihlar, T. *Novel targets for HIV therapy.* Antiviral Research, 2008. **80** (3): p. 251-265.
70. De Clercq, E., *The design of drugs for HIV and HCV.* Nature Reviews Drug Discovery, 2007. **6** (12): p. 1001-1018.
71. De Clercq, E., *Antivirals and antiviral strategies.* Nature Reviews Microbiology, 2004. **2** (9): p. 704-720.
72. De Clercq, E., *Antiviral drugs in current clinical use.* Journal of Clinical Virology, 2004. **30** (2): p. 115-133.
73. Martinand-Mari, C., B. Lebleu, and I. Robbins, *Oligonucleotide-based Strategies to Inhibit Human Hepatitis C Virus.* Oligonucleotides, 2003. **13** (6): p. 539-548.

74. Highleyman, L., *Fomivirsen.* BETA bulletin of experimental treatments for AIDS : a publication of the San Francisco AIDS foundation, 1998.
75. Highleyman, L., *FDA approves fomivirsen, famciclovir, and Thalidomide. Food and Drug Administration.* BETA bulletin of experimental treatments for AIDS : a publication of the San Francisco AIDS foundation, 1998: p. 5.
76. *Clinical Pharmacology of Fomivirsen, Rxlist.* 2008 [cited 04/08/08]; Available from: http://www.rxlist.com/cgi/generic2/fomivirsen_cp.html.
77. Jing, N. and X. Xu, *Rational drug design of DNA oligonucleotides as HIV inhibitors.* Current drug targets. Infectious disorders, 2001. **1** (2): p. 79-90.
78. Arzumanov, A., Walsh, A. P., Liu, X., Rajwanshi, V. K., Wengel, J. and Gait, M. J *Oligonucleotide analogue interference with the HIV-1 Tat protein-TAR RNA interaction.* Nucleosides, Nucleotides and Nucleic Acids, 2001. **20** (4-7): p. 471-480.
79. Arzumanov, A., Walsh, A. P., Rajwanshi, V. K., Kumar, R., Wengel, J. and Gait, M. J. *Inhibition of HIV-1 Tat-dependent trans activation by steric block chimeric 2'-O-methyl/LNA oligoribonucleotides.* Biochemistry, 2001. **40** (48): p. 14645-14654.
80. Arzumanov, A., Stetsenko, D. A., Malakhov, A. D., Reichelt, S., Sorensen, M. D., Babu, B. R., Wengel, J. and Gait, M. J. *A Structure-Activity Study of the Inhibition of HIV-1 Tat-Dependent Trans-Activation by Mixmer 2'-O-Methyl Oligoribonucleotides Containing Locked Nucleic Acid (LNA), α-L-LNA, or 2'-Thio-LNA Residues.* Oligonucleotides, 2003. **13** (6): p. 435-453.
81. Elmen, J., Zhang, H. Y., Zuber, B., Ljungberg, K., Wahren, B., Wahlestedt, C. and Liang, Z. *Locked nucleic acid containing antisense oligonucleotides enhance inhibition of HIV-1 genome dimerization and inhibit virus replication.* FEBS Letters, 2004. **578** (3): p. 285-290.
82. Dean, N.M. and C. Frank Bennett, *Antisense oligonucleotide-based therapeutics for cancer.* Oncogene, 2003. **22** (56 REV. ISS. 8): p. 9087-9096.
83. Orr, R.M. and B.P. Monia, *Antisense therapy for cancer.* IDrugs, 1998. **1** (2): p. 199-205.
84. Orr, R.M. and F.A. Dorr, *Clinical studies of antisense oligonucleotides for cancer therapy.* Methods in molecular medicine, 2005. **106**: p. 85-111.
85. Hadaschik, B.A. and M.E. Gleave, *Therapeutic options for hormone-refractory prostate cancer in 2007.* Urologic Oncology: Seminars and Original Investigations, 2007. **25**(5): p. 413-419.
86. Hadaschik, B.A., R.D. Sowery, and M.E. Gleave, *Novel targets and approaches in advanced prostate cancer.* Current Opinion in Urology, 2007. **17** (3): p. 182-187.
87. Jansen, B., Schlagbauer-Wadl, H., Brown, B. D., Bryan, R. N., van Elsas, A., Muller, M., Wolff, K., Eichler, H. G. and Pehamberger, H. *Bcl-2 antisense therapy chemosensitizes human melanoma in SCID mice.* Nat Med, 1998. **4** (2): p. 232-4.
88. Paz-Ares, L., Douillard, J. Y., Koralewski, P., Manegold, C., Smit, E. F., Reyes, J. M., Chang, G. C., John, W. J., Peterson, P. M., Obasaju, C. K., Lahn, M. and Gandara, D. R. *Phase III study of gemcitabine and cisplatin with or without aprinocarsen, a protein kinase C-alpha antisense oligonucleotide, in patients with advanced-stage non-small-cell lung cancer.* Journal of Clinical Oncology, 2006. **24** (9): p. 1428-1434.
89. *Oncogenex Product Candidate: OGX-427 Overview.* 2009 [cited 16/07/09]; Available from: http://www.oncogenex.com/products/ogx427.html.

90. Chang, Q., Qin, R., Huang, T., Gao, J. and Feng, Y. *Effect of antisense hypoxia-inducible factor 1α on progression, metastasis, and chemosensitivity of pancreatic cancer.* Pancreas, 2006. **32** (3): p. 297-305.
91. Ziello, J.E., I.S. Jovin, and Y. Huang, *Hypoxia-Inducible Factor (HIF)-1 regulatory pathway and its potential for therapeutic intervention in malignancy and ischemia.* Yale J Biol Med, 2007. **80** (2): p. 51-60.
92. Greenberger, L.M., Horak, I. D., Filpula, D., Sapra, P., Westergaard, M., Frydenlund, H. F., Albaek, C., Schroder, H. and Orum, H. *A RNA antagonist of hypoxia-inducible factor-1α, EZN-2968, inhibits tumor cell growth.* Molecular Cancer Therapeutics, 2008. **7** (11): p. 3598-3608.
93. Potera, C., *Antisense - Down, but not out.* Nature Biotechnology, 2007. **25** (5): p. 497-499.
94. Komiyama, M. and J. Sumaoka, *Progress towards synthetic enzymes for phosphoester hydrolysis.* Curr Opin Chem Biol, 1998. **2** (6): p. 751-7.
95. Koroleva, L.S., Serpokrylova, I. Yu., Vlassov, V. V. and Silnikov, V. N. *Design and synthesis of metal-free artificial ribonucleases.* Protein Pept Lett, 2007. **14** (2): p. 151-63.
96. Beloglazova, N.G., Fabani, M. M., Zenkova, M. A., Bichenkova, E. V., Polushin, N. N., Sil'nikov, V. V., Douglas, K. T. and Vlassov, V. V. *Sequence-specific artificial ribonucleases. I. Bis-imidazole-containing oligonucleotide conjugates prepared using precursor-based strategy.* Nucleic Acids Research, 2004. **32** (13): p. 3887-3897.
97. Huber, P.W., *Chemical nucleases: Their use in studying RNA structure and RNA-protein interactions.* FASEB Journal, 1993. **7** (14): p. 1367-1375.
98. Desai, N.A. and V. Shankar, *Single-strand-specific nucleases.* FEMS Microbiology Reviews, 2003. **26** (5): p. 457-491.
99. Johannes, L. and D. Decaudin, *Protein toxins: Intracellular trafficking for targeted therapy.* Gene Therapy, 2005. **12** (18): p. 1360-1368.
100. Arnold, U. and R. Ulbrich-Hofmann, *Natural and engineered ribonucleases as potential cancer therapeutics.* Biotechnology Letters, 2006. **28** (20): p. 1615-1622.
101. Leland, P.A. and R.T. Raines, *Cancer chemotherapy--ribonucleases to the rescue.* Chem Biol, 2001. **8** (5): p. 405-13.
102. *Malignant Mesothelioma: Focus on new therapeutic approaches.* 2009 [cited 03/06/09]; Available from: http://www.mesotheliomaweb.org/newchemo.html.
103. Lee, J.E., Bae, E., Bingman, C. A., Phillips Jr, G. N. and Raines, R. T. *Structural Basis for Catalysis by Onconase.* Journal of Molecular Biology, 2008. **375** (1): p. 165-177.
104. Horiuchi, H., Yanai, K., Takagi, M., Yano, K., Wakabayashi, E., Sanda, A., Mine, S., Ohgi, K. and Irie, M. *Primary structure of a base non-specific ribonuclease from Rhizopus niveus.* Journal of Biochemistry, 1988. **103** (3): p. 408-418.
105. Schulenburg, C., Ardelt, B., Ardelt, W., Arnold, U., Shogen, K., Ulbrich-Hofmann, R. and Darzynkiewicz, Z. *The interdependence between catalytic activity, conformational stability, and cytotoxicity of onconase.* Cancer Biology and Therapy, 2007. **6** (8): p. 1233-1239.
106. *The Alfacell corporation website: Onconase clinical trial results.* 2009 [cited 12/06/09]; Available from: http://www.alfacell.com/products/onconase_clinical_results.html.
107. *Onconase New Drug Application.* 2009 [cited 15/05/2009]; Available from: http://www.drugs.com/nda/onconase_090128.html.

108. Mironova, N.L., Pyshnyi, D. V., Shtadler, D. V., Fedorova, A. A., Vlassov, V. V. and Zenkova, M. A. *RNase T1 mimicking artificial ribonuclease.* Nucleic Acids Research, 2007. **35** (7): p. 2356-2367.
109. McPherson, A., Brayer, G., Cascio, D. and Williams, R. *The mechanism of binding of a polynucleotide chain to pancreatic ribonuclease.* Science, 1986. **232** (4751): p. 765-8.
110. Perreault, D.M. and E.V. Anslyn, *Unifying the Current Data on the Mechanism of Cleavage-Transesterification of RNA.* Angewandte Chemie (International Edition in English), 1997. **36** (5): p. 432-450.
111. Oivanen, M., S. Kuusela, and H. Lonnberg, *Kinetics and mechanisms for the cleavage and isomerization of the phosphodiester bonds of RNA by bronsted acids and bases.* Chemical Reviews, 1998. **98** (3): p. 961-990.
112. Anslyn, E. and R. Breslow, *Geometric evidence on the ribonuclease model mechanism.* Journal of the American Chemical Society, 1989. **111**(15): p. 5972-5973.
113. Breslow, R., *How do imidazole groups catalyze the cleavage of RNA in enzyme models and in enzymes? Evidence from "negative catalysis".* Accounts of Chemical Research, 1991. **24** (11): p. X1-324.
114. Breslow, R., *Kinetics and mechanism in RNA cleavage.* Proceedings of the National Academy of Sciences of the United States of America, 1993. **90** (4): p. 1208-1211.
115. Breslow, R., Dong, S. D., Webb, Y. and Xu, R. *Further studies on the buffer-catalyzed cleavage and isomerization of uridyluridine. Medium and ionic strength effects on catalysis by morpholine, imidazole, and acetate buffers help clarify the mechanisms involved and their relationship to the mechanism used by the enzyme ribonuclease and by a ribonuclease mimic.* Journal of the American Chemical Society, 1996. **118** (28): p. 6588-6600.
116. Anslyn, E. and R. Breslow, *On the mechanism of catalysis by ribonuclease: Cleavage and isomerization of the dinucleotide UpU catalyzed by imidazole buffers.* Journal of the American Chemical Society, 1989. **111**(12): p. 4473-4482.
117. Wayne Schultz, L., D.J. Quirk, and R.T. Raines, *HisÂ·Â·Â·Asp catalytic dyad of ribonuclease A: Structure and function of the wild-type, D121N, and D121A enzymes.* Biochemistry, 1998. **37** (25): p. 8886-8898.
118. delCardayre, S.B. and R.T. Raines, *A residue to residue hydrogen bond mediates the nucleotide specificity of ribonuclease A.* Journal of Molecular Biology, 1995. **252** (3): p. 328-336.
119. Beloglazova, N.G., Fabani, M. M., Zenkova, M. A., Bichenkova, E. V., Polushin, N. N., Sil'nikov, V. V., Douglas, K. T. and Vlassov, V. V. *Sequence-specific artificial ribonucleases. I. Bis-imidazole-containing oligonucleotide conjugates prepared using precursor-based strategy.* Nucleic Acids Res, 2004. **32** (13): p. 3887-97.
120. Kuznetsova, I.L., Zhdan, N. S., Zenkova, M. A., Vlassov, V. V. and Silnikov, V. N. *Synthesis and ribonuclease activity of tripeptides composed of amino acids involved in catalytic centers of natural ribonucleases.* Russian Chemical Bulletin, International Edition, 2004. **53** (2): p. 455-462
121. Wlodawer, A., *Neutron diffraction of crystalline proteins.* Prog Biophys Mol Biol, 1982. **40** (1-2): p. 115-59.
122. Wlodawer, A. and L. Sjolin, *Structure of ribonuclease A: results of joint neutron and X-ray refinement at 2.0-A resolution.* Biochemistry, 1983. **22** (11): p. 2720-8.

123. Silnikov, V.N. and V.V. Vlassov, *Design of site-specific RNA-cleaving reagents.* Russian Chemical Reviews, 2001. **70** (6): p. 491-508.
124. Konevetz, D.A., Beck, I. E., Beloglazova, N. G., Sulimenkov, I. V., Sil'nikov, V. N., Zenkova, M. A., Shishkin, G. V. and Vlassov, V. V. *Artificial ribonucleases: Synthesis and RNA cleaving properties of cationic conjugates bearing imidazole residues.* Tetrahedron, 1999. **55** (2): p. 503-512.
125. Garipova, I.Y. and V.N. Silnikov, *Site-specific synthetic ribonucleases based on oligonucleotide conjugates with metal-independent organic catalysts of hydrolysis of phosphodiester bonds.* Russian Chemical Bulletin, 2002. **51** (7): p. 1112-1117.
126. Sidorov, A.V., J.A. Grasby, and D.M. Williams, *Sequence-specific cleavage of RNA in the absence of divalent metal ions by a DNAzyme incorporating imidazolyl and amino functionalities.* Nucleic Acids Research, 2004. **32** (4): p. 1591-1601.
127. Ushijima, K., Gouzu, H., Hosono, K., Shirakawa, M., Kagosima, K., Takai, K. and Takaku, H. *Site-specific cleavage of tRNA by imidazole and/or primary amine groups bound at the 5'-end of oligodeoxyribonucleotides.* Biochimica et Biophysica Acta - General Subjects, 1998. **1379** (2): p. 217-223.
128. Mironova, N.L., Pyshnyi, D. V., Ivanova, E. M., Zarytova, V. F., Zenkova, M. A., Gross, H. J. and Vlassov, V. V. *Sequence-specific RNA cleavage by oligonucleotide-peptide conjugates.* Russian Chemical Bulletin, 2002. **51** (7): p. 1177-1186.
129. Mironova, N.L., Pyshnyi, D. V., Ivanova, E. M., Zenkova, M. A., Gross, H. J. and Vlassov, V. V. *Covalently attached oligodeoxyribonucleotides induce RNase activity of a short peptide and modulate its base specifity.* Nucleic Acids Research, 2004. **32** (6): p. 1928-1936.
130. Kuznetsova, I.L., Zhdan, N. S., Zenkova, M. A., Vlassov, V. V. and Silnikov, V. N. *Artificial ribonucleases. 5. Synthesis and ribonuclease activity of tripeptides composed of amino acids involved in catalytic centers of natural ribonucleases.* Russian Chemical Bulletin, 2004. **53** (2): p. 455-462.
131. Tung, C.H., Wei, Z., Leibowitz, M. J. and Stein, S. *Design of peptide-acridine mimics of ribonuclease activity.* Proceedings of the National Academy of Sciences of the United States of America, 1992. **89** (15): p. 7114-7118.
132. Endo, M., Azuma, Y., Saga, Y., Kuzuya, A., Kawai, G. and Komiyama, M. *Molecular Design for a Pinpoint RNA Scission. Interposition of Oligoamines between Two DNA Oligomers.* Journal of Organic Chemistry, 1997. **62** (4): p. 846-852.
133. Komiyama, M. and K. Yoshinari, *Kinetic Analysis of Diamine-Catalyzed RNA Hydrolysis.* Journal of Organic Chemistry, 1997. **62** (7): p. 2155-2160.
134. Komiyama, M. and T. Inokawa, *Selective hydrolysis of tRNA by ethylenediamine bound to a DNA oligomer.* Journal of Biochemistry, 1994. **116** (4): p. 719-720.
135. Cotton, F.A., E.E. Hazen Jr, and M.J. Legg, *Staphylococcal nuclease: Proposed mechanism of action based on structure of enzyme-thymidine 3',5'-bisphosphate-calcium ion complex at 1.5-Ã... resolution.* Proceedings of the National Academy of Sciences of the United States of America, 1979. **76** (6): p. 2551-2555.
136. Judice, J.K., Gamble, T. R., Murphy, E. C., De Vos, A. M. and Schultz, P. G. *Probing the mechanism of staphylococcal nuclease with unnatural amino acids: Kinetic and structural studies.* Science, 1993. **261** (5128): p. 1578-1581.
137. Smith, J., K. Ariga, and E.V. Anslyn, *Enhanced imidazole-catalyzed RNA cleavage induced by a bis-alkylguanidinium receptor.* Journal of the American Chemical Society, 1993. **115** (1): p. 362-364.

138. Matsuda, S., Ishikubo, A., Kuzuya, A., Yashiro, M. and Komiyama, M. *Conjugates of a dinuclear zinc(II) complex and DNA oligomers as novel sequence-selective artificial ribonucleases.* Angewandte Chemie - International Edition, 1998. **37** (23): p. 3284-3286.
139. Husken, D., Goodall, G., Blommers, M. J. J., Jahnke, W., Hall, J., Haner, R. and Moser, H. E. *Creating RNA bulges: Cleavage of RNA in RNA/DNA duplexes by metal ion catalysis.* Biochemistry, 1996. **35** (51): p. 16591-16600.
140. Niittymaki, T., Kaukinen, U., Virta, P., Mikkola, S. and Lonnberg, H. *Preparation of Azacrown-Functionalized 2'-O-Methyl Oligoribonucleotides, Potential Artificial RNases.* Bioconjugate Chemistry, 2004. **15**(1): p. 174-184.
141. Niittymaki, T., Virta, P., Ketomaki, K. and Lonnberg, H. *Di(azacrown) conjugates of 2'-O-methyl oligoribonucleotides as sequence-selective artificial ribonucleases.* Bioconjugate Chemistry, 2007. **18** (5): p. 1583-1592.
142. Niittymaki, T. and H. Lonnberg, *Artificial ribonucleases.* Organic and Biomolecular Chemistry, 2006. **4** (1): p. 15-25.
143. Gunnlaugsson, T., J.E. O'Brien, and S. Mulready, *Glycine-alanine conjugated macrocyclic lanthanide ion complexes as artificial ribonucleases.* Tetrahedron Letters, 2002. **43** (47): p. 8493-8497.
144. Hall, J., D. Husken, and R. Haner, *Towards artificial ribonucleases: The sequence-specific cleavage of RNA in a duplex.* Nucleic Acids Research, 1996. **24** (18): p. 3522-3526.
145. Komiyama, M., *Lanthanide ion-mediated peptide hydrolysis.* Metal ions in biological systems, 2001. **38**: p. 25-41.
146. Jenkins, L.A., J.K. Bashkin, and M.E. Autry, *The embedded ribonucleotide assay: A chimeric substrate for studying cleavage of RNA by transesterification.* Journal of the American Chemical Society, 1996. **118** (29): p. 6822-6825.
147. Haner, R., J. Hall, and G. Rihs, *37. Synthesis and Structure of a Macrocyclic Europium Complex and Its Possible Role as a Catalyst for Phosphodiester Transesterification.* Helvetica Chimica Acta, 1997. **80** (2): p. 487-494.
148. Stulz, E., H.B. Burgi, and C. Leumann, *ZrIV-tetraphenylporphyrinates as nuclease mimics: Structural, kinetic and mechanistic studies on phosphate diester transesterification.* Chemistry - A European Journal, 2000. **6** (3): p. 523-536.
149. Roigk, A. and H.J. Schneider, *Noncovalently bound cofactors for chemical nucleases.* European Journal of Organic Chemistry, 2001(1): p. 205-209.
150. Niittymaki, T., et al., *Preparation of Azacrown-Functionalized 2â€²-O-Methyl Oligoribonucleotides, Potential Artificial RNases.* Bioconjugate Chemistry, 2004. **15** (1): p. 174-184.
151. Klug, A., *The discovery of zinc fingers and their development for practical applications in gene regulation.* Proceedings of the Japan Academy Series B: Physical and Biological Sciences, 2005. **81** (4): p. 87-102.
152. Klug, A., *Towards therapeutic applications of engineered zinc finger proteins.* FEBS Letters, 2005. **579** (4 SPEC. ISS.): p. 892-894.
153. Klug, A., *Zinc finger peptides for the regulation of gene expression.* Journal of Molecular Biology, 1999. **293** (2): p. 215-218.
154. Klug, A. and J.W.R. Schwabe, *Zinc fingers.* FASEB Journal, 1995. **9** (8): p. 597-604.
155. Bibikova, M., Beumer, K., Trautman, J. K. and Carroll, D. *Enhancing gene targeting with designed zinc finger nucleases.* Science, 2003. **300** (5620): p. 764.

156. Bibikova, M., Golic, M., Golic, K. G. and Carroll, D. *Targeted chromosomal cleavage and mutagenesis in Drosophila using zinc-finger nucleases.* Genetics, 2002. **161** (3): p. 1169-1175.
157. Barbier, B. and A. Brack, *Search for catalytic properties of simple polypeptides.* Origins of Life and Evolution of the Biosphere, 1987. **17** (3-4): p. 381-390.
158. Brack, A. and B. Barbier, *Chemical activity of simple basic peptides.* Origins of Life and Evolution of the Biosphere, 1990. **20** (2): p. 139-144.
159. Mironova, N.L., Pyshnyi, D. V., Ivanova, E. M., Zenkova, M. A., Gross, H. J. and Vlassov, V. V. *Ribonuclease activity of the peptides with alternating arginine and leucine residues conjugated to tetrathymidilate.* Nucleosides, Nucleotides and Nucleic Acids, 2004. **23** (6-7): p. 885-890.
160. Pyshnyi, D.V. and E.M. Ivanova, *The influence of nearest neighbours on the efficiency of coaxial stacking at contiguous stacking hybridization of oligodeoxyribonucleotides.* Nucleosides, Nucleotides and Nucleic Acids, 2004. **23** (6-7): p. 1057-1064.
161. Burakova, E.A. and V.N. Silnikov, *Molecular design of artificial ribonucleases using electrostatic interaction.* Nucleosides, Nucleotides and Nucleic Acids, 2004. **23** (6-7): p. 915-920.
162. Bailly, C. and J.P. Henichart, *DNA recognition by intercalator - minor-groove binder hybrid molecules.* Bioconjugate Chemistry, 1991. **2** (6): p. 379-393.
163. Baraldi, P.G., et al., *DNA minor groove binders as potential antitumor and antimicrobial agents.* Medicinal Research Reviews, 2004. **24** (4): p. 475-528.
164. Usman, N. and R. Cedergren, *Exploiting the Chemical Synthesis of Rna.* Trends in Biochemical Sciences, 1992. **17** (9): p. 334-339.
165. Lown, J.W., *Lexitropsins in antiviral drug development.* Antiviral Research, 1992. **17** (3): p. 179-196.
166. Anthony, N.G., Breen, D., Clarke, J., Donoghue, G., Drummond, A. J., Ellis, E. M., Gemmell, C. G., Helesbeux, J. J., Hunter, I. S., Khalaf, A. I., Mackay, S. P., Parkinson, J. A., Suckling, C. J. and Waigh, R. D. *Antimicrobial lexitropsins containing amide, amidine, and alkene linking groups.* Journal of Medicinal Chemistry, 2007. **50** (24): p. 6116-6125.
167. Bichenkova, E.V., Frau, S., Fedorova, O. S. and Douglas, K. T. *Binding of a desmetallo-porphyrin conjugate of Hoechst 33258 to DNA. III. Strong bonding to single-strand oligonucleotides.* Nucleosides Nucleotides Nucleic Acids, 2001. **20** (1-2): p. 157-68.
168. Frau, S., Bichenkova, E. V., Fedorova, O. S., Lokhov, S. and Douglas, K. T. *Binding of a porphyrin conjugate of Hoechst 33258 to DNA. I. UV-visible and melting studies detect multiple binding modes to a 12-mer nonself-complementary duplex.* Nucleosides Nucleotides Nucleic Acids, 2001. **20** (1-2): p. 131-43.
169. Frau, S., Bichenkova, E. V., Morris, G. A. and Douglas, K. T. *Binding of a porphyrin conjugate of Hoechst 33258 to DNA. II. NMR spectroscopic studies detect multiple binding modes to a 12-mer nonself-complementary duplex DNA.* Nucleosides Nucleotides Nucleic Acids, 2001. **20** (1-2): p. 145-56.
170. Nakanuma, K., Moriguchi, T., Suzuki, H. and Shinozuka, K. *Synthesis of small multifunctional molecules having nucleic acid binding property.* Nucleic Acids Res Suppl, 2001 (1): p. 69-70.
171. Kuzuya, A., R. Mizoguchi, and M. Komiyama, *Site-selective artificial ribonuclease using pinpoint RNA activation.* Nucleic Acids Res Suppl, 2001 (1): p. 131-132.

172. Asseline, U., Delarue, M., Lancelot, G., Toulme, F., Thuong, N. T., Montenaygarestier, T. and Helene, C. *Nucleic-Acid Binding-Molecules with High-Affinity and Base Sequence Specificity - Intercalating Agents Covalently Linked to Oligodeoxynucleotides.* Proceedings of the National Academy of Sciences of the United States of America-Biological Sciences, 1984. **81** (11): p. 3297-3301.
173. Anthony, N.G., Huchet, G., Johnston, B. F., Parkinson, J. A., Suckling, C. J., Waigh, R. D. and Mackay, S. P. *In silico footprinting of ligands binding to the minor groove of DNA.* Journal of Chemical Information and Modeling, 2005. **45** (6): p. 1896-1907.
174. Parkinson, J.A., Barber, J., Douglas, K. T., Rosamond, J. and Sharples, D. *Minor-groove recognition of the self-complementary duplex d(CGCGAATTCGCG)2 by Hoechst 33258: a high-field NMR study.* Biochemistry, 1990. **29** (44): p. 10181-90.
175. Parkinson, J.A., Khalaf, A. I., Anthony, N. G., MacKay, S. P., Suckling, C. J. and Waigh, R. D. *Comparison of DNA complex formation behaviour for two closely related lexitropsin analogues.* Helvetica Chimica Acta, 2009. **92**(5): p. 795-822.
176. Anthony, N.G., Fox, K. R., Johnston, B. F., Khalaf, A. I., Mackay, S. P., McGroarty, I. S., Parkinson, J. A., Skellern, G. G., Suckling, C. J. and Waigh, R. D. *DNA binding of a short lexitropsin.* Bioorganic and Medicinal Chemistry Letters, 2004. **14**(5): p. 1353-1356.
177. Shi, Y., Kuzuya, A., Machida, K. and Komiyama, M. *Crucial role of linker portion in acridine-bearing oligonucleotides for highly efficient site-selective RNA scission.* Tetrahedron Letters, 2004. **45** (19): p. 3703-3706.
178. Komiyama, M., Sumaoka, J., Kuzuya, A. and Yamamoto, Y. *Sequence-selective artificial ribonucleases*, in *Methods in Enzymology*. 2001. p. 455-468.
179. Tung, C.H. and S. Stein, *Preparation and applications of peptide-oligonucleotide conjugates.* Bioconjugate Chemistry, 2000. **11** (5): p. 605-618.
180. Haner, R. and J. Hall, *The sequence-specific cleavage of RNA by artificial chemical ribonucleases.* Antisense and Nucleic Acid Drug Development, 1997. **7** (4): p. 423-430.
181. Haner, R., Hall, J., Pfutzer, A. and Husken, D. *Development of artificial ribinucleases.* Pure and Applied Chemistry, 1998. **70** (1): p. 111-116.
182. Guvakova, M.A., Yakubov, L. A., Vlodavsky, I., Tonkinson, J. L. and Stein, C. A. *Phosphorothioate oligodeoxynucleotides bind to basic fibroblast growth factor, inhibit its binding to cell surface receptors, and remove it from low affinity binding sites on extracellular matrix.* Journal of Biological Chemistry, 1995. **270** (6): p. 2620-2627.
183. Brown, D.A., Kang, S. H., Gryaznov, S. M., DeDionisio, L., Heidenreich, O., Sullivan, S., Xu, X. and Nerenberg, M. I. *Effect of phosphorothioate modification of oligodeoxynucleotides on specific protein binding.* Journal of Biological Chemistry, 1994. **269** (43): p. 26801-26805.
184. Kurreck, J., Wyszko, E., Gillen, C. and Erdmann, V. A. *Design of antisense oligonucleotides stabilized by locked nucleic acids.* Nucleic Acids Research, 2002. **30** (9): p. 1911-1918.
185. Petersen, L., De Koning, M. C., Van Kuik-Romeijn, P., Weterings, J., Pol, C. J., Platenburg, G., Overhand, M., Van Der Marel, G. A. and Van Boom, J. H. *Synthesis and in vitro evaluation of PNA-peptide-DETA conjugates as potential cell penetrating artificial ribonucleases.* Bioconjugate Chemistry, 2004. **15** (3): p. 576-582.

186. Larsen, H.J., T. Bentin, and P.E. Nielsen, *Antisense properties of peptide nucleic acid.* Biochimica et Biophysica Acta - Gene Structure and Expression, 1999. **1489** (1): p. 159-166.
187. Baker, B.F. and B.P. Monia, *Novel mechanisms for antisense-mediated regulation of gene expression.* Biochimica et Biophysica Acta - Gene Structure and Expression, 1999. **1489** (1): p. 3-18.
188. Jakobsen, M.R., Haasnoot, J., Wengel, J., Berkhout, B. and Kjems, J. *Efficient inhibition of HIV-1 expression by LNA modified antisense oligonucleotides and DNAzymes targeted to functionally selected binding sites.* Retrovirology, 2007. **4**: p. 29.
189. Fischer, P.M., *Cellular uptake mechanisms and potential therapeutic utility of peptidic cell delivery vectors: Progress 2001-2006.* Medicinal Research Reviews, 2007. **27**(6): p. 755-795.
190. Gait, M.J., *Peptide-mediated cellular delivery of antisense oligonucleotides and their analogues.* Cellular and Molecular Life Sciences, 2003. **60** (5): p. 844-853.
191. Prochiantz, A., *Getting hydrophilic compounds into cells: Lessons from homeopeptides. Commentary.* Current Opinion in Neurobiology, 1996. **6** (5): p. 629-634.
192. Vives, E., Granier, C., Prevot, P. and Lebleu, B. *Structure-activity relationship study of the plasma membrane translocating potential of a short peptide from HIV-1 Tat protein.* Letters in Peptide Science, 1997. **4**(4-6): p. 429-436.
193. Vives, E., Granier, C., Prevot, P. and Lebleu, B. *Structure-activity relationship study of the plasma membrane translocating potential of a short peptide from HIV-1 Tat protein.* International Journal of Peptide Research and Therapeutics, 1997. **4** (4-6): p. 429-436.
194. Pooga, M., Habrink, M., Zorko, M. and Langel, U. *Cell penetration by transportan.* FASEB Journal, 1998. **12** (1): p. 67-77.
195. Lindsay, M.A., *Peptide-mediated cell delivery: Application in protein target validation.* Current Opinion in Pharmacology, 2002. **2** (5): p. 587-594.
196. Vicennati, P., Giuliano, A., Ortaggi, G., Masotti, A. *Polyethylenimine in medicinal chemistry.* Current Medicinal Chemistry, 2008. **15** (27): p. 2826-2839.
197. Kichler, A., *Gene transfer with modified polyethylenimines.* Journal of Gene Medicine, 2004. **6** (SUPPL. 1): p. S3-S10.
198. Turner, J.J., Jones, S., Fabani, M. M., Ivanova, G., Arzumanov, A. A. and Gait, M. J. *RNA targeting with peptide conjugates of oligonucleotides, siRNA and PNA.* Blood Cells, Molecules, and Diseases, 2007. **38** (1): p. 1-7.
199. Fischer, P.M., E. Krausz, and D.P. Lane, *Cellular delivery of impermeable effector molecules in the form of conjugates with peptides capable of mediating membrane translocation.* Bioconjugate Chemistry, 2001. **12** (6): p. 825-841.
200. Dawson D.C., Elliot K.M. *Data for biochemical research.* 1986: Clarendon Press. Oxford.
201. Godovikova TS, Z.V., Mal'tseva TV, Khalimskaia LM., *Active derivatives of oligonucleotides with a zwitterionic terminal phosphate group for design of affinity reagents and probes.* Bioorganicheskaia Khimiia, 1989. **15** (9): p. 1246-1252.
202. Vlassov V.V., Z.G., Felden B., Behr J., Giege R., *Cleavage of tRNA with imidazole and spermine imidazole constructs: a new approach for probing RNA structure.* Nucleic Acids Research, 1995. **23** (16): p. 3161-3167.
203. Maltseva, T., Sandstrom, A., Ivanova, I. M., Sergeyev, D. S., Zarytova, V. F. and Chattopadhyaya, J. *Structural studies of the 5'-phenazinium-tethered matched*

and G-A-mismatched DNA duplexes by NMR spectroscopy. Journal of Biochemical and Biophysical Methods, 1993. **26** (2-3): p. 173-236.
204. Maltseva, T.V., Agback, A., Repkova, M. N., Venyaminova, A. G., Ivanova, E. M., Sandstrom, A., Zarytova, V. F. and Chattopadhyaya, J. *The solution structure of a 3'-phenazinium (Pzn) tethered DNA-RNA duplex with a dangling adenosine: r(5'GAUUGAA3'):d(5'TCAATC3'-Pzn).* Nucleic Acids Research, 1994. **22** (25): p. 5590-5599.
205. Lokhov, S.G., Podyminogin, M. A., Sergeev, D. S., Silnikov, V. N., Kutyavin, I. V., Shishkin, G. V. and Zarytova, V. P. *Synthesis and high stability of complementary complexes of N-(2-hydroxyethyl)phenazinium derivatives of oligonucleotides.* Bioconjugate Chemistry, 1992. **3** (5): p. 414-419.
206. Pyshnyi, D.V., Pyshnaya, I. A., Lokhov, S. G., Podyminogin, M. A., Ivanova, E. M. and Zarytova, V. F. *New approach to enhancing the efficiency and specificity of interaction in duplexes by the use of tandem structure.* Pure and Applied Chemistry, 1996. **68** (6): p. 1321-1328.
207. Denisov, A.Y., D.V. Pyshnyi, and E.M. Ivanova, *The nature of stabilization of the tandem DNA duplex pTGGAGCTG Â· (pCAGC + (Phn-NH-(CH2)3-NH)pTCCA) Basing on the UV, CD, and two-dimensional NMR spectroscopy data.* Bioorganicheskaya Khimiya, 2000. **26** (5): p. 385-386.
208. Denisov, A.Y., D.V. Pyshnyi, and E.M. Ivanova, *The nature of stabilization of the tandem DNA duplex pTGGAGCTG Â· (pCAGC + (Phn-NH-(CH2)3-NH)pTCCA) basing on the UV, CD, and two-dimensional NMR spectroscopy data.* Russian Journal of Bioorganic Chemistry, 2000. **26** (5): p. 337-349.
209. Bodanszky, M., *Principles of Peptide Synthesis*. 1984: Springer-Verlag.
210. Gorenstein, D.G., *Nucleotide conformational analysis by 31P nuclear magnetic resonance spectroscopy.* Annual review of biophysics and bioengineering, 1981. **10**: p. 355-386.
211. Letsinger, R.L. and M.E. Schott, *Selectivity in Binding a Phenanthridinium-Dinucleotide Derivative to Homopolynucleotides.* Journal of the American Chemical Society, 1981. **103** (24): p. 7394-7396.
212. Asseline, U., N.T. Thuong, and C. Helene, *Oligonucleotides Covalently Linked to Intercalating Agents - Influence of Positively Charged Substituents on Binding to Complementary Sequences.* Journal of Biological Chemistry, 1985. **260** (15): p. 8936-8941.
213. Garipova, I.Y. and V.N. Silnikov, *New synthetic approaches to multifunctional phenazinium salt derivatives.* Molecules, 2003. **8** (6): p. 505-519.
214. Bichenkova, E.V., Gorenshtein L.A., Vorob'ev Yu.N., Tenne E.Yu., Zarytova V.F., Ivanova E.M., Maltseva T.V., Lebedev A.V. *Study of the spatial structure of the duplex (Phn-NH(CH2)NH)pd(CCAAACA).pd(TGTTTGGC) with covalently bound 10-(2-hydroxyethyl)phenazine by in aqueous solution by 2D-^{1}H-NMR and by limited molecular mechanics.* Bioorganicheskaya Khimia, 1992. **18** (7): p. 901-910.
215. Maltseva, T.V., V.F. Zarytova, and J. Chattopadhyaya, *Base-pair exchange kinetics of the imino and amino protons of the 3'-phenazinium tethered DNA-RNA duplex, r((5')GAUUGAA(3')):d((5')TCAATC(3')-Pzn), and their comparison with those of B-DNA duplex.* Journal of Biochemical and Biophysical Methods, 1995. **30** (2-3): p. 163-177.
216. Yurchenko, L., Silnikov, V., Godovikova, T., Shishkin, G., Toulme, J. J. and Vlassov, V. *Cleavage of Leishmania mini-exon sequence by oligonucleotides*

conjugated to a diimidazole construction. Nucleosides and Nucleotides, 1997. **16** (7-9): p. 1721-1725.
217. Vlassov, V., Abramova, T., Godovikova, T., Giege, R. and Silnikov, V. *Sequence-specific cleavage of yeast tRNA(Phe) with oligonucleotides conjugated to a diimidazole construct.* Antisense and Nucleic Acid Drug Development, 1997. **7** (1): p. 39-42.
218. Petyuk, V., Serikov, R., Tolstikov, V., Potapov, V., Giege, R., Zenkova, M. and Vlassov, V. *Invasion of strongly binding oligonucleotides into tRNA structure.* Nucleosides, Nucleotides and Nucleic Acids, 2000. **19** (7): p. 1145-1158.
219. Kuznetsova, I.L., Zenkova, M. A., Gross, H. J. and Vlassov, V. V. *Enhanced RNA cleavage within bulge-loops by an artificial ribonuclease.* Nucleic Acids Research, 2005. **33** (4): p. 1201-1212.
220. Koval'ov, N., Kuznetsova, I., Burakova, E., Sil'nikov, V., Zenkova, M., and Vlassov, V. *Ribonuclease activity of cationic structures conjugated to lipophilic groups.* Nucleosides, Nucleotides and Nucleic Acids, 2004. **23** (6-7): p. 977-981.
221. Kovalev, N.A., Medvedeva, D. A., Zenkova, M. A. and Vlassov, V. V. *Cleavage of RNA by an amphiphilic compound lacking traditional catalytic groups.* Bioorganic Chemistry, 2008. **36** (2): p. 33-45.
222. Soukup, G.A. and R.R. Breaker, *Relationship between internucleotide linkage geometry and the stability of RNA.* RNA, 1999. **5** (10): p. 1308-1325.